



Universitat Autònoma de Barcelona

ADVERTIMENT. L'accés als continguts d'aquesta tesi queda condicionat a l'acceptació de les condicions d'ús establertes per la següent llicència Creative Commons:  http://cat.creativecommons.org/?page_id=184

ADVERTENCIA. El acceso a los contenidos de esta tesis queda condicionado a la aceptación de las condiciones de uso establecidas por la siguiente licencia Creative Commons:  <http://es.creativecommons.org/blog/licencias/>

WARNING. The access to the contents of this doctoral thesis it is limited to the acceptance of the use conditions set by the following Creative Commons license:  <https://creativecommons.org/licenses/?lang=en>



Universitat Autònoma de Barcelona

Biological response to implanted intraneural electrodes

Memòria de la Tesi Doctoral presentada per Natalia de la Oliva Muñoz per optar al grau de Doctor en Neurociències per la Universitat Autònoma de Barcelona

Aquesta tesi doctoral ha estat realitzada sota la direcció del Dr. Xavier Navarro Acebes i Dr. Jaume del Valle Macià.

Director de Tesi

Dr. Xavier Navarro Acebes

Director de Tesi

Dr. Jaume del Valle Macià

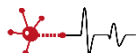
Doctoranda

Natalia de la Oliva Muñoz

Bellaterra, Desembre del 2017

Unitat de Fisiologia Mèdica. Departament de Biologia Cel·lular, Fisiologia i Immunologia. Institut de Neurociències

NeuroPlasticity
& Regeneration



The research described in this thesis was conducted at the Department of Cellular Biology, Physiology and Immunology, Institute of Neurosciences, of the Universitat Autònoma de Barcelona in the Group of Neuroplasticity and Regeneration (Faculty of Medicine).

This research was supported by the European Union FP7-ICT project NEBIAS number 611687 and CIBERNED funds from the Instituto de Salud Carlos III of Spain.

Summary	5
List of Abbreviations	7
Introduction	9
PERIPHERAL NERVE INTERFACES	9
1.1 Peripheral nervous system	9
1.2 Prostheses	11
1.3 Peripheral nerve electrodes	16
BIOCOMPATIBILITY AND FOREIGN BODY RESPONSE	24
2.1 Foreign Body Reaction	24
2.2 Biocompatibility	30
THE FBR TO INTERFACES WITH THE NERVOUS SYSTEM	35
3.1 CNS interfaces and the FBR	35
3.2 PNS interfaces and the FBR	36
3.3 Strategies to reduce the FBR to neural interfaces	37
Objectives	41
Chapter 1: In vivo biocompatibility and functionality of a new parylene c-based transversal intraneural electrode	43
Chapter 2: Time course study of long-term biocompatibility and foreign body reaction to intraneural implants	57
Chapter 3: Dexamethasone reduces the foreign body response to intraneural electrode implants in the peripheral nerve of the rat	89
Chapter 4: Dexamethasone improves long-term function of transversal intraneural electrodes	113
General discussion	135
Conclusions	145
References	149
Annex	167

SUMMARY

The foreign body reaction (FBR) is an immune-mediated response to any device implanted in the body. Several studies have shown that it is characterized by a first inflammatory phase followed by a tissue remodeling phase, which results in the encapsulation of the foreign body. This encapsulation is thought to cause, among other factors, the progressive decline in function reported in neural electrodes, which should remain chronically implanted in the body to generate and record nerve signals from the nervous tissue.

In this thesis, a detailed characterization of the FBR to intraneural electrodes has been performed, in order to determine feasible therapeutic strategies to reduce the FBR and to improve the long-term function of chronic implanted intraneural electrodes.

Our results show that the immune infiltration in the nerve peaked after two weeks of implant, without differences between two polymers intended to be used as electrode substrate (i.e., polyimide and Parylene C). However, the tissue deposition around both polymers evolved differently at chronic time points. While the capsule around polyimide devices peaked after two weeks and was stabilized after that up to 8 months, the capsule around Parylene C devices had a first peak at week 2 and it continued increasing after a resting period of 4-8 weeks to reach a second maximum at week 16. Molecular analysis of implanted nerves showed no differences between the FBR to both polymers in the inflammatory and tissue remodeling studied factors.

The two main phases described in the FBR in peripheral nerves have determined possible therapeutic strategies to reduce this reaction. Among the several drugs tested, only dexamethasone significantly reduced the infiltration of macrophages and the thickness of the capsule around both polymers. Moreover, dexamethasone treatment improved the long-term function of transversal intraneural electrodes, particularly in terms of stimulation properties.

In conclusion, the FBR to intraneural devices shows a similar pattern than the reported in other host tissues such as the subcutaneous and the peritoneal spaces. Moreover, differences in the FBR between polyimide and Parylene C have

been observed, which would rule Parylene C out as a substrate for chronically implanted intraneural electrodes. The FBR characterization has allowed testing several therapeutic strategies to reduce this response, such as dexamethasone. In fact, dexamethasone treatment has improved the outcome of chronic implanted intraneural electrodes, may be due to a reduction in the cellular infiltration and tissue deposition.

LIST OF ABBREVIATIONS

CCL	C-C motif ligand
CCR	C-C chemokine receptor
CD90	cluster of differentiation 90
CMAP	compound muscle action potential
CNAP	compound nerve action potential
CNS	central nervous system
CXCL	chemokine C-X-C motif ligand
DRG	dorsal root ganglia
ECG	electrocardiographic
ECM	extracellular matrix
EMG	electromyographic
ENG	electroneurographic
FBGCs	foreign body giant cells
FBR	foreign body reaction
GM	gastrocnemius medialis
IL	interleukin
Iba1	ionized calcium-binding adapter molecule 1
LIFE	longitudinal intrafascicular electrode
MEA	multielectrode array
ParC	Parylene C
PI	polyimide
PL	plantar interossei

PNS	peripheral nervous system
SNR	signal-to-noise ratio
TA	tibialis anterior
TGF β	transforming growth factor beta
TIME	transversal intrafascicular multi-channel electrode
TNF α	tumor necrosis factor alpha

PERIPHERAL NERVE INTERFACES

1.1 Peripheral nervous system

The function of the peripheral nervous system (PNS) is to interconnect and communicate the central nervous system (CNS) with the limbs and the internal organs. The PNS is constituted by neurons whose cell bodies are located in the spinal cord and within ganglia and its axons, which are bundled together within peripheral nerves to reach the target organs (Fig. 1). The flow of information has to occur in both directions, from the CNS to organs and vice versa. External and internal stimuli (e.g., arterial pressure, mechanical stimuli in the skin...) detected by receptors are transmitted by afferent axons of sensory neurons located in the dorsal root ganglia (DRGs), that will synapse and transduce the signals to CNS neurons in specific regions of the spinal cord or the brainstem. Once the CNS has processed the afferent sensory information at different levels, a response may be necessary. The CNS then generates an adequate motor response that will lead to impulses along the efferent motor axons to activate the appropriate effectors (muscles and glands). Thus, the nervous system is able to get and transduce the environmental information, to process it and to give a proper response in a fast and reliable way (Tortora and Derrickson, 2014).

Afferent and efferent axons that innervate different target organs such as muscles, skin or viscera, are grouped into bundles or fascicles surrounded by connective tissue to form the peripheral nerves. Peripheral nerves have three supportive layers: epineurium, perineurium, and endoneurium (Fig. 1). The epineurium is the outermost sheath, surrounds the whole nerve and is mainly composed of loose connective tissue and blood vessels for nerve supply. The perineurium surrounds each fascicle in the nerve and is composed of perineurial cells and collagen fibers so that it is the responsible for the tensile strength and flexibility of the nerve. Finally, the endoneurium is the connective tissue matrix that surrounds each axon individually and occupies all the space between fibers. It is composed of fibroblasts, collagen and other extracellular matrix (ECM) proteins and Schwann cells, which either myelinate or surround the axons.

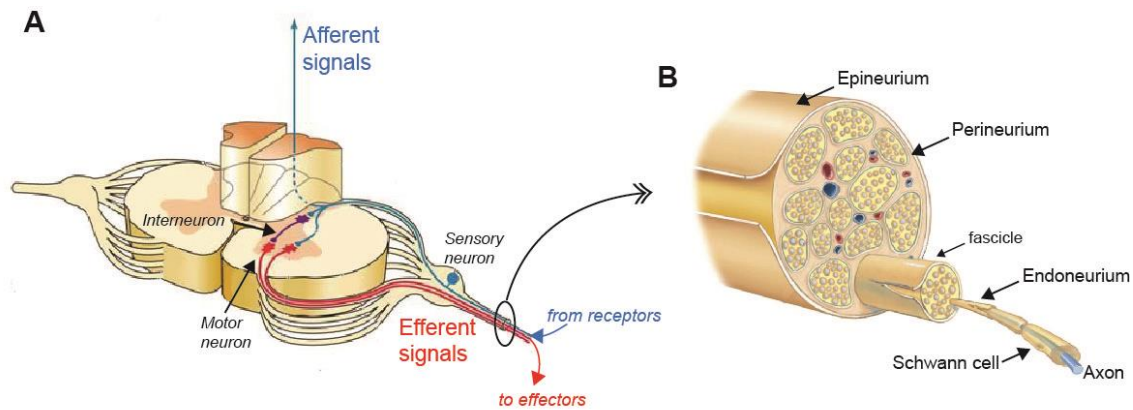


Figure 1. Anatomy of peripheral nerves. (A) Peripheral nerves contain both motor and sensory axons. Flow of afferent information in sensory axons from sensory neurons located in dorsal root ganglia to upper structures. Efferent signals from CNS to effectors through motor axons from motor neurons located in the ventral horn of the spinal cord. (B) Transversal section of peripheral nerve with the epineurium, perineurium, forming nerve fascicles, and endoneurium connective layers. Schwann cells surround both myelinated and unmyelinated axons. Modified from (A) RCI Rutgers and (B) Pearson education.

Peripheral nerves are formed by different types of axons: motor axons from motoneurons located in the spinal cord, sensory axons from sensory neurons in the DRGs and autonomic axons. The number and types of fibers present in peripheral nerves are highly variable, but most of them are mixed nerves containing motor, sensory and autonomic fibers to innervate a target territory. The nerve fibers are commonly classified depending on their diameter and myelination, which will determine the conduction velocity of these axons (Table 1, Erlanger and Gasser, 1937). Efferent motor fibers are myelinated fibers and can be mainly divided into alpha-motor fibers that innervate skeletal extrafusal muscle fibers and gamma-motor fibers that innervate the muscle spindle. Afferent sensory axons can be myelinated or unmyelinated and can range from 0.5 to 20 μm in diameter. Sensory fibers in the skin, muscles and deep tissues can process different types of stimuli - mainly mechanical, thermal, noxious and proprioceptive - through different specific membrane receptors. The intensity of stimulation is coded by the frequency of action potentials and the number of recruited sensory afferents.

<i>Fiber type</i>	<i>Function</i>		<i>Diameter</i> (μm)	<i>Conduction velocity</i> (m/s)
<i>Myelinated</i>	A α	Alpha-motor efferents, Proprioception	12 – 20	80 – 120
	A β	Tactile, Proprioception	8 – 12	30 – 80
	A γ	Gamma-motor efferents	3 – 8	15 – 40
	A δ	Pain, Temperature	1 – 3	5 – 30
	B	Preganglionic autonomic efferents	1 – 3	3 – 15
<i>Unmyelinated</i>	C	Pain, Temperature	0,5 – 2	0,5 – 2

Table 1. Classification of nerve fibers (Erlanger and Gasser, 1937).

An injury to peripheral nerves means the partial or total disconnection of the area innervated by the affected nerves from the CNS, with the subsequent loss of the conveyed functions. The regeneration of injured axons needs a complex and well-coordinated process in which axotomized neurons change to a regrowing state, the distal stump debris is cleared in a process called Wallerian degeneration and then axons can regenerate through the distal stump (Allodi et al., 2012). Several surgical strategies have been developed to repair the injured nerves (Navarro and Verdú, 2004). Nevertheless, the functional recovery achieved after a nerve injury is usually limited due to the misdirection of regenerating axons, the formation of a neuroma and the chronic denervation and atrophy of target organs. On the other hand, mechanical hand prostheses have become very advanced and they constitute a valid option for hand amputee patients to recover some functionality (Cordella et al., 2016; Schultz and Kuiken, 2011). Even more, the possibility of substituting the patient's own non-functional arm by an artificial one in cases of severe plexus and nerve injuries is now under debate (Aszmann et al., 2016; Smith et al., 2014).

1.2 Prostheses

After a nerve injury or limb amputation, especially of a hand or upper limb, loss of function of denervated areas cause the inability to perform activities of daily living and ultimately determines people's lifestyle. Besides the evident inability to grasp and manipulate surrounding objects, amputee people lose its capacity to interact and communicate with its environment or to express emotions without gestures properly.

The desire and need to restore and replace the lost functions due to injuries to the nervous system, limb amputations and degenerative diseases have been historically present (Finch, 2011; Nerlich et al., 2000). Several strategies have been developed, from a merely

aesthetic objective to more complex ideas based on artificial systems (Fliegel and Feuer, 1966; Zuo and Olson, 2014). Aesthetic prostheses were the first strategy to ameliorate the loss of a limb, but without any functional recovery aim (Nerlich et al., 2000). With further developments in engineering, artificial systems and mechanical prostheses are intended to substitute the lost limb in amputee people and recover its normal functions. To ensure a good outcome, a prosthesis has:

- to mimic and look like the natural limb, as do the aesthetic prosthesis,
- to be naturally felt and controlled by the patient,
- to allow for multiple degrees of freedom to have all the functions of a natural limb,
- to provide sensory feedback to achieve the natural control needed by the subject.

Thus, an ideal prosthesis would use the subject motor commands to induce movement of the mechanical limb and then provide sensory feedback from sensors present in the robotic arm (Ciancio et al., 2016; Cordella et al., 2016). However, this is not an easy and feasible objective and several different strategies have been developed in order to achieve the ideal prosthesis.

1.2.1 Body-powered prostheses

Body-powered prostheses consist of a socket attached to the residual limb that finishes in a terminal device. Patients wear them by means of harnesses (Fig. 2). They work by using cables to link the body movement to control the prosthesis motion. Thus, moving the body or the remaining limb stump in a certain way (e.g., extending the arm or flexing the shoulder) will pull on the cable attached to the harness on the user back, opening, closing or bending the attached terminal device. Besides, in some of these prostheses it is possible to interchange the terminal device in order to do more specific actions (e.g. hooks, mechanical hands...).

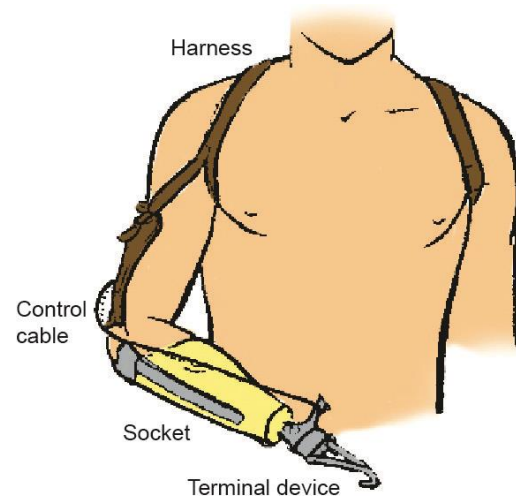


Figure 2. Body-powered prosthesis with the terminal device attached to a socket. The prosthesis is fixed to the patient by means of a harness and controlled with a cable. Adapted from Upperlimbprosthetics.info

These kinds of prostheses are a good option to solve some basic daily problems and with an excellent aesthetic satisfaction. Besides, they are usually more durable and less expensive than other more sophisticated systems. However, they do not have a satisfactory

functional restoring due to the limited degrees of freedom offered (Biddiss et al., 2007; Millstein et al., 1986).

1.2.2 Myoelectric prostheses

Myoelectric prostheses are a more complex solution for functional restoration. These prostheses are motorized and controlled by surface electromyographical (EMG) signals recorded from muscles in the residual limb or the body (e.g., chest muscles). Electrodes placed on the remaining muscles detect the muscle activity (triggered by the user) and translate it into information that electric motors in the prosthesis use to control the artificial limb movement. The user can control the strength and speed of the limb movement by proportional control according to the EMG signal amplitude (Zecca et al., 2002).

A significant advance was made in this field with the development of the *targeted muscle reinnervation* (TMR) strategy (Fig. 3). With TMR, the remaining nerves of the upper limb, such as median, ulnar and radial nerves, that have been disconnected from their targets, are transferred and inserted into the residual limb or chest muscles that are no longer useful due to the loss of the limb (Kuiken et al., 2011). Thus, the re-innervated muscles with

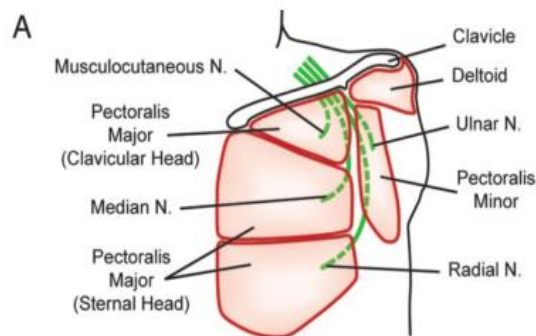


Figure 3. Targeted muscle reinnervation strategy. Nerves innervating the hand (green) were rerouted to chest muscles. Extracted from Kuiken et al., 2007.

amputated nerves are now the target muscles of the lost limb. Patients control the prosthetic system by the efferent signals from injured nerves that now reach the reinnervated muscles, which will result in the contraction of those muscles. The strong EMG signals generated are used for powered hand, wrist and elbow control. User people find that myoelectric prostheses allow for a wide range of motion, a more natural appearance and they are more comfortable as the harness is almost eliminated (Miller et al., 2008).

However, there are some crucial points in the use of myoelectric prostheses that cause the incomplete acceptance of these systems by the patients (Biddiss and Chau, 2007). When using EMG signals, some delay appears due to the data processing, which results in longer time to perform easy movements in comparison to the natural limb (Chadwell et al., 2016). Even the advances in prosthetic arm designs, which now offer up to 17 degrees of

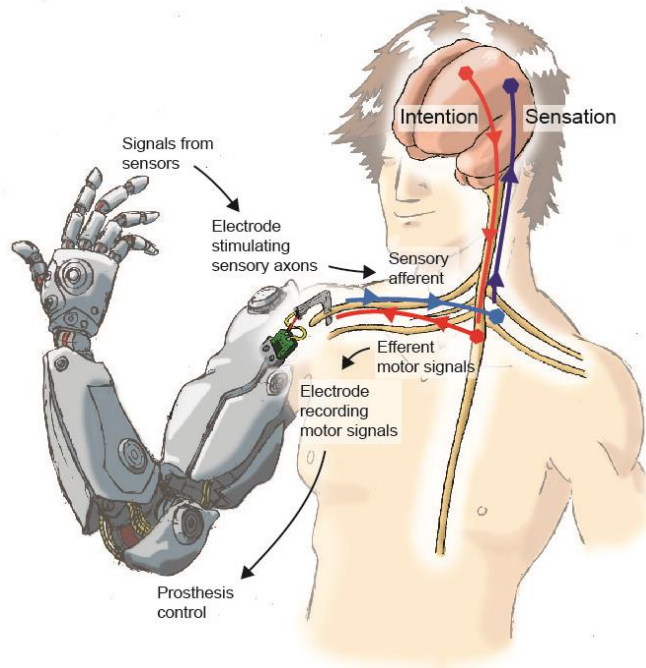
freedom (Burck et al., 2011; Resnik et al., 2014), still these prostheses are far from the natural limb performance (Cowley et al., 2017). Besides, users have to rely on visual feedback constantly due to the lack of sensory feedback from the prosthesis. In line with this, studies with TMR have demonstrated some recovery of tactile sensory feedback in the skin overlying the reinnervated muscles, which eventually could be used to improve control of mechanical prostheses (Kuiken et al., 2007).

1.2.3 Neuroprostheses and bionic systems

Very advanced hand prostheses have been fabricated in the last decade, which can eventually produce almost the same amount and variety of movements than the natural human hand (Hashim et al., 2017; Kyberd, 2017). Thus, a parallel improvement is needed to offer a proper somatosensory feedback and a more complex voluntary control of the prosthesis than provided with the powered and myoelectric prosthetic systems. To achieve a more natural and intuitive control, directly interfacing the nervous system would allow to record information from motor commands and to stimulate the sensory system. It appears as a significant improvement for solving some of the problems with the systems mentioned above. Tyler and coworkers have used electrodes placed around the peripheral nerves of the upper limb to stimulate specific nerve fibers to give the prosthesis users sensory feedback (Schiefer et al., 2016; Tan et al., 2014). They showed an improved in task performance of upper limb amputee patients using myoelectric prosthesis based on EMG-signals control when the nerves innervating the lost limb were stimulated.

Thus, neuroprostheses are the next step to directly interconnect the nervous system of the patient with a robotic limb by means of interfaces with the nervous tissue. Unlike myoelectric prostheses, in which EMG signals are recorded from close muscles to control the mechanical limb, neuroprostheses systems are based in the recording of efferent motor signals directly from the nervous system to control the robotic prosthesis (Fig. 4). In addition, the same interfaces can also stimulate afferent sensory fibers to provide a proper somatosensory feedback to the patient from sensors present in the mechanical part (Fig. 4).

Figure 4. Neuroprosthesis closed loop control by means of peripheral nerve electrodes. Efferent motor signals (red) are recorded to control the mechanical prosthesis. Sensory signals from the robotic limb conveyed to the user through selective electrical stimulation of the amputated nerve. The sensory stimulus travels to upper structures to provide sensory feedback.



Neural signals can be intercepted from different places in the nervous system, depending on the individual characteristics and applications, such as the brain (Wang et al., 2013), the spinal cord (Capogrosso et al., 2016) and the peripheral nerves (Navarro et al., 2005). For restoring a functional arm lost, peripheral nerves are a suitable option due to easier accessibility and reduced invasiveness in comparison with the CNS. Besides, peripheral nerves contain both motor and sensory fibers, so that it would be possible to intercept motor commands for prosthetic device control and also to stimulate sensory fibers to provide somatosensory feedback more specifically than in higher areas.

The interface is an essential part of a neuroprosthesis since it includes the electrode in direct contact with the nervous tissue and the wires to connect to the external processor and controller (Fig. 4). The neural electrode should record efferent bioelectrical activity in peripheral nerves that came from commands in the brain and transform these impulses into electrical signals to control the motors of the prosthetic limb. Besides, the electrode should also be able to translate signals from the mechanical sensors in the device into bioelectrical inputs to stimulate afferent fibers to provide a sensory feedback (del Valle and Navarro, 2013).

Electrodes functionality and characteristics are described in detail in the following section.

1.3 Peripheral nerve electrodes

1.3.1 Bases of stimulation and recording from the nervous tissue

Electrical stimulation and recording from an excitable tissue as the nervous tissue are the basis of electrophysiological research and neuroprostheses development. Any interface capable of interacting in both ways with the nervous tissue can be considered as a bidirectional electrical interface.

An adequate nerve electrode has to be composed of inert materials, both passively and when subjected to electrical stimulation, since deterioration of the device may result in implant failure and the release of toxic products. In general, neural electrodes are composed of a substrate isolating material and the conductive metal lines. Materials typically used are gold, platinum, iridium, tungsten and stainless steel as conductors, and silicon, silicone elastomer, polytetrafluoroethylene and polyimide as insulating carriers (Heiduschka and Thanos, 1998; Navarro et al., 2005). For the substrate, silicon and flexible polymers like polyimide are the most widespread materials used with micromachining techniques.

The active sites on the electrode are the uncovered parts of the conductive material that effectively serve to record or deliver an electrical charge to the nerve fibers. They are made of different materials (e.g., gold, platinum, iridium) with different physical and chemical properties that will determine the amount of injected charge available, the degradation process that could suffer or its impedance (Merrill et al., 2005; Stieglitz et al., 2000). Besides, depending on their application (e.g., cortical, peripheral nerves), the electrode and its active sites will have specific shape and size, which will also determine the maximum charge it may deliver and the impedance since smaller active sites typically have a higher impedance (Tyler et al., 2015).

a) Extracellular stimulation of the nervous tissue

In terms of extracellular nerve stimulation, when a difference of potential is applied between two electrodes in contact with neural tissue, electric current flows between them and an electrical field is generated. This electric field activates the voltage-gated sodium and potassium channels of the nerve fibers in the neighborhood. When enough channels are opened and the threshold potential is achieved, an action potential is generated and propagated away from the site of stimulation. Action potentials conducted in motor fibers will ultimately provoke the release of acetylcholine in the neuromuscular junction and the consequent excitation and contraction of the innervated skeletal muscle. On the other hand,

action potentials generated in sensory axons will transduce the sensory input and will be conducted along the sensory pathways to upper structures.

Different parameters modulate the extracellular stimulation capacity of electrodes.

The first one is the distance between the active site delivering the current and the axon to stimulate. The closer the active site and the axon are, the lower current will be needed to activate the axon. The minimum current intensity needed to evoke an action potential and a specific response is known as the *threshold of stimulation* and it increases as the distance between the active site and the axon to stimulate increases (Ranck, 1975).

A second factor is the resistance of the nerve fibers to the electrical flow. Nerve fibers with a large diameter are activated at smaller currents and have a lower threshold of stimulation than small ones (Blair and Erlanger, 1933; McNeal, 1976). This difference is particularly important between myelinated and unmyelinated nerve fibers.

Parameters such amplitude, duration, and frequency of the stimuli applied are also relevant to determine the stimulation threshold and the input generated (Gorman and Mortimer, 1983). These variables are inversely related: as the amplitude of the pulse increases, the duration required to stimulate the fiber decreases (Bostock, 1983), and vice versa. Modulation of the pattern of activation by changes in amplitude and duration may produce differences in the transduction along the neural pathways. In fact, Tan and coworkers showed that repeated stimulation with pulses of constant amplitude and width were perceived by the subject as paresthesia, whereas modulation of both parameters produced a more natural sensation when stimulating amputated arm nerves (Tan et al., 2014).

Hence, the position of the active site with respect to the fibers inside the nerve will determine not only the current needed to stimulate the fibers (based on the distance and fiber diameter) but also which fibers will be stimulated (based on fiber type and topography). This, in fact, will determine the *selectivity of stimulation*, i.e., the specific activation of those axons related to a specific response. *Topographical or anatomical selectivity* describes the ability of an electrode to stimulate only the fibers related to a specific anatomical region and target (muscle or skin), usually located bundled in a fascicle, without activating other fibers linked to other targets. On the other hand, *functional selectivity* determines the activation of distinct classes of nerve fibers, that relates with the type of function conveyed by the targeted axons, for example, excite sensory or motor fibers (Grill and Mortimer, 1996).

In summary, to achieve a selective stimulation of only those fibers related to the desired output, active sites in the implanted electrode have to be close to the specific axons. Therefore, detailed knowledge of the topographical organization of the implanted nerve is required (Badia et al., 2010) to guide adequate placement of the electrode active sites as near as possible to the target bundle of axons. The intensity of the stimuli may be increased to obtain a specific response, but then the electrical field also diffuses to a wider area and can activate all the fibers in the vicinity, thus decreasing the selectivity for that specific response. Hence, when evaluating the selectivity achieved with a particular electrode design, it is usually expressed as the ratio of the specific response obtained with respect to others responses relying on the same nerve (Badia et al, 2011a, Veraart et al, 1993).

b) Extracellular recording of nerve signals from nerve fibers

When an action potential runs along an axon, ions flow across the membrane. This ion movement, equivalent to a current flow, also generates a small potential that can be detected by the metal active sites of the implanted electrode. Thus, recording nerve signals is based on the capacity of the electrode to detect changes in the membrane potential. In nerve electrophysiology, the general recording setting is based on the differential recording between two electrode sites placed relatively close to the excited tissue.

Alike the stimulation of nerve fibers, many of the parameters above-mentioned are also crucial to obtain good quality nerve signals. The magnitude of the potential sensed depends on: a) the distance between the active site and the axons that have generated it, b) the impedance of the active site, and c) the tissue impedance between the axon and the active site. Moreover, the potential sensed can be the result of the summed current when many axons are excited synchronously and they produce a larger signal (compound nerve action potential, CNAP). During standard excitation produced by natural sensory stimuli, axons fire asynchronously during the stimulus duration, so the signal recorded of the nerve activity (electroneurography, ENG) is smaller and disperse compared to the CNAP (Tyler et al., 2015).

Another critical factor in order to obtain proper quality signals is the signal to noise ratio (SNR), it is, the amplitude of the signal of interest with respect to the noise. Extracellularly recorded neural signals are very small, ranging from 10 to 100 μV within microns of the axon without a resistant tissue in between, in comparison to different environmental (e.g., circuit) and biological (e.g., ECG, EMG) noise sources. Thus, recording needs a very low-noise, high-gain amplifier system. Therefore, to record high-quality nerve signals, the active

site should be as close as possible to the axons. However, smaller active sites will have a higher impedance, which will reduce the signal to amplify.

On the other hand, since different sources produce electrical signals with different frequency components, the recording can be processed with adequate filters to reduce the input of undesired signals, thus increasing the SNR of the targeted signal. For example, EMG signals usually have a peak around 300Hz, while for ENG it is around 1000Hz (Haugland et al., 1994; Upshaw and Sinkjaer, 1998). Moreover, with an adequate processing, recorded signals can be differentiated using different features according to the stimulus type (Raspopovic et al., 2010). Thus, the limiting factor to having good quality recordings is the SNR, which, even with digital processing, depends on the neurophysiological nature of the signal, electrochemical changes in the metal active sites, electrode position and tissue deposition over time.

1.3.2 Types of peripheral nerve electrodes

Consequently, an equilibrium is needed between the interface design, active site size and position, the stimulation/recording properties desired and the ratio benefit/risk. For

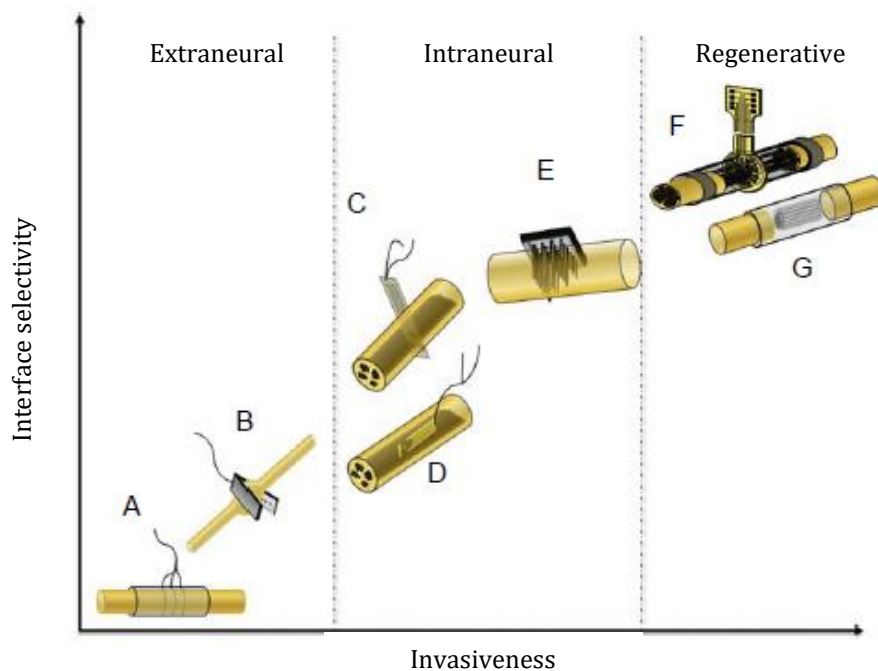


Figure 5. Classification of peripheral nerve electrodes regarding its invasiveness and selectivity. Images show examples of extraneural electrodes such as (A) cuff and (B) flat interface neural electrode (FINE), intraneural electrodes such as (C) transversal intraneural multichannel electrode (TIME), (D) longitudinal intrafascicular electrode (LIFE), (E) multielectrode array (MEA) and regenerative electrode such as (F) sieve and (G) multichannel electrode. From del Valle and Navarro, 2013.

different biomedical applications, several electrode designs for the PNS have been developed based on their location within the nerve anatomy: extraneural, intrafascicular and regenerative electrodes, that can be in turn classified according to their invasiveness and selectivity (Fig. 5) (Navarro et al., 2005). For example (see following sections), surface and muscular electrodes can record EMG activity from and stimulate only the underlying or implanted muscles. Extraneural electrodes, such as cuff and epineurial, provide a simultaneous interface with many axons in the nerve, whereas intrafascicular and regenerative electrodes inserted in the nerve may interface small groups of axons within a nerve fascicle. On the other hand, the state of the nerve varies; cuff and intrafascicular electrodes can be applied to intact nerves in acute or chronic studies, whereas by definition regenerative electrodes are implanted in transected nerves that need to regenerate across the electrode over several months.

a) Extraneural electrodes

Extraneural electrodes, such as cuffs (Loeb and Peck, 1996; Rodriguez et al., 2000; Tan et al., 2013) (Fig.5), are designed to be placed surrounding a nerve trunk and to provide simultaneously interfacing with many axons in the nerve (Navarro et al., 2005). They are composed of an insulating tubular sheath with the active sites placed on the inner surface. This leads to confine the stimulating current to the inner space, avoiding stimulation of other neighboring nerves and tissues (Loeb and Peck, 1996).

Cuff electrodes may induce selective activation of nerve fibers within a nerve or fascicle (Tan et al., 2013), but due to its design, mainly only those fibers in the periphery (Badia et al., 2011a). This fact leads to a lower selectivity and an increase in current injection needed to activate the most internal fibers. Additionally, although cuff electrodes have been implanted in patients for decades due to their robustness and relatively low invasiveness (Fisher et al., 2009; Polasek et al., 2009), nerves can be damaged by the presence of the cuff due to the differences in stiffness between the electrode and the nervous tissue (Krarup et al., 1989; Larsen et al., 1998), especially in those nerves subjected to a wide range of motion. Nevertheless, the reduced size and thickness of recent polymer cuffs (Stieglitz et al., 2000) have brought the possibility to implant several small cuffs around different fascicles or branches of nerves to achieve a higher selective functional stimulation without significant nerve damage (Rodriguez et al., 2000), although it implies more aggressive implantation methods. Recently, promising results from human amputee patients have demonstrated the ability to provide sensory feedback using extraneural cuff electrodes over extended periods of time (Tan et al., 2013).

A variation of the cuff electrode was developed to change the nerve conformation, the Flat Interface Nerve Electrode (FINE) (Tyler and Durand, 2002). With this type of electrode, the nerve is flattened and there are more nerve fibers close to the active sites in the surrounding electrode. Comparative studies with cuff electrode showed that it is possible to selectively activate more individual fascicles with the FINE, as well as groups of fibers within the fascicles (Leventhal and Durand, 2004; Tyler and Durand, 2002). Besides, it also pointed out the strong dependency of selectivity on the relative locations of the fascicle and the electrode contacts. However, chronic studies in laboratory animals with implanted FINE over 1 to 3 months showed that electrodes applying high reshaping force induced nerve damage, whereas those with moderate and small forces did not cause significant changes in nerve physiology and histology (Leventhal et al., 2006). Besides, electrodes that moderately flattened the nerve demonstrated the best selectivity for limb motion measurements that was maintained throughout the implant time (Leventhal and Durand, 2004; Park and Durand, 2015; Schiefer et al., 2013).

In terms of nerve recording, cuff electrodes are usually less used than other designs due to a low SNR, mainly caused by the low conductance that the tissue between the active sites and the axons have (Tyler et al., 2015). However, some studies have shown the ability of cuff electrodes to record nerve signals (Y. J. Lee et al., 2017; Loeb and Peck, 1996).

b) Intrafascicular electrodes

In order to enhance stimulation selectivity and improve the recordings quality with respect to extraneural electrodes, more invasive electrodes have been developed, as intrafascicular and regenerative electrodes intended to be placed inside the nerve, in closer contact with the axons in the endoneurium (Navarro et al., 2005).

Intrafascicular electrodes, such as the longitudinal intrafascicular electrode (LIFE) and the transversal intrafascicular multichannel electrode (TIME), are placed inside the nerve, within a given fascicle, in close contact with the nerve fibers to activate or record from them. Stimulation with them specifically activates axons in the nerve fascicle in which the active sites of the electrode are placed, with little cross-talk to adjacent fascicles. Due to the proximity to nerve fibers, lower intensity current is needed to achieve equivalent stimulation than with extraneural electrodes (Yoshida et al., 2000). Besides, as they are inside fascicles, they avoid the perineurium tissue and its low conductance in comparison to the epi- and endoneurium layers (Tyler et al., 2015).

LIFE electrodes are longitudinally implanted within nerve fascicles, parallel to the longitudinal direction of the axons. They can interface a restricted group of axons within that fascicle. The initial LIFEs were composed by thin insulated conducting wires, such as Pt-Ir or metalized Kevlar fibers with a short active site zone of the wire bared of insulation (Malagodi et al., 1989; McNaughton and Horch, 1996; Yoshida et al., 2000). Histological analysis revealed no damage to nerve fibers or to the fascicular architecture due to the implant (Lawrence et al., 2002). Nevertheless, the use of flexible polymers such as polyimide (Lago et al., 2007) improved the flexibility and long-term biocompatibility of LIFE electrodes. Several studies in human amputee patients have proved the applicability of LIFEs to stimulate and record from amputee's peripheral nerves even years after the limb amputation (Dhillon and Horch, 2005; Horch et al., 2011). In fact, stimulation of nerve fibers and recording of efferent signals allowed users to better control a motorized hand prosthesis (Horch et al., 2011; Rossini et al., 2010). However, while the selectivity of the LIFE within one fascicle is excellent, it is challenging to implant a few of these electrodes in different fascicles of the same nerve to interface several targets.

In order to improve the connection with different fascicles within the same nerve, the TIME electrode was developed. The TIME consists of a thin, strip-like polyimide-based structure with multiple active sites along the structure (Boretius et al., 2010). The TIME is designed to be implanted transversally in the peripheral nerve, thereby accessing different groups of axons within different fascicles in the same nerve (Badia et al., 2011b). The rationale for the TIME design is to enhance the selectivity of recording from and stimulating different populations of axons localized within different fascicles in the nerve with respect to longitudinally implanted electrodes. In the case of TIME, several fabrication modifications were made to adapt the length and number of active sites to the nerve anatomical requirements. Besides, studies in the rat model have shown the capability of differentiating between sensory stimuli applied to different sites in the paw according to the TIME recordings by different active sites within a peripheral nerve (Badia et al., 2016). Recent studies in human amputee patients implanted with TIME electrodes have shown that by providing sensory feedback it was possible to improve the accuracy to perform different grasping movements, and also to distinguish different shapes and stiffness (Raspopovic et al., 2014) and even discriminate between different coarseness of objects (Oddo et al., 2016).

Moreover, a recent modification of the TIME basic structure, the self-opening intraneural peripheral interface (SELINe), improves the anchorage to the nerves, thus

increasing the stability and stimulation selectivity in experiments performed in animal models (Cutrone et al., 2015).

Finally, a third type of intrafascicular electrode design has been used to interface the peripheral nerve, based on previous designs for the brain cortex. The multielectrode array (MEA) consists of an array of tens of needles incorporated in glass, silicon or polyimide carriers inserted into the nervous system (Rutten et al., 1999). The shaft of the needles is isolated while only the very tip is uncovered to serve as the active site. A modified version, the Utah slanted electrode array (USEA), has been developed with different lengths of the needle rows (Branner et al., 2001). Hence, once implanted in peripheral nerves, stimulation or recording may affect not only surface axons but also inner fibers at defined depths in the nerve. They have been implanted in animal models with slight nerve damage due to the rigidity of the silicon material (Christensen et al., 2014), and successfully used to produce nerve fibers stimulation (Branner et al., 2004; Rutten et al., 1991; Smit et al., 1999), while nerve signals recording was not as good as the stimulation (Branner et al., 2004; Clark et al., 2011). Besides, studies in human volunteers have shown successful recordings and stimulation of nerve fibers for short-term and sub-chronic periods of time (Christensen et al., 2015; Clark et al., 2014; Davis et al., 2016; Warwick et al., 2003). Some shortcomings are due to failure of the active sites with time, and to the fact that the length of the spikes was not enough to reach the mid part of large nerves in humans.

c) Regenerative electrodes

Regenerative electrodes are probably the most invasive interface to the PNS but are also the ones that might offer the highest selectivity. Regenerative electrodes are designed to be implanted not in intact nerves but between the severed stumps of a peripheral nerve after a section, provided that axons will grow across the electrode device distally. Thus, the applicability of regenerative electrodes is directly related to the need of successful regeneration of transected axons (Navarro et al., 1996; Rosen et al., 1990). Regenerating axons will eventually grow through, along or near the electrode, making it possible to record action potentials from and to stimulate individual axons or small groups.

The sieve electrode has been the most used design in regenerative nerves (Stieglitz et al., 1997b) and it consists of an array of holes with metal ring active sites built around them. Ideally, individual or small bundles of axons will grow through each hole, thus resulting in a high number of selective contacts. The first electrodes were made on hard materials, like epoxy, and later on silicon dice (Edell, 1986; Kovacs et al., 1992), that represented some problems due to poor adaptability and late compression of the

regenerated axons within the via holes (Navarro et al., 1998). Better results have been obtained with sieve electrodes made on a flexible polyimide substrate with a large number of via holes (Ceballos et al., 2002; Lago et al., 2005), although further investigation is needed to overcome the technical and biological problems (e.g., scar tissue, axon compression within holes) with these interfaces.

New designs have been developed in order to improve the regenerative process through the regenerative electrode. For example, the micro-channel electrode array, which showed successfully regenerated axons after 1 month, but of a limited number of axons due to the added difficulty of axons to grow through narrow long microchannels (Lacour et al., 2009). A recent new design focused on increasing the transparency of the electrode to facilitate the growth of a more substantial number of axons have been developed. Tubular devices containing a longitudinal planar electrode with several active sites allow the separate regeneration of different nerve fascicles (Clements et al., 2013; Delgado-Martinez et al., 2017). With such dual aisle design, it was possible to selectively stimulate the two different fascicles in acute and chronic experiments in rats, demonstrating that it allowed for better nerve regeneration than the sieve electrodes, but also it can be used as an interface with the regenerating axons grouped in small new fascicles.

BIOCOMPATIBILITY AND FOREIGN BODY REACTION

The potential usability of peripheral nerve interfaces to control mechanical prostheses relies directly on its performance as chronically implanted devices. Therefore, it is mandatory for these implanted devices not only to be biocompatible but also to accomplish with its function in the long-term. However, any implanted device represents a strange body that will induce a host response that could ultimately compromise the functional outcome. The host response to an implanted device – known as foreign body reaction (FBR) – is determined by factors related to both, the material of which the device is made and the tissue in which the device is placed. Efforts have been made to characterize the FBR to different materials and in different tissues and organs in order to determine targets and strategies to reduce the FBR and improve the long-term applicability of medical devices (Anderson et al., 2008; Burgess et al., 2015; Kenneth Ward, 2008).

2.1 Foreign Body Reaction

Biocompatibility is the most commonly used term to describe an optimal host response to implanted medical devices. Biocompatible materials have been defined as those which do not induce an adverse tissue reaction (e.g., necrosis, organ failure) (Williams, 1987). However, a more helpful definition would be that biocompatibility is the ability of a medical

device to accomplish a specific application with an appropriate host response (Williams, 2008). This definition links the device properties and the tissue reaction with the performance in a specific biomedical function. Therefore, it is necessary to characterize thoroughly the tissue responses which could be harmful to the host but which could also lead to the device failure, facing both the biological and the engineering perspectives.

After the surgical implantation of any medical device in the body, several biological processes occur, from protein adsorption on the material surface to inflammation and scar formation around the device. These are comprehended in the foreign body reaction (FBR) (Corradetti, 2017). The tissue reaction also occurs to heal the damage caused by the implantation of a foreign body in the tissue. A difference must be noted between the normal wound healing process after a tissue injury and the process after a device implantation. The objective of wound healing after tissue damage is to heal clean incisions in which wound edges have been approximated by surgical sutures. If this is not possible, scar tissue is formed to fill the damaged tissue and the reactive process will be solved. However, after a material implantation, despite a healing process is also activated to repair the damage, complete tissue remodeling will not happen because the implant constitutes a physical impediment. Therefore, a capsule or scar tissue appears around the implant, as the

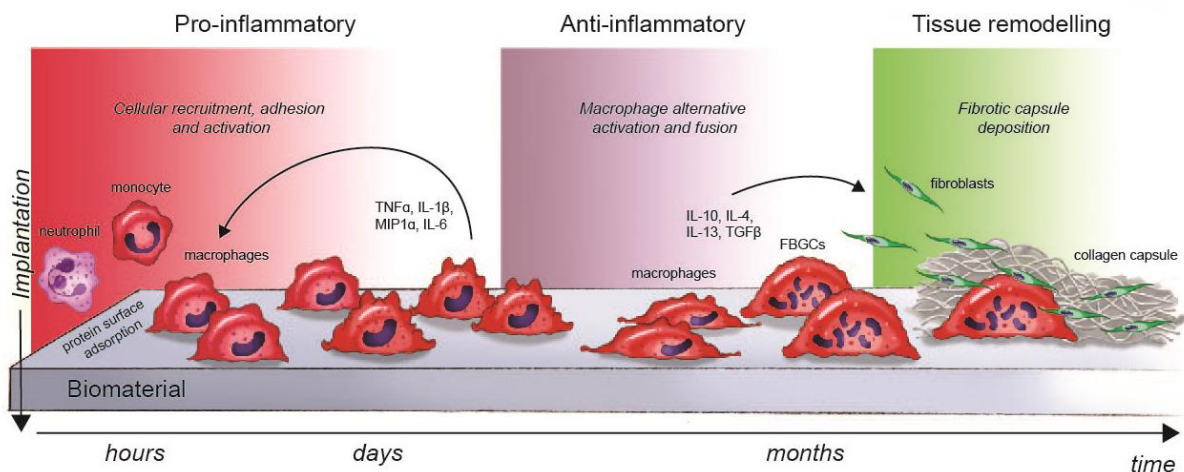


Figure 6. Foreign body reaction following biomaterial implantation. Proteins from serum adsorb to the material surface and inflammatory cells such as neutrophils and monocytes/macrophages infiltrate in response to tissue damage. Macrophages are initially classical activated and secrete pro-inflammatory mediators, which stimulate additional cellular recruitment and activation. After several days, macrophages polarize towards an anti-inflammatory and pro-healing phenotype and release anti-inflammatory and tissue remodeling factors. At final stages, macrophages fuse into foreign body giant cells (FBGCs) and recruit fibroblasts, which generate a fibrotic capsule around the biomaterial.

reconstitution of damaged tissue cannot completely occur. The amount of tissue formed is related to the extension of tissue damage and the material area.

Specific material characteristics (e.g., shape, size, physical and chemical properties) and particularities of different organs and tissues determine the overall FBR in each case (Boddupalli et al., 2016). Nonetheless, the general sequence of events (Fig. 6) following implantation of a device is described in detail in the following sections.

2.1.1 Acute inflammation and protein adsorption

Several molecular and cellular mechanisms are activated after the implantation of any device in response to the surgical damage. These are mediated by the innate immune system to restore the tissue homeostasis (Janeway et al., 2001). Rapidly after the injury, the damage to the blood vessels let fluid, plasma proteins and blood cells into the tissue and activation of acute inflammatory response occurs, with infiltration of leucocytes and macrophages. Initially, inflammation serves to contain possible infectious or injurious agents. Besides, acute inflammation will stimulate following mechanisms to heal and reconstitute the injured tissue by native parenchymal cells, fibroblastic scar tissue or a combination of both.

The implantation procedure cause coagulation around the implant, initiated by blood coagulation pathways, i.e., platelet, fibrinogen and complement cascades. Clot formation on the material surface is induced by the Vroman effect (Vroman et al., 1985, 1980), which regulates the early changes in protein adsorption to the material surface, saturating it with a protein layer within seconds to minutes after implantation (Kenneth Ward, 2008), mainly composed of albumin, fibrinogen, complement, fibronectin, integrins and others. The Vroman effect depends on chemical composition, roughness and shape of the material and the protein composition of the tissue implanted (Vroman, 1988). It has been of great interest in the last years (Geelhood et al., 2007; Hirsh et al., 2013; Kim, 2002; Mohan et al., 2017) because when infiltrating cells approach the material surface, they do not actually interact with the molecular structure of the material itself but with the adsorbed protein layer (Latour, 2008). This first cellular contact would determine the mechanisms initiated by the first interacting cells with the material and, in turn, determines the biocompatibility and the FBR to the implanted device (Hirsh et al., 2013; Vroman et al., 1985).

The adsorbed proteins and cells present from minutes to hours after implantation are considered as a provisional matrix and they initiate the following resolution,

reorganization and repair processes in the FBR. In fact, this provisional matrix can be seen as a natural and biodegradable sustained release system of several inflammatory and wound healing mediators (cytokines, chemokines and growth factors) (Baldwin and Hunt, 2008; Luttikhuisen et al., 2006). Considering the critical role that adsorbed layers have in the modulation of the acute inflammation and subsequent FBR, different studies have focused in the modulation of the FBR by means of protein coatings on implanted devices (Balaji et al., 2015; Geelhood et al., 2007; Young et al., 2017).

Protein mediators present in the provisional matrix regulate the acute inflammatory response, which usually is of short duration (from minutes to hours or days) and depends on the surgical injury and the origin and size of the biomaterial. The most studied molecular mediators that regulate this inflammatory phase and the attraction and activation of neutrophils and macrophages to the injury site are tumor necrosis factor alpha (TNF α), interleukin 1 β (IL-1 β), platelet-derived growth factor (PDGF), fibroblast growth factor (FGF) and transforming growth factor beta (TGF β) and proteins from the complement and the coagulation systems (Hu et al., 2001; Luttikhuisen et al., 2006).

Neutrophils and other polymorphonuclear cells are the first to infiltrate the damaged tissue, predominate during the first days after implantation (McDonald et al., 2010) and are subsequently substituted by monocytes/macrophages (Lawrence and Gilroy, 2007; Martin and Leibovich, 2005). This cell replacement is mainly due to the short life of neutrophils and its rapid chemoattraction, while monocytes/macrophages are very long-lived in tissue (up to months) and their chemoattractive signals last longer (Lech and Anders, 2013). Both neutrophils and macrophages are phagocytic cells and clean cellular debris, damaged tissue and try to eliminate the foreign body. However, the elimination of the foreign body may or may not occur depending on the type and size of the biomaterials. If it is not possible to degrade and eliminate the foreign body, only recognition and cellular attachment occur. This will not lead to engulfment of the foreign body but to the extracellular release of products in order to degrade the biomaterial. Thus, the degree of acute inflammatory reaction depends on the type of biomaterial implanted and if it can be phagocytosed or not.

2.1.2 Chronic inflammation

The presence of monocytes/macrophages and lymphocytes together with blood vessels proliferation and connective tissue contributes to the chronic inflammatory phase.

While general chronic inflammation in toxicity and infectious situations is characterized by the presence of monocytes/macrophages and lymphocytes, the foreign body reaction to biomaterials is generally composed of monocytes/macrophages and foreign body giant cells (Kenneth Ward, 2008). The chronic inflammatory phase to biomaterials is usually of short duration and limited to the implant site. However, chronic inflammation may last longer if toxic products are released from the biomaterial or due to micromotions between the implant and the tissue.

Macrophages are the most critical cell type involved in the chronic inflammatory phase and the FBR to biomaterials, since they can release a vast range of products, from pro-inflammatory (e.g., IL-1 β , TNF α , reactive oxygen species) to anti-inflammatory (e.g., IL-10, IL-4) and tissue remodeling (e.g., TGF β , vascular endothelial growth factor A - VEGF-A, matrix metalloproteinase 9 - MMP9) factors (Klopffleisch, 2016). They can play different roles within the FBR, from phagocytosis of the foreign body and damaged tissue to the resolution of inflammation and stimulation of wound-healing and remodeling processes. Macrophage phenotype and function are heterogeneous, depending on the molecular and cellular environment. There are two major phenotypes that macrophages can display, defined as M1 and M2 *in vitro* (Kigerl et al., 2009; Tarique et al., 2015). M1 or pro-inflammatory macrophages are the first to appear after an injury, along with neutrophils. They are potent producers of inflammatory factors such as TNF α , IL-1 and reactive oxygen species to destroy the foreign material (Moore et al., 2015). After acute inflammation, M2 or pro-wound-healing macrophages become the predominant subtype, secreting anti-inflammatory cytokines such as interleukin 10 (IL-10) and pro-regeneration factors such as TGF β . Thus, it is hypothesized that a low ratio M1/M2 is needed to stimulate resolution of the inflammatory phase and to start the wound healing process. In the case of the FBR, if the implant can be degraded, M2 macrophages will recruit fibroblasts to continue with the remodeling and wound healing processes. On the contrary, if the device cannot be degraded – as usually occurs with medical and prosthetic devices – M2 macrophages will recruit fibroblasts to generate new matrix and fibrous capsule around the implant and will stimulate new vessels formation. Unlike in the normal wound healing process in which M1 and M2 macrophages are temporally separate, in the FBR to biomaterials both phenotypes are concurrently observed in the tissue-material interface (Moore and Kyriakides, 2015; Sussman et al., 2014).

Foreign-body giant cells (FBGCs) are typically found in the FBR to most biomaterials. FBGCs are fused macrophages intended to phagocytose the implant when individual macrophages are unable to do so. These multinucleated cells can have up to one hundred

nuclei (McNally and Anderson, 2011) and may persist in the tissue-implant interface, together with the fibrous encapsulation, for the lifetime of the implant. However, it is not known if these cells remain activated, releasing its lysosomal content to degrade the biomaterial or become quiescent (McNally and Anderson, 2011; Sheikh et al., 2015). The formation of FBGCs due to macrophage fusion seems to be IL-4 and IL-13-dependant (McNally et al., 1996), what suggests their presence is related to an anti-inflammatory and tissue remodeling environment.

2.1.3 Tissue remodeling phase

A hallmark of the healing inflammation during the FBR is the formation of granulation tissue around the biomaterial and the injury site. Fibroblasts, together with macrophages, are typically found within this newly formed tissue.

After the inflammatory phase, macrophages, by means of anti-inflammatory and tissue remodeling secreted factors (e.g., TGF β , PDGF), stimulate the recruitment of fibroblasts to mediate the matrix remodeling (Anderson et al., 2008; Wynn, 2013). Fibroblasts are active in synthesizing collagen, proteoglycans and fibronectin. All these components mediate the FBR to biomaterials, depending on the biomaterial type and topography and the amount of tissue damage (Bota et al., 2010; Veisoh et al., 2015). Due to high levels of TGF β released by M2 macrophages, a constant influx of fibroblasts and collagen deposition occurs. Moreover, myofibroblasts and fibrocytes (resident and circulating mesenchymal progenitor cells) may also have a role in the formation and maintenance of the fibrous capsule around implants (Abe et al., 2001; Bucala et al., 1994; Darby et al., 2014).

For the vast majority of biomaterials, the end-stage of the FBR is the formation of a fibrotic capsule around them. The intention of this encapsulation is, on the one hand, to reconstitute the damaged tissue and the organ structure and, on the other hand, to isolate the implant and localize the FBR. However, tissue characteristics may lead to different wound healing outcome. Thus, repair of the implant site can involve two distinct processes: tissue reconstitution with the same type of parenchymal cells or replacement by connective tissue, which is fibrous encapsulation. This dichotomy is based mainly in 1) the regenerative capacity of tissue cell type and the extent of the injury and 2) the persistence of the original extracellular matrix (ECM) after injury, which will favor normal tissue restitution. Related with the regenerative capacity, perfect tissue repair (i.e., without connective tissue deposition) is theoretically only possible in those tissues in which cells can regenerate themselves continuously during lifetime (e.g., liver, kidney, pancreas, smooth muscle,

epithelial cells). After an injury, while tissues with permanent cells (i.e., nerve tissue, cardiac muscle) will give rise to fibrosis with little normal tissue restitution, tissues with regenerative cells may undergo fibrosis or may undergo resolution of inflammation and restitution of natural tissue structure (Anderson et al., 2008).

In summary, implantation of a biomaterial in the body elicits a well-orchestrated process known as the FBR. Although this reaction shares most of the features of the wound healing process, some differences arise. In wound healing, resolution of inflammation and subsequent tissue remodeling lead to the restoration of the original tissue. In contrast, during the FBR there is no complete inflammatory resolution as macrophages are found on the material surface and it results in the encapsulation of the implant by fibrotic tissue (Anderson et al., 2008; Luttikhuisen et al., 2006). Therefore, the material has to be seen as an impediment to the normal wound healing process of damaged tissue and this is sometimes understood as a sign of rejection.

However, regarding prosthetics and regenerative medicine, this could have a negative or positive impact and different scenarios can be developed depending on material type and intended function (Klopfleisch, 2016). For some implants, such as breast implants, the fibrous encapsulation has a positive impact, since it markedly reduces the motion of the implant, stabilizing it within the tissue and reducing the chronic inflammation due to motion (Anderson and Jiang, 2017). On the contrary, FBR results in a severe problem with implants intended to interact with the tissue in which they are implanted (i.e., glucose sensors, drug delivery systems or electrodes). In that case, fibrous encapsulation may lead to functional failure of the implant, with negative consequences. Thus, a classification could be done regarding the intended function of the implants: those with an acute or temporal function (i.e., tissue regeneration), in which the material should be degradable and FBR should not be developed; 2) materials with a chronic supporting function (i.e. joint replacement), which should have excellent durability and embodiment of the implant could be positive, and 3) chronic implants intended to interact with the tissue (i.e., sensors, neural interfaces), which have to be durable and no encapsulation should occur to ensure its chronic functionality (Boddupalli et al., 2016).

2.2 Biocompatibility

Despite the progress achieved in biomaterial, polymer science and immunology fields to reduce the FBR, all known materials induce an FBR and the formation of a fibrous capsule once implanted in the human body (DiEgidio et al., 2014; Morais et al., 2010). Material origin, shape and properties have an important impact on the progression of the FBR.

Moreover, location within the body and the intended function of the device are also critical factors, as they determine the type and design of the implant. These factors are summarized in the next sections.

2.2.1 Material specificities

Ideally, in order to avoid rejection, modulate the inflammatory response and reduce the FBR, the implanted devices intended to interact with the tissue should be invisible to the host.

Based on their sources, biomaterials can be classified as naturally derived (i.e., ECM proteins, polysaccharides, decellularized matrices...) or artificial (i.e., polymers, metals...) biomaterials. Both types may induce different host reactions and are intended for different clinical applications (Sarkar et al., 2017).

Natural biomaterials derive from living organisms and its main advantage is that they may not produce toxicity problems (Ige et al., 2012). Besides, they could be bioactive, as they present specific protein binding sites and biochemical signals, so they can interact through cellular activities such as cell attachment, cell-cell communication and tissue regeneration (Lapidot et al., 2012). However, although they are considered biocompatible, they can still present problems of immunogenicity and contamination (Badylak and Gilbert, 2008). Moreover, they do not show a very long-term stability, which may result in mechanical failure and premature decomposition (Badylak and Gilbert, 2008). Natural biomaterials with biodegradable characteristics have many potential applications within tissue regeneration and wound healing fields (Nair and Laurencin, 2007).

However, for long-term applications more stable biomaterials are needed. Synthetic materials, such as polymers, may show less biocompatibility than naturally-derived biomaterials, but they are easy and less expensive to produce (Fattahi et al., 2014). Moreover, they offer the opportunity to control degradation rate, mechanical strength, porosity, microstructure and surface properties through different modifications.

Polymer chemistry can be modified to adjust functional aspects such as hydrophilicity, surface pore size, degradation rate and degradation released products. These modifications alter protein adsorption and, consequently, immune cell interaction and activation (Sheikh et al., 2015). For example, hydrophobic surfaces promote greater protein adsorption and cellular adhesion (Hezi-Yamit et al., 2009), because water is easily replaced from these surfaces by hydrophobic proteins (Sarkar et al., 2017). In contrast, hydrophilic surfaces show less monocyte adhesion and FBGC formation, although they

produce higher levels of cytokines and chemokines (Jones et al., 2007). On the other hand, biomaterials present multiple structures, from the molecular level (individual polymer chain form porous network) to the microscopic level (surface characteristics). Materials with small pore size present less area for protein adsorption and smaller capsule formation while larger porous size allows for more protein binding (Bota et al., 2010; Sussman et al., 2014). Moreover, aligned fibers also reduce capsule formation in comparison to non-aligned fibers (Cao et al., 2009). Modification of the chemical surface with proteins or specific peptide sequences also alter protein adsorption and the FBR (Balaji et al., 2015; Noorisafa et al., 2016; Pacelli et al., 2015). In addition, overall geometry and size of the implanted device also have a role in the FBR developed (Veisheh et al., 2015; Weyhe et al., 2015), as it will determine the ability of immune cells to phagocyte and degrade them.

In summary, both naturally-derived and synthetic biomaterials show different advantages, in which natural materials seem to be more biocompatible while synthetic allow for chemical and mechanical modifications (Boddupalli et al., 2016). Thus, a combination of both types of materials become essential to improve implant acceptance. Tissue specificities and clinical applications will finally determine the material used. Therefore, it is mandatory to dissect the specific cues in different tissues to know macrophages and fibroblasts phenotypes and modulate them.

2.2.2 Strategies to reduce the FBR

Ideally, implanted devices intended to interact with the surrounding tissue should be inert or non-recognizable by the body to avoid the host response. In addition, to choosing the appropriate biomaterial according to the intended medical function, host tissue and physical and chemical characteristics, different strategies such as surface modification, coatings, and local release systems have been proposed to improve the biocompatibility of implanted polymers and make them more similar to self-body molecules.

a) Surface modification by molecular adsorption

The most attractive method is the pre-adsorption of common biomolecules such as proteins, peptides, drugs or lipids onto the biomaterial surface to modulate cell signaling and the subsequent FBR.

Proteins are essential to regulate cell structure and function and to regenerate tissues and organs and the pre-adsorption of proteins (e.g., plasma proteins, ECM proteins) onto polymer surface has been widely studied to modulate the FBR (Balaji et al., 2015). Materials coated with plasma protein such as albumin and fibrinogen showed less platelet activation

and cell adhesion on its surface (Amiji et al., 1992; Chang et al., 1977; Mohan et al., 2017). In contrast, titanium implants intended for orthopedic and bone regeneration showed increased osseoprogenitor cell attachment and matrix deposition after plasma protein coating in vitro (Oughlis et al., 2016). Regarding ECM proteins, while laminin and vitronectin enhanced rat islet cells adhesion, fibronectin, collagen I, II and IV did not produce any significant effect in vitro (Chen et al., 2008).

b) Coatings

Polysaccharides as chitosan and heparin are used for surface coating to improve biocompatibility and also as drug delivery systems (Boehler et al., 2011; DiEgidio et al., 2014). Heparin is widely known for its anticoagulant properties and some studies have demonstrated better compatibility for heparin-coated materials than non-coated ones (Bayramoğlu et al., 2008; Cui and Schwendeman, 2007; Zhang et al., 2016). Further, chitosan has been widely used in polymer coatings, together with other hydrogels, for reducing clot formation and anti-bacterial properties. Several studies have reported an increase in cellular growth and tissue regeneration in chitosan-coated implants (Deng et al., 2017; Mighri et al., 2015; Yuan et al., 2008) and in chitosan-ECM proteins coated materials (Haipeng et al., 2000).

Most of the strategies cited above result in enhanced cellular adhesion and tissue regeneration. They may be promising for tissue regeneration and chronic supporting implants, but not be suitable options for devices intended to interact with the tissue. Enhanced cellular adhesion may not result in reduced FBR and capsule formation. Alike biomaterial choice, strategies to improve the biocompatibility of implanted devices should keep in mind the intended chronic function and the host tissue too. To address this issue, coatings with silk fibroin protein have shown a reduce cellular adhesion to different devices (Borkner et al., 2017; Can et al., 2016). However, the exact molecular mechanisms by which these strategies modulate and, indeed, reduce the implant encapsulation for long-term devices is unclear.

c) Local and systemic treatments

In addition to surface modifications and coatings, local drug release and systemic treatments can also be used to modulate the immune response to implanted materials (Boehler et al., 2011).

Bioactive molecules, such as cytokines and anti-inflammatory drugs, can be incorporated in the material surface, within hydrogel coatings or as a systemic therapy. To

extend the presence of these cues in the implanted area, localized delivery systems such as microspheres can be used, incorporated within the material (Norton et al., 2007, 2005). Molecules such as endothelial growth factor (EGF), FGF, VEGF or TGF β are responsible for adhesion, migration, proliferation and differentiation of the cells implicated in wound healing. Therefore, it has been suggested that releasing of these molecules from coatings could have an immunomodulatory effect during the FBR (Kastellorizios et al., 2015a; Norton et al., 2007). In the same vein, coating with nitric oxide (NO)-releasing layer has been another suggested strategy to modulate the immune response to reduce the FBR (Hetrick et al., 2007). However, other authors have pointed out the role of NO in wound healing, increasing the amount of tissue deposition around the implant (Kang et al., 2015).

Glucocorticoids, such as dexamethasone, have anti-inflammatory and immunosuppressive properties. They act through glucocorticoid receptor, inhibiting the phospholipase 2A (PLA2) and cyclooxygenases (COX1 and COX2), thus reducing the production of pro-inflammatory molecules (e.g., leukotrienes, prostaglandins) (Cain and Cidlowski, 2017). Glucocorticoid treatment results in less infiltrating inflammatory cells, less capillary permeability and reduced fibroblast proliferation (Coutinho and Chapman, 2011). However, it also reduces the secretion of VEGF, downregulating angiogenesis and potentially inhibiting wound healing. Studies with dexamethasone-loaded microparticles implanted in the subcutaneous space have reported a reduction in inflammatory cells and fibroblasts infiltration and less collagen deposition up to 1 month (Dang et al., 2011; Kastellorizios et al., 2015b). Similar results were reported using subcutaneous polyimide implants soaked with dexamethasone, in which a reduced inflammatory response was observed both *in vitro* and *in vivo* (Heo et al., 2016a).

In conclusion, surface coatings can contribute to improving biocompatibility by improving cellular adhesion to implants intended to stimulate tissue regeneration. Different immune modulators can reduce the inflammatory response or the wound healing process. Strategies developed nowadays try to polarize the inflammatory environment to a more M2 and tissue remodeling phenotype in order to resolve inflammation and wound healing. Despite the promising results, it is mandatory to evaluate these strategies in an *in vivo* implant, also considering the intended function of specific medical devices. Thus, surface modifications and drug-release coatings should also try to repulse cell adhesion and reduce the FBR for implants with long-term applications (Balaji et al., 2015).

THE FBR TO INTERFACES WITH THE NERVOUS SYSTEM

Regarding neuroprostheses, the main objective of interfaces implanted within the nervous system is to stimulate and record the information from neurons and nerve fibers. The potential usability of neural interfaces relies on its performance as chronically implanted devices, that depends, at least in part, on the FBR. In fact, several studies have reported a decrease in signal recording and electrode stability over time following electrode implantation (Davis et al., 2016; Gunasekera et al., 2015; Kozai et al., 2015). As opposed to the PNS, where the electrode interface axons, in the CNS there are neuronal somas close to the interface. The position of neuronal soma with respect to the implanted electrode determines the strength and the quality of bioelectric signal recordings. In fact, there is a maximal distance between neuronal soma and electrode (i.e. 50-100 μm) to ensure good quality signal recordings (Henze et al., 2000; Rosenthal, 1972). Thus, tissue encapsulation and neuronal death after electrode implantation reduce signal recordings. As it occurs in other tissues, the tissue reaction and FBR after the implantation of a device varies between peripheral nerves and CNS. One of the main differences is regarding the cells implicated in the tissue response.

3.1 CNS interfaces and the FBR

After an injury to the CNS, astrocytes become reactive, enlarge their projections, proliferate and increase matrix production. Astrocytes are the responsible for scar formation around the injury or the device implanted, in order to isolate the implant and the subsequent inflammatory response from healthy tissue (Seymour and Kipke, 2007). Microglial cells change their appearance from the quiescent inactive ramified state after an injury, becoming reactive amoeboid cells. Principally, both cell types act as cytotoxic cells killing pathogenic organisms or as phagocytes of damaged tissue and foreign materials by upregulation of production and secretion of lytic enzymes. Although CNS is considered as an immune-privileged site, the BBB is damaged after an injury and blood-derived immune cells enter the brain parenchyma due to platelet and cytokines recruitment. Once inside, monocytes/macrophages are indistinguishable from microglial cells and seem to perform the same functions (Polikov et al., 2005). Microglial cells release several factors involved in the immune response, such as macrophage chemoattractant protein 1 (MCP1), IL-1, IL-6 and $\text{TNF}\alpha$ (Smith et al., 2011). Besides, they release not only factors to ensure neuronal survival as nerve growth factor (NGF), brain-derived neurotrophic factor (BDNF) and neurotrophin 3 (NT-3) but can also produce various cytotoxic and neurotoxic factors which could lead to neuronal death (Hanisch and Kettenmann, 2007). As in the FBR in other tissues, it has been suggested that non-degradable materials lead to a “frustrated wound

healing” state, in which macrophages are unable to remove the foreign body and therefore remain activated, causing more tissue damage (Polikov et al., 2005).

Tissue reaction after penetrating electrodes implanted in the brain has been well studied (Polikov et al., 2005) and is similar to the fibrotic encapsulation of implanted devices in other soft tissues. The mechanical damage of insertion causes a first injury to the tissue now occupied by the electrode. A first inflammatory response is observed with activated microglia and infiltration of blood-derived immune cells. Once acute inflammation declines, the chronic inflammatory response occurs, characterized by reactive astrocytes and activated microglia at the surface of the device (Polikov et al., 2005; Xie et al., 2014). This chronic inflammation is maintained as long as the device remains within the brain tissue, noted by the continued presence of microglial cells in the surface of the device (Hascup et al., 2009; Szarowski et al., 2003). The most common feature of the chronic CNS response to implanted electrodes is the encapsulation by glial cells, forming the so-called “glial scar” (Biran et al., 2005; Seymour and Kipke, 2007). While soft tissue encapsulation involves other types of cells and matrix production, astrocytes in the CNS are the main cell population involved. The glial scar isolates the electrode from the neurons to interface, increasing the distance and the impedance. In addition, neuronal loss also occurs around the electrode (Biran et al., 2005; Nolte et al., 2015), contributing to progressive decay in signal recording and electrode function (McCreery et al., 2016).

3.2 PNS interfaces and the FBR

In contrast, the PNS does not have a specific immune-cell population, being scarce the resident macrophages (Müller et al., 2010; Vass et al., 1993). After a peripheral nerve injury, immune blood cells infiltrate the injury site and are the main responsible for the reparative process in peripheral nerves (Bosse, 2012; Gaudet et al., 2011). However, the FBR to peripheral nerve electrodes has been less studied. This is due to, mostly, the wide range of electrode designs available, summarized in section 1.3. Different studies have focused on the tissue response to implanted multielectrode arrays (Christensen et al., 2015, 2014), extraneural (Leventhal et al., 2006), longitudinal (Lago et al., 2007) and transversal (Badia et al., 2011b) electrodes. However, the description of the FBR in these studies was not as complete as in those for subcutaneous implants and even of brain electrode implants.

Recently, a more detailed characterization of the FBR to implanted transversal electrodes has been done, correlating biological features with the functional performance (Wurth et al., 2017). One of the main conclusions of previous works regarding nerve interfaces is that improvement in the long-term functional performance is still needed. For

that, it is mandatory to know the progression of the FBR in peripheral nerves in order to develop strategies to reduce this response and to improve the chronic stability of implanted electrodes.

3.3 Strategies to reduce the FBR to neural interfaces

Similar to implanted devices in other tissues, many efforts have been made in the development of neural interfaces that would reduce local inflammation and FBR. As previously described, surface properties of implanted electrodes are critical factors for tissue capsule formation (Fattahi et al., 2014; Kim and Romero-Ortega, 2012; Lacour et al., 2016). In a neural electrode, both the isolating-supporting material and the active sites material may contribute to the FBR development.

The FBR leads to the formation of scar tissue around the implanted electrode, but also may degrade the active sites, contributing to the increase of impedance and electrode failure. Active sites are fabricated from a variety of conductive materials, including gold, platinum, platinum-iridium or iridium oxide deposited over isolating non-conductive substrates (Merrill et al., 2005). Although these metals are considered safe, biocompatible and corrosion-resistive materials, the release of ions due to hydrolyzation of metals can affect tissue response after chronic implantation. On the other hand, although impedance could be reduced by increasing the area of the active sites, this is not always possible according to the implant site. If the active site area increases, so would do the stimulated/recorded area of the nerve and the selectivity will decrease. Coating the active sites with conducting polymers or carbon nanotubes may allow for smaller active sites but with better electrochemical characteristics (i.e., low impedance, safe charge injection capacity and high charge storage density). Conducting polymers such as polypyrrole (PPy), polythiophene (PTh) and poly-(3,4-ethylenedioxythiophene) (PEDOT) have been used to improve electrode-tissue communication in nerve electrodes (Green et al., 2008). These coatings are non-cytotoxic (Asplund et al., 2009) and improve the electrochemical characteristics compared to bare active sites (Heo et al., 2016b; Jan et al., 2009).

Another critical parameter is the mechanical mismatch (difference in elasticity and stiffness) between the device implanted and the host tissue, usually evaluated with the Young's modulus (YM). The YM of nerve tissue is around 0.45MPa, while current polymers used range from 1MPa to 8GPa and silicon is around 150GPa (Fekete and Pongrácz, 2017; Tyler et al., 2015). Since polymers are typically soft materials, it is hypothesized that coated devices or polymers with lower Young's modulus and less mechanical mismatch would reduce the inflammatory response and the FBR (H. C. Lee et al., 2017). Several polymer

substrates have been tested to reduce the mechanical mismatch between the electrode surface and the neural tissue (Fekete and Pongrácz, 2017):

- *Silicone or polydimethylsiloxane (PDMS)*: is one of the most used materials for polymer implants (Donalson, 1989; Lawrence et al., 2004). Although there are different PDMS types, all have a backbone of siloxanes in common. Methyl-groups can be replaced by others (e.g., nitrogen, vinyl), changing the material properties drastically. All silicones have a high permeability for oxygen and water vapor but are impermeable to ions, which make them suitable for isolating coat for electrical implants. Besides, it has a tissue-like YM close to 1 MPa. As they are FDA approved, there are many clinical products and applications (Gebelein and Carraher, 2007).
- *Polyimide (PI)*: represents a class of polymer of imide monomers. It is a good candidate for flexible neural implants due to its good chemical and mechanical durability, low water uptake and low hydrolysis, electrical insulation properties and its processing with standard cleanroom equipment (Rubehn and Stieglitz, 2010). Studies have shown good biocompatibility for PI (Stieglitz et al., 2000) and good stability over long-term studies *in vitro* (Rubehn and Stieglitz, 2010). However, it has a high YM around 8500 MPa and is still not FDA approved. Different PI-based designs have been developed for PNS (Boretius et al., 2010; Lago et al., 2007, 2005; Rodriguez et al., 2000; Stieglitz, 2001) and CNS applications (Rousche et al., 2001; Stieglitz et al., 1997a).
- *Parylene C (ParC)*: is the most promising and used type of poly(p-xylylene) polymers in microelectromechanical and biomedical systems (Kim and Meng, 2016). Currently, it is mainly used as a biocompatible coating for CNS interfaces (Schmidt et al., 1988; Seymour and Kipke, 2007), although it is being adopted for other applications due to its biocompatibility and chemical inertness (P.-C. Chang et al., 2007; Lecomte et al., 2017). However, since it delaminates easier than other polymer substrates due to its low tensile strength, its chronic use as substrate is still limited (Fekete and Pongrácz, 2017). Regarding neural interfaces, its mechanical properties could allow for an improved manufacturing process of neural electrodes (Lecomte et al., 2017; Mueller et al., 2016). Besides, Parylene C is more hydrophilic than polyimide, showing higher contact angles (T. Y. Chang et al., 2007), which could be interesting in terms of FBR control. Since it is an FDA approved material, further research is needed to determine its suitability as neural electrodes substrate.

Biological coatings have also been proposed to modulate the tissue response to neural electrodes. Neural probes coated with biomolecules such as laminin (Bossi et al., 2010) or

fibronectin (Cui et al., 2001) showed promising results *in vitro*. Fibronectin-coated brain probes had a positive effect on recording during the first week of implant, although no longer effect was observed after three weeks (Cui et al., 2003). In fact, *in vitro* studies demonstrated better adhesion of glial rat cells to coated probes while neuroblastoma cells did not show any preference (Cui et al., 2001). These results suggest that chemical modifications of the surface may improve electrode performance, and also the biocompatibility (i.e., cell attachment) but do not reduce the FBR (i.e., glial scar formation). Some other coatings as polyethylene glycol (PEG) or silk fibroin (SF) showed improved material-tissue mismatching and can also be used as drug delivery systems to modulate the local FBR (Lecomte et al., 2015; Metallo and Trimmer, 2015).

The search of drug delivery systems was motivated since it was reported that systemic administration of anti-inflammatory glucocorticoids reduced the number of glial cells forming the glial scar around penetrating cortical implants (Spataro et al., 2005). Since then, strategies to locally deliver such agents have been proposed (Willerth and Sakiyama-Elbert, 2007). Indeed, dexamethasone-coating neural probes implanted in brain demonstrated to efficiently reduce the inflammatory response for one week while the number of reactive astrocytes was reduced for four weeks (Zhong and Bellamkonda, 2007). Furthermore, coatings of dexamethasone-encapsulated nanoparticles seemed also able to reduce glial scar and electrode impedance after 14 and 46 days of implant (Kim and Martin, 2006; Mercanzini et al., 2010). Such system could be combined with conductive coatings such as PEDOT to improve not only the inflammatory reaction but also the electrochemical characteristics of the electrodes (Boehler et al., 2017; Park et al., 2015; Zhong et al., 2017). All these local delivery strategies have been mainly developed for CNS implants. Regarding PNS interfaces, a recent study with a dexamethasone eluting regenerative electrode indicated a reduction of scar tissue deposition (FitzGerald, 2016). Dexamethasone or glucocorticoids in the PNS have been mainly used for nerve blockages or to improve nerve regeneration through the expression of regeneration-associated genes such as growth associated protein 43 (GAP43) (Albrecht et al., 2015; Wang et al., 2015; Yao and Kiyama, 1995; Zhang et al., 2016). Targeting molecules involved in inflammation or the FBR in other tissues could be a suitable option also to modulate the FBR in the PNS. For example, it has been shown that TNF α neutralizing antibodies could have a positive effect in reducing the early tissue reaction around the nerve after cuff electrode implantation (Vince et al., 2005), although there is no evidence if it affects electrode performance.

In summary, although there are different strategies to reduce the FBR to neural implants, still further research is needed to develop feasible options to reduce this response

in peripheral nerves and to improve the long-term performance of peripheral nerve interfaces.

OBJECTIVES

Intraneural electrodes are a key element to bidirectionally interconnect a bionic prosthetic limb with the PNS due to its high selectivity of stimulation with a relatively low invasiveness. However, any device implanted in the body induces the development of a foreign body reaction (FBR) that results in the encapsulation and isolation of the electrode from the nervous tissue, thus decreasing its functionality after chronic implantation. Strategies to reduce and avoid the FBR have been attempted for improving the chronic use of nerve electrodes, from different substrate polymers to molecule-releasing coatings or pharmacological treatments. The main objective of this thesis is to improve the long-term functionality of chronic implanted intraneural electrodes by means of improving the knowledge about the FBR to intraneural devices. In the mainframe of the European project NEBIAS, a new polymer-based interface has been developed and tested *in vivo*.

To accomplish this general objective, specific objectives have been established:

1. To study the biocompatibility and suitability of the Parylene C polymer as a substrate of neural electrodes.
2. To characterize the progression of the FBR developed around longitudinal polyimide and Parylene C devices implanted in peripheral nerves.
3. To identify the cellular and molecular mechanisms involved in the FBR to both materials used as a substrate for electrodes in peripheral nerves.
4. To evaluate different pharmacological treatments to reduce the FBR in peripheral nerves.
5. To evaluate whether pharmacological treatments can improve the long-term functionality of intraneural interfaces in terms of chronic stimulation and recording capabilities.







CHAPTER 1: *IN VIVO* BIOCOMPATIBILITY AND FUNCTIONALITY OF A NEW PARYLENE C-BASED TRANSVERSAL INTRANEURAL ELECTRODE

In this chapter, the biocompatibility and the chronic functionality of a new intraneural interface made in Parylene C have been evaluated. Nerve damage, nerve function and stimulation properties of the new electrode have been analyzed after chronic implantation in rat sciatic nerve.

Parylene C is a polymer that has been widely used as an insulator for brain interfaces (Hassler et al., 2010; Seymour and Kipke, 2007) and other medical devices (Kim and Meng, 2016). It is an FDA approved material for different clinical applications, and different studies have shown its good biocompatible characteristics both in vitro (Chang et al., 2007) and in vivo (Lecomte et al., 2017; Winslow et al., 2010) models. Regarding intraneural interfaces, its mechanical properties offer the possibility, together with a new double-sided fabrication process (Mueller et al., 2016), to integrate several metal contacts in both sides of the polymer substrate, thus reducing the total thickness of the electrode in comparison to the previous transversal design made in polyimide, the TIME electrode (Boretius et al., 2010).

This study has been published in collaboration with Matthias Mueller and Thomas Stieglitz, from the Laboratory for Biomedical Microtechnology, Department of Microsystems Engineering (IMTEK) from the University of Freiburg, Germany. They are responsible for the fabrication and electrode in vitro characterization, studies that are part of the Ph.D. thesis of Matthias Mueller.

Rapid prototyping of flexible intrafascicular electrode arrays by picosecond laser structuring

Matthias Mueller¹ , Natalia de la Oliva^{2,3} , Jaume del Valle^{2,3} ,
Ignacio Delgado-Martínez^{2,3} , Xavier Navarro^{2,3}  and Thomas Stieglitz¹ 

¹ Laboratory for Biomedical Microtechnology, Department of Microsystems Engineering (IMTEK), University of Freiburg, Georges-Koehler-Allee 102, D-79110 Freiburg, Germany

² Group of Neuroplasticity and Regeneration, Institute of Neurosciences, Department of Cell Biology, - Physiology and Immunology, Universitat Autònoma de Barcelona, Edifici M, Avinguade de Can Domènech, 08193 Bellaterra, Spain

³ Centro de Investigación Biomédica en Red sobre Enfermedades Neurodegenerativas (CIBERNED), 08193 Bellaterra, Spain

E-mail: matthias.mueller@imtek.uni-freiburg.de

Received 10 March 2017, revised 22 May 2017

Accepted for publication 11 July 2017

Published 23 November 2017




Abstract

Objective. Interfacing the peripheral nervous system can be performed with a large variety of electrode arrays. However, stimulating and recording a nerve while having a reasonable amount of channels limits the number of available systems. Translational research towards human clinical trial requires device safety and biocompatibility but would benefit from design flexibility in the development process to individualize probes. **Approach.** We selected established medical grade implant materials like precious metals and Parylene C to develop a rapid prototyping process for novel intrafascicular electrode arrays using a picosecond laser structuring. A design for a rodent animal model was developed in conjunction with an intrafascicular implantation strategy. Electrode characterization and optimization was performed first in saline solution *in vitro* before performance and biocompatibility were validated in sciatic nerves of rats in chronic implantation. **Main results.** The novel fabrication process proved to be suitable for prototyping and building intrafascicular electrode arrays. Electrochemical properties of the electrode sites were enhanced and tested for long-term stability. Chronic implantation in the sciatic nerve of rats showed good biocompatibility, selectivity and stable stimulation thresholds. **Significance.** Established medical grade materials can be used for intrafascicular nerve electrode arrays when laser structuring defines structure size in the micro-scale. Design flexibility reduces re-design cycle time and material certificates are beneficial support for safety studies on the way to clinical trials.

Keywords: peripheral nerve, interface, electrode, Parylene C, laser fabrication, neural prostheses

(Some figures may appear in colour only in the online journal)

 Original content from this work may be used under the terms of the [Creative Commons Attribution 3.0 licence](https://creativecommons.org/licenses/by/3.0/). Any further distribution of this work must maintain attribution to the author(s) and the title of the work, journal citation and DOI.

1. Introduction

Ongoing research in biomedical engineering gave rise to a multitude of implantable electrode arrays and their numerous applications. A classification of these electrode arrays can be done by their intended implantation site or the mechanical properties of the substrate. The first approach leads to surface, extraneural and penetrating electrode arrays [1]. The second approach further classifies into flexible and non-flexible arrays [2]. Well known examples for flexible substrates are silicone rubber and polyimide, non-flexible substrates are usually fabricated from silicon wafers. Silicone rubbers have traditionally been used as encapsulants and substrates in precision-machined devices, while they are now also used as substrate materials for laser fabricated electrode arrays [3, 4]. Polyimides were investigated for application in cochlea implants and were later on used in implantable, high-density electrode arrays due to their compatibility with standard microelectromechanical (MEMS) processes [5, 6]. Silicon based microelectrodes have been in application since 1969, mainly used for measurements in the brain cortex [7].

Concerning flexible electrode arrays, silicone rubber offers large stretchability and a high degree of freedom for the designer, if used with laser fabrication of metal foils. However, this leads to relative thick arrays of several 100 μm which are mainly used for surface applications [4] or as a carrier for stiffer penetrating elements [8]. Cleanroom fabricated polyimide electrodes are only minimally stretchable but offer a high degree of flexibility, while offering a thickness of about 10 μm [9, 10]. A drawback of this technology is the need for several lithography masks and sophisticated process technology, which contradicts the need for multiple design iterations during development of the electrode arrays. Moreover, there is no medical-grade polyimide available that has records for long-term human implantation. During the recent years, research in ultra-flexible electrodes based on biocompatible substrate materials has been conducted. However, flexibility goes hand in hand with utilizing very thin substrate layers and thus limited application *in vivo* due to low mechanical stability [11, 12]. The intended application has to be taken into consideration, while choosing the right type of electrode array and the right fabrication method.

This study proceeds with the development of intraneural electrode arrays for peripheral nerves. Ultrashort pulse lasers in the picosecond (ps) and femtosecond (fs) range offer new possibilities in high-resolution metal cutting and subsequent thinning due to cold ablation [13]. This allows to combine the advantages of laser fabricated and lithography based electrode arrays. Both, the variability in the design process and the tenuity of the substrate, are necessary to have a feasible implantation procedure in a peripheral nerve. A comparable electrode array, called the TIME electrode (transverse intra-fascicular multichannel electrode), has been fabricated in a lithographic process with polyimide and implanted in human to treat phantom limb pain and to restore sensory feedback in prosthesis control [14, 15]. Due to the absence of a double-sided fabrication process the electrodes were folded, which resulted in an arrow shaped structure of about 20 μm thickness. Next to increasing the integration density, the transversal

penetration of the nerve was simplified. Two pilot studies have been carried out to gain first insight in the new technology and limitations of the utilization of Parylene C in combination with ablated metal foils [16, 17]

Parylene C, in contrast to other thin film polymers used as substrates, has the advantage of being classified for chronic implantation by the United States Pharmacopoeia (USP class VI). However, due to a relatively low Young's modulus of 2.7 GPa small filament electrodes cannot withstand much force. This challenge has been addressed by coating biodegradable layers like silk or maltose to enhance the robustness, which is, however, not suitable for intraneural electrodes due to an increase in thickness of several 100 μm [18, 19]. Thus, in this work we propose alternatively to increase the stiffness with the embedded metal layer as well as adding a guidance directly to the array. To address the limited capability of plain metal to transfer charge, the possibilities to increase the active surface by laser hatching as well as the electrochemical deposition of nanostructures were investigated [20]. Ultrashort pulse lasers offer the possibility to structure a metal surface by arranging sub-micron ripples, which develop on a material due to surface plasmon interference (SPI) of the incident laser light, to form interference patterns [21, 22]. All these research items were integrated in a novel fabrication process, electro-chemically investigated *in vitro* and transferred into rodent animal models for acute and chronic *in vivo* experiments.

2. Materials and methods

2.1. Electrode fabrication

2.1.1. Design considerations. Whereas the initial electrode design was inspired by the TIME electrodes, the task of rethinking the implantation strategy arose due to deviating material parameters. Thin film polyimide electrodes like LIFE and TIME have a thickness of roughly 10 μm and can thus be folded, forming an arrow-like tip which can incorporate a needle with suture, to be easily pulled through a nerve [23, 24]. Parylene C based ps laser fabricated intraneural electrodes cannot be fabricated this thin due to the lower Young's modulus compared to polyimide as well as due to use of a metal foil instead of evaporated metal layers. The general thickness of these electrodes imposes the necessity of changing the implantation strategy. Due to the design freedom the tip of the electrode can be extended to form an elongation to be used as suture material (figure 1(A)). Inspired by the TIME electrodes, two electrode arrays can be fabricated at the same time and stay connected via a bridge of Parylene C. After placing a loop of medical suture inside the electrodes can be folded alongside the symmetric axis to form an arrow-like structure. Along the sharpened tip, the two single-sided electrodes can be pulled through the nerve, forming a double-sided electrode array (figure 1(B)). The possibility to freely change the thickness and layout of the metal foil with a ps laser allows to terminate the electrode tip in a thin metal beam. In contrast to thin film metals a conductive wire can be resistance welded on top of it. In this case a medical grade MP35N wire is sharpened and resistance welded to the tip, replacing the demand for a surgical needle (figure 1(C)).

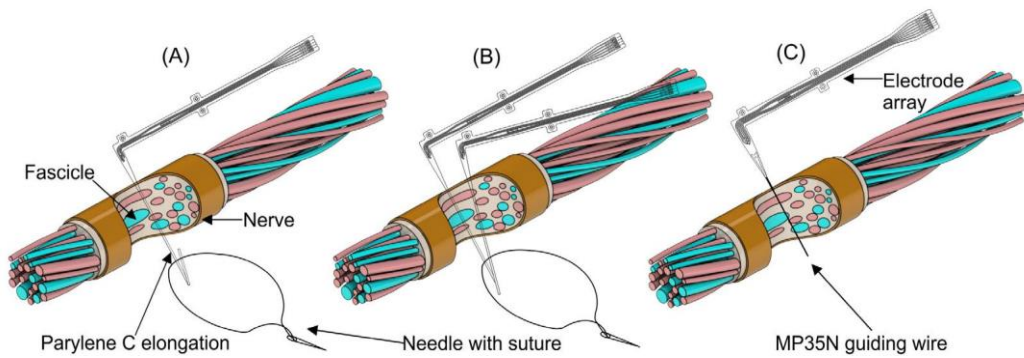


Figure 1. Three different concepts for the transversal implantation strategy of Parylene C based ps laser structured intrafascicular electrode arrays. (A) Elongated Parylene C tip which can be used as suture material to pull the electrode through the nerve. (B) Two single-sided electrodes, which are folded during assembly, form an arrow-like tip that incorporates a needle with fixed suture. (C) The electrode tip terminates in thin and narrow metal fiber on which a sharpened MP35N wire is resistance welded. The wire acts as a needle that guides the electrode through the nerve.

2.1.2. Fabrication process. All intrafascicular electrode arrays were fabricated with a passively mode-locked Nd:YVO4 picosecond laser (Rapid 10, Coherent Inc., Santa Clara, CA). Through internal frequency tripling the native wavelength is converted to 355 nm. Movement and focusing of the 12 μm laser spot is implemented by a two axis deflection unit with an integrated f-theta lens (Superscan II, Raylase AG, Wesslingen, Germany) inside a process chamber.

Two types of intrafascicular electrode arrays were fabricated in this setup; electrode arrays with a silicone rubber interlayer in a single- and double-sided configuration (figure 2 left column) and electrodes that only consist out of Parylene C and a metal foil electrodes (figure 2 right column). All fabrication routes started with the lamination of adhesive poly-imide tape (No. 5413, 3M Co., St.Paul, MN) on a 2" by 2" mechanical carrier (96% pure alumina ceramic substrate) (figure 2(1)). The tape was used as a release layer at the end of the fabrication process.

For single- and double-sided electrodes the deviations in the individual routes are minor. Making use of the ‘Gorham process’ [25] a 10 μm layer of Parylene C (Dimer DPX-C, Coater PDS 2010, Speciality Coating Systems Inc., Indianapolis, IN) was deposited on top of the carrier structure (figure 2(2, left)). To offer adhesion for the metal foil a 10 μm thick layer of n-heptane-diluted MED-1000 silicone adhesive (NuSil Technology LLC, Carpinteria, CA) was spin-coated on top of the Parylene C (figure 2(3, left)). With 5 min of curing, if needed, the structures that later on form the backside contacts were lasered and ablated (figure 2(4, left)). Afterwards a 25 μm thick metal foil (Pt90/Ir10, Goodfellow Cambridge Ltd, Huntington, United Kingdom) was laminated (figure 2(5, left)). Applying a hatching pattern with the ps laser allowed to thin down the metal to 10 μm at desired areas before patterning the interconnection sites, conducting tracks and electrodes (figures 2(6, left) and (7, left)). Excess material was peeled off and the remaining electrode array again covered with Parylene C (figures 2(8, left) and (9, left)). Afterwards laser hatching was used to open as well as roughen the electrode sites and the contact pads for MicroFlex Interconnects and resistance welding (figure 2(10, left)) [26]. At his step some electrodes were also subjected to structured laser interference patterning (SLIP), by continuously hatching across

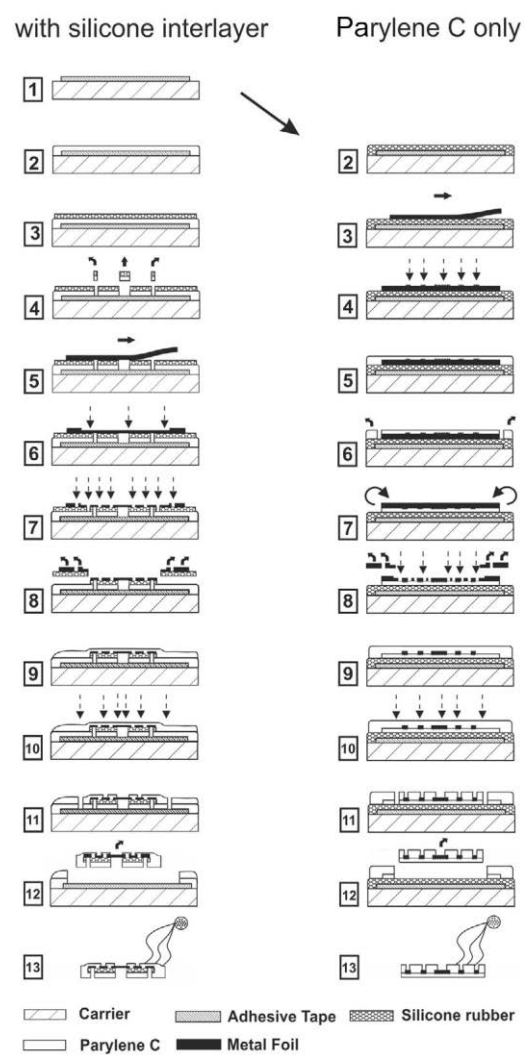


Figure 2. Fabrication process of Parylene C based intrafascicular electrode arrays for peripheral nerves. Left: fabrication process for single- or double-sided arrays with silicone rubber interlayer. Right: fabrication process for arrays that consist only of metal and Parylene C.

the electrode surface with 0°, 4° and 135° angled lines of 8 μm spacing, at the minimal possible power level necessary for cold ablation [21]. The intrafascicular electrode arrays

were released by laser cutting the outer perimeters through the Parylene C and subsequent peeling from the release layer (figures 2(11, left) and (12, left)).

Electrode arrays consisting of only metal and Parylene C follow an altered fabrication route (all following steps: figure 2 right column). A 100 μm thick MED-1000 silicone adhesive was spin-coated as a release layer (figure 2(2, right)). After the layer was cured for a week to decrease the adhesion properties a 25 μm thick metal foil (Pt90/Ir10) was laminated on top and transferred to the ps laser (figure 2(3, right)). There, a mirrored version of the electrode array design was hatched in the metal foil before coating it with a 10 μm thick layer of Parylene C (figures 2(4, right) and (5, right)). Next, the boundaries of the metal foil were laser cut and flipped with the Parylene C facing downwards (figures 2(6, right) and (7, right)). By applying a hatch pattern the metal layer was thinned down to 10 μm , before transferring the electrode the design by ablating the metal not completely through to the Parylene C (figure 2(8, right)). The excess metal could be peeled whereas the intended structures adhered to the Parylene C layer. Afterwards a second Parylene C layer was deposited on top, completely encasing the complete electrode array (figure 2(9, right)). With hatching the electrode sites were opened, releasing the array was achieved by laser cutting completely through the two layers of Parylene C (figures 2(10, right) and (11, right)). To decrease the adhesion of the silicone adhesive ethanol was applied, so that the array could be peeled of (figure 2(12, right)).

All electrode types were interconnected via a ceramic adaptor to a cable; the double-sided arrays were additionally resistance welded with a 75 μm diameter MP35N wire at the tip to facilitate implantation into the nerve (figure 2(13)).

2.1.3. Imaging of electrode samples. The fabricated samples were optically characterized with a scanning electron micro-copy (SEM) system (Phenom PRO Desktop SEM, Phenom-World BV., Eindhoven, Netherlands) in a configuration with 10 kV acceleration voltage. Hatched and SLIP electrodes were also investigated with a Zeiss Auriga 60 (Carl Zeiss AG, Oberkochen, Germany) focused ion beam setup (FIB) with integrated SEM. A focused gallium ion beam was used to create a cross section in the metal surface, before cross sectional images were taken via SEM.

2.2. Mechanical characterization

A T-pull test and a peel test were performed [27] to investigate the adhesion between the different material interfaces inside the intrafascicular electrode array. Both tests were performed with a bond tester (type 4000 with WP10kg measurement cartridge, Dage Holdings Ltd, Buckinghamshire, United Kingdom). Samples for adhesion measurements of two Parylene C layers were prepared by depositing two layers with an individual thickness of 8 μm , with a small strip of Polyimide tape between them at one end. Utilizing the ps laser system the samples were cut in stripes of 28 mm in length and 5 mm in width. One layer was fixated in a chuck, the second layer was clamped and pulled away in an 180° angle. Adhesion

was calculated with (1), in which F_A is the applied average force while delamination and b the width of the samples [28]:

$$P_{180} = 2 * F_A/b. \quad (1)$$

For the investigation of the adhesion between Pt90/Ir10 and Parylene C metal samples were hatched and cut to measure 28 mm in length and 5 mm in width. One series of the samples were hatched with 2 μm deep lines of 29 μm spacing and an inclination of 90° and 45° towards each other. For further investigation on the effect of the roughness of the Pt90/Ir10, two rectangular hatch patterns with a spacing of 288 μm between the lines and a varying depth of 2 μm and 5 μm were fabricated, others remained unhatched. After a deposition of a 8 μm thick Parylene C layer the samples were submitted to a 90° peel-test.

Adhesion was calculated with (2), in which F_A is the applied average force while delamination and b the width of the samples [28]:

$$P_{90} = F_A/b. \quad (2)$$

2.3. Electrochemical characterization

Electrode arrays were investigated with electrochemical impedance spectroscopy (EIS). Measurements ranged between 100 kHz to 1 Hz at a sinusoidal excitation amplitude of 10 mV with a potentiostat and a frequency analyzer (Solartron 1260&1287, Solartron Analytical, Farnborough, United Kingdom) in a three-electrode configuration. As working electrode (WE), a large-area platinum counter electrode (CE) and as reference electrode (RE) Ag/AgCl (3M KCL) were placed in phosphate buffered saline solution (PBS). Analysis of the data was performed with the software Zplot v2.8 (Scribner Associates Inc., Southern Pines, NC). An electrochemical cleaning step, using cyclic voltammetry (CV) (100 times with 300 mV s⁻¹ from -0.6 V to 0.8 versus Ag|AgCl in PBS), was performed before starting the measurements.

Pulse testing was done in a two-electrode setup (WE: front or back side electrodes; CE: 1 cm² Pt/Ir) in PBS with a PlexStim Electrical Stimulator system (Plexon Inc., Dallas, TX) [29]. Stimulus was a rectangular, symmetrical, charged balanced pulse (cathodic first, pulse width: 200 μs with 10 μs interpulse delay, repetition frequency: 200 Hz). The voltage response across the phase boundary (V_{PB}) was recorded, while varying the amplitude of the current. Due to an open circuit potential (OCP) of 300 mV the safe charge injection limit was reached at a potential of $V_{PB} = -900$ mV (with a cathodic water window of -600 mV in PBS).

Platinum with nanorough surface was deposited to improve electrochemical behavior of the electrodes, thus gaining a better insight of the enlargement of the real surface by ps laser hatching. Details of the deposition process can be found in [20].

2.4. In vivo evaluation

2.4.1. Implantation procedure. Experiments were conducted implanting Parylene C based electrodes in the rat (Sprague-Dawley, 250 \pm 20 g) sciatic nerve. Implants were made at

the distal half of the thigh, where the sciatic nerve divides into the tibial, peroneal and sural branches, but they are still bundled together and enclosed by a common epineurium. All procedures were performed under ketamine and xylazine anaesthesia (90/10 mg kg⁻¹ i.p.) and in compliance to protocols approved by the Ethical Committee of the Universitat Autònoma de Barcelona, Spain in accordance with the European Communities Council Directive 2010/63/EU.

The implantation procedure was based on already established methods with the TIME electrode [24]. In the case of Parylene C electrodes, the MP35N guiding wire (figure 1(C)) was added to help penetration in the nerve. Thus, the MP35N thin wire was used to pierce the nerve branches and pull the flexible electrode through the sciatic nerve until the correct positioning. All the process was monitored under a dissection microscope to ensure that the electrode active sites were located inside the nerve tissue. Then, the electrode was fixed to the closest muscles with a 10-0 suture stitch to prevent motion. The PCB of the connected electrodes was placed and fixed on the gluteus muscles while the silicone wire was placed subcutaneously, leaving the Omnetics connector fixed over the skin with a plastic base on the back of the animals at the hip level. After implant, animals were left to recover in warm pads and then housed in plastic cages at 22 ± 2 °C under a 12:12 h light cycle with free access to food and tap water with amitriptyline.

Furthermore, to evaluate the long-term biocompatibility of these new electrodes, non-connected devices without wires were also implanted in other animals following the same procedure and nerve function tests were performed for up to twelve months. These non-connected devices were chosen to avoid forces and tensions on the nerve due to the PCB and wires of the functional electrodes to evaluate possible nerve damage due to the implanted electrode only.

Three months post implantation for both functional and nonfunctional electrode groups and twelve months post implantation for the nonfunctional electrode groups, animals were deeply anesthetized with an overdose of pentobarbital and perfused transcardially with 4% PFA in phosphate buffer (PB). After the perfusion, the sciatic nerve segment including the implant was collected and paraffin embedded, and the distal part of the nerve was kept in 3% glutaraldehyde-3% paraformaldehyde in PB for epon embedding.

2.4.2. Nerve function evaluation. The functional properties of the nerves that had been implanted were evaluated by means of nerve conduction, algometry and locomotion tests from 2 weeks up to 12 months after the implant of the non-connected devices. Nerve conduction tests were performed by stimulating the sciatic nerve proximally with single electrical pulses and recording the compound muscle action potentials (CMAPs) of tibialis anterior (TA), gastrocnemius medialis (GM) and plantar interossei (PL) muscles as previously described [30, 31]. The nociceptive threshold to mechanical stimuli was evaluated by means of an electronic Von Frey algometer (Bioseb, Chaville, France) following the same protocol than in [32]. Briefly, rats were placed on a wire net platform in plastic chambers, and a metal tip applied to the

sole of the hindpaw until the rat withdrew the paw in response to the stimulus. Finally, the walking track test was performed to assess locomotor function after the implant. The plantar surface of the hindpaws was painted with black ink and the rat was left to walk on top of a white paper along a corridor [33]. The print length, the distance between the 1st and 5th toes and between the 2nd and 4th toes were measured to calculate the sciatic functional index (SFI) [34].

2.4.3. Histological evaluation. To identify the location of the electrode inside the nerve, paraffin embedded nerve segments were cut in transverse sections (10 μm thick), mounted in silane-coated slides and dried overnight. The sections were deparaffinized and a standard luxol fast blue (LFB) staining was performed overnight to visualize myelin in nerve samples and then a hematoxylin-eosin (HE) staining was performed in the same nerve slices. Then, samples were dehydrated and mounted with DPX (Sigma-Aldrich, St. Louis, MO).

In order to evaluate the potential damage to the implanted nerves, distal nerve segments were postfixed in 2% OsO₄ for 2 h, dehydrated through ethanol series and embedded in epon resin. Semithin sections (0.5 μm thick) were stained with toluidine blue and examined by light microscopy. The number of myelinated fibers in the distal tibial nerve was counted in images taken with a BX51 light microscope and a DP50 digital camera (Olympus K.K., Tokyo, Japan) at 100× chosen by systematic random sampling of squares representing at least 30% of the nerve cross-sectional area. The cross-sectional area of the tibial nerve was measured at 4× and the total number of myelinated fibers estimated.

2.4.4. Electrode functionality evaluation. To assess the electrode nerve stimulation capabilities over time, monophasic rectangular voltage pulses with a width of 20 μs and amplitude from 5 to 100 V were delivered through each one of the different electrode active sites against a small needle electrode placed subcutaneously in the back of the animal. Simultaneously, electromyographic (EMG) signals were recorded from TA, GM and PL muscles, which are innervated by different fascicles or subfascicles of the sciatic nerve [35] using needle recording electrodes placed in each muscle. Signals were amplified (P511 AC; Grass; WestWarwick, RI) by 200× or 1000×, and digitized with a PowerLab recording system (PowerLab16SP, ADInstruments, Bella Vista, Australia). The same experiment was repeated in five implanted rats at 0, 7, 15, 30, 45 and 60 days post implant. The amplitude of the CMAP was measured from baseline to the positive peak and normalized to the maximum CMAP amplitude obtained in each experiment. The EMG data was used to calculate the stimulation threshold at which a 5% of maximal muscle response was achieved. Moreover, the selectivity index (SI) was also calculated to quantify the activation of a single muscle among the set of three muscles (TA, GM, PL) when stimulating by each one of the active sites, as previously described [30, 36]. Thus, the maximum CMAP obtained for one active site (as) was used to calculate the maximum selectivity index (SI_{as max}) for each muscle and each electrode and the mean of the maximum SI_{as} (SI_{as max}) was plotted. Besides, the selectivity

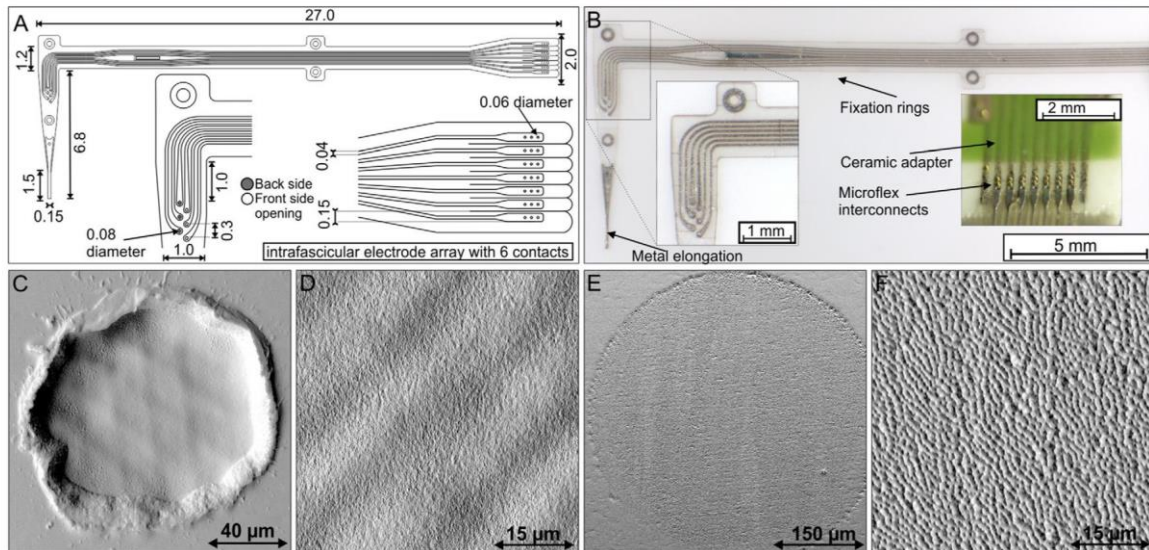


Figure 3. Optical and SEM images of a Parylene C based intraneural electrode array. (A) Design of an electrode array with 6 electrode contacts and one ground electrode. All dimensions in mm. (B) Optical image of the same electrode array. Close up of the Microflex interconnects to a ceramic adaptor. (C) SEM image of front side 80 μm electrode with hatching pattern. (D) Surface of the rough hatching pattern. (E) SLIP patterned Pt90/Ir10 surface. (F) Close up of the SLIP patterned surface.

index for the device (SId) was also calculated following the described formulae by [30].

2.4.5. Statistics. Results are expressed as mean \pm SEM. Statistical analysis of mean were performed using one or two-way ANOVA followed by Tukey post hoc test for differences between groups or time-points using GraphPad Prism software. Differences among groups or times were considered significant when $p < 0.05$.

3. Results

3.1. In vitro characterization

3.1.1. Sample fabrication. All electrode arrays were fabricated following the proposed fabrication route. The arrays featured a ground electrode outside the nerve and 4–6 active sites for intraneural implantation (figures 3(A) and (B) version with 6 electrode contacts). However, the 80 μm electrode contacts showed small deviations in actual geometry due to the use of a mechanical deflection system for the laser movement (figure 3(C)). An optical observable roughening of the surface could be achieved with normal hatching patterns (figure 3(D)). The metal surface showed a wave structure that represent the laser path as well as a grainy roughening on the surface. With SLIP patterning the grains were formed multiple times over and interacted forming an interference pattern on the metal surface (figure 3(E)). Close up a very rough pattern with deep pores could be observed (figure 3(F)). Cross section views revealed a clear difference in the penetration depth of the created structures for hatched and SLIP electrodes. Whereas the hatched surfaces exhibit a distinct 3D surface enlargement, the penetration depth of the grains is in the range of several 10 nm (figure 4(A)). Pores of the SLIP pattern were observed to penetrate the metal surface for at least 1.5 μm (figures

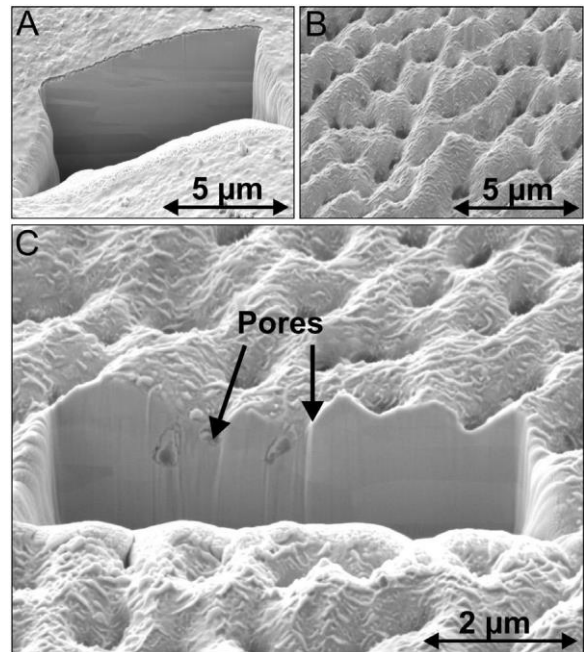


Figure 4. SEM micrographs of cross sections, cut with FIB in Pt electrode surfaces. (A) Cross section of hatched electrode surface. The wave structure and the low penetration depth of the grainy structures can be observed. (B) 10k magnification of SLIP surface. (C) Cross section through SLIP structures. Two pores can be seen penetrating out of the viewing field into the bulk.

4(B), (C)). However, while running the ps laser beam across the surface a faint light was observed on the backside, implying some pores might penetrate deeper into the bulk.

3.1.2. Mechanical measurements. The mean adhesion of Parylene C on bare, untreated Pt90/Ir10 foil was found to be roughly 60 mN cm^{-1} . However, between two 10 μm thick layers of Parylene C a mean adhesion of 4400 mN cm^{-1} was

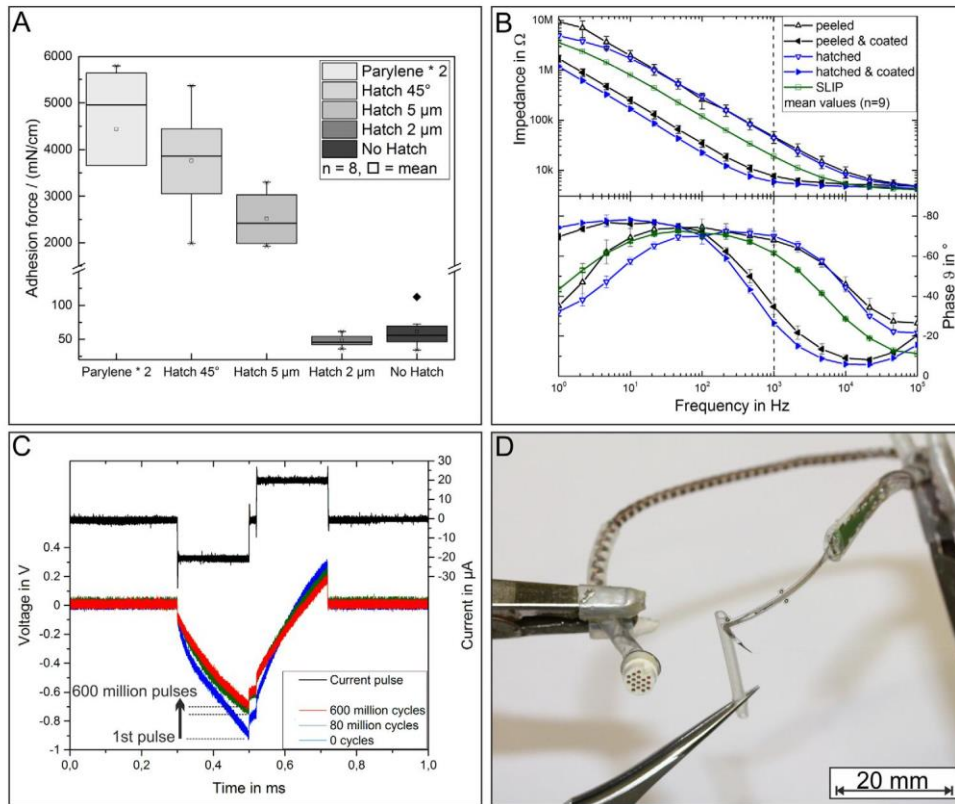


Figure 5. (A) Left to right: adhesion force of: 2 10 μm thick Parylene C layers; Pt/Ir with 10 μm Parylene C layer on top and 45° inclined mesh (2 μm depth, 29 μm distance); Pt90/Ir10 with 10 μm Parylene C layer on top and rectangular hatch (5 μm/2 μm depth, 288 μm distance); untreated Pt/Ir foil with 10 μm Parylene C layer on top (n = 14, others n = 8). (B) Impedance and phase angles of peeled and hatched 80 μm Pt/Ir electrodes, both pure and coated with platinum nanostructures, as well as SLIP roughened electrodes. (C) Long-term pulse testing of a hatched (non-coated) 80 μm Pt90/Ir10 electrode. (D) Complete assembly of intrafascicular Parylene C based electrode used for the measurements.

measured. Applying the hatch pattern with 2 μm depth lowered the mean adhesion to 47 mN cm⁻¹, whereas an increase of depth to 5 μm led to an increase in mean adhesion to 3053 mN cm⁻¹. Narrowing the hatching pattern and providing crossing points of 4 μm depth led to an increase in mean adhesion to 4012 mN cm⁻¹ (figure 5(A)).

3.1.3. Electrochemical measurements. The fabricated electrodes showed the anticipated high pass behavior. This correlates to a R||C-R electrode model which can be fitted to all electrodes.

Access resistance R_A of the peeled electrodes was measured to be 5540 Ω (standard deviation (std.) 541 Ω) whereas for the hatched electrodes 4762 Ω (std. 47 Ω) were determined. At 1 kHz the impedance magnitudes were measured to 55.5 kΩ (std. 12.5 kΩ) and 43.8 kΩ (std. 3081 Ω) respectively. After coating the electrodes according to [20] the impedance magnitude at 1 kHz dropped to 7.6 kΩ (std. 941 Ω) for the peeled and 5.8 kΩ (std. 182 Ω) for the hatched electrodes. Without coating, both types featured a cutoff frequency of over 50 kHz. Coating the electrodes lowered the cutoff frequency to 1 kHz. SLIP electrodes yielded an R_A of 4105 Ω (std. 177 Ω) and an impedance magnitude at 1 kHz of 18.7 kΩ (std. 632 Ω) (figure 5(B)).

Over the phase boundary of a peeled electrode a mean charge of 2.97 nC per phase (maximum charge injection

capacity (Q_{maxinj}) resulted in 59.64 μC cm⁻²) could be delivered before reaching the cathodic water window. Hatched electrodes were able to support a mean charge of 9.93 nC (Q_{maxinj} : 197.63 μC cm⁻²). With the coating the mean delivered charge of peeled electrodes was boosted to 31.20 nC (Q_{maxinj} : 635.75 μC cm⁻²) whereas the hatched electrodes were raised to 37.89 nC (Q_{maxinj} : 753.24 μC cm⁻²). SLIP electrodes exhibited a Q_{maxinj}^{max} of 272.18 μC cm⁻².

Prior to their implantation, a long-term pulse test of hatched 80 μm electrodes with a charge of 4 nC per pulse was performed over five weeks (figure 5(C)). The lower border of the water window is shifted from -600 mV to -900 mV due to an OCP of 300 mV. Whereas the initial voltage response was -850 mV it dropped to -668 mV after one week where it rested relatively stable for the remaining experiment.

3.2. In vivo tests

3.2.1. In vivo biocompatibility. To evaluate functional changes in the nerves with implanted electrodes, neurophysiological tests were performed at different time points. In electrophysiological tests, there were no differences in the CMAP amplitude (figure 6(A)) and latency to the onset of the response of TA, GM or PL muscles between the implanted and the contralateral intact limb of the rats during the 12 months follow-up. Regarding

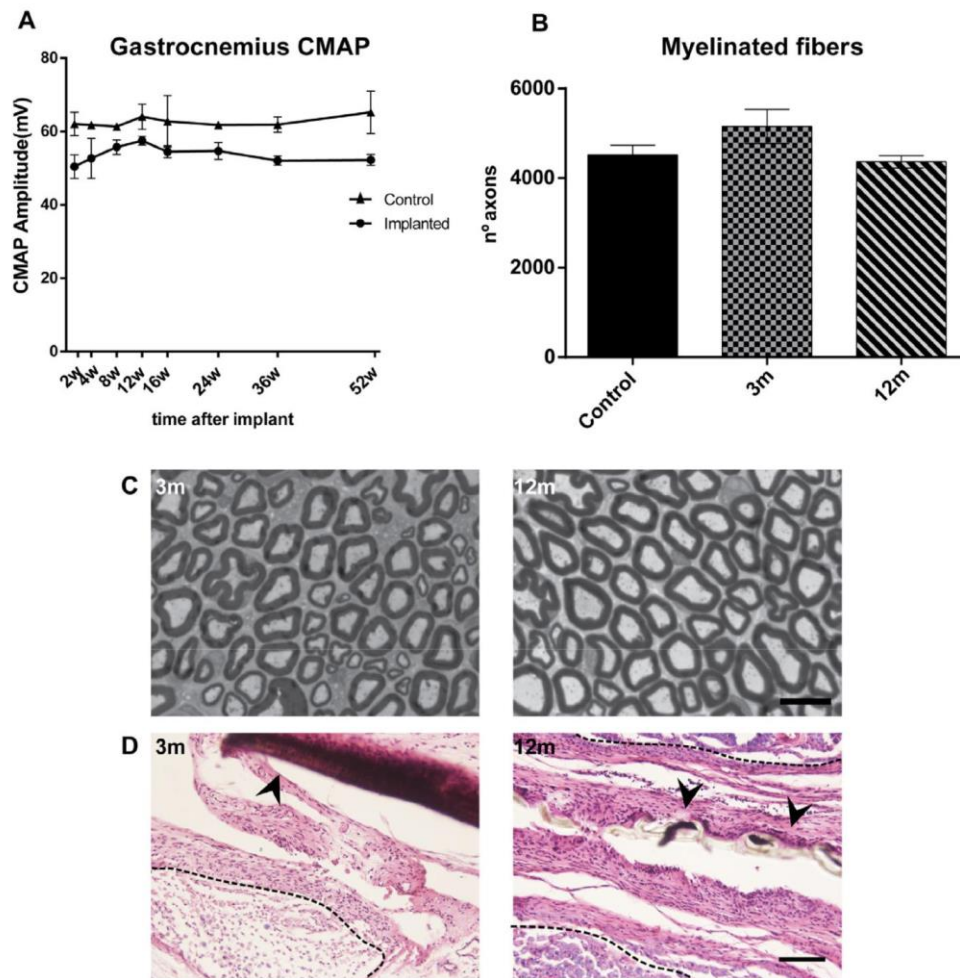


Figure 6. (A) Gastrocnemius CMAPs amplitude for implanted and contralateral paws over time. (B) Total number of myelinated fibers from control, 3 months and 12 months implanted nerves. (C) Representative images of distal nerves after 3 or 12 months of implant. Scale bar = 10 μm . (D) *H-E* representative images of implanted nerves. Arrows indicate the electrode implanted and dotted line delimitates nerves fascicles. Scale bar = 100 μm .

pain assessment, pain threshold of animals implanted with both connected and non-connected devices remained around 30 g throughout all the studied time points. Besides, no alterations in the locomotion pattern were found during the year of implantation at any of the implanted animals.

Evaluation of the distal segment of nerves implanted with both non-connected and connected electrodes showed no morphological alterations, differences in the total number of myelinated fibers (figure 6(B)) neither signs of degeneration after three or twelve months of implant for the non-connected devices or after three months for the connected electrodes.

The histological analysis showed that at the segment where the electrodes were implanted, there were no signs of nerve degeneration and that the fascicular architecture of the nerve was preserved (figures 6(C) and (D)) after 3 or 12 months of implant. Besides, no important changes in the matrix accumulation around the electrode seem to occur from 3 months onward for both connected and non-connected devices. Thus, the main matrix deposition surrounding the electrodes occurs during the first weeks after the implantation.

3.2.2. *In vivo* electrodes functionality. The threshold of stimulation needed to elicit a 5% of the total muscle response

showed significant changes over time (figure 7(A)) and two different phases could be observed over time. During the first weeks of implant, an increase in the stimulation threshold was observed compared to acute tests; then, a plateau was reached from 2 weeks to 2 months of implant.

Regarding the stimulation selectivity of the electrodes no significant differences were observed from acute stimulation at the implant day to chronic stimulation over 2 months of implant (figure 7(B)), with a SI for each muscle around 0.55 during all the follow-up. The SI for the device was also maintained stable (figure 7(C)). These results proved that parylene electrodes are able to selectively stimulate different axonal subpopulations of the sciatic nerve, depending on the active site used and the intensity of stimulation.

4. Discussion

In this work we describe a new method for the fabrication of a novel intrafascicular electrode array. Even though the individual electrode sites are rather small, a precise fabrication over several transfer steps during the process is possible. Utilizing ps laser technology the adhesion of the individual

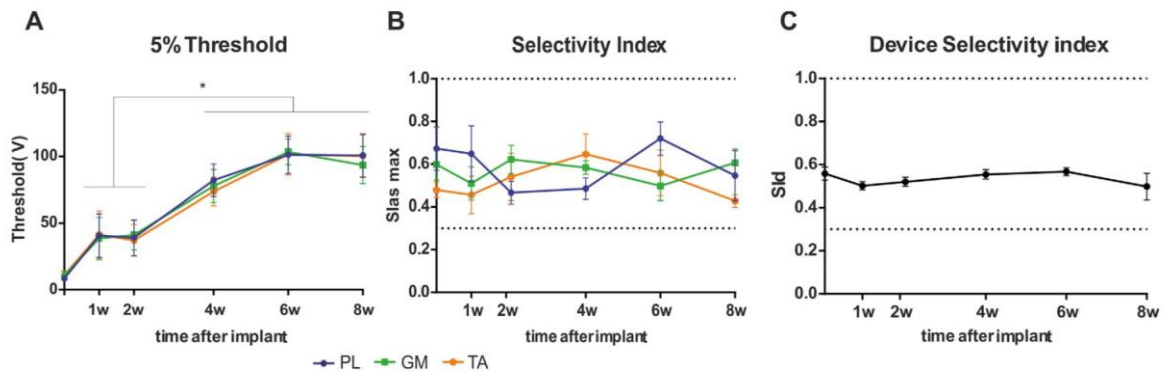


Figure 7. (A) Threshold of stimulation to achieve 5% of the maximal muscular response over 8 weeks of follow-up for GM, TA and PL muscles. (B) Maximal selectivity index for GM, TA and PL muscles after 8 weeks of implant. (C) Progression of device selectivity index over time. * $p < 0.05$, two-way ANOVA.

layers can be adjusted to each other, forming a mechanical stable system. Disparities in the peeled and hatched electrodes were observable optically and by electrochemical measurements. Larger standard deviations reflect the disadvantageous manual peeling of the small contacts in comparison to a touch-free direct hatching. The fabrication process now allows for quick design changes which are only limited by the maximum work area of the deflection unit.

Coating the electrodes gave insights on the difference in active area of the two processes. At 1 kHz the peeled electrodes have a 1.27 times higher impedance compared to the hatched electrodes.

This factor changed to 1.31 after the coating. In terms of $Q_{\max inj}$ a factor of 3.34, which dropped to 1.21 after the coating, was measured. The same investigation on SLIP electrodes hints towards a surface enlargement by a factor of 3, which is about 15% higher compared to Green *et al* [21], however small changes in diameter strongly influences the electro-chemical characteristics of microelectrodes [29]. Considering widespread use of iridium oxide covered microelectrodes a comparison needs to be addressed. Over the phase boundary

of such a 80 μm electrode results a $Q_{\max inj}$ of 2.3 mC cm^{-2} [37], which is over 10 times larger than the hatched electrodes (3 times for the coated electrodes), but the impedances can be roughly matched by coating a hatched electrode. However, the hatched electrodes have a 3–4 times larger $Q_{\max inj}$ compared to bare platinum electrodes [38] and show a good long-term stability during pulse testing. A future shift to SLIP electrodes might further improve application. The nanorough Pt coating has already been investigated for long-term stability over 240 million pulses and *in vitro* cytotoxicity [20].

Furthermore, parylene-based electrodes have shown good biocompatibility and safety after long-term implantation in an *in vivo* rat model. As shown by the electromyography studies, no changes in the nerve function were observed. Besides, no signs of pain or locomotion alterations were found after 1 year follow-up. These results agree to those shown with similar electrode designs [24] or with other intrafascicular electrodes [39]. Moreover, histological analysis revealed no evidence of nerve damage due to the devices implanted.

However, tissue accumulation surrounding the implanted devices was observed after months of implant in both connected and non-connected electrodes, as reported for other neural electrodes [39, 40]. The increase of threshold stimulation

necessary to induce a response in the first two weeks indicate that matrix accumulation around the implanted device mainly occur during the first weeks after implantation, similar to other studies [41]. The later stabilization implies that after 4–8 weeks there is no more tissue deposition around the electrodes, although changes in its cellular nature may occur [42]. Such tissue deposition surrounding the electrodes explain, among other facts, the increase in the voltage needed to stimulate nerve fibers, as the distance between the active sites and the nervous tissue is widened. Nevertheless, the electrodes showed a stable SI of stimulation, without significant changes over time, indicating stable position in the implanted nerve. Thus, parylene-based electrodes meet the needs for chronic implants in animals or even in humans [43]. However, further studies are needed to elucidate if these new Parylene C electrodes are able to record neural signals after long-term implantation.

5. Conclusions

A novel fabrication process and implantation technique for thin intrafascicular Parylene C based electrode arrays was implemented and used to create arrays for a small animal model. During chronic implantation the electrode arrays exhibited good biocompatibility and functionality. A design change for including more electrode sites and for adaptation to larger nerve diameters has to be made to prove feasibility in a larger animal model and ultimately the application in human patients. The published fabrication process allows for rapid prototyping of novel biocompatible electrode arrays.

Acknowledgments

This work has received funding from the European Community's Seventh Framework Programme (FP7/2007-2013) under grant agreement no.611687 (NEBIAS-NEurocontrolled Bidirectional Artificial upper limb and hand prosthesis).

FIB measurements were carried out with the support of the Karlsruhe Nano Micro Facility (KNMF, www.knmf.kit.edu), a Helmholtz Research Infrastructure at Karlsruhe Institute of Technology (KIT, www.kit.edu) under KNMF proposal 2016-017-016529. The authors would like to thank Ms Dr Sabine Schlabach for her expertise.

The authors would like to thank Mr Christian Boehler for his help in coating the electrodes.

The authors would like to thank Ms Linda Rudmann for taking the SEM pictures

ORCID iDs

Matthias Mueller  <https://orcid.org/0000-0003-2074-144X>
 Natalia de la Oliva  <https://orcid.org/0000-0002-1263-2705>
 Jaume del Valle  <https://orcid.org/0000-0002-6703-8244>
 Ignacio Delgado-Martínez  <https://orcid.org/0000-0003-1616-8943>
 Xavier Navarro  <https://orcid.org/0000-0001-9849-902X>
 Thomas Stieglitz  <https://orcid.org/0000-0002-7349-4254>

References

- [1] Navarro X, Krueger T B, Lago N, Micera S, Stieglitz T and Dario P 2005 A critical review of interfaces with the peripheral nervous system for the control of neuroprostheses and hybrid bionic systems *J. Peripher. Nerv. Syst.* **10** 229–58
- [2] Ordóñez J, Schuettler M, Boehler C, Boretius T and Stieglitz T 2012 Thin films and microelectrode arrays for neuroprosthetics *MRS Bull.* **37** 590–8
- [3] Donaldson P E K 1991 Aspects of silicone rubber as an encapsulant for neurological prostheses *Med. Biol. Eng. Comput.* **29** 34–9
- [4] Schuettler M, Stieglitz T, King B V and Suanning G J 2005 Fabrication of implantable microelectrode arrays by laser cutting of silicone rubber and platinum foil *J. Neural Eng.* **2** S121–8
- [5] Shamma-Donoghue S A, May G A, Cotter N E, White R L and Simmons F B 1982 Thin-film multielectrode arrays for a cochlear prosthesis *IEEE Trans. Electron Devices* **29** 136–44
- [6] Stieglitz T, Beutel H and Meyer J-U 1997 A flexible, light-weight multichannel sieve electrode with integrated cables for interfacing regenerating peripheral nerves *Sensors Actuators A* **60** 240–3
- [7] Wise K D, Angell J B and Starr A 1970 An integrated-circuit approach to extracellular microelectrodes *IEEE Trans. Biomed. Eng.* **17** 238–47
- [8] Tyler D J and Durand D M 1997 A slowly penetrating interfascicular nerve electrode for selective activation of peripheral nerves *IEEE Trans. Rehabil. Eng.* **5** 51–61
- [9] Stieglitz T, Beutel H, Schuettler M and Meyer J-U 2000 Micromachined, polyimide-based devices for flexible neural interfaces *Biomed. Microdevices* **2** 283–94
- [10] Lacour S P, Wagner S, Huang Z and Suo Z 2003 Stretchable gold conductors on elastomeric substrates *Appl. Phys. Lett.* **82** 2404–6
- [11] Kaltenbrunner M et al 2013 An ultra-lightweight design for imperceptible plastic electronics *Nature* **499** 458–63
- [12] Wagner S and Bauer S 2012 Materials for stretchable electronics *MRS Bull.* **37** 207–13
- [13] Nebel A, Herrmann T, Henrich B and Knappe R 2005 Fast micromachining using picosecond lasers *Lasers and Applications in Science and Engineering (SPIE Proc.)* ed J T Schriempf (San Jose, CA, 22 January 2005) pp 87–98
- [14] Raspopovic S et al 2014 Restoring natural sensory feedback in real-time bidirectional hand prostheses *Sci. Transl. Med.* **6** 222ra19
- [15] Oddo C M et al 2016 Intraneural stimulation elicits discrimination of textural features by artificial fingertip in intact and amputee humans *Elife* **5** e09148
- [16] Mueller M, Boehler C, Jaeger J, Asplund M and Stieglitz T 2016 A double-sided fabrication process for intrafascicular Parylene C based electrode arrays *Conf. Proc. IEEE Engineering in Medicine and Biology Society* vol 2016 pp 2798–801
- [17] Mueller M, Ulloa M, Schuettler M and Stieglitz T 2015 Development of a single-sided Parylene C based intrafascicular multichannel electrode for peripheral nerves *Proc. of the 7th Internat. IEEE/EMBS Conf. on Neural Engineering (NER)* vol 2015 pp 537–40
- [18] Wu F, Tien L W, Chen F, Berke J D, Kaplan D L and Yoon E 2015 Silk-backed structural optimization of high-density flexible intracortical neural probes *J. Microelectromech. Syst.* **24** 62–9
- [19] Xiang Z, Yen S-C, Xue N, Sun T, Tsang W M, Zhang S, Liao L-D, Thakor N V and Lee C 2014 Ultra-thin flexible polyimide neural probe embedded in a dissolvable maltose-coated microneedle *J. Micromech. Microeng.* **24** 65015
- [20] Boehler C, Stieglitz T and Asplund M 2015 Nanostructured platinum grass enables superior impedance reduction for neural microelectrodes *Biomaterials* **67** 346–53
- [21] Green R A, Matteucci P B, Dodds C W D, Palmer J, Dueck W F, Hassarati R T, Byrnes-Preston P J, Lovell N H and Suanning G J 2014 Laser patterning of platinum electrodes for safe neurostimulation *J. Neural Eng.* **11** S6017
- [22] Bouhelier A, Ignatovich F, Bruyant A, Huang C, Des Colas Francis G, Weeber J-C, Dereux A, Wiederrecht G P and Novotny L 2007 Surface plasmon interference excited by tightly focused laser beams *Opt. Lett.* **32** 2535
- [23] Lago N, Udina E, Ramachandran A and Navarro X 2007 Neurobiological assessment of regenerative electrodes for bidirectional interfacing injured peripheral nerves *IEEE Trans. Biomed. Eng.* **54** 1129–37
- [24] Badia J, Boretius T, Pascual-Font A, Udina E, Stieglitz T and Navarro X 2011 Biocompatibility of chronically implanted transverse intrafascicular multichannel electrode (TIME) in the rat sciatic nerve *IEEE Trans. Biomed. Eng.* **58** 2324–32
- [25] Gorham W F 1966 A new, general synthetic method for the preparation of linear poly-p-xylylenes *J. Polym. Sci. A* **4** 3027–39
- [26] Meyer J-U, Stieglitz T, Scholz O, Haberer W and Beutel H 2001 High density interconnects and flexible hybrid assemblies for active biomedical implants *IEEE Trans. Adv. Packag.* **24** 366–74
- [27] ASTM D1876-08 2008 *Standard Test Method for Peel Resistance of Adhesives (T-Peel Test)* (West Conshohocken, PA: ASTM International) (<https://doi.org/10.1520/D1876-08>)
- [28] Packham D E 2005 *Handbook of Adhesion* 2nd edn (New York: Wiley) pp 311–5
- [29] Cogan S F 2008 Neural stimulation and recording electrodes *Annu. Rev. Biomed. Eng.* **10** 275–309
- [30] Badia J, Boretius T, Andreu D, Azevedo-Coste C, Stieglitz T and Navarro X 2011 Comparative analysis of transverse intrafascicular multichannel, longitudinal intrafascicular and multipolar cuff electrodes for the selective stimulation of nerve fascicles *J. Neural Eng.* **8** 36023
- [31] Cutrone A, Del Valle J, Santos D, Badia J, Filippeschi C, Micera S, Navarro X and Bossi S 2015 A three-dimensional self-opening intraneural peripheral interface (SELINe) *J. Neural Eng.* **12** 16016
- [32] Santos D, Wieringa P, Moroni L, Navarro X and Valle J D 2016 PEOT/PBT guides enhance nerve regeneration in long gap defects *Adv. Healthc. Mater.* **6** 160029
- [33] Navarro X 2016 Functional evaluation of peripheral nerve regeneration and target reinnervation in animal models: a critical overview *Eur. J. Neurosci.* **43** 271–86

- [34] de Medinaceli L, Freed W J and Wyatt R J 1982 An index of the functional condition of rat sciatic nerve based on measurements made from walking tracks *Exp. Neurol.* **77** 634–43
- [35] Badia J, Pascual-Font A, Vivo M, Udina E and Navarro X 2010 Topographical distribution of motor fascicles in the sciatic-tibial nerve of the rat *Muscle Nerve* **42** 192–201
- [36] Veraart C, Grill W M and Mortimer J T 1993 Selective control of muscle activation with a multipolar nerve cuff electrode *IEEE Trans. Biomed. Eng.* **40** 640–53
- [37] Boretius T, Yoshida K, Badia J, Harreby K, Kundu A, Navarro X, Jensen W and Stieglitz T 2012 A transverse intrafascicular multichannel electrode (TIME) to treat phantom limb pain—towards human clinical trials *Proc. IEEE RAS EMBS Int. Conf. Biomedical Robotics and Biomechatronics* vol 2012 pp 282–7
- [38] Donaldson N d N and Donaldson P E K 1986 Performance of platinum stimulating electrodes mapped on the limitvoltage plane *Med. Biol. Eng. Comput.* **24** 431–8
- [39] Lago N, Yoshida K, Koch K P and Navarro X 2007 Assessment of biocompatibility of chronically implanted polyimide and platinum intrafascicular electrodes *IEEE Trans. Biomed. Eng.* **54** 281–90
- [40] Christensen M B, Pearce S M, Ledbetter N M, Warren D J, Clark G A and Tresco P A 2014 The foreign body response to the Utah slant electrode array in the cat sciatic nerve *Acta Biomater.* **10** 4650–60
- [41] Wurth S et al 2017 Long-term usability and bio-integration of polyimide-based intra-neural stimulating electrodes *Biomaterials* **122** 114–29
- [42] del Valle J, de La Oliva N, Muller M, Stieglitz T and Navarro X 2015 Biocompatibility evaluation of Parylene C and polyimide as substrates for peripheral nerve interfaces *Proc. of the 7th Int. IEEE/EMBS Conf. on Neural Engineering (NER)* vol 2015 pp 442–5
- [43] Micera S 2016 Staying in touch: toward the restoration of sensory feedback in hand prostheses using peripheral neural stimulation *IEEE Pulse* **7** 16–9

CHAPTER 2: TIME COURSE STUDY OF LONG-TERM BIOCOMPATIBILITY AND FOREIGN BODY REACTION TO INTRANEURAL IMPLANTS

Natàlia de la Oliva¹, Matthias Müller², Thomas Stieglitz², Xavier Navarro¹, Jaume del Valle^{1,3}

¹ Institute of Neurosciences, Department of Cell Biology, Physiology and Immunology, Universitat Autònoma de Barcelona, and Centro de Investigación Biomédica en Red en Enfermedades Neurodegenerativas (CIBERNED), Bellaterra, Spain.

² Laboratory for Biomedical Microtechnology, Department of Microsystems Engineering IMTEK, Albert-Ludwig-University Freiburg, Freiburg, Germany.

³ Catalan Institute of Nanoscience and Nanotechnology (ICN2), CSIC and BIST, Campus UAB, Bellaterra, 08193 Barcelona, Spain

ABSTRACT

The foreign body reaction (FBR) against an implanted device is characterized by the formation of a fibrotic tissue around the implant. In the case of electrodes for peripheral nerves, used to stimulate a specific group of axons and to record different nerve signals, the FBR induces a matrix deposition around the implant creating a physical separation between nerve fibers and the electrode that may reduce its functionality over time.

In order to understand the FBR to intraneural electrodes, polyimide and Parylene C non-functional devices were implanted longitudinally in the rat sciatic nerve. Functional tests (electrophysiological, pain and locomotion) and histological evaluation demonstrated that implanted devices did not cause any alteration in nerve function, in myelinated axons or in nerve architecture. The inflammatory response due to the surgical implantation was decreased after 2 weeks. In contrast, inflammation was higher and more prolonged in the device implanted nerves with a peak at 2 weeks. With regard to tissue deposition, a tissue capsule appeared soon around the devices, acquiring maximal thickness at 2 weeks and being remodeled subsequently. The capsule increased in thickness until 8 weeks, and then stabilized on polyimide devices, but continued to increase on Parylene C devices. Immunohistochemical analysis revealed two different cell types implicated in the FBR in the nerve: macrophages as the first cells in contact with the interface and fibroblasts that appear after 8 weeks at the edge of the capsule. Our results describe how the FBR against an intraneural implant in the peripheral nerve occurs and which are the main cellular players. Moreover, the FBR dynamics is determined not only by the tissue but also by the material implanted. Increasing knowledge of these responses will help to improve strategies to decrease the FBR against intraneural electrodes and to extend their usability.

Keywords: foreign body reaction, intraneural electrode, Parylene C, polyimide.

INTRODUCTION

Advanced neuroprostheses are based on their capability to interface specific groups of motor axons within a nerve to obtain different motor signals and to stimulate specific sensory afferent fibers to provide feedback, thus allowing for a bidirectional communication between the nervous system and the mechanical prosthesis by means of neural electrodes (del Valle and Navarro, 2013; Navarro et al., 2005; Tyler et al., 2015). Some authors consider intraneural electrodes as the most adequate type, as they allow for higher selectivity of recording and stimulation, lower intensity for stimulation and increased signal-to-noise ratio of recordings compared to extraneural electrodes (Badia et al., 2011a; Yoshida et al., 2000). Several intraneural electrodes, such as multielectrode arrays (Branner et al., 2001; Branner and Normann, 2000; Clark et al., 2014, 2011; Wark et al., 2013), longitudinal (LIFE) (Lago et al., 2007; Malmstrom et al., 1998) and transversal (TIME) (Badia et al., 2011b; Boretius et al., 2010) intrafascicular electrodes have shown good performance for a bidirectional interface with the peripheral nerve. Such intraneural interfaces should have good biocompatibility and stability to remain inside the nerves for months or years, and be able to record neural signals with high signal-to-noise ratio, to extract motor efferent information to drive a prosthetic limb, and also to selectively stimulate axons to evoke sensory feedback of the use of the prosthesis.

However, after the implantation of any device in the body, an immune-mediated response – known as foreign body reaction (FBR) – occurs. The FBR results in the encapsulation of the implant with immune cells and fibrotic tissue (Anderson et al., 2008; Kenneth Ward, 2008) and it may finally lead to the failure of the device due to the lack of interaction with the tissue environment (Chen and Young, 2016; Yu et al., 2007). In fact, several studies have shown a progressive reduction in the functionality of intraneural electrodes after days/weeks of implantation (Raspopovic et al., 2014; Rossini et al., 2010; Warwick et al., 2003), thus limiting the prospective use of intraneural electrodes. Such failures could be attributed to electromechanical erosion of the metal sites, fatigue of the connections, changes in conductivity, cell death and to the biological response of the nerve tissue against the electrode implant. Regarding the latter, experimental studies have reported that the implanted electrode becomes encapsulated by host cells, creating a separation between the electrode and the nerve fibers to be interfaced (Lago et al., 2007).

Despite the FBR has been widely studied and the progression of this response is well known in subcutaneous (Fet et al., 2014; Gretzer et al., 2006; Kastellorizios et al., 2015), peritoneal (Le et al., 2010; Robitaille et al., 2005) and even central nervous system implants

(Biran et al., 2005; Polikov et al., 2005; Yanagihara et al., 1967), few studies have focused in the peripheral nervous system (Christensen et al., 2016, 2014; Wark et al., 2014) and a detailed description of the long-term response and its time-course against implanted interfaces in peripheral nerves is still needed.

Moreover, the substrate material on which the electrode is made has an essential role in the FBR developed (Boddupalli et al., 2016). It has to be biocompatible and biostable, avoiding the release of degrading particles that will induce an inflammatory reaction. Another recognized problem is the mismatch of compliance between neural tissue and the implant material; indeed, reducing biomaterial stiffness can reduce the activation of immune cells leading to a less severe FBR (Blakney et al., 2012). Regarding the advances in biocompatible materials, several polymers have emerged as feasible options as substrates of flexible neural electrodes, such as polyimide and Parylene C.

Polyimide is currently used in the fabrication of peripheral nerve interfaces (Boretius et al., 2010; Cutrone et al., 2015; Lago et al., 2007; Wurth et al., 2017). This polymer has good chemical, mechanical and electrical insulation properties (Rubehn and Stieglitz, 2010) and good biocompatibility and long-term stability (Rubehn and Stieglitz, 2010; Stieglitz et al., 2000). Parylene C is a highly flexible polymer used in many biomedical applications, such as sensors, coatings or as substrate for neural electrodes (Chen and Young, 2016; Haggren et al., 2017; Kim and Meng, 2016; Ordonez et al., 2012) due to its good biocompatibility and biostability (Chang et al., 2007; Lecomte et al., 2017). Unlike polyimide and other polymers used, Parylene C allows for thinner layers that could improve the implantation procedure and reduce the damage to the nerves (Mueller et al., 2017, 2016).

In order to characterize the cellular processes participating in the FBR to an intraneural electrode, which may allow identifying new targets to modulate this response and enhance the interface functionality, we have studied from 1 day to 8 months the progression of the FBR to longitudinal nerve implants made of polyimide or Parylene C.

MATERIAL AND METHODS

Animals and surgical procedures

All animal experiments were performed with the approval of the Ethical Committee of the Universitat Autònoma de Barcelona in accordance with the European Communities Council Directive 2010/63/EU.

Female Sprague-Dawley rats weighing 250-300g were used (n = 6-8/group). All surgeries were performed under ketamine and xylazine anesthesia (90 / 10 mg/kg i.p.). The sciatic nerve was surgically exposed at the mid thigh and carefully freed from adhesions to surrounding tissues. Passive devices of polyimide or Parylene C (20 mm long, 200 μ m wide and 10 μ m thick) (Fig. 1A) were inserted longitudinally in the tibial branch of the sciatic nerve with the help of a straight needle attached to a 10-0 loop thread (STC-6, Ethicon). The thread was passed between the two arms of the device and pulled the arrow-shaped center of the electrode strip (Fig. 1B-C), as previously described for the insertion of LIFE s (Lago et al., 2007). Then, the surrounding muscles and the skin were closed and the wound disinfected with povidone-iodine. A longitudinal implant was chosen because of its better reproducibility in comparison with transversal implants and to better study only the FBR inside the nerve. A group of animals underwent a sham operation with the same procedures but leaving no implant inside the nerve and another group of intact animals was included for reference of normal nerves. Animals were left to recover under warm environment. They were housed at 22 \pm 2 $^{\circ}$ C under a 12:12h light cycle with ad libitum food and water access.

After 6 hours, 1, 2, 4 days and 2, 4, 8, 16 and 32 weeks post-implant, animals were deeply anesthetized with an overdose of pentobarbital and transcardially perfused with 4% PFA in phosphate buffer (PB) or sterile saline to obtain the sciatic nerve including the implanted device for histological or molecular analyses.

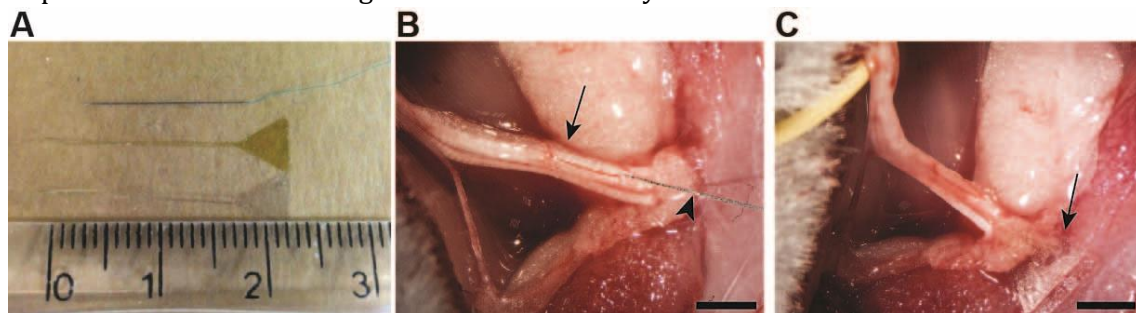


Figure 1. Surgical procedure. (A) Photograph of the longitudinal polyimide (above) or Parylene C (middle) devices implanted and the needle used (bottom). (B) Needle used for the implantation piercing (arrowhead) the sciatic nerve (arrow) of a rat. (C) Device implanted (arrow points to the triangle base) in the sciatic nerve. Scale bar in (B-C) = 1mm.

Functional evaluation

To evaluate functional properties of the implanted nerves, nerve conduction, algesimetry and locomotion tests were performed at different time points. Nerve conduction test was performed by stimulating the sciatic nerve proximally with single electrical pulses and recording the compound action potentials (CMAPs) of the gastrocnemius medialis (GM) muscle as previously described (Badia et al., 2011b; Lago et al., 2007). Pain threshold to mechanical stimuli was assessed by means of an electronic Von Frey algesimeter (Bioseb, Chaville, France). Briefly, rats were placed on a wire net platform in plastic chambers 10 min before the experiment for habituation. Then, the hindpaw plantar surface was stimulated by applying a non-noxious pointed probe slowly increasing the pressure until the rat mice withdrew the paw in response to the stimulus (Cobianchi et al., 2014). The walking track test was performed to assess locomotor function after the implant. The plantar surface of the hind paws was painted with black ink and the rat was left to freely walk along a corridor. The print length, the distance between the 1st and the 5th toes and between the 2nd and the 4th toes were measured to calculate the Sciatic Functional Index (SFI) (de Medinaceli et al., 1982).

Morphological evaluation

To evaluate the microstructure of implanted nerves and the myelinated axons, a segment of the tibial nerve was fixed in 3% glutaraldehyde-3% paraformaldehyde and postfixed in 2% OsO₄ for 2h, dehydrated through ethanol series and embedded in epon resin. Semithin sections (0.5 μm thick) were stained with toluidine blue and examined by light microscopy. To estimate the number of myelinated fibers in the tibial nerve, axons were counted in images at 100x, chosen by systematic selection and representing at least the 30% of the nerve cross-section area. The whole area of the tibial nerve was measured in 4x images, and the number of axons was estimated. Using the same sections, the thickness of the tissue capsule around the devices implanted was measured as the distance between each side of the device and the closest myelinated axon, using ImageJ software.

Transmission electron microscopy (TEM) was performed to analyze the tissue and the collagen deposition around the implanted devices. Ultrathin sections (70 nm) were cut, mounted on formvar 200 mesh copper grids and contrasted with uranyl acetate/lead citrate. Images of the area with the device were taken using a TEM microscope (JEM 1400) to evaluate the encapsulating tissue at different time points.

Immunohistochemistry

Another nerve segment containing the device implanted was serially cut (15 μm) with a cryostat (Leica CM190, Leica Microsystems). After blocking with normal donkey serum, slides were incubated overnight at 4°C with primary antibodies rabbit anti-iba1 (Wako, 191947, 1:500) for macrophages and mouse anti-CD90 clone OX-7 (BD Pharmingen, 554897, 1:150) for fibroblasts. Slides were then washed with 0.1% tween 20 buffer solution and incubated with AlexaFluor 594 donkey anti-rabbit (Invitrogen, A21207, 1:200) and 488 donkey anti-mouse (Invitrogen, A21202, 1:200) secondary antibodies for 1 h at room temperature. Finally, slides were mounted with mowiol containing DAPI (0.1 $\mu\text{g}/\text{ml}$, Sigma).

The number of infiltrating macrophages labeled with Iba1 marker was quantified using images of the whole tibial nerve. Images were taken with an epifluorescence microscope (Olympus BX51) attached to a digital camera (Olympus DP73) and equally treated to adjust brightness and contrast. The background was subtracted, and a threshold of detection and binarization was applied using ImageJ software. Iba1 positive cells in the whole tibial nerve, excluding the implanted device and tissue surrounding, were counted using the plugin “Analyze Particles” of ImageJ.

Hematoxylin-eosin staining

To determine the amount of foreign body giant cells (FBGCs) around the implant, cryostat sections were immersed in hematoxylin Harris solution (Fluka, Sigma) for 7 min, and washed in water followed by 1% HCl in ethanol solution for 20 sec. Then, sections were rewashed with water and stained with Eosin Y (Merck Millipore) for 5 min. Sections were dehydrated with series of graded ethanol rinses and mounted with DPX (Sigma). The number of FBGC was counted under the microscope in each stained section and expressed as FBGC per mm of implant width. Moreover, pictures of every FBGC were taken and the diameter was measured with ImageJ.

Cytokine protein expression

A group of animals were transcardially perfused with sterile saline after 6 hours, 1 and 4 days, 2 and 8 weeks post-implant and 1 centimeter of the sciatic nerve including the implanted device was taken, snap-frozen with liquid nitrogen and kept at -80°C. Sciatic nerves were homogenized with HEPES buffer, and the protein concentration was determined using Pierce BCA assay kit (Thermo Fisher). To ensure equal amounts of protein, all samples were diluted with HEPES to 4 $\mu\text{g}/\mu\text{l}$. Cytokines (EGF, CCL11,

Fraktalkine/CX3CL1, GCSF, GMCSF, CXCL1, IFN γ , IL1 α , IL1 β , IL2, IL4, IL5, IL6, IL10, IL12, IL13, IL17A, IL18, IP10/CXCL10, Leptin, LIX/CXCL6, MCP1/CCL2, MIP1 α /CCL3, MIP2/CXCL2, RANTES/CCL5, TNF α , VEGF-A) and TGF β (TGF β 1, TGF β 2, TGF β 3) protein levels were analyzed using the Milliplex map Rat Cytokine/Chemokine magnetic bead panel (RECYMAG65PMX27BK, Merck Millipore) or the Milliplex map TGF β magnetic bead 3 Plex Kit (TGFBMAG-64K-03, Merck Millipore), according to the manufacturer protocol. Proteins with levels lower than detection limit are not shown.

Statistical analysis

All reported values are the mean \pm SEM. Differences between groups or times were analyzed by one or two-way ANOVA followed by Bonferroni post hoc tests (GraphPad Prism). Statistical significance was considered at $p < 0.05$. For protein levels, results are expressed as the ratio with intact, sham or polyimide values in heatmaps.

RESULTS

Longitudinal neural implants do not cause damage to the implanted nerves

Alterations in nerve function were assessed by means of different functional tests. Electrophysiological tests of gastrocnemius muscle showed no differences in CMAP amplitude (Fig. 2A) or initial latency (Fig. 2B) between both Parylene C or polyimide implanted and sham animals. Moreover, Von Frey test showed no changes in pain thresholds (Fig. 2C) between groups and, according to the SFI values, implanted rats displayed normal locomotor patterns comparable to sham rats (Fig. 2D).

Histological evaluation of polyimide and Parylene C implanted nerves revealed that all the implanted devices were placed within the tibial nerve (Fig. 2E). Light microscopy observations showed a normal fascicular architecture and axonal morphology of both implanted and sham nerves, similar to intact sciatic nerves (Fig. 2E-F) and the number of myelinated fibers showed no differences between groups (Fig. 2G). Moreover, no signs of axonal degeneration or demyelination due to the surgery or the implanted device within the nerve were found, indicating that the implant model used was useful to assess the FBR to longitudinal devices, without confounding factors that might be due to tissue damage.

Nerve response and tissue capsule formation

The tissue capsule formed around the implant was evaluated under light microscopy. Whereas in the sham nerves there was no evidence of wound or tissue aggregation at any time point, the surrounding of the implant was rapidly modified in the device implanted nerves (Fig. 3A). Quantification of tissue deposition thickness around the implant showed a gradual increase from 2 days to 2 weeks post-implant and a slight decrease and compaction thereafter for both polyimide and Parylene C devices. However, while the thickness of the capsule formed around polyimide showed no changes from 4 to 32 weeks post-implant, in Parylene C devices it increased again at 16 weeks and then was stabilized up to 8 months post-implant (Fig. 3A-B).

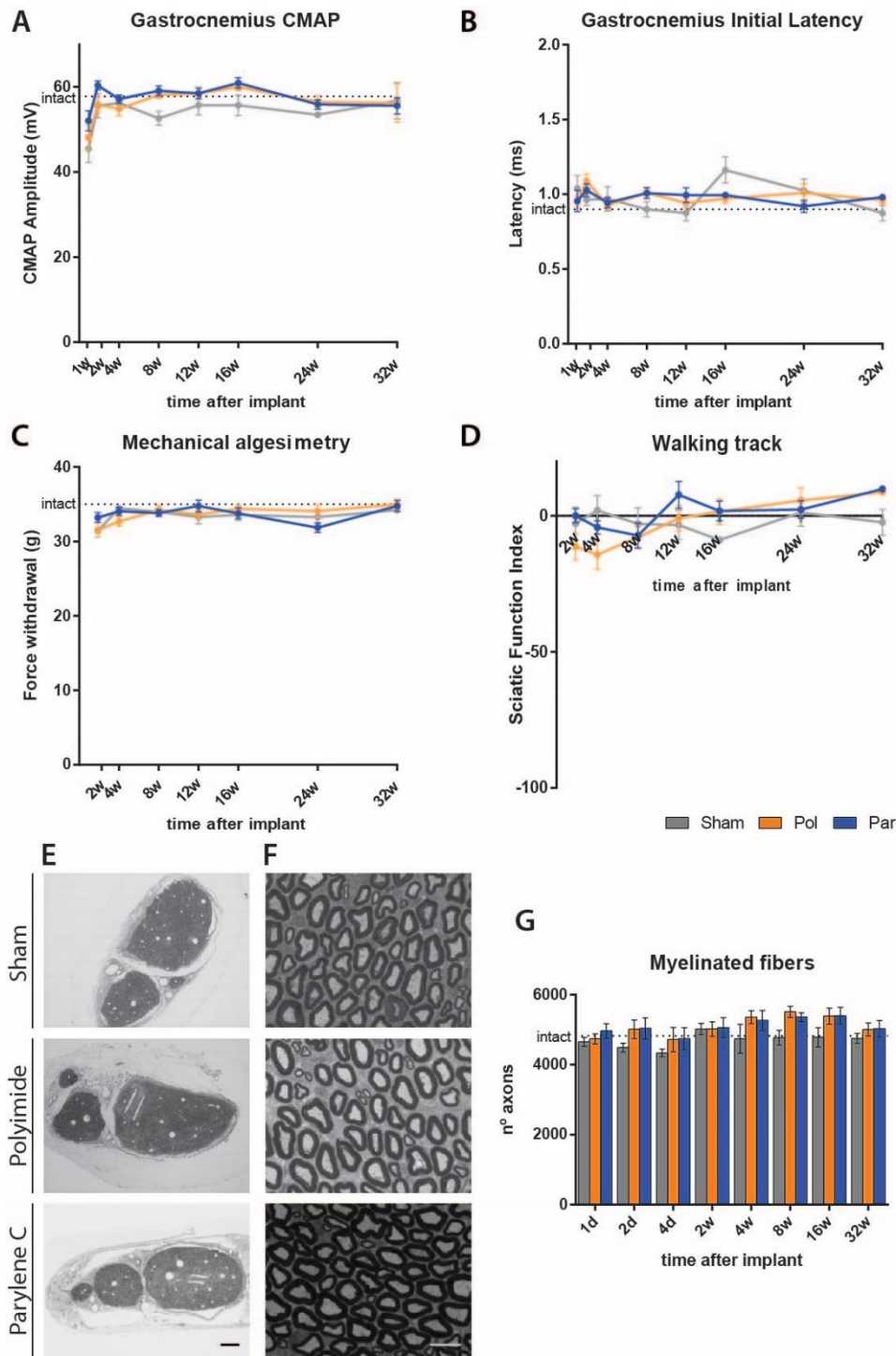


Figure 2. Functional and histological evaluation of implanted nerves. No differences were found in (A) amplitude or (B) initial latency of the gastrocnemius CMAP between Parylene C, polyimide, and sham groups. (C) No alterations in pain threshold assessed by Von Frey mechanical allgesimetry in the paw due to the surgery or the device implanted. (D) No differences in SFI values of sham and implanted animals. (E) Low and (F) high magnification of sham and polyimide and Parylene C implanted nerves. Scale bar in (E) = 150 μ m and in (F) = 10 μ m. (G) Number of myelinated fibers in the tibial nerve of rats with polyimide or Parylene C implants in comparison with the sham group. Dotted line indicates values from intact animals.

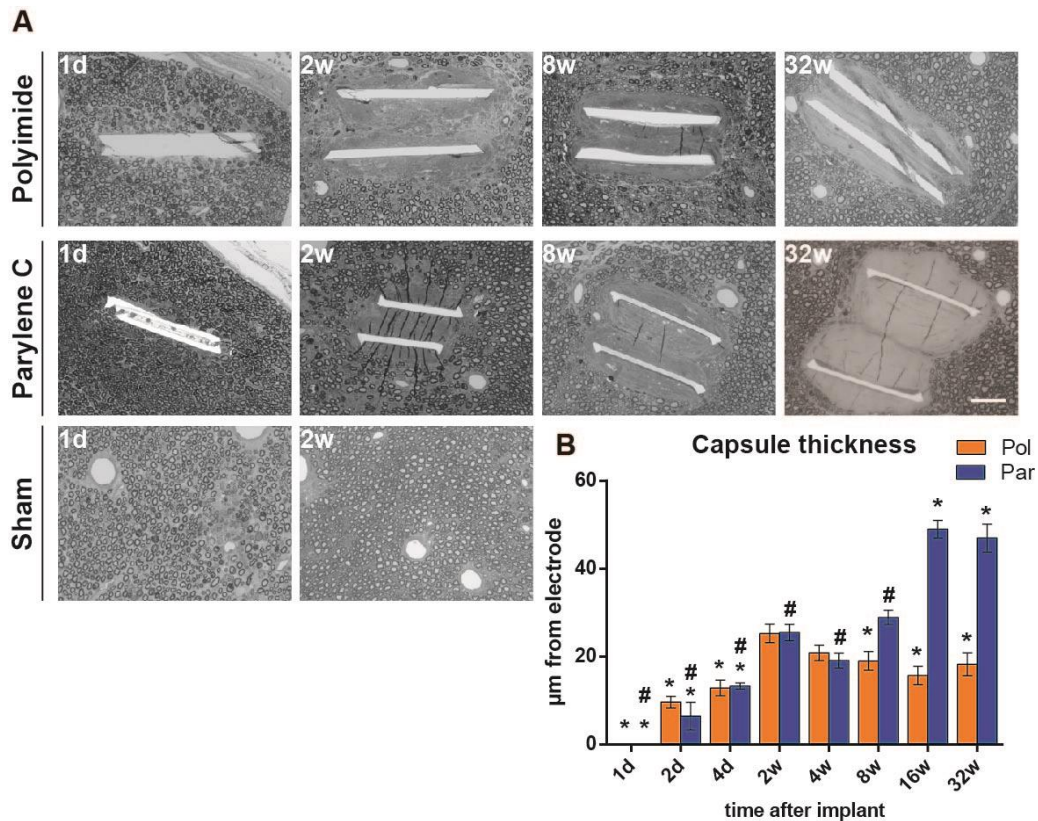


Figure 3. Progression of tissue capsule formation observed by light microscopy. (A) Representative images of capsule deposition around devices and in sham animals at different time-points. Scale bar = 50µm. (B) Increase in tissue capsule thickness over time. * $p < 0.05$ vs respective value at 2w. # $p < 0.05$ vs Parylene C at 16w.

Detailed analysis of the encapsulating tissue under light and transmission electron microscopy showed several changes in the surroundings of the device (Fig. 4). At day one only some erythrocytes could be seen near the implant and axons were still in close contact with both polyimide and Parylene C devices (Fig. 4). After 2 and 4 days, amoeboid cells were easily recognizable in the space between axons and the device embedded in a loose and disorganized matrix (Fig. 4A-B, J-K). At 2 and 4 weeks post-implant, the capsule that separated the axons and the polyimide implant appeared as a more compacted tissue containing mainly amoeboid-shaped cells and the characteristic collagen organization of the endoneurium was not distinguished in the surroundings of the implant (Fig. 4C, L). After 8 weeks, spindle-shaped cells started to appear on the edge of the capsule, in contact with axons (Fig. 4E, M). Two zones could be differentiated in the capsule: an inner area with amoeboid cells in contact with the device as in the previous time points, and an outer region composed of layers of parallel spindle-shaped cells. However, from this time point, differences between the capsules around polyimide or Parylene C devices were found. In the case of polyimide devices, disposition and thickness of the two different zones were maintained after 16 weeks, and the presence of amoeboid cells seemed to slightly decrease

(Fig. 4F). By week 32, only spindle-shape cells were seen in the polyimide capsule without presence of amoeboid cells (Fig. 4I). In contrast, after 16 weeks of Parylene C devices implantation, although the inner area remained more or less similar, the outer zone appeared thicker and with more spindle-shape cells present than seen on polyimide implants (Fig. 4N). After 8 months post-implant, the tissue around the device appeared as a compact and organized matrix with spindle-shape cells and some amoeboid cells in the inner zone (Fig. 4O). The changes in the cellular type from 8 to 32 weeks were related with a progressive organization of the extracellular matrix of the capsule in both groups, with an increasing deposition and organization of collagenous fibers that invaded the area occupied by spindle-shaped cells (Fig. 4G-I, R-U). This was more obvious by week 16 in the case of Parylene C devices, when in the inner area amoeboid cells occupied all the space (Fig. 4S) while most of the outer zone was full of collagen fibers (Fig. 4T).

Cellular characterization of the FBR

To evaluate the inflammatory response due to the surgery or the implant, we assessed the presence of Iba1 labeled macrophages in the whole tibial nerve. Whereas in intact nerves a few macrophages were seen, the number of Iba1 positive macrophages started to increase within the implanted nerves one day after surgery in device implanted and in sham nerves (Fig. 5A). The inflammatory response caused solely by the surgery, evaluated in sham rats with no implant left within the nerve, peaked at 4 days and decreased noticeably at 2 and 4 weeks, reaching similar values than intact animals from week 8 onwards (Fig. 5B). In contrast, the inflammatory reaction due to implanted devices peaked at 2 weeks and took more time to resolve, with a slight decrease at 4 weeks that persisted 8 weeks after the implant for both materials. Finally, at weeks 16 and 32, the number of macrophages showed a further decrease but with still significantly more Iba1+ cells than sham and intact animals (Fig. 5B).

To further investigate how the tissue capsule is formed around the implant, we focused on the two main cell populations involved in the FBR process: macrophages and fibroblasts (Anderson, 2016). In the host response in the implanted peripheral nerves, macrophages were the first cells to arrive (Fig. 6A, I) and rapidly surrounded the device from day 2-4 up to 4 weeks after implant (Fig. 6B-E, J-M). Indeed, after 2 and 4 weeks, the capsule around the device was mainly formed by compacted macrophagic cells expressing Iba1 in close contact with the device, in a similar disposition of the round-shape cells observed by TEM in figure 4. By week 8, some CD90+ fibroblasts started to appear in the edge of the capsule for both materials, between the inner macrophage layer and the

Polyimide

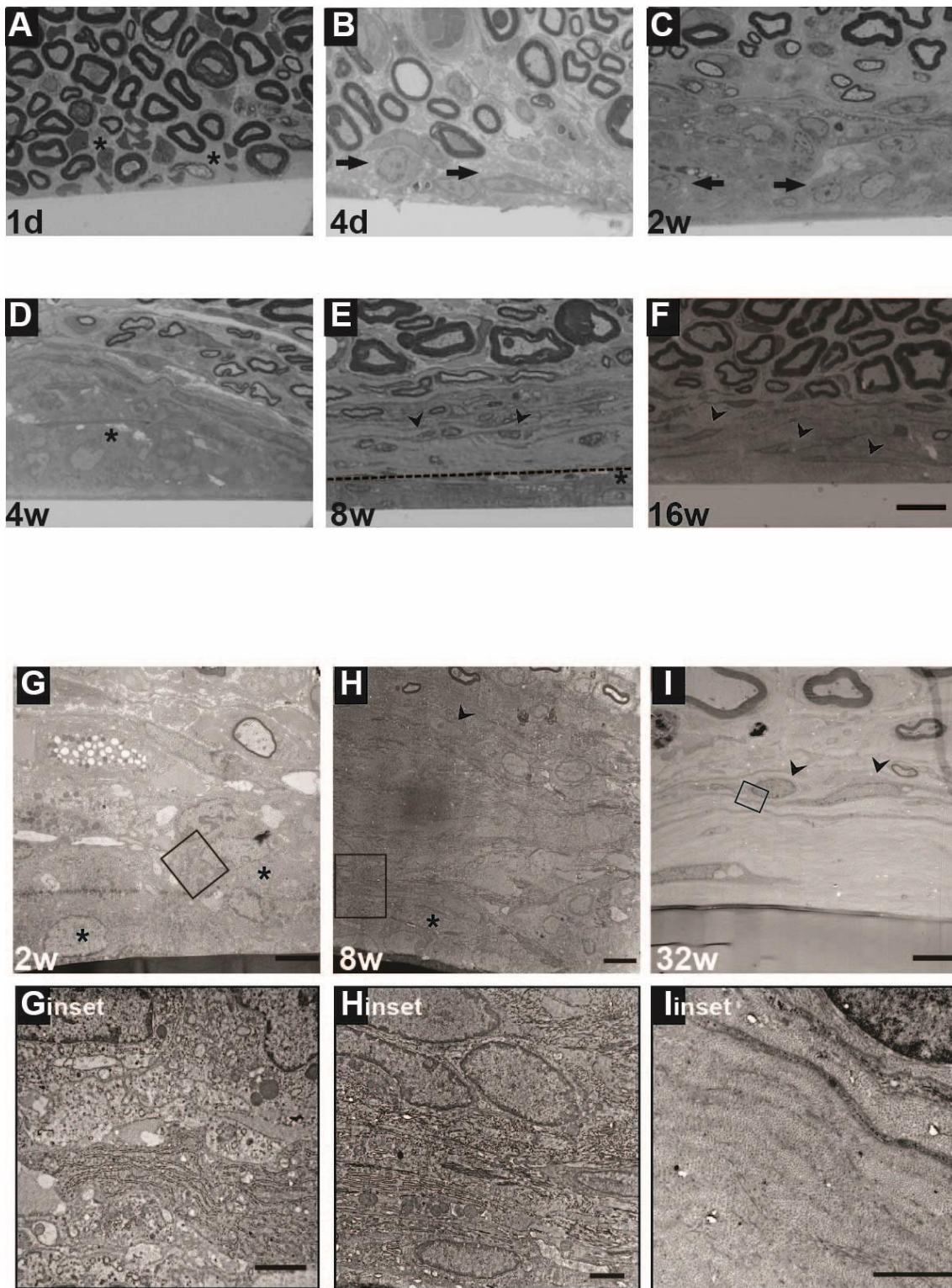
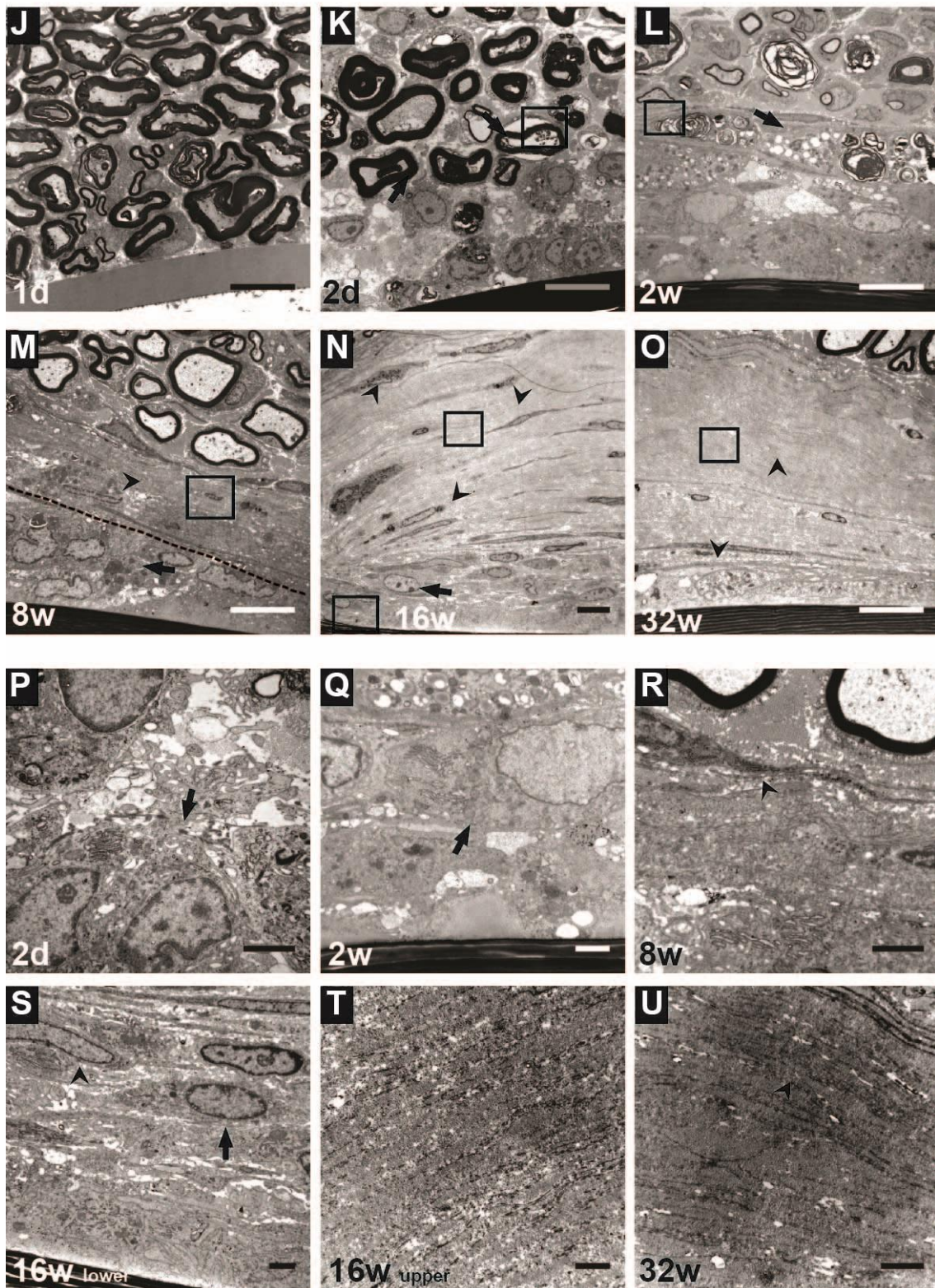


Figure 4. Detailed evaluation of tissue capsule by light and transmission microscopy. Representative images of tissue capsule changes around (A-F) polyimide and (M-O) Parylene C devices. Scale bar = 10µm. At (A, J) 1 day, (B, K) 2-4 days and (C, L) 2 weeks only erythrocytes (asterisks) and amoeboid cells (arrows) were seen in the vicinity of the device. From (E, M) week 8, two different zones can be distinguished within the capsule (dotted line), *(continued on the next page)*

Parylene C



(continued from previous page) with spindle-shaped cells localized in the periphery of the capsule (arrowheads). After (F, N-O) 16 and 32 weeks post-implant, the capsule was mainly formed by spindle-shape cells and collagen fibers (insets, I, R-U). Insets show the progressive change from (G, P-Q) amoeboid cells at early time points to (H-I, R-U) spindle-shape cells, together with an increase in collagen deposition from 8 weeks. Scale bar = 2 μ m.

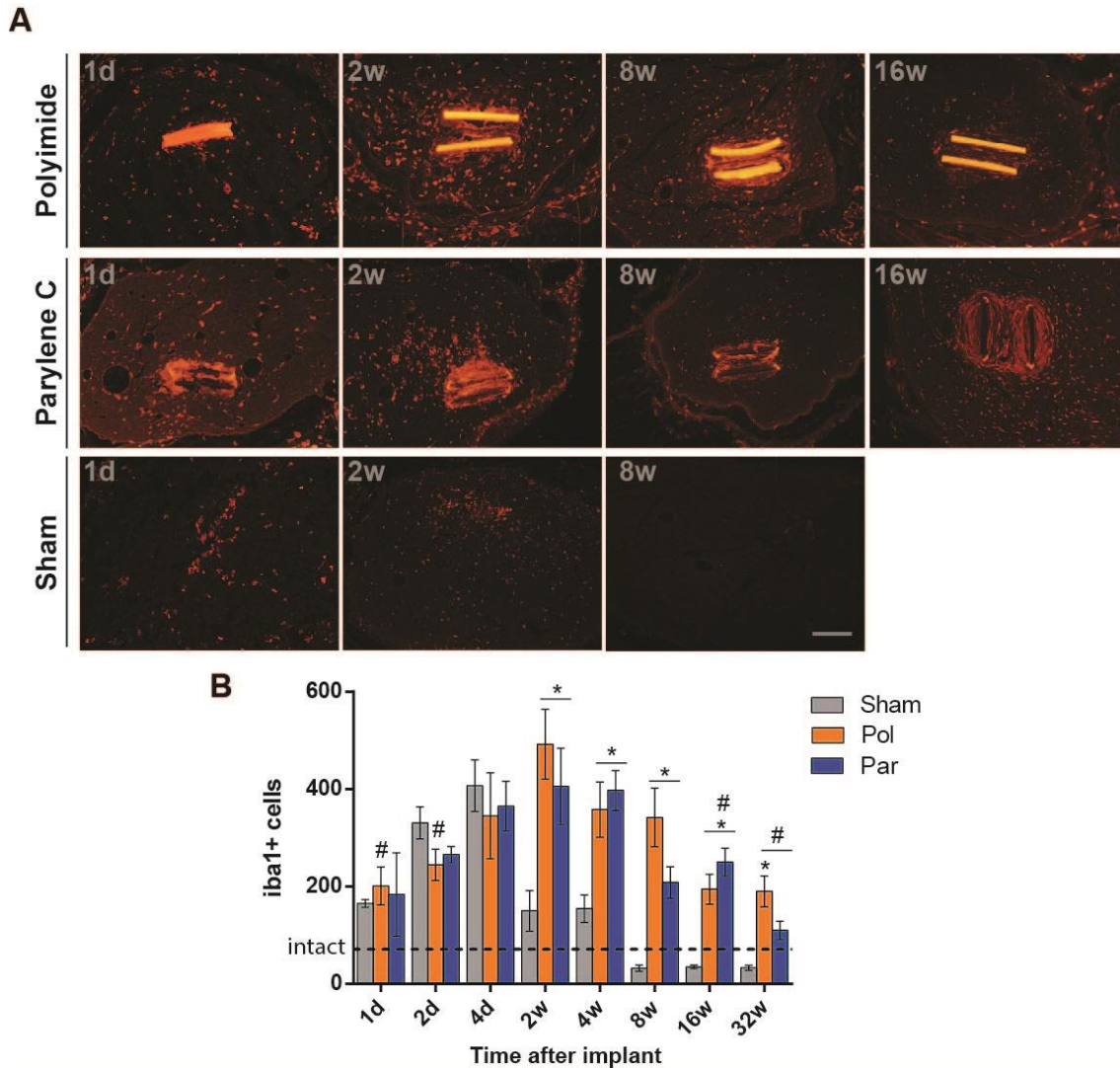


Figure 5. Iba1 labeling for infiltrating macrophages in the tibial nerve. (A) Representative images of implanted and sham nerves at different time-points. Scale bar = 100 μ m. (C) Number of Iba1 positive cells in the whole tibial nerve over time. * $p < 0.05$ vs sham animals. # $p < 0.05$ vs 2w implanted.

surrounding nerve fibers (Fig. 6F, N), confirming the observations of light and electron microscopy. After 16 weeks, while the number of cells in the polyimide capsule seemed to decrease (Fig. 6G), a higher organization of Iba1 positive cells could be appreciated in the Parylene C capsule, being these cells flattened (Fig. 6O). After 32 weeks of implant, most cells in the capsule were CD90+ fibroblasts within a well-organized extracellular matrix for both materials, without presence of Iba1+ cells (Fig 6H, P) and a higher number of CD90+ cells was observed in Parylene C than in polyimide surrounding capsule.

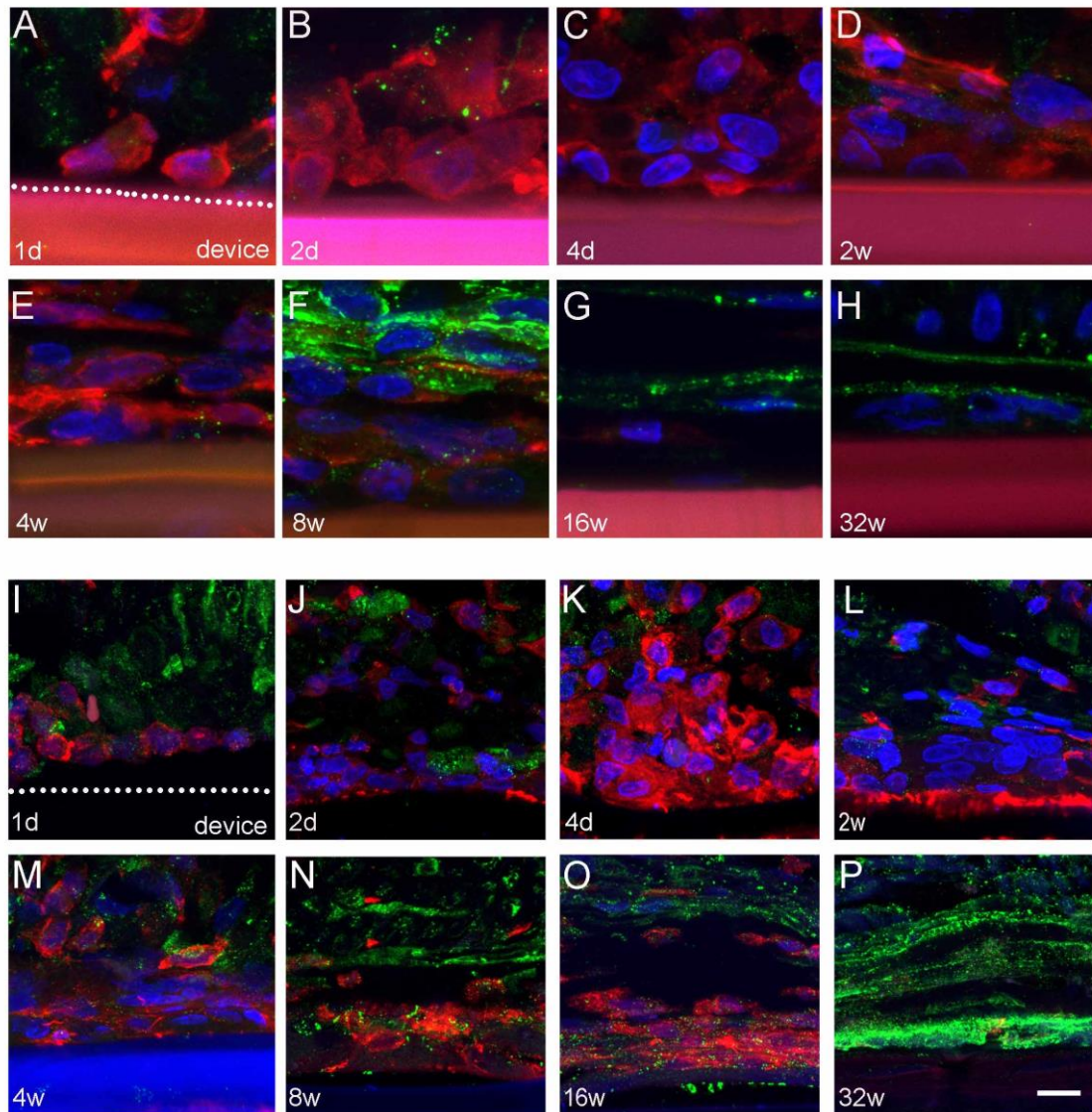


Figure 6. Cellular integration of the capsule visualized under confocal imaging. Representative images of Iba1 and CD90 labeling in the capsule of (A-H) polyimide and (I-P) Parylene C devices. Only Iba1+ macrophages were observed from 1 day to 4 weeks post-implant. From 8 to 16 weeks, CD90+ fibroblasts were located in the periphery of the capsule, and by week 32w, CD90+ fibroblasts occupied most of the area of the capsule for both materials. Scale bar = 5 μ m.

The amount of FBGCs (Fig. 7A) was also measured as another hallmark of the FBR. These cells resulting from macrophage fusion appeared soon after the device implantation and increased in number over time (Fig. 7B) for both materials. The FBGCs seen in this model had many nuclei mainly in the cellular periphery, as expected with the presence of foreign bodies (McNally and Anderson, 2011). By week 2 these cells were easily recognized around the implant, becoming stabilized in number and size (Fig. 7B-C) up to 8 weeks. From week 16 onwards, the amount of these cells remained stable and it was slightly increase at 32 weeks in the capsule around both materials.

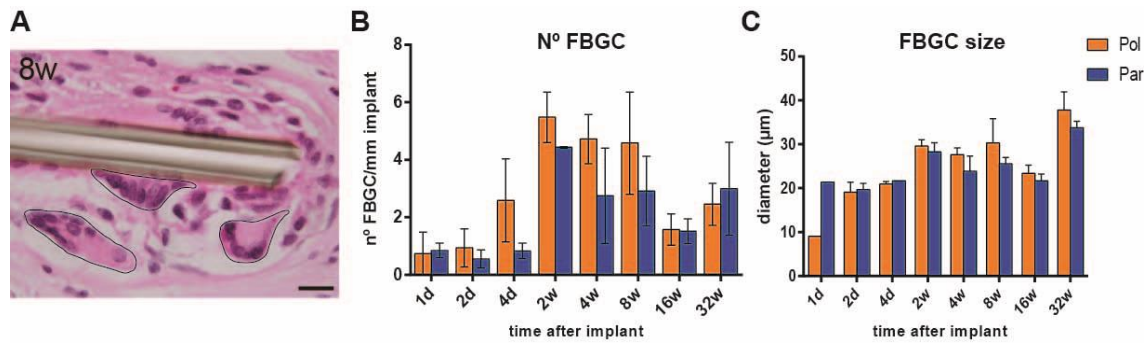


Figure 7. FBGCs presence in the capsule. (A) Representative photograph of FBGCs due to FBR at 8 weeks around an implanted polyimide device. Scale bar = 20μm. Changes in (B) number and (C) diameter of FBGCs over time for both materials.

Molecular environment of the FBR

Although the inflammatory pattern in Parylene C and polyimide implanted nerves is similar, the tissue deposition dynamics appears to be different. To further characterize the immune response to devices implanted in the peripheral nerve and to compare the response between these two materials, cytokines and TGFβ levels were quantified using Luminex technology from 6 hours to 8 weeks of implantation.

The analysis showed an increase for most of the studied factors at 6 hours and 1 day after surgery in the implanted (Fig. 8A-A', B-B') and sham (Fig. 8C-C') animals in comparison to intact nerves, and levels for most cytokines recovered to control values from 4 days onwards. On the other hand, there were no differences in the levels of the main pro-inflammatory, anti-inflammatory or tissue-remodeling factors between sham animals and Parylene C (Fig. 9A-A') or polyimide (Fig. 9B-B') implanted nerves with the exception of an increase in the levels of CCL2 and CCL3 in both materials in comparison to sham animals at chronic time points. Moreover, a comparison between materials was performed, but the analysis did not point out any different factor at any time point between the response to Parylene C or polyimide devices (Fig. 9C-C'). Some interleukins such as IL1a, IL1b, IL17A, and IL13 showed disparate values at 6 hours and 1 day after implant in comparison with polyimide devices. At chronic time points, there were no clear differences between materials in any of the studied cytokines. MIP2/CXCL2 was the only one to show different levels between Parylene C and polyimide from 4 days to 8 weeks, although there were no statistical differences.

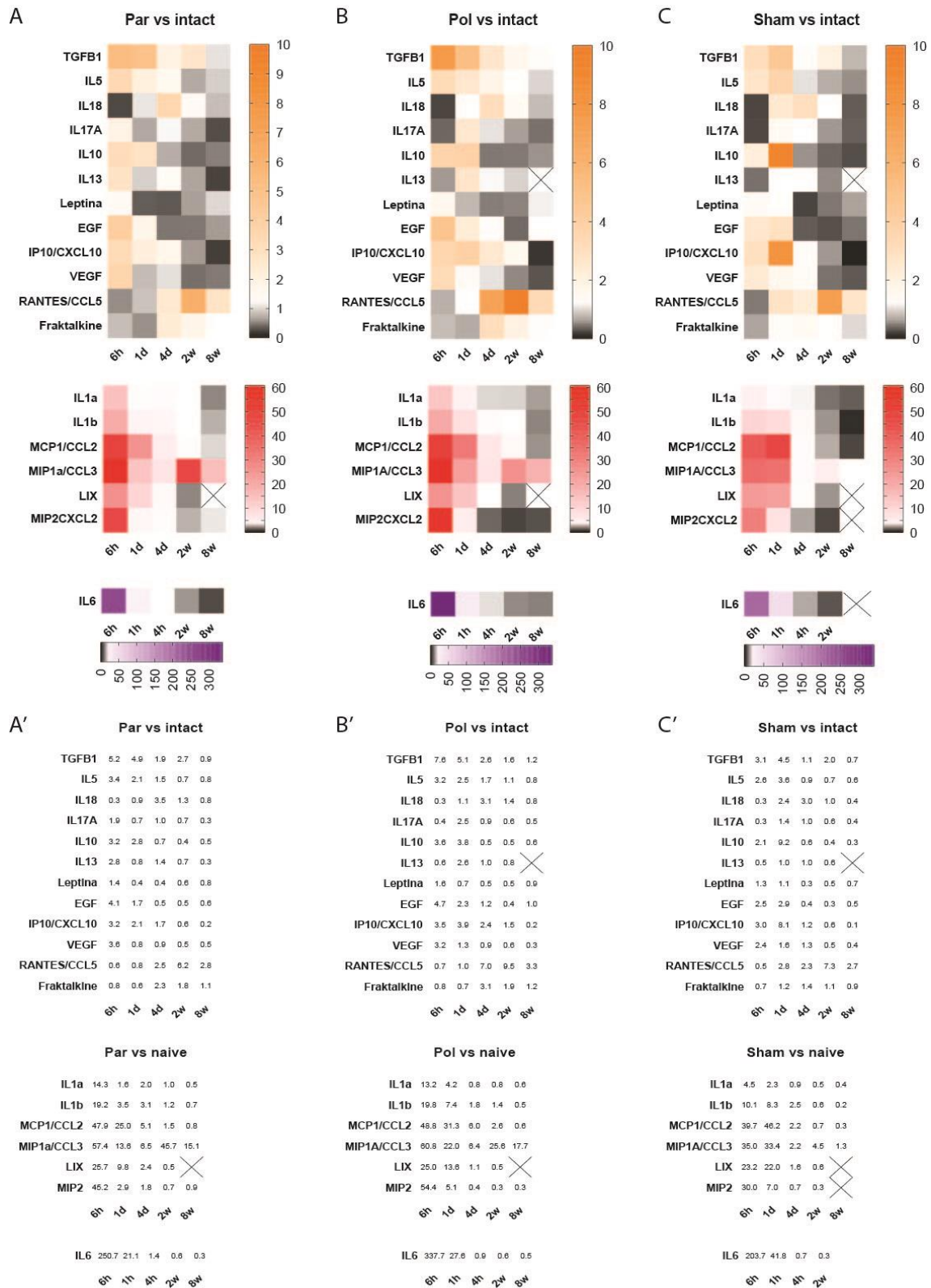


Figure 8. Dynamic changes of cytokine levels after sham or device implantation in comparison to intact nerves. Heatmaps (A-C) and ratio values (A'-C') showing the changes in protein levels of relevant pro-inflammatory, anti-inflammatory and tissue remodeling-related factors in (A, A') Parylene, (B, B') polyimide and (C, C') sham implanted nerves. Results expressed as the mean of the ratio between each group and intact values. Crossed out squares means no protein detected.

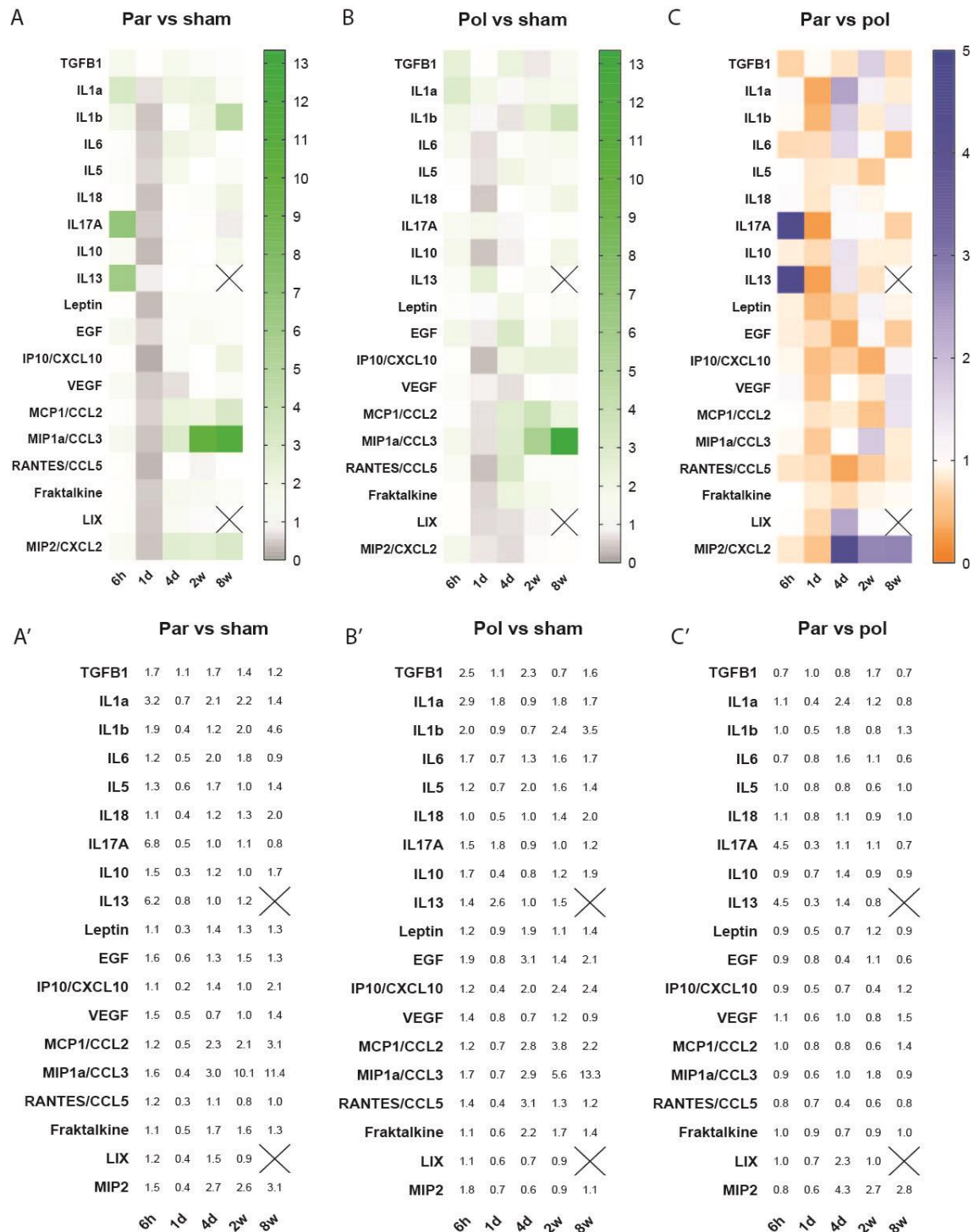


Figure 9. Cytokine levels analyzed by Milliplex map. Heatmaps and ratio values showing the changes in different proteins at different time points in (A-A') Parylene C and (B-B') polyimide implanted animals versus sham animals. Results expressed as the mean of the ratio between each group and sham values. (C) Heatmap and (C') ratio values representing the changes in Parylene C implanted nerves with respect to polyimide implanted nerves. Results expressed as the mean of the ratio between Parylene C and polyimide values. Crossed out squares means no protein detected.

Discussion

The FBR is the first response of the immune system after the implant of any device in the body (Anderson et al., 2008; Luttikhuisen et al., 2006) and it includes an inflammatory response and the tissue encapsulation of the implanted device (Kenneth Ward, 2008; Sheikh et al., 2015). The peripheral nervous system is not an exception (Lago et al., 2007) and it is a severe problem when the active sites of implanted intraneural interfaces have to be in close contact with nerve fibers to have a proper functionality. Although many studies have reported good results regarding stimulation and recording of nerve signals in short-term studies, a progressive loss of function of intraneural electrodes that reduces the useful life of the interface has been reported (Raspopovic et al., 2014; Rossini et al., 2010; Wark et al., 2014; Warwick et al., 2003). The encapsulating tissue reduces the amplitude of recordable axonal impulses and increases the intensity needed for axonal excitation due to the interposition of the fibrous tissue between the active sites in the electrode and the axons. Although stimulation can be maintained over time at the cost of increasing the intensity of stimuli (Raspopovic et al., 2014), recording of nerve signals is more critically affected given the low amplitude, in the range of microvolts, of axonal impulses recorded extracellularly (Bisoni et al., 2017). Provided these signals cannot be increased, the amplitude and quality of signal recordings decline as the distance between the active sites and axons is increased (Kamondi et al., 1998). However, whereas the rationale to explain the functional decrease in chronic electrodes has been hypothesized and modeled (Micera et al., 2010; Raspopovic et al., 2011), the exact mechanisms that explain the possible role of the FBR in electrode failure have not yet been elucidated (Raspopovic et al., 2017).

Some reports have previously characterized the FBR to nerve electrodes in cats (Christensen et al., 2014) and humans (Christensen et al., 2016), but these studies were conducted after the implantation of rigid multielectrode Utah slanted arrays, and the stiffness of these electrodes has been reported to contribute to traumatic nerve injuries due to mechanical tension, increasing the FBR (Lacour et al., 2010). Thus, the use of passive non-functional longitudinal devices and the absence of wires that may induce some tethering forces in the nerve (Navarro et al., 2005) avoids external artifacts in the creation of a FBR and focus only in the material reaction in comparison with those studies that used wired or active electrodes (Christensen et al., 2016, 2014; Wark et al., 2014; Wurth et al., 2017). The results exposed in this work describe in detail the progression of the FBR to longitudinal intraneural devices fabricated with polyimide or Parylene C, two polymers used as a substrate for neural electrodes (Boretius et al., 2010; Cutrone et al., 2015; Mueller et al., 2017).

Unlike other fibrotic responses in pathological conditions where scar tissue impairs proper function of the organ (Duffield, 2014; Gross and Hunninghake, 2001), our results showed that the new tissue formation in the peripheral nerve does not have a negative impact on its function after careful implantation. No alterations in nerve conduction, nociception or locomotion were observed due to implanted devices along eight months follow-up. These results were corroborated by histological observations of implanted and sham nerves, where the regular fascicular architecture was preserved, and no evidence of axonal damage or distal degeneration were observed at all the studied time points. Taking into account that the model used is a longitudinal device, these results are not surprising according to previous studies with longitudinal electrodes (Lago et al., 2007). Besides, these results confirm the biocompatible characteristics of both materials (Chang et al., 2007; Richardson et al., 1993).

Regarding the progression of the FBR, several studies, mainly with subcutaneous and intraperitoneal implants (Anderson et al., 2008; Kenneth Ward, 2008; Sheikh et al., 2015), have shown that it has a first inflammatory phase followed by an anti-inflammatory and tissue remodeling phase. Here we have observed a similar pattern to that reported in other peripheral nerve FBR studies (Christensen et al., 2016, 2014; Wurth et al., 2017). Whereas in the sham group the inflammatory reaction was low and resolved rapidly, inflammation was longer in time in both implanted groups. Inflammatory macrophages surrounded the device after 1 day, generating a cellular capsule that peaks in thickness after 2 weeks (Fig. 3B), coinciding with the maximum inflammatory reaction (Fig. 5B). However, while the inflammatory reaction was solved by week 8 in both implanted materials, the formation of the capsule evolved differently between materials. In the case of polyimide devices, the thickness of the capsule peaked at 2 weeks and then decreased until stabilization after 8 weeks. In contrast, capsule around Parylene C devices also peaked after 2 weeks but continued increasing up to a maximum after 16 weeks. Therefore, these results indicate that Parylene C promotes a slightly different pattern of FBR than polyimide.

During the first phase of the FBR, tissue damage from the implantation and protein adsorption to the device surface stimulate resident nerve macrophages and recruitment and infiltration of macrophages and polymorphonuclear cells into the nerve. These cells try to phagocyte the foreign body. If this is not possible, macrophages fuse to generate FBGCs, a hallmark of the response to non-degradable implants. This leads to the second phase, in which FBGCs and recruited fibroblasts isolate the device generating a capsule. Hence, the general pattern of the FBR for non-degradable implants is a switch from a pro-inflammatory to an anti-inflammatory and tissue deposition environment (Doloff et al., 2017; Vince et al.,

2005). However, a slight independence from the inflammatory phase seems to occur with Parylene C devices. Thus, despite the inflammatory reaction decreases, the tissue deposition continues increasing. This scenario implies a difference between the response in the whole implanted nerve and the local response around the implant. Thus, the inflammation in the nerve is solved after 8 weeks (i.e. reduced Iba1+ cells), but it is maintained in areas surrounding the implant (i.e. tissue capsule). When fibroblasts start to surround the implant and to deposit collagen between 8 and 16 weeks post-implant, the macrophages remain in the inner zone and continue stimulating fibroblast recruitment and collagen deposition. In fact, higher number of fibroblasts was observed around Parylene C devices after 32 weeks. The reason for such stronger macrophage activation phase with Parylene C implants needs further analysis. Differences in FBR can have their origin in differences in the surface or chemical structure of polyimide and Parylene C (Ordóñez et al., 2012; Veisheh et al., 2015; Zhou et al., 2016). While the aromatic rings in the polyimide are in stable configurations, Parylene C is known to have non-saturated radicals at the carbon atoms that might result in different surface potentials (Zeta-potential) that influence interaction with proteins at the material-tissue interface (Goda et al., 2007; Myllymaa et al., 2010).

Molecular analyses were also performed to clarify if there were differences regarding the mediators inducing the cellular events. However, no changes in the amount of several inflammation-related cytokines were observed between Parylene C and polyimide implants at any time point, which were also similar to sham-implanted nerves. In our results, as well as in most injury models, the highest levels of cytokines are normally produced within the first hours or days after a tissue injury (Baldwin and Hunt, 2008; Luttkhuizen et al., 2006; Rodríguez et al., 2009). Moreover, in our model, the levels of the cytokines were already decreased by 2 weeks when the injury of the implantation is mainly resolved. Intriguingly, CCL3 and CCL5 have been found as potential targets to pharmacologically reduce the tissue deposition around implanted devices since they were increased compared with sham nerves. It has been shown that CCL3/MIP1 α (macrophage inflammatory protein 1) and CCL5/RANTES recruit polymorphonuclear cells and macrophages (Luttkhuizen et al., 2006; Rodríguez et al., 2009; Sahin and Wasmuth, 2013), thus increasing the first inflammatory phase of the FBR to implanted devices. On the other hand, CXCL2 levels are also increased in Parylene C in comparison to polyimide implanted nerves at chronic time points, although no significant, so further analyses are needed to clarify the differences between both materials.

In conclusion, our results show how the FBR against a polyimide or a Parylene C implant in the peripheral nerve occurs and which are the main players. It should be taken

into account that the specificities of the FBR seem to be determined not only by the tissue in which the device is implanted but also by the material implanted (Boddupalli et al., 2016). Thus, differences between the FBR to both materials have been found, particularly in the chronic phase. The understanding of these changes will let to a better development of new strategies that would reduce the FBR against intraneural implants and thus lengthen their lifespan.

ACKNOWLEDGEMENTS

This research was supported by the European Union FPT-ICT project NEBIAS under contract number 611687, FEDER funds, and TERCEL (RD12/0019/0011) and CIBERNED (CB06/05/1105) funds from the Instituto de Salud Carlos III of Spain. The ICN2 is funded by the CERCA programme / Generalitat de Catalunya, and it is also supported by the Severo Ochoa programme of the Spanish Ministry of Economy, Industry, and Competitiveness (MINECO, grant no. SEV-2013-0295). The authors thank Monica Espejo and Jessica Jaramillo for the technical help and Servei de Microscopia (UAB) for help with TEM images.

REFERENCES

- Anderson, J.M., 2016. Future challenges in the *in vitro* and *in vivo* evaluation of biomaterial biocompatibility. *Regen. Biomater.* rbw001. <https://doi.org/10.1093/rb/rbw001>
- Anderson, J.M., Rodriguez, A., Chang, D.T., 2008. Foreign body reaction to biomaterials. *Semin. Immunol.* <https://doi.org/10.1016/j.smim.2007.11.004>
- Badia, J., Boretius, T., Andreu, D., Azevedo-Coste, C., Stieglitz, T., Navarro, X., 2011a. Comparative analysis of transverse intrafascicular multichannel, longitudinal intrafascicular and multipolar cuff electrodes for the selective stimulation of nerve fascicles. *J. Neural Eng.* 8, 36023. <https://doi.org/10.1088/1741-2560/8/3/036023>
- Badia, J., Boretius, T., Pascual-Font, A., Udina, E., Stieglitz, T., Navarro, X., 2011b. Biocompatibility of chronically implanted transverse intrafascicular multichannel electrode (TIME) in the rat sciatic nerve. *IEEE Trans. Biomed. Eng.* 58, 2324–2332. <https://doi.org/10.1109/TBME.2011.2153850>
- Baldwin, L., Hunt, J.A., 2008. The *in vivo* cytokine release profile following implantation. *Cytokine* 41, 217–222. <https://doi.org/10.1016/j.cyto.2007.11.015>
- Biran, R., Martin, D.C., Tresco, P.A., 2005. Neuronal cell loss accompanies the brain tissue response to chronically implanted silicon microelectrode arrays. *Exp. Neurol.* 195, 115–126. <https://doi.org/10.1016/j.expneurol.2005.04.020>
- Bisoni, L., Carboni, C., Puddu, R., Barabino, G., Pani, D., Raffo, L., Mueller, M., Stieglitz, T., del Valle, J., De La Oliva, N., Delgado-Martínez, I., Navarro, X., Barbaro, M., 2017. A 64-channels neural interface for biopotentials recording and PNS stimulation, in: *Proceedings of the Annual International Conference of the IEEE Engineering in Medicine and Biology Society, EMBS.* pp. 1938–1941. <https://doi.org/10.1109/EMBC.2017.8037228>
- Blakney, A.K., Swartzlander, M.D., Bryant, S.J., 2012. The effects of substrate stiffness on the *in vitro* activation of macrophages and *in vivo* host response to poly(ethylene glycol)-based hydrogels. *J. Biomed. Mater. Res. - Part A* 100 A, 1375–1386. <https://doi.org/10.1002/jbm.a.34104>
- Boddupalli, A., Zhu, L., Bratlie, K.M., 2016. Methods for Implant Acceptance and Wound Healing: Material Selection and Implant Location Modulate Macrophage and Fibroblast Phenotypes. *Adv. Healthc. Mater.* <https://doi.org/10.1002/adhm.201600532>
- Boretius, T., Badia, J., Pascual-Font, A., Schuettler, M., Navarro, X., Yoshida, K., Stieglitz, T., 2010. A transverse intrafascicular multichannel electrode (TIME) to interface with the peripheral nerve. *Biosens. Bioelectron.* 26, 62–69. <https://doi.org/10.1016/j.bios.2010.05.010>
- Branner, A., Normann, R.A., 2000. A multielectrode array for intrafascicular recording and

- stimulation in sciatic nerve of cats. *Brain Res. Bull.* 51, 293–306. [https://doi.org/10.1016/S0361-9230\(99\)00231-2](https://doi.org/10.1016/S0361-9230(99)00231-2)
- Branner, A., Stein, R.B., Normann, R.A., 2001. Selective Stimulation of Cat Sciatic Nerve Using an Array of Varying-Length Microelectrodes. *J. Neurophysiol.* 85.
- Chang, T.Y., Yadav, V.G., De Leo, S., Mohedas, A., Rajalingam, B., Chen, C.L., Selvarasah, S., Dokmeci, M.R., Khademhosseini, A., 2007. Cell and protein compatibility of parylene-C surfaces. *Langmuir* 23, 11718–11725. <https://doi.org/10.1021/la7017049>
- Chen, X., Young, D., 2016. Robust implantable blood pressure sensor packaging for long-term laboratory animals monitoring, in: 2016 IEEE SENSORS. IEEE, pp. 1–3. <https://doi.org/10.1109/ICSENS.2016.7808969>
- Christensen, M.B., Pearce, S.M., Ledbetter, N.M., Warren, D.J., Clark, G.A., Tresco, P.A., 2014. The foreign body response to the Utah Slant Electrode Array in the cat sciatic nerve. *Acta Biomater.* 10, 4650–4660. <https://doi.org/10.1016/j.actbio.2014.07.010>
- Christensen, M.B., Wark, H.A., Hutchinson, D.T., 2016. A histological analysis of human median and ulnar nerves following implantation of Utah slanted electrode arrays. *Biomaterials* 77, 235–242. <https://doi.org/10.1016/j.biomaterials.2015.11.012>
- Clark, G.A., Ledbetter, N.M., Warren, D.J., Harrison, R.R., 2011. Recording sensory and motor information from peripheral nerves with Utah Slanted Electrode Arrays. *Proc. Annu. Int. Conf. IEEE Eng. Med. Biol. Soc. EMBS* 4641–4644. <https://doi.org/10.1109/IEMBS.2011.6091149>
- Clark, G.A., Wendelken, S., Page, D.M., Davis, T., Wark, H.A.C., Normann, R.A., Warren, D.J., Hutchinson, D.T., 2014. Using multiple high-count electrode arrays in human median and ulnar nerves to restore sensorimotor function after previous transradial amputation of the hand. 2014 36th Annu. Int. Conf. IEEE Eng. Med. Biol. Soc. EMBC 2014 1977–1980. <https://doi.org/10.1109/EMBC.2014.6944001>
- Cobianchi, S., de Cruz, J., Navarro, X., 2014. Assessment of sensory thresholds and nociceptive fiber growth after sciatic nerve injury reveals the differential contribution of collateral reinnervation and nerve regeneration to neuropathic pain. *Exp. Neurol.* 255, 1–11. <https://doi.org/10.1016/j.expneurol.2014.02.008>
- Cutrone, A., Del Valle, J., Santos, D., Badia, J., Filippeschi, C., Micera, S., Navarro, X., Bossi, S., 2015. A three-dimensional self-opening intraneural peripheral interface (SELINe). *J. Neural Eng.* 12, 16016. <https://doi.org/10.1088/1741-2560/12/1/016016>
- de Medinaceli, L., Freed, W.J., Wyatt, R.J., 1982. An index of the functional condition of rat sciatic nerve based on measurements made from walking tracks. *Exp. Neurol.* 77, 634–643. [https://doi.org/10.1016/0014-4886\(82\)90234-5](https://doi.org/10.1016/0014-4886(82)90234-5)

- del Valle, J., Navarro, X., 2013. Interfaces with the peripheral nerve for the control of neuroprostheses. *Int. Rev. Neurobiol.* 109, 63–83. <https://doi.org/10.1016/B978-0-12-420045-6.00002-X>
- Doloff, J.C., Veiseh, O., Vegas, A.J., Tam, H.H., Farah, S., Ma, M., Li, J., Bader, A., Chiu, A., Sadraei, A., Aresta-Dasilva, S., Griffin, M., Jhunjhunwala, S., Webber, M., Siebert, S., Tang, K., Chen, M., Langan, E., Dholokia, N., Thakrar, R., Qi, M., Oberholzer, J., Greiner, D.L., Langer, R., Anderson, D.G., 2017. Colony stimulating factor-1 receptor is a central component of the foreign body response to biomaterial implants in rodents and non-human primates. *Nat. Mater.* <https://doi.org/10.1038/nmat4866>
- Duffield, J.S., 2014. Cellular and molecular mechanisms in kidney fibrosis. *J. Clin. Invest.* 124, 2299–2306. <https://doi.org/10.1172/JCI72267.a>
- Fet, N., Alizai, P.H., Fragoulis, A., Wruck, C., Pufe, T., Tolba, R.H., Neumann, U.P., Klinge, U., 2014. In vivo characterisation of the inflammatory reaction following mesh implantation in transgenic mice models. *Langenbecks. Arch. Surg.* 399, 579–88. <https://doi.org/10.1007/s00423-014-1192-8>
- Goda, T., Konno, T., Takai, M., Ishihara, K., 2007. Photoinduced phospholipid polymer grafting on Parylene film: Advanced lubrication and antibiofouling properties. *Colloids Surfaces B Biointerfaces* 54, 67–73. <https://doi.org/10.1016/j.colsurfb.2006.09.006>
- Gretzer, C., Emanuelsson, L., Liljensten, E., Thomsen, P., 2006. The inflammatory cell influx and cytokines changes during transition from acute inflammation to fibrous repair around implanted materials. *J. Biomater. Sci. Polym. Ed.* 17, 669–687. <https://doi.org/10.1163/156856206777346340>
- Gross, T.J., Hunninghake, G.W., 2001. Idiopathic pulmonary fibrosis. *English J.* 345, 517–525. <https://doi.org/10.1056/NEJMra003200>
- Haggren, T., Shah, A., Autere, A., Kakko, J.-P., Dhaka, V., Kim, M., Huhtio, T., Sun, Z., Lipsanen, H., 2017. Nanowire encapsulation with polymer for electrical isolation and enhanced optical properties. *Nano Res.* 1–10. <https://doi.org/10.1007/s12274-017-1468-8>
- Kamondi, A., Acsády, L., Buzsáki, G., 1998. Dendritic spikes are enhanced by cooperative network activity in the intact hippocampus. *J. Neurosci.* 18, 3919–3928.
- Kastellorizios, M., Papadimitrakopoulos, F., Burgess, D.J., 2015. Multiple tissue response modifiers to promote angiogenesis and prevent the foreign body reaction around subcutaneous implants. *J. Control. Release* 214, 103–11. <https://doi.org/10.1016/j.jconrel.2015.07.021>
- Kenneth Ward, W., 2008. A review of the foreign-body response to subcutaneously-implanted devices: the role of macrophages and cytokines in biofouling and fibrosis. *J. Diabetes Sci. Technol.* 2, 768–77. <https://doi.org/10.1177/193229680800200504>

- Kim, B.J., Meng, E., 2016. Micromachining of Parylene C for bioMEMS. *Polym. Adv. Technol.* 27, 564–576. <https://doi.org/10.1002/pat.3729>
- Lacour, S.P., Benmerah, S., Tarte, E., FitzGerald, J., Serra, J., McMahon, S., Fawcett, J., Graudejus, O., Yu, Z., Morrison, B., 2010. Flexible and stretchable micro-electrodes for in vitro and in vivo neural interfaces. *Med. Biol. Eng. Comput.* 48, 945–54. <https://doi.org/10.1007/s11517-010-0644-8>
- Lago, N., Yoshida, K., Koch, K.P., Navarro, X., 2007. Assessment of biocompatibility of chronically implanted polyimide and platinum intrafascicular electrodes. *IEEE Trans. Biomed. Eng.* 54, 281–290. <https://doi.org/10.1109/TBME.2006.886617>
- Le, S.J., Gongora, M., Zhang, B., Grimmond, S., Campbell, G.R., Campbell, J.H., Rolfe, B.E., 2010. Gene expression profile of the fibrotic response in the peritoneal cavity. *Differentiation* 79, 232–243. <https://doi.org/10.1016/j.diff.2010.03.001>
- Lecomte, A., Degache, A., Descamps, E., Dahan, L., Bergaud, C., 2017. In vitro and in vivo biostability assessment of chronically-implanted Parylene C neural sensors. *Sensors Actuators B Chem.* <https://doi.org/10.1016/j.snb.2017.05.057>
- Luttikhuisen, D.T., Harmsen, M.C., Van Luyn, M.J.A., 2006. Cellular and molecular dynamics in the Foreign Body Reaction. *Tissue Eng.* 12, 1955–1970. <https://doi.org/10.1089/ten.2006.12.ft-126>
- Malmstrom, J. a, McNaughton, T.G., Horch, K.W., 1998. Recording properties and biocompatibility of chronically implanted polymer-based intrafascicular electrodes. *Ann. Biomed. Eng.* 26, 1055–1064. <https://doi.org/10.1114/1.35>
- McNally, A.K., Anderson, J.M., 2011. Macrophage fusion and multinucleated giant cells of inflammation. *Adv. Exp. Med. Biol.* 713, 97–111. https://doi.org/10.1007/978-94-007-0763-4_7
- Micera, S., Citi, L., Rigosa, J., Carpaneto, J., Raspopovic, S., Di Pino, G., Rossini, L., Yoshida, K., Denaro, L., Dario, P., Rossini, P.M., 2010. Decoding information from neural signals recorded using intraneural electrodes: Toward the development of a neurocontrolled hand prosthesis. *Proc. IEEE* 98, 407–417. <https://doi.org/10.1109/JPROC.2009.2038726>
- Mueller, M., Boehler, C., Jaeger, J., Asplund, M., Stieglitz, T., 2016. A double-sided fabrication process for intrafascicular parylene C based electrode arrays, in: *Proceedings of the Annual International Conference of the IEEE Engineering in Medicine and Biology Society, EMBS. IEEE*, pp. 2798–2801. <https://doi.org/10.1109/EMBC.2016.7591311>
- Mueller, M., de la Oliva, N., del Valle, J., Delgado Martinez, I., Navarro, X., Stieglitz, T., 2017. Rapid prototyping of flexible intrafascicular electrode arrays by picosecond laser structuring. *J. Neural Eng.* <https://doi.org/10.1088/1741-2552/aa7eea>

- Myllymaa, S., Myllymaa, K., Korhonen, H., Lammi, M.J., Tiitu, V., Lappalainen, R., 2010. Surface characterization and in vitro biocompatibility assessment of photosensitive polyimide films. *Colloids Surfaces B Biointerfaces* 76, 505–511. <https://doi.org/10.1016/j.colsurfb.2009.12.011>
- Navarro, X., Krueger, T.B., Lago, N., Micera, S., Stieglitz, T., Dario, P., 2005. A critical review of interfaces with the peripheral nervous system for the control of neuroprostheses and hybrid bionic systems. *J. Peripher. Nerv. Syst.* 10, 229–58. <https://doi.org/10.1111/j.1085-9489.2005.10303.x>
- Ordonez, J., Schuettler, M., Boehler, C., Boretius, T., Stieglitz, T., 2012. Thin films and microelectrode arrays for neuroprosthetics. *MRS Bull.* 37, 590–598. <https://doi.org/10.1557/mrs.2012.117>
- Polikov, V.S., Tresco, P.A., Reichert, W.M., 2005. Response of brain tissue to chronically implanted neural electrodes. *J. Neurosci. Methods* 148, 1–18. <https://doi.org/10.1016/j.jneumeth.2005.08.015>
- Raspopovic, S., Capogrosso, M., Micera, S., 2011. A computational model for the stimulation of rat sciatic nerve using a transverse intrafascicular multichannel electrode. *IEEE Trans. Neural Syst. Rehabil. Eng.* 19, 333–344. <https://doi.org/10.1109/TNSRE.2011.2151878>
- Raspopovic, S., Capogrosso, M., Petrini, F.M., Bonizzato, M., Rigosa, J., Di Pino, G., Carpaneto, J., Controzzi, M., Boretius, T., Fernandez, E., Granata, G., Oddo, C.M., Citi, L., Ciancio, a. L., Cipriani, C., Carrozza, M.C., Jensen, W., Guglielmelli, E., Stieglitz, T., Rossini, P.M., Micera, S., 2014. Restoring Natural Sensory Feedback in Real-Time Bidirectional Hand Prostheses. *Sci. Transl. Med.* 6, 222ra19–222ra19. <https://doi.org/10.1126/scitranslmed.3006820>
- Raspopovic, S., Petrini, F.M., Zelechowski, M., Valle, G., 2017. Framework for the Development of Neuroprostheses: From Basic Understanding by Sciatic and Median Nerves Models to Bionic Legs and Hands. *Proc. IEEE* 105, 34–49. <https://doi.org/10.1109/JPROC.2016.2600560>
- Richardson, R.R., Miller, J.A., Reichert, W.M., 1993. Polyimides as biomaterials: preliminary biocompatibility testing. *Biomaterials* 14, 627–635. [https://doi.org/10.1016/0142-9612\(93\)90183-3](https://doi.org/10.1016/0142-9612(93)90183-3)
- Robitaille, R., Dusseault, J., Henley, N., Desbiens, K., Labrecque, N., Hall, J.P., 2005. Inflammatory response to peritoneal implantation of alginate-poly-L-lysine microcapsules. *Biomaterials* 26, 4119–4127. <https://doi.org/10.1016/j.biomaterials.2004.10.028>
- Rodriguez, A., Meyerson, H., Anderson, J.M., 2009. Quantitative in vivo cytokine analysis at synthetic biomaterial implant sites. *J. Biomed. Mater. Res. - Part A* 89, 152–159. <https://doi.org/10.1002/jbm.a.31939>
- Rossini, P.M., Micera, S., Benvenuto, A., Carpaneto, J., Cavallo, G., Citi, L., Cipriani, C., Denaro, L., Denaro,

- V., Di Pino, G., Ferreri, F., Guglielmelli, E., Hoffmann, K.P., Raspopovic, S., Rigosa, J., Rossini, L., Tombini, M., Dario, P., 2010. Double nerve intraneural interface implant on a human amputee for robotic hand control. *Clin. Neurophysiol.* 121, 777–783. <https://doi.org/10.1016/j.clinph.2010.01.001>
- Rubehn, B., Stieglitz, T., 2010. In vitro evaluation of the long-term stability of polyimide as a material for neural implants. *Biomaterials* 31, 3449–3458. <https://doi.org/10.1016/j.biomaterials.2010.01.053>
- Sahin, H., Wasmuth, H.E., 2013. Chemokines in tissue fibrosis. *Biochim. Biophys. Acta - Mol. Basis Dis.* 1832, 1041–1048. <https://doi.org/10.1016/j.bbadis.2012.11.004>
- Sheikh, Z., Brooks, P.J., Barzilay, O., Fine, N., Glogauer, M., 2015. Macrophages, foreign body giant cells and their response to implantable biomaterials. *Materials (Basel)*. <https://doi.org/10.3390/ma8095269>
- Stieglitz, T., Beutel, H., Schuettler, M., Meyer, J.-U., 2000. Micromachined, Polyimide-Based Devices for Flexible Neural Interfaces. *Biomed. Microdevices* 2, 283–294. <https://doi.org/10.1023/A:1009955222114>
- Tyler, D.J., Polasek, K.H., Schiefer, M.A., 2015. *Peripheral Nerve Interfaces, Nerves and Nerve Injuries*. Elsevier Ltd. <https://doi.org/10.1016/B978-0-12-802653-3.00112-3>
- Weiseh, O., Doloff, J.C., Ma, M., Vegas, A.J., Tam, H.H., Bader, A.R., Li, J., Langan, E., Wyckoff, J., Loo, W.S., Jhunjunwala, S., Chiu, A., Siebert, S., Tang, K., Hollister-Lock, J., Aresta-Dasilva, S., Bochenek, M., Mendoza-Elias, J., Wang, Y., Qi, M., Lavin, D.M., Chen, M., Dholakia, N., Thakrar, R., Lacić, I., Weir, G.C., Oberholzer, J., Greiner, D.L., Langer, R., Anderson, D.G., 2015. Size- and shape-dependent foreign body immune response to materials implanted in rodents and non-human primates. *Nat. Mater.* 14, 643–51. <https://doi.org/10.1038/nmat4290>
- Vince, V., Brelén, M.E., Delbeke, J., Colin, I.M., 2005. Anti-TNF α reduces the inflammatory reaction associated with cuff electrode implantation around the sciatic nerve. *J. Neuroimmunol.* 165, 121–128. <https://doi.org/10.1016/j.jneuroim.2005.04.019>
- Wark, H.A., Mathews, K.S., Normann, R.A., Fernandez, E., 2014. Behavioral and cellular consequences of high-electrode count Utah Arrays chronically implanted in rat sciatic nerve. *J. Neural Eng.* 11, 46027. <https://doi.org/10.1088/1741-2560/11/4/046027>
- Wark, H.A., Sharma, R., Mathews, K.S., Fernandez, E., Yoo, J., Christensen, M.B., Tresco, P., Rieth, L., Solzbacher, F., Normann, R. a, Tathireddy, P., 2013. A new high-density (25 electrodes/mm²) penetrating microelectrode array for recording and stimulating sub-millimeter neuroanatomical structures. *J. Neural Eng.* 10, 45003. <https://doi.org/10.1088/1741-2560/10/4/045003>

- Warwick, K., Gasson, M., Hutt, B., Goodhew, I., Kyberd, P., Andrews, B., Teddy, P., Shad, A., 2003. The Application of Implant Technology for Cybernetic Systems. *Arch. Neurol.* 60, 1369. <https://doi.org/10.1001/archneur.60.10.1369>
- Wurth, S., Capogrosso, M., Raspopovic, S., Gandar, J., Federici, G., Kinany, N., Cutrone, A., Piersigilli, A., Pavlova, N., Guiet, R., Taverni, G., Rigosa, J., Shkorbatova, P., Navarro, X., Barraud, Q., Courtine, G., Micera, S., 2017. Long-term usability and bio-integration of polyimide-based intra-neural stimulating electrodes. *Biomaterials* 122, 114–129. <https://doi.org/10.1016/j.biomaterials.2017.01.014>
- Yanagihara, T., Goldstein, N.P., Svien, H.J., Bahn, R.C., 1967. Foreign body reaction of the brain: Enzyme-histochemical study in dogs. *Neurology* 17, 337. <https://doi.org/10.1212/WNL.17.4.337>
- Yoshida, K., Jovanović, K., Stein, R.B., 2000. Intrafascicular electrodes for stimulation and recording from mudpuppy spinal roots. *J. Neurosci. Methods* 96, 47–55. [https://doi.org/10.1016/S0165-0270\(99\)00176-4](https://doi.org/10.1016/S0165-0270(99)00176-4)
- Yu, B., Ju, Y., West, L., Moussy, Y., Moussy, F., 2007. An Investigation of Long-Term Performance of Minimally Invasive Glucose Biosensors. *Diabetes Technol. Ther.* 9, 265–275. <https://doi.org/10.1089/dia.2006.0020>
- Zhou, G., Niepel, M.S., Saretia, S., Groth, T., 2016. Reducing the inflammatory responses of biomaterials by surface modification with glycosaminoglycan multilayers. *J. Biomed. Mater. Res. Part A* 104, 493–502. <https://doi.org/10.1002/jbm.a.35587>

CHAPTER 3: DEXAMETHASONE REDUCES THE FOREIGN BODY REACTION TO INTRANEURAL ELECTRODE IMPLANTS IN THE PERIPHERAL NERVE OF THE RAT

Natàlia de la Oliva¹, Xavier Navarro¹, Jaume del Valle^{1, 2}

¹ Institute of Neurosciences, Department of Cell Biology, Physiology and Immunology, Universitat Autònoma de Barcelona, and Centro de Investigación Biomédica en Red en Enfermedades Neurodegenerativas (CIBERNED), Bellaterra, Spain.

² Catalan Institute of Nanoscience and Nanotechnology (ICN2), CSIC and BIST, Campus UAB, Bellaterra, 08193 Barcelona, Spain

ABSTRACT

Intraneural electrodes must be in intimate contact with nerve fibers to have a proper function, but this interface is compromised due to the foreign body reaction (FBR). The FBR is characterized by a first inflammatory phase followed by a second anti-inflammatory and fibrotic phase, which results in the formation of a tissue capsule around the device, causing physical separation between the active sites of the electrode and the nerve fibers. We have tested several anti-inflammatory drugs such as dexamethasone, ibuprofen and maraviroc to reduce macrophage activation, as well as clodronate liposomes to reduce monocyte/macrophage infiltration, and sildenafil as an antifibrotic drug to reduce collagen deposition in an FBR model with longitudinal Parylene C intraneural devices implanted in the rat sciatic nerve. Treatment with dexamethasone, ibuprofen or clodronate significantly reduced the inflammatory response in the nerve in comparison to the saline group after two weeks of the implant, whereas sildenafil and maraviroc had no effect on infiltration of macrophages in the nerve. However, only dexamethasone was able to significantly reduce the matrix deposition around the implant. Similar positive results were obtained with dexamethasone in the case of polyimide-based intraneural implants, another polymer substrate for the electrode. These results indicate that inflammation triggers the FBR in peripheral nerves, and that anti-inflammatory treatment with dexamethasone may have beneficial effects on lengthening intraneural interface functionality.

Keywords: dexamethasone, foreign body reaction, intraneural electrodes, polyimide, Parylene C.

INTRODUCTION

Advanced neuroprostheses are intended to link the human nervous system with electronic or robotic prostheses, with the aim of restoring motor and sensory functions lost after neural injuries or amputations. Various neuroprosthetic systems include an interface with the peripheral nerve. Although different peripheral nerve interfaces have been developed, all of them are based on their capability to contact with specific groups of axons within a nerve to obtain neural signals and to stimulate their activity, thus achieving a bidirectional communication (del Valle and Navarro, 2013; Navarro et al., 2005). Interfaces designed to achieve a high resolution, in terms of recording the small amplitude of neural signals and of stimulation with high selectivity small fascicles of axons with a common target, require a close positioning of axons and electrode. Hence, intraneural electrodes have been proposed as showing an adequate trade-off thanks to a reduced invasiveness and a good selectivity (Micera et al., 2008). The most used designs of electrodes that are implanted within a peripheral nerve include the multielectrode arrays (MEAs), the longitudinal intra-fascicular electrode (LIFE) and the transversal intraneural multichannel electrode (TIME), all of them providing several (ten to hundred) small electrical active sites in one device. Compared with extraneural electrodes, such as cuff types, intraneural electrodes are placed within a fascicle in the nerve and have closer contact to the targeted axons. This intraneural positioning increases the signal-to-noise ratio of recordings, reduces the stimulus intensity needed to depolarize the axons, and enhances selectivity (Badia et al., 2011).

However, any implanted device in the body induces a host response, known as the foreign body reaction (FBR), that may ultimately compromise the long-term functional outcome of a biomedical device. The FBR is the response of the immune system to any external device implanted in the body (Ward 2008; Onuki et al. 2008). It is characterized by an initial inflammatory phase, followed by an inflammatory resolution and tissue remodeling phase that results in the formation of a fibrous tissue capsule around the device (Luttikhuisen et al. 2006; Anderson et al. 2008). In the case of an intraneural electrode, this encapsulation results in a progressive decline in signal level and increase in stimulation threshold, because the scar tissue gradually separates axons away from the contacts (Christensen et al., 2014; Lago et al., 2007; Raspopovic et al., 2014; Rossini et al., 2010; Wurth et al., 2017).

To improve the long-term functional outcome of implanted electrodes, different strategies have been developed. From the biomaterials field, different polymers (Sommakia et al. 2014; Skousen et al. 2014; Lee et al. 2017) and surface coatings (Cui et al. 2001; Balaji et al. 2015; Noorisafa et al. 2016) have been investigated to reduce the FBR. In fact, these

coatings have been used as local delivery systems of active molecules or drugs to modulate the inflammatory response in subcutaneous (Hetrick et al., 2007; Norton et al., 2007) and brain (Mercanzini et al. 2010; Zhong et al. 2017) implants. Besides, a combination of conductive polymers and anti-inflammatory treatment have shown better recording properties and closer neurons to implants over time (Boehler et al., 2017). However, only a few of these strategies have been applied to peripheral nerve interfaces, such as cuff (Vince et al. 2005; Heo et al. 2016b) and regenerative (FitzGerald, 2016) devices. In the case of intraneural interfaces, there are some limitations (i.e. nerve size) that limit the use of bulky local administration strategies. Moreover, the effective time window to improve the FBR for intraneural electrodes is still unknown.

We have recently characterized the extent of the inflammatory and the remodeling phases of the FBR to devices longitudinally implanted in the peripheral nerve (de la Oliva et al., 2017), thus determining possible targets for reducing the encapsulation and improving electrode functional outcome. The aim of this study is to evaluate the effect of different treatments to modulate the FBR and to reduce capsule thickness around longitudinal Parylene C intraneural devices inserted in the rat sciatic nerve. Hence, anti-inflammatory drugs such as dexamethasone, ibuprofen and maraviroc were administered for 2 weeks to reduce macrophage activation, as well as clodronate liposomes to reduce monocyte/macrophage infiltration. Sildenafil was also assayed as an antifibrotic drug to reduce collagen deposition around the device (Percival et al., 2012). The effects have been assessed in terms of anatomical and histological measures of the capsule and the infiltrating cells. Finally, the effects of dexamethasone have been also evaluated in the FBR to polyimide electrode implants, for comparing the differences between device substrates.

MATERIAL AND METHODS

Surgical procedures and drug administration

All animal experiments conducted were performed with the approval of the Ethical Committee of the Universitat Autònoma de Barcelona in accordance with the European Communities Council Directive 2010/63/EU.

Female Sprague-Dawley rats of 200-250 g of weight were used. Surgery was performed under ketamine and xylazine anaesthesia (90/10 mg/kg, i.p.). The implantation procedure was performed as previously described for LIFEs (Lago et al., 2007). Briefly, the sciatic nerve was surgically exposed at the mid thigh and freed from surrounding adhesions. Parylene C and polyimide strips of 20 mm length, 200 μ m width and 10 μ m thickness, mimicking the structure of the thin-film LIFE (Lago et al., 2007) were longitudinally implanted in the tibial branch of the sciatic nerve with the help of a straight needle attached to a 10-0 loop thread (STC-6, Ethicon). A longitudinal implant was chosen because of its better reproducibility in comparison with transversal implants and to better study only the FBR inside the nerve. Finally, the surrounding muscles and the skin were sutured and disinfected with povidone-iodine. Animals were housed at $22\pm 2^{\circ}\text{C}$ on a 12h light-dark cycle with food and water ad libitum.

Treatments to reduce FBR to the Parylene C intraneural devices started 2 days before surgery to ensure appropriate systemic levels and were daily administered for 2 weeks since we have previously found that at this time postimplant the thickness of the encapsulation reaches stable maximal values (de la Oliva et al., 2017). We have assayed three anti-inflammatory drugs, dexamethasone, ibuprofen and maraviroc, to reduce macrophage activation; clodronate liposomes to reduce monocyte/macrophage infiltration, and sildenafil to reduce collagen deposition around the device. Animal distribution, doses and administration pathways are summarized in Table 1. Dosage was selected according to previous reports in the literature. In a second part of the study, the most effective drug treatment found, i.e. dexamethasone, was administered at three different doses to assess dose-effect response. Finally, dexamethasone was administered to rats with either Parylene C or polyimide implants for comparing possible differences between electrode substrates, and during 1, 2 or 8 weeks for comparing the differences in duration of treatment.

For each drug and material group, a saline group was studied as control. However, as there were no differences between administration pathways, all the saline animals were combined in a unique group for Parylene C or polyimide devices.

Table 1. Drugs, doses and administration pathways used in this work.

Group	Material	Treatment duration	Dose	Administration	N
Dexamethasone	ParC	2w	400 µg/kg/s.i.d. ¹	s.c	6
			200 µg/kg/s.i.d. ¹		12
			50 µg/kg/s.i.d. ¹		6
		1w	200 µg/kg/s.i.d. ¹		8
		2w			8
		8w			8
	Pol	1w	200 µg/kg/s.i.d. ¹		8
		2w			8
		8w			8
Ibuprofen	ParC	2w	30 mg/kg/s.i.d. ¹	p.o.	6
Clodronate	ParC	2w	10 ml/kg/q.a.d. ²	i.v.	6
Sildenafil	ParC	2w	25 mg/kg/s.i.d. ¹	p.o.	6
Dex+Sild	ParC	2w		s.c., p.o.	6
Maraviroc	ParC	2w	30 mg/kg/b.d.s. ³	p.o.	10
Saline	ParC			s.c/p.o/i.v.	28
Saline	Pol			s.c.	8

¹s.i.d.: once a day, ²q.a.d.: every other day, ³b.d.s.: twice a day.

Morphological evaluation

After 2 or 8 weeks post-implant, animals were deeply anaesthetized with an overdose of pentobarbital and transcardially perfused with 4% PFA in phosphate buffer (PB) to obtain the sciatic nerve including the implanted device for histological and immunohistochemical analyses.

To evaluate the microstructure of the nerve and the thickness of the tissue capsule around the device, nerve segments were postfixed in 3% glutaraldehyde-3% paraformaldehyde and postfixed in 2% OsO₄ for 2h, dehydrated through ethanol series and embedded in epon resin. Semithin sections (0.5 µm thick) were stained with toluidine blue and examined by light microscopy. The thickness of the tissue capsule was measured as the distance between each side of the device and the closest myelinated axon using ImageJ software.

Analysis of infiltrating macrophages in the implanted nerves was performed using immunohistochemical labeling. Nerve segments containing the device implanted were serially cut (15 µm) with a cryostat (Leica CM190, Leica Microsystems). After thawing and blocking with normal donkey serum, slides were incubated overnight at 4°C with primary

antibody rabbit anti-Iba1 (Wako, 191947, 1:500). Slides were then washed with 0.1% Tween 20 buffer solution and incubated with AlexaFluor 555 donkey anti-rabbit secondary antibody (Invitrogen, A21207, 1:200) for 1 h at room temperature. Finally, slides were mounted with Mowiol containing DAPI (0.1 µg/ml, Sigma). The number of Iba1 positive macrophages that infiltrate the whole tibial nerve was quantified in images taken with an epifluorescence microscope (Olympus BX51). Images were equally treated to adjust brightness and contrast, and background subtraction. A threshold of detection and binarization was applied using ImageJ software. Iba1 positive cells in the whole tibial nerve, excluding the implant and the tissue capsule, were counted using the plugin “Analyze particles” of ImageJ.

Hematoxylin-eosin staining was performed to evaluate the formation of foreign body giant cells (FBGCs) as a result of macrophage fusion around the implant. Other cryostat sections were immersed in hematoxylin Harys solution (Fluka, Sigma) for 7 min, washed in water and immersed in 1% HCl in ethanol for 20 sec. Then, sections were washed again in water and stained with Eosin Y (Merck Millipore) for 5 min. Finally, sections were dehydrated with series of graded ethanol rinses and mounted with DPX (Sigma). The number of FBGCs in each stained section was counted under the microscope and results expressed as FBGC per mm of implant width. In addition, the diameter of each FBGC counted was measured using ImageJ.

Statistical analysis

All reported values are the average \pm SEM. Differences between groups or times postimplant were analyzed by one or two-way ANOVA followed by Bonferroni post hoc tests, using the GraphPad Prism software. Statistical significance was considered at $p < 0.05$.

RESULTS

Anti-inflammatory treatment reduces the infiltration of macrophages in implanted nerves

The infiltration of macrophages in Parylene C implanted nerves was significantly reduced by treatment with ibuprofen, clodronate and dexamethasone compared to the saline administered group (Fig. 1). In contrast, maraviroc and sildenafil did not reduce the number of macrophages present after 2 weeks of treatment. The combination of

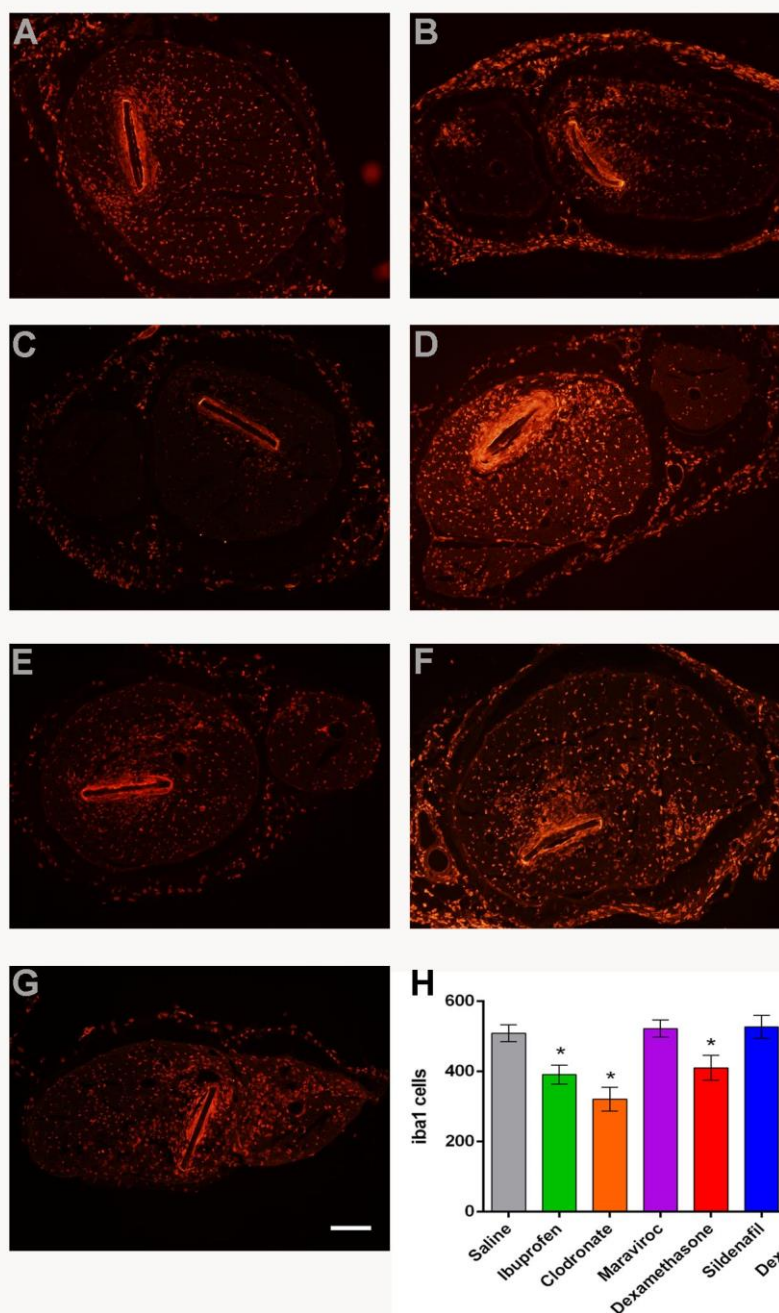


Figure 1. Representative images of Iba1 labeled infiltrating macrophages in the tibial nerve 2 weeks after implant of a Parylene C electrode device, following administration of (A) saline, (B) ibuprofen, (C) clodronate, (D) maraviroc, (E) dexamethasone, (F) sildenafil or (G) dexamethasone and sildenafil. (H) Quantification of the number of Iba1 positive cells in the nerve after the different treatments. Scale bar = 150µm. * p < 0.05 vs saline group.

dexamethasone and sildenafil significantly reduced the infiltration of iba1+ cells to similar levels than dexamethasone alone (Fig. 1).

As a hallmark of the final phase of the FBR, the number of FBGCs was evaluated. These cells are the result of the fusion of macrophages when they are not able to phagocytose the foreign body and are associated with an anti-inflammatory and tissue remodeling environment (McNally et al. 2011; Sheikh et al. 2015). No changes in the number of FBGCs around the implant were found for any of the treatments administered except for maraviroc (Fig. 2), which caused a marked increase in FBGCs in the capsule around the devices in comparison to saline-treated animals. No changes in the diameter of these cells were observed between groups (Fig. 2).

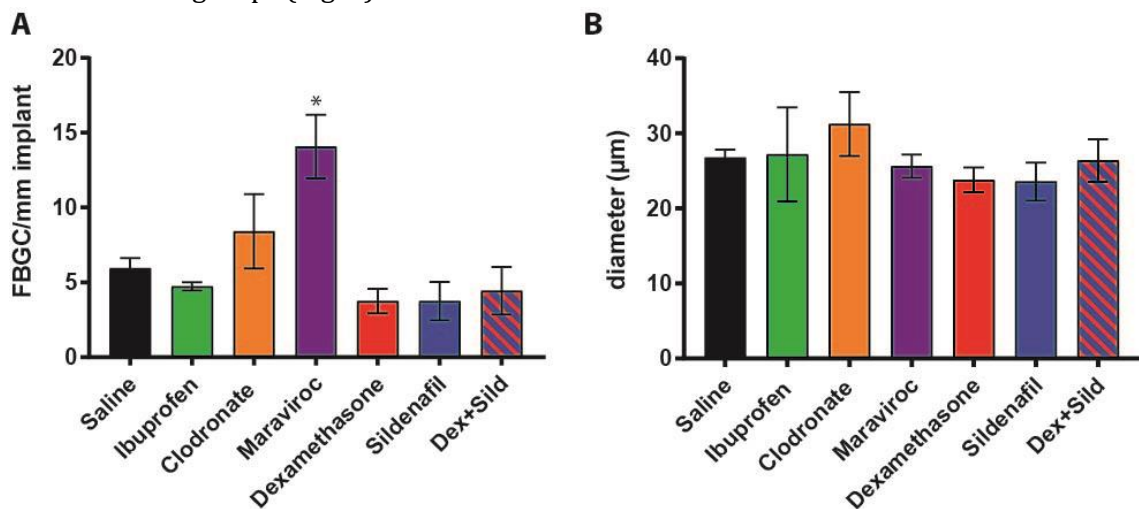
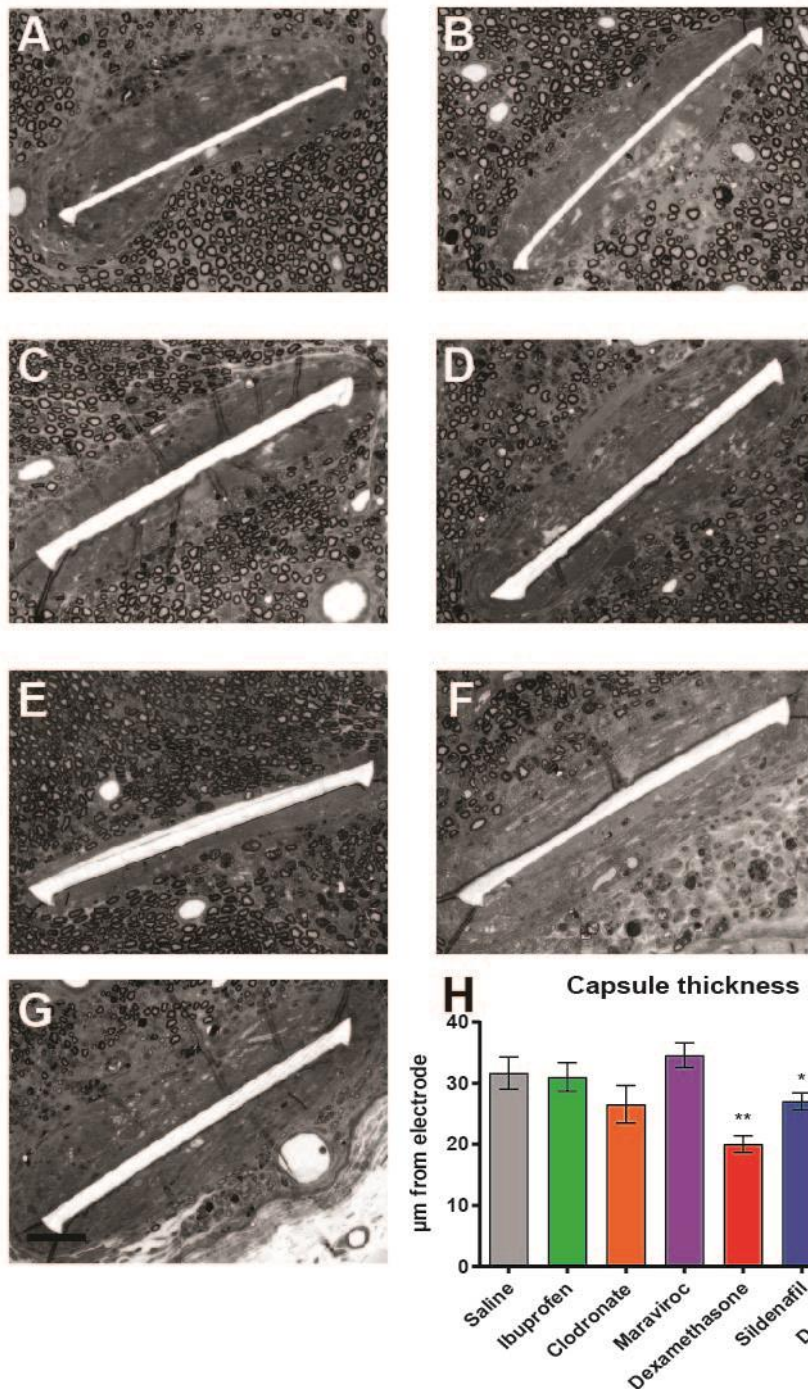


Figure 2. Foreign body giant cells (FBGCs) in the capsule around the Parylene C electrode device. Changes in (A) number and (B) diameter of FBGCs after 2 weeks under the different treatments. * $p < 0.05$ vs saline group.

The FBR results in the formation of a tissue capsule around the implanted devices in the peripheral nerve. Among the anti-inflammatory drugs used only dexamethasone significantly reduced the thickness of the capsule compared with the saline controls (Fig. 3). Sildenafil also reduced the formation of this capsule, although to a lesser degree. The combination of both treatments, dexamethasone plus sildenafil during 2 weeks did not show any additive effect.



Since dexamethasone was the most effective drug in reducing inflammatory cell infiltration and encapsulation of the intraneural devices, we further investigated the dose-effect relation. Thus, dexamethasone was given daily at 400, 200 and 50 μ g/kg in different groups of rats. The results showed that the lowest dose was not able to reduce significantly cell infiltration and tissue encapsulation, whereas the highest and the medium doses were similarly effective (Fig.4).

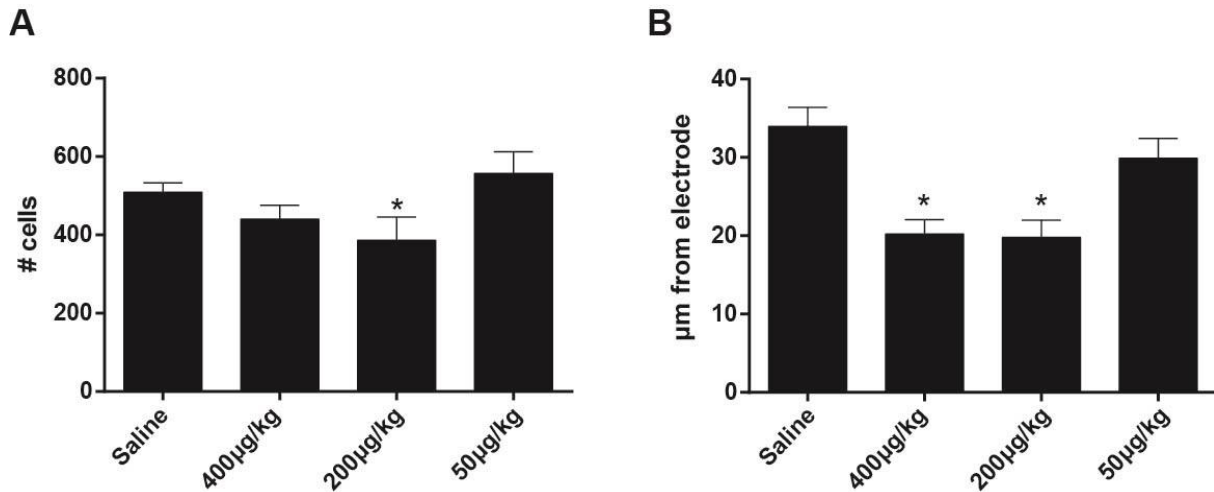


Figure 4. Dose-response effect of dexamethasone on (A) iba1+ cells infiltration, and (B) capsule formation around parylene C devices implanted in the nerve during 2 weeks. * p < 0.01 vs saline

Evaluation of dexamethasone effect on the FBR to different polymers

We also tested the effects of systemic dexamethasone administration on the FBR to intraneural devices made of polyimide, another polymer used as electrode substrate (Lacour et al., 2009; Lago et al., 2007; Rodriguez et al., 2000). As expected, dexamethasone treatment also reduced the infiltration of iba1+ macrophages in polyimide implanted nerves and the tissue capsule thickness around the device (Fig. 5). Comparatively, the characteristics of the FBR were similar for both Parylene C and polyimide substrates. The beneficial effect of dexamethasone was slightly more marked for the polyimide device, particularly in the limitation of macrophage infiltration after 2 weeks.

Finally, to know whether the reduction in macrophage infiltration and tissue deposition persisted over time after treatment withdrawal to avoid secondary adverse effects, groups of rats were administered for either 1, 2 or 8 weeks with dexamethasone at 200 µg/kg/s.i.d. and followed for 2 or 8 weeks of implant. The analyses made at 2 weeks after implant showed that only 1 week of treatment was not enough to reduce macrophage infiltration nor thickness of the capsule around both polyimide and Parylene C devices (Fig. 5). On the contrary, the results after 8 weeks of implant showed that only 2 weeks of dexamethasone administration were sufficient to reduce the capsule thickness, even though, treatment maintained for 8 weeks resulted in a more marked effect for both materials (Fig. 6).

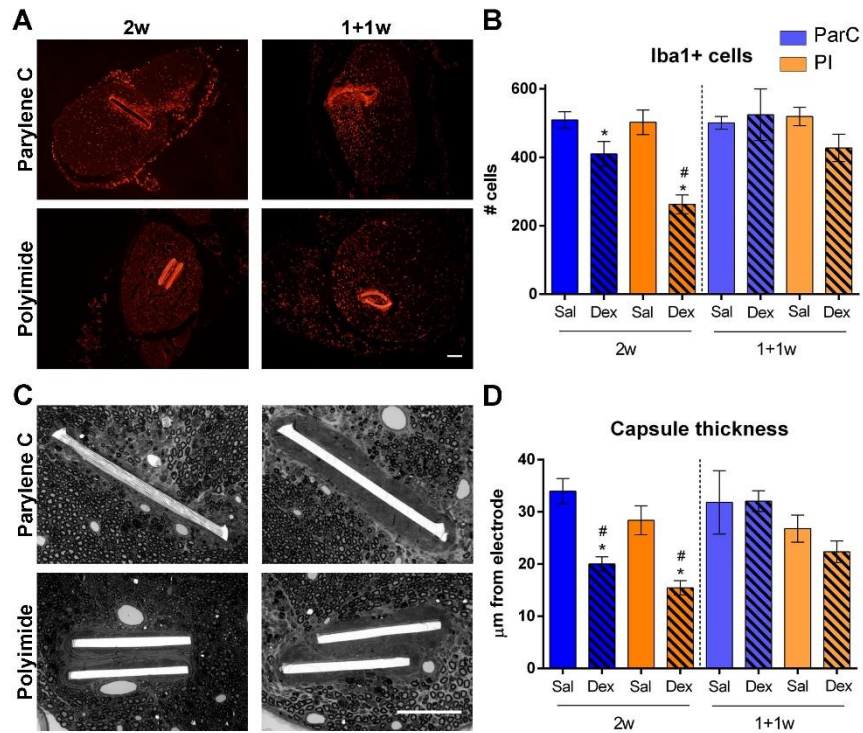


Figure 5. Effects of dexamethasone on FBR to parylene C and polyimide devices after 2 weeks implantation. (A) Representative images of iba1 labeling after 1 or 2 weeks of dexamethasone treatment in parylene C and polyimide implanted nerves. Scale bar = 100µm. (B) Quantification of iba1 positive cells after treatment with saline (Sal) or dexamethasone (Dex) during 2 (left) or 1 (right) week following intraneural implantation of parylene (blue) or polyimide (orange) devices. *p<0.05 vs respective saline group. #p<0.05 vs respective 1+1w treated group. (C) Representative images of tissue capsule after 2 or 1 week of dexamethasone treatment around parylene C and polyimide devices implanted in the nerve. Scale bar = 100µm. (D) Capsule thickness measurement after treatment with saline (Sal) or dexamethasone (Dex) during 2 (left) or 1 (right) week in parylene (blue) or polyimide (orange) devices. * p< 0.05 vs respective saline group. # p<0.05 vs respective 1+1w treated group.

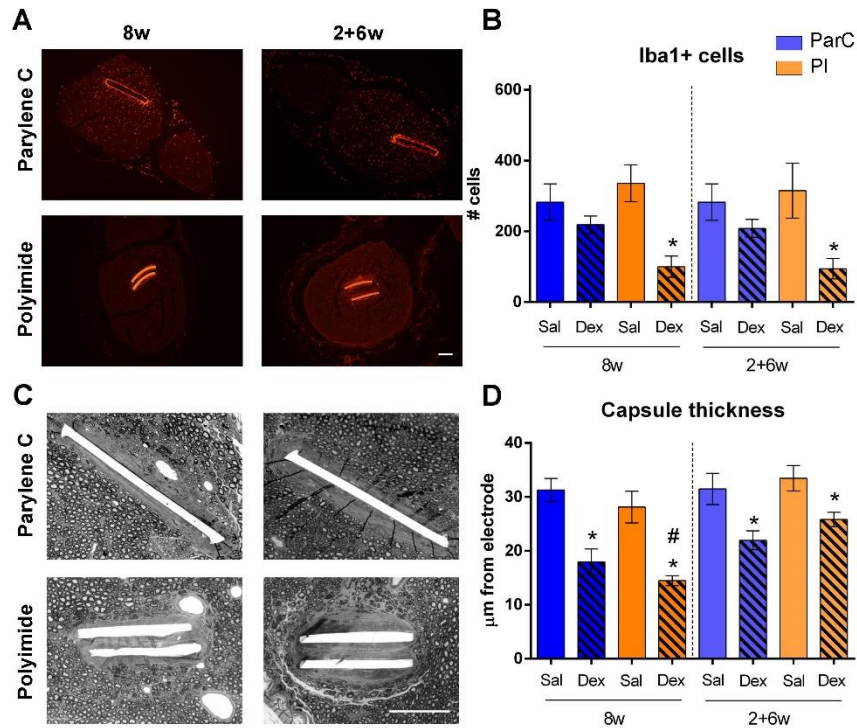


Figure 6. Effects of dexamethasone on FBR to parylene C and polyimide devices after 8 weeks implantation. (A) Representative images of iba1 labeling after 2 or 8 weeks of dexamethasone treatment in parylene C and polyimide implanted nerves. Scale bar = 100μm. (B) Quantification of iba1 positive cells after treatment with saline (Sal) or dexamethasone (Dex) during 8 (left) or 2 (right) weeks after parylene (blue) or polyimide (orange) devices implant. * $p < 0.05$ vs respective saline group. (C) Representative images of tissue capsule after 2 or 8 weeks of dexamethasone treatment in parylene C and polyimide implanted devices. Scale bar = 100μm. (D) Capsule thickness measurement after treatment with saline (Sal) or dexamethasone (Dex) during 8 (left) or 2 (right) weeks around parylene (blue) or polyimide (orange) implanted devices. * $p < 0.05$ vs respective saline group. # $p < 0.05$ vs respective 2+6w treated group.

DISCUSSION

The results of this study demonstrate that dexamethasone is effective in reducing the inflammatory reaction and the fibrous encapsulation seen as the response to electrodes implanted in the peripheral nerve. This is an important issue in the application of nerve interfaces for neuroprostheses because progressive scarring will impair long-term interface function. Even with recent advances in the electrode design to make them more adaptive and stable (Lago et al., 2007; Boretius et al., 2010; Cutrone et al., 2015) and in the use of biocompatible materials (Sommakia et al. 2014), the FBR still compromises the long-term functional performance of implanted neural interfaces.

In this study, systemic administration of different drugs has been tested to reduce the tissue encapsulation of longitudinal intraneural devices. Dexamethasone has been found as the most effective treatment to modulate the FBR, by reducing the infiltration of macrophages and the capsule thickness around both Parylene C and polyimide devices. Our results agree with those previously found with systemic (Spataro et al., 2005) and local (Zhong and Bellamkonda 2007; FitzGerald 2016) administration of dexamethasone, in which a reduction of scar tissue formation was reported. Moreover, improvement in electrode functionality due to local release of dexamethasone has also been described (Kim and Martin 2006; Mercanzini et al. 2010). However, most of the local release studies have been made on brain (Kim and Martin 2006; Zhong and Bellamkonda 2007; Mercanzini et al. 2010) and subcutaneous implants (Dang et al. 2011; Kastellorizios et al. 2015; Heo et al. 2016a). Only a few works have focused on strategies to focally release anti-inflammatory drugs in peripheral nerves (Park et al. 2015; FitzGerald 2016; Heo et al. 2016b). Indeed, by using systemic administration we aimed to make a feasible screening of different drugs with the potential to prevent the FBR. Eventually, modifications in the design of current intraneural electrodes may allow to include systems for focal, controlled release, either by coating their surface with biodegradable hydrogels or by adapting a microfluidic system. Nevertheless, the volume limits within the peripheral nerve must be considered, so these options should avoid an increase in the thickness of the electrode.

On the other hand, systemic administration facilitates the combination of different FBR modulatory drugs at different time points after implantation, according to the time-window of effectiveness for each drug. As our results show, at least two weeks of dexamethasone administration (at a dose of 200 µg/kg/s.i.d.) are needed to significantly reduce the infiltration of immune cells and the thickness of the capsule. The effect achieved during the first two weeks is maintained after 8 weeks of implant, suggesting that this initial period is predictive of the later chronic FBR. Despite the reduction of the FBR to electrode

polymers (i.e. Parylene C and polyimide) obtained with dexamethasone, still some encapsulation appeared around the implanted devices. Therefore, the ultimate question is how this reduction in capsule thickness may improve the functionality of intraneural interfaces in terms of stimulation and nerve signals recording. Current experiments will determine the potential effect of dexamethasone in improving the functional characteristics of chronically implanted intraneural electrodes. Given the similarities in the FBR with other types of devices, such as multielectrode arrays (Christensen et al., 2014) and transversal electrodes (Wurth et al., 2017), dexamethasone treatment will be likely useful to modulate the FBR to different electrode designs for peripheral nerves.

The differences found between the several anti-inflammatory drugs assayed in this work point out the mechanisms through which dexamethasone is doing its positive effect. Ibuprofen is a NSAID, known to exert anti-inflammatory effect by the inhibition of cyclooxygenase 1 and 2 enzymes. Clodronate induces apoptosis of circulating monocytes/macrophages. Dexamethasone acts through the glucocorticoid receptor, having a much wider spectrum of actions (Coutinho and Chapman, 2011), from anti-inflammatory to immunosuppressive effects. Thus, the reduction of infiltrating macrophages and the decrease of immune mediators achieved also with ibuprofen and clodronate treatments, would not be enough to reduce the encapsulation of implanted devices. In the same line, maraviroc, an antagonist of CCR5, did not reduce macrophages infiltration nor tissue deposition in the implanted nerves. Despite the role of CCR5 in different fibrotic models (Berres et al., 2010; Sahin and Wasmuth, 2013; Seki et al., 2009), we did not observe any beneficial effect of its blockage in our model of FBR in peripheral nerves. However, CCR5 is not the only chemokine receptor implicated in tissue fibrosis (Ishida et al., 2007; Sahin and Wasmuth, 2013).

As expected from previous studies using sildenafil for reducing fibrosis development (Valente et al. 2003; Noel et al. 2012; Percival et al. 2012), we found a significant reduction in capsule thickness. However, the effect was not as marked as with dexamethasone. This could be due to the two main phases of the FBR, one pro-inflammatory followed by a second one anti-inflammatory and tissue remodeling (Anderson et al. 2008). Thus, dexamethasone might be modulating both phases while the other treatments assessed only act by reducing either activation of the inflammatory cells or the matrix deposition.

In conclusion, systemic administration of dexamethasone could be a feasible option to improve the long-term usability of neural electrodes in peripheral nerves without modifications on electrodes design. Further advances can be expected if the FBR might be

modulated according to the cellular and molecular players within each phase, with sequential administration of appropriate drugs for each phase.

ACKNOWLEDGEMENTS

This research was supported by the European Union FPT-ICT project NEBIAS under contract number 611687, FEDER funds, and TERCEL (RD12/0019/0011) and CIBERNED (CB06/05/1105) funds from the Instituto de Salud Carlos III of Spain. The ICN2 is funded by the CERCA programme of Generalitat de Catalunya and supported by the Severo Ochoa programme of the Spanish Ministry of Economy, Industry and Competitiveness (MINECO, grant no. SEV-2013-0295). The authors thank Monica Espejo and Jessica Jaramillo for the technical help. The authors would like to express their special appreciation to Matthias Müller and Thomas Stieglitz from IMTEK, University of Freiburg, for providing the polymer devices used in the study.

REFERENCES

- Anderson, J.M., Rodriguez, A., Chang, D.T., 2008. Foreign body reaction to biomaterials. *Semin. Immunol.* 20, 86–100. <https://doi.org/10.1016/j.smim.2007.11.004>
- Badia, J., Boretius, T., Andreu, D., Azevedo-Coste, C., Stieglitz, T., Navarro, X., 2011. Comparative analysis of transverse intrafascicular multichannel, longitudinal intrafascicular and multipolar cuff electrodes for the selective stimulation of nerve fascicles. *J. Neural Eng.* 8, 36023. <https://doi.org/10.1088/1741-2560/8/3/036023>
- Balaji, A., Jaganathan, S.K., Vellayappan, M. V., John, A.A., Subramanian, A.P., SelvaKumar, M., Mohandas, H., Sundar Raj, M., Supriyanto, E., 2015. Prospects of common biomolecules as coating substances for polymeric biomaterials. *RSC Adv.* 5, 69660–69679. <https://doi.org/10.1039/c5ra12693b>
- Bellamkonda, R. V., Pai, S.B., Renaud, P., 2012. Materials for neural interfaces. *MRS Bull.* 37, 557–561. <https://doi.org/10.1557/mrs.2012.122>
- Berres, M.-L., Koenen, R.R., Rueland, A., Zaldivar, M.M., Heinrichs, D., Sahin, H., Schmitz, P., Streetz, K.L., Berg, T., Gassler, N., Weiskirchen, R., Proudfoot, A., Weber, C., Trautwein, C., Wasmuth, H.E., 2010. Antagonism of the chemokine Ccl5 ameliorates experimental liver fibrosis in mice. *J. Clin. Invest.* 120, 4129–40. <https://doi.org/10.1172/JCI41732>
- Boehler, C., Kleber, C., Martini, N., Xie, Y., Dryg, I., Stieglitz, T., Hofmann, U.G.G., Asplund, M., 2017. Actively controlled release of Dexamethasone from neural microelectrodes in a chronic in vivo study. *Biomaterials* 129, 176–187. <https://doi.org/10.1016/j.biomaterials.2017.03.019>
- Chen, S., Allen, M., 2012. Extracellular matrix-based materials for neural interfacing. *MRS Bull.* 37, 606–615.
- Christensen, M.B., Pearce, S.M., Ledbetter, N.M., Warren, D.J., Clark, G. a, Tresco, P. a, 2014. The foreign body response to the Utah Slant Electrode Array in the cat sciatic nerve. *Acta Biomater.* 10, 4650–60. <https://doi.org/10.1016/j.actbio.2014.07.010>
- Coutinho, A.E., Chapman, K.E., 2011. The anti-inflammatory and immunosuppressive effects of glucocorticoids, recent developments and mechanistic insights. *Mol. Cell. Endocrinol.* 335, 2–13. <https://doi.org/10.1016/j.mce.2010.04.005>
- Cui, X., Lee, V.A., Raphael, Y., Wiler, J.A., Hetke, J.F., Anderson, D.J., Martin, D.C., 2001. Surface modification of neural recording electrodes with conducting polymer/biomolecule blends. *J. Biomed. Mater. Res.* 56, 261–272. [https://doi.org/10.1002/1097-4636\(200108\)56:2<261::AID-JBM1094>3.0.CO;2-I](https://doi.org/10.1002/1097-4636(200108)56:2<261::AID-JBM1094>3.0.CO;2-I)
- Dang, T.T., Bratlie, K.M., Bogatyrev, S.R., Chen, X.Y., Langer, R., Anderson, D.G., 2011. Spatiotemporal effects of a controlled-release anti-inflammatory drug on the cellular dynamics of host response. *Biomaterials* 32, 4464–4470. <https://doi.org/10.1016/j.biomaterials.2011.02.048>
- de la Oliva, N., Navarro, X., del Valle, J., 2017. Time course study of long-term biocompatibility and foreign body reaction to intraneural polyimide-based implants. *J. Biomed. Mater. Res. Part A.* <https://doi.org/10.1002/jbm.a.36274>
- del Valle, J., Navarro, X., 2013. Interfaces with the peripheral nerve for the control of neuroprostheses.

- Int. Rev. Neurobiol. 109, 63–83. <https://doi.org/10.1016/B978-0-12-420045-6.00002-X>
- FitzGerald, J.J., 2016. Suppression of scarring in peripheral nerve implants by drug elution. *J. Neural Eng.* 13, 26006. <https://doi.org/10.1088/1741-2560/13/2/026006>
- Heo, D.N., Ko, W.-K., Lee, W.J., Lee, S.J., Lee, D., Heo, M., Rim, H., Bae, M.S., Lee, J.B., Ahn, B.-S., Kwon, I.K., 2016a. Enhanced Biocompatibility of Polyimide Film by Anti-Inflammatory Drug Loading. *J. Nanosci. Nanotechnol.* 16, 8800–8804. <https://doi.org/10.1166/jnn.2016.12482>
- Heo, D.N., Song, S.J., Kim, H.J., Lee, Y.J., Ko, W.K., Lee, S.J., Lee, D., Park, S.J., Zhang, L.G., Kang, J.Y., Do, S.H., Lee, S.H., Kwon, I.K., 2016b. Multifunctional hydrogel coatings on the surface of neural cuff electrode for improving electrode-nerve tissue interfaces. *Acta Biomater.* 39, 25–33. <https://doi.org/10.1016/j.actbio.2016.05.009>
- Hetrick, E.M., Prichard, H.L., Klitzman, B., Schoenfisch, M.H., 2007. Reduced foreign body response at nitric oxide-releasing subcutaneous implants. *Biomaterials* 28, 4571–4580. <https://doi.org/10.1016/j.biomaterials.2007.06.036>
- Ishida, Y., Kimura, A., Kondo, T., Hayashi, T., Ueno, M., Takakura, N., Matsushima, K., Mukaida, N., 2007. Essential Roles of the CC Chemokine Ligand 3-CC Chemokine Receptor 5 Axis in Bleomycin-Induced Pulmonary Fibrosis through Regulation of Macrophage and Fibrocyte Infiltration. *Am. J. Pathol.* 170, 843–854. <https://doi.org/10.2353/ajpath.2007.051213>
- Kastellorizios, M., Papadimitrakopoulos, F., Burgess, D.J., 2015. Multiple tissue response modifiers to promote angiogenesis and prevent the foreign body reaction around subcutaneous implants. *J. Control. Release* 214, 103–11. <https://doi.org/10.1016/j.jconrel.2015.07.021>
- Kenneth Ward, W., 2008. A review of the foreign-body response to subcutaneously-implanted devices: the role of macrophages and cytokines in biofouling and fibrosis. *J. Diabetes Sci. Technol.* 2, 768–77. <https://doi.org/10.1177/193229680800200504>
- Kim, D.H., Martin, D.C., 2006. Sustained release of dexamethasone from hydrophilic matrices using PLGA nanoparticles for neural drug delivery. *Biomaterials* 27, 3031–3037. <https://doi.org/10.1016/j.biomaterials.2005.12.021>
- Kim, Y., Romero-Ortega, M.I., 2012. Material considerations for peripheral nerve interfacing. *MRS Bull.* 37, 573–581. <https://doi.org/10.1557/mrs.2012.99>
- Lacour, S.P., FitzGerald, J.J., Lago, N., Tarte, E., McMahon, S., Fawcett, J., 2009. Long micro-channel electrode arrays: A novel type of regenerative peripheral nerve interface. *IEEE Trans. Neural Syst. Rehabil. Eng.* 17, 454–460. <https://doi.org/10.1109/TNSRE.2009.2031241>
- Lago, N., Yoshida, K., Koch, K.P., Navarro, X., 2007. Assessment of biocompatibility of chronically implanted polyimide and platinum intrafascicular electrodes. *IEEE Trans. Biomed. Eng.* 54, 281–290. <https://doi.org/10.1109/TBME.2006.886617>
- Lee, Y.J., Kim, H.J., Kang, J.Y., Do, S.H., Lee, S.H., 2017. Biofunctionalization of Nerve Interface via Biocompatible Polymer-Roughened Pt Black on Cuff Electrode for Chronic Recording. *Adv. Healthc. Mater.* 6. <https://doi.org/10.1002/adhm.201601022>
- Luttikhuisen, D.T., Harmsen, M.C., Van Luyn, M.J.A., 2006. Cellular and molecular dynamics in the Foreign Body Reaction. *Tissue Eng* 12, 77–96; discussion 97. <https://doi.org/10.1089/ten.2006.12.1955>

- McNally, A.K., Anderson, J.M., 2011. Macrophage fusion and multinucleated giant cells of inflammation. *Adv. Exp. Med. Biol.* 713, 97–111. https://doi.org/10.1007/978-94-007-0763-4_7
- Mercanzini, A., Reddy, S.T., Velluto, D., Colin, P., Maillard, A., Bensadoun, J.C., Hubbell, J.A., Renaud, P., 2010. Controlled release nanoparticle-embedded coatings reduce the tissue reaction to neuroprostheses. *J. Control. Release* 145, 196–202. <https://doi.org/10.1016/j.jconrel.2010.04.025>
- Micera, S., Navarro, X., Carpaneto, J., Citi, L., Tonet, O., Rossini, P.M., Carrozza, M.C., Hoffmann, K.P., Viv??, M., Yoshida, K., Dario, P., 2008. On the use of longitudinal intrafascicular peripheral interfaces for the control of cybernetic hand prostheses in amputees. *IEEE Trans. Neural Syst. Rehabil. Eng.* 16, 453–472. <https://doi.org/10.1109/TNSRE.2008.2006207>
- Navarro, X., Krueger, T.B., Lago, N., Micera, S., Stieglitz, T., Dario, P., 2005. A critical review of interfaces with the peripheral nervous system for the control of neuroprostheses and hybrid bionic systems. *J. Peripher. Nerv. Syst.* 10, 229–58. <https://doi.org/10.1111/j.1085-9489.2005.10303.x>
- Noel, S., Dhooghe, B., Leal, T., 2012. PDE5 Inhibitors as Potential Tools in the Treatment of Cystic Fibrosis. *Front. Pharmacol.* 3, 167. <https://doi.org/10.3389/fphar.2012.00167>
- Noorisafa, F., Razmjou, A., Emami, N., Low, Z.-X., Korayem, A.H., Kajani, A.A., 2016. Surface modification of polyurethane via creating a biocompatible superhydrophilic nanostructured layer: role of surface chemistry and structure. *J. Exp. Nanosci.* 8080, 1–23. <https://doi.org/10.1080/17458080.2016.1188223>
- Norton, L.W., Koschwanetz, H.E., Wisniewski, N.A., Klitzman, B., Reichert, W.M., 2007. Vascular endothelial growth factor and dexamethasone release from nonfouling sensor coatings affect the foreign body response. *J. Biomed. Mater. Res. - Part A* 81, 858–869. <https://doi.org/10.1002/jbm.a.31088>
- Onuki, Y., Bhardwaj, U., Papadimitrakopoulos, F., Burgess, D.J., 2008. A review of the biocompatibility of implantable devices: current challenges to overcome foreign body response. *J. Diabetes Sci. Technol.* 2. [https://doi.org/10.1016/S0091-679X\(07\)83003-2](https://doi.org/10.1016/S0091-679X(07)83003-2)
- Park, S.J., Lee, Y.J., Heo, D.N., Kwon, I.K., Yun, K.S., Kang, J.Y., Lee, S.H., 2015. Functional nerve cuff electrode with controllable anti-inflammatory drug loading and release by biodegradable nanofibers and hydrogel deposition. *Sensors Actuators, B Chem.* 215, 133–141. <https://doi.org/10.1016/j.snb.2015.03.036>
- Percival, J.M., Whitehead, N.P., Adams, M.E., Adamo, C.M., Beavo, J. a, Froehner, S.C., 2012. Sildenafil reduces respiratory muscle weakness and fibrosis in the mdx mouse model of Duchenne muscular dystrophy. *J. Pathol.* 228, 77–87. <https://doi.org/10.1002/path.4054>
- Raspopovic, S., Capogrosso, M., Petrini, F.M., Bonizzato, M., Rigosa, J., Di Pino, G., Carpaneto, J., Controzzi, M., Boretius, T., Fernandez, E., Granata, G., Oddo, C.M., Citi, L., Ciancio, A.L., Cipriani, C., Carrozza, M.C., Jensen, W., Guglielmelli, E., Stieglitz, T., Rossini, P.M., Micera, S., 2014. Restoring Natural Sensory Feedback in Real-Time Bidirectional Hand Prostheses. *Sci. Transl. Med.* 6, 222ra19–222ra19. <https://doi.org/10.1126/scitranslmed.3006820>

- Rodriguez, F.J., Ceballos, D., Schuttler, M., Valero, A., Valderrama, E., Stieglitz, T., Navarro, X., 2000. Polyimide cuff electrodes for peripheral nerve stimulation. *J. Neurosci. Methods* 98, 105–118. [https://doi.org/10.1016/S0165-0270\(00\)00192-8](https://doi.org/10.1016/S0165-0270(00)00192-8)
- Rossini, P.M., Micera, S., Benvenuto, A., Carpaneto, J., Cavallo, G., Citi, L., Cipriani, C., Denaro, L., Denaro, V., Di Pino, G., Ferreri, F., Guglielmelli, E., Hoffmann, K.P., Raspopovic, S., Rigosa, J., Rossini, L., Tombini, M., Dario, P., 2010. Double nerve intraneural interface implant on a human amputee for robotic hand control. *Clin. Neurophysiol.* 121, 777–783. <https://doi.org/10.1016/j.clinph.2010.01.001>
- Sahin, H., Wasmuth, H.E., 2013. Chemokines in tissue fibrosis. *Biochim. Biophys. Acta - Mol. Basis Dis.* 1832, 1041–1048. <https://doi.org/10.1016/j.bbadis.2012.11.004>
- Seki, E., De Minicis, S., Gwak, G.Y., Kluwe, J., Inokuchi, S., Bursill, C.A., Llovet, J.M., Brenner, D.A., Schwabe, R.F., 2009. CCR1 and CCR5 promote hepatic fibrosis in mice. *J. Clin. Invest.* 119, 1858–1870. <https://doi.org/10.1172/JCI37444.1858>
- Sheikh, Z., Brooks, P.J., Barzilay, O., Fine, N., Glogauer, M., 2015. Macrophages, foreign body giant cells and their response to implantable biomaterials. *Materials (Basel)*. <https://doi.org/10.3390/ma8095269>
- Skousen, J.L., Bridge, M.J., Tresco, P. a, 2014. A strategy to passively reduce neuroinflammation surrounding devices implanted chronically in brain tissue by manipulating device surface permeability. *Biomaterials* 36, 33–43. <https://doi.org/10.1016/j.biomaterials.2014.08.039>
- Sommakia, S., Lee, H.C., Gaire, J., Otto, K.J., 2014. Materials approaches for modulating neural tissue responses to implanted microelectrodes through mechanical and biochemical means. *Curr. Opin. Solid State Mater. Sci.* 18, 319–328. <https://doi.org/10.1016/j.cossms.2014.07.005>
- Spataro, L., Dilgen, J., Retterer, S., Spence, a. J., Isaacson, M., Turner, J.N., Shain, W., 2005. Dexamethasone treatment reduces astroglia responses to inserted neuroprosthetic devices in rat neocortex. *Exp. Neurol.* 194, 289–300. <https://doi.org/10.1016/j.expneurol.2004.08.037>
- Valente, E.G. a, Vernet, D., Ferrini, M.G., Qian, A., Rajfer, J., Gonzalez-Cadavid, N.F., 2003. L-Arginine and phosphodiesterase (PDE) inhibitors counteract fibrosis in the Peyronie's fibrotic plaque and related fibroblast cultures. *Nitric Oxide - Biol. Chem.* 9, 229–244. <https://doi.org/10.1016/j.niox.2003.12.002>
- Vince, V., Brelen, M.E., Delbeke, J., Colin, I.M., 2005. Anti-TNF α reduces the inflammatory reaction associated with cuff electrode implantation around the sciatic nerve. *J. Neuroimmunol.* 165, 121–128. <https://doi.org/10.1016/j.jneuroim.2005.04.019>
- Wurth, S., Capogrosso, M., Raspopovic, S., Gandar, J., Federici, G., Kinany, N., Cutrone, A., Piersigilli, A., Pavlova, N., Guiet, R., Taverni, G., Rigosa, J., Shkorbatova, P., Navarro, X., Barraud, Q., Courtine, G., Micera, S., 2017. Long-term usability and bio-integration of polyimide-based intra-neural stimulating electrodes. *Biomaterials* 122, 114–129. <https://doi.org/10.1016/j.biomaterials.2017.01.014>
- Zhong, C., Ke, D., Wang, L., Lu, Y., Wang, L., 2017. Bioactive interpenetrating polymer networks for improving the electrode/neural-tissue interface. *Electrochem. commun.* 79, 59–62. <https://doi.org/10.1016/j.elecom.2017.04.015>

Zhong, Y., Bellamkonda, R. V, 2007. Dexamethasone-coated neural probes elicit attenuated inflammatory response and neuronal loss compared to uncoated neural probes. *Brain Res.* 1148, 15–27. <https://doi.org/10.1016/j.brainres.2007.02.024>

CHAPTER 4: DEXAMETHASONE IMPROVES LONG-TERM FUNCTION OF TRANSVERSAL INTRANEURAL ELECTRODES

Natàlia de la Oliva¹, Jaume del Valle^{1,2}, Ignacio Delgado-Martínez¹, Xavier Navarro¹

¹ Institute of Neurosciences, Department of Cell Biology, Physiology and Immunology, Universitat Autònoma de Barcelona, and Centro de Investigación Biomédica en Red en Enfermedades Neurodegenerativas (CIBERNED), Bellaterra, Spain.

² Catalan Institute of Nanoscience and Nanotechnology (ICN2), CSIC and BIST, Campus UAB, Bellaterra, 08193 Barcelona, Spain

ABSTRACT

Neuroprostheses aimed to restore lost functions after a limb amputation are based on the interaction with the nervous system by means of neural interfaces. Among the different designs, intraneural electrodes implanted in peripheral nerves represent a good strategy to stimulate nerve fibers to send sensory feedback and also to record nerve signals to control the prosthetic limb. However, any device implanted in the body undergoes a process called foreign body reaction (FBR). The FBR is an immune-mediated response to any device implanted in the body that includes a first pro-inflammatory phase followed by a second anti-inflammatory and tissue remodeling phase, which results in the tissue encapsulation of the device implanted. In the case of intraneural electrodes, which should remain chronically implanted to interact with nerve fibers, the FBR causes a progressive decline of function over time due to the physical separation between the electrode and the axons to interface. Administration of anti-inflammatory drugs such as dexamethasone might reduce the FBR and maintain electrode functionality. In this work, transversal intraneural multi-channel electrodes (TIMEs) implanted in rat sciatic nerve have been tested during 3 months to evaluate its stimulation and recording capabilities. Dexamethasone treatment significantly reduced the current needed to evoke a muscle response during the follow-up compared to saline-treated animals, without affecting the selectivity of stimulation. However, dexamethasone treatment did not improve the signal-to-noise ratio (SNR) of the recorded neural signals in comparison to the saline group. Dexamethasone treatment was associated with more working active sites than with saline treatment. Thus, systemic administration of dexamethasone appears as a useful treatment to improve the functionality of chronically implanted neural electrodes.

INTRODUCTION

The interface of neuroprosthetic systems intended to substitute an amputated limb is based in the stimulation of remaining sensory nerves to evoke sensory feedback and in the recording of motor nerve signals to control the prosthetic device (Navarro et al., 2005; Tyler et al., 2015). Peripheral nerve electrodes are a key component of neuroprostheses, as they are the active part that will interact with the nervous tissue to stimulate and record signals from nerve fibers. Despite the different designs of neural interfaces, all of them consist on a polymer substrate where metal active sites are embedded to deliver current to stimulate nerve fibers or to record nerve signals due to changes in the membrane potentials. Therefore, the relative position and distance to the nerve fibers will determine the intensity needed to stimulate the axons and the quality of the recorded signals. Among the different designs developed, intraneural electrodes, such as the transversal intrafascicular multichannel electrode (TIME), have shown good capabilities for selective stimulation and high quality recorded neural signals in comparison to extraneural electrodes, as the active sites in the electrode are closer to nerve fibers than with perineural electrodes, such as cuffs (Badia et al., 2011a).

However, studies in human volunteers and animal experiments have shown a progressive decline in the intraneural electrode functionality over time (Oddo et al., 2016; Raspopovic et al., 2014; Rossini et al., 2010). It has been shown that an immune-mediated response, known as the foreign body reaction (FBR), is triggered after the implantation of any device in the body (Anderson et al., 2008; Ward, 2008). Regarding neural interfaces, it is characterized by an inflammatory phase, where polymorphonuclear cells and monocytes/macrophages infiltrate the tissue from 1 day up to 8 weeks after the implant. This first phase induces a second anti-inflammatory and tissue remodeling phase by week 8 post-implant, mainly orchestrated by fibroblasts (Christensen et al., 2014; de la Oliva et al., 2017; Wurth et al., 2017). The FBR to neural interfaces results in a progressive tissue encapsulation, leading to physical separation of the electrode from the nervous tissue and an increase in tissue resistance. Since the relative position and distance to the nerve fibers is critical to determine the intensity needed to stimulate the axons and the quality of the recorded signals, the capsule tissue around the electrode will affect its functionality.

Different strategies have been pursued to improve the long-term functional outcome of implanted electrodes, including the use of different polymers as a substrate of the electrode (Kim and Romero-Ortega, 2012; Skousen et al., 2014; Sommakia et al., 2014), diverse surface coatings (Balaji et al., 2015; Chen and Allen, 2012; Noorisafa et al., 2016)

and pharmacological modulators of the FBR (Kastellorizios et al., 2015; Norton et al., 2007). One of the most used drugs to modulate this reaction is dexamethasone, a glucocorticoid known for its anti-inflammatory and immune-depressant effects (Coutinho and Chapman, 2011). Dexamethasone administration has shown good results in reducing the inflammatory reaction to implanted electrodes in the central nervous system (Spataro et al., 2005; Zhong and Bellamkonda, 2007) as well as improving brain recordings (Boehler et al., 2017). However, not all the strategies mentioned above are suitable for peripheral nerves, as they may increase the size of the electrode to implant. Some studies have applied these strategies to peripheral nerve electrodes, as for example, dexamethasone-releasing cuff (Park et al., 2015) or dexamethasone-loaded regenerative (FitzGerald, 2016) electrodes. However, these studies did not take into account the time-window in which such modulators may be effective or if the modulation of the FBR has positive effects on the functional performance of the electrodes for stimulation and recording. Systemic administration of modulators of the FBR allows for a better control of dosage and timing without modifications in the design of current nerve electrodes. We have made a comparative assay of several compounds with potential anti-inflammatory and/or anti-fibrotic properties in the previous chapter and found that dexamethasone was the most effective drug to reduce the capsule thickness. Thus, this study aims to evaluate if dexamethasone treatment improves the long-term functional outcome of TIME electrodes implanted in the rat sciatic nerve.

MATERIAL AND METHODS

Surgical procedures and drug administration

All animal experiments conducted in this study were performed according to protocols approved by the Ethical Committee of the Universitat Autònoma de Barcelona in accordance with the European Communities Council Directive 2010/63/EU.

The electrode used was a transversal intrafascicular multichannel electrode (TIME version 3H; developed by the Department of Microsystems Engineering-IMTEK, University of Freiburg, Germany) (Boretius et al., 2010). It contains seven active sites (AS) made of iridium oxide at each arm of the device, with a diameter of 80 μm in one arm and a diameter ranging from 20 to 60 μm in the other. In this study, only the AS of 80 μm at one arm were evaluated. The TIME electrodes were implanted in the sciatic nerve of female Sprague-Dawley rats ($n=12$, $220\pm 20\text{g}$). Animals were anesthetized with ketamine and xylazine (90/10 mg/kg, i.p.) and the sciatic nerve was surgically exposed at the mid thigh and freed from adhesions to surrounding tissues. Following the same procedure as in Badia *et al.*, 2011, the TIME was transversally inserted across the sciatic nerve with the help of a straight needle attached to a 10-0 loop thread. All the process was monitored under a dissection microscope to ensure the correct position of the active sites (AS) inside the nerve fascicles (Fig. 1). Since the TIME used was originally designed for human nerves, in most cases, only 2-3 of seven contacts per arm were positioned within the rat sciatic nerve at the same time. Then, the electrode tip was fixed to the closest muscle with a 10-0 suture to avoid motion. The PCB, where the TIME tracks are connected to wires, was fixed on the gluteus muscles to reduce tethering forces on the electrode. The wires were routed inside a thin silicone tube subcutaneously and finished in a Nano Plastic Circular Omnetic connector that was fixed with a custom-made plastic base on the back of the animal to facilitate the connection during the electrophysiological tests and covered with a metal protection cap. The surrounding muscles and the skin were closed with sutures and the wounds disinfected with povidone-iodine (Fig. 1). After the surgical procedure, animals were left to recover in warm pads. During the follow-up, they were housed at $22\pm 2^\circ\text{C}$ under a 12:12h light cycle with food and water access ad libitum.

Half of the rats were administered daily with dexamethasone ($n=6$, 200 $\mu\text{g}/\text{kg}$ subcutaneous; Merck) from two days before the surgery to ensure systemic levels and during all the follow-up. The other half received an injection of the same volume of saline vehicle. After 12 weeks post-implant, animals were deeply anesthetized with an overdose

of pentobarbital, transcardially perfused with 4% paraformaldehyde in phosphate buffer and the sciatic nerve including the implanted device harvested for histological analysis.

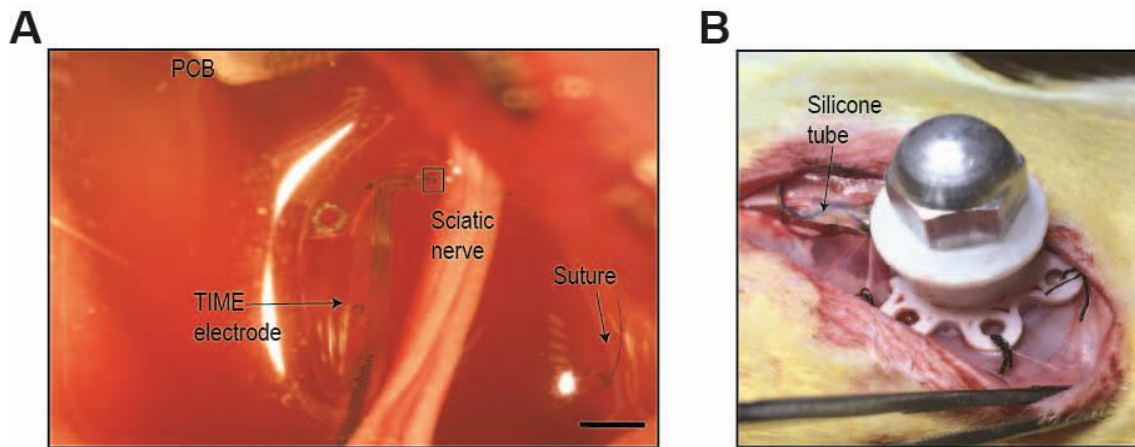


Figure 1. Surgical implantation of TIME electrode. (A) Photograph of the TIME inserted transversally in the rat sciatic nerve, with the tip sutured to the close muscle to avoid motion. Active site 1 (square) can be seen near the nerve. Scale bar = 1cm. (B) View of the back of the animal with the subcutaneous silicone tube protecting the wires and the plastic base holding the Omnetics connector sutured to the fascia. The metal cup is used to prevent damage to the connector.

Histological studies

To identify the location of TIME electrode inside the nerve and to evaluate the presence of foreign body giant cells (FBGCS), the nerve segment including the intraneural electrode was embedded in paraffin. Transverse sections (10 μm thick) were cut, mounted on silane-coated slides and dried overnight. Sections were deparaffinized and successively stained, first overnight with standard luxol fast blue (LFB) for myelin visualization, after that with hematoxylin Harris solution (Fluka, Sigma) for 7 min, washed with water and stained with Eosin Y (Merck Millipore) for 5 min. Sections were dehydrated with series of graded ethanol rinses and mounted with DPX (Sigma).

Nerve stimulation protocol

To assess the stimulation capabilities of implanted TIMEs, biphasic rectangular current pulses with a width of 100 μs and an intensity up to 1 mA were delivered (Stimulator DS4, Digitimer) through each one of the active sites against a small needle electrode placed subcutaneously. Simultaneously, the compound muscle action potentials (CMAP) were recorded from gastrocnemius medialis (GM), tibialis anterior (TA) and plantar interossei (PL) muscles using small needle electrodes placed in each muscle (Badia et al., 2011a). EMG data was amplified x200 for GM and TA and x1000 for PL muscles (P511AC amplifiers,

Grass), band-pass filtered (3 Hz to 3 kHz) and digitized with a Powerlab recording system (PowerLab16SP, ADInstruments) at 20 kHz. The amplitude of each CMAP (M wave) was measured peak to peak and normalized to the maximum CMAP amplitude obtained in each experiment by monopolar stimulation of the sciatic nerve with a stainless-steel needle electrode. For each active site (AS), the current of stimulation that elicited a 5, 36, 50 and 95% of the maximum CMAP was determined. The threshold current was defined as the minimal current needed to elicit the above-mentioned percentages of CMAP. Due to nerve dimension, only 2 or 3 ASs out of 7 could be properly accommodated inside the nerve. Therefore, only the best AS with the lowest threshold value was used for data analysis and comparison between groups. Finally, the selectivity index (SI) was calculated to quantify the specific activation of a single muscle among the set of three muscles (GM, PL, TA) when stimulating from each active site, as previously described (Badia et al., 2011a; Veraart et al., 1993) and the maximum SI (SI_{max}) from each TIME for each muscle was analysed.

Nerve signals recording protocol

To assess the recording capabilities of TIME electrodes over time, two different protocols were performed a previously described (Badia et al., 2016).

First, the compound nerve action potentials (CNAPs) were recorded from each one of the active sites in the TIME following electrical stimulation of the distal tibial nerve. Monophasic rectangular pulses of 100 μ s and up to 5 mA (Stimulator DS4, Digitimer) were delivered using two small needles inserted on the medial side of the paw. The CNAP amplitude was measure peak to peak for each active site in each electrode and the mean of the maximum amplitude recorded from each TIME was analyzed. On the other hand, evoked neural activity after fast scratching with a plastic blunt probe the plantar surface of the paw (10 repetitions) was also recorded from each active site. Signals recorded were amplified x5000, band-pass filtered (between 300 Hz and 10 kHz) and fed to a power-line noise eliminator (Hum Bug, Quest Scientific), then digitized at 20 kHz and recorded with Chart software (PowerLab System, ADInstruments). The total power of the recorded signals and the noise was obtained after applying the short-time Fourier transform with a window of 1 ms, and an overlap of 87.5% (Chart software) and the signal-to-noise ratio (SNR) was calculated.

Animal body temperature was maintained constant using a thermostatic heating pad during the stimulation and recording session. Both stimulation and recording protocols were performed acutely (0 days, 30 minutes after the implantation) and at chronic time points (7, 14, 30, 60 and 90 days after implant) or until failure of the interface.

Statistical analysis

Results are expressed as the average \pm SEM. Differences between groups or times were analyzed by two-way ANOVA followed by Bonferroni post hoc tests (GraphPad Prism). Statistical significance was considered at $p < 0.05$.

RESULTS

Animals implanted with TIME electrodes and administered with dexamethasone or saline were followed for 3 months to evaluate electrode functionality. Unfortunately, many times the wiring system resulted damaged too early, and the experiment had to be aborted ahead of time. Therefore, the comparison between the two groups with respect to electrophysiological results was only performed up to 1 month of implant.

Nerve stimulation results

The plot of the current needed to achieve a CMAP of 5% of the maximal amplitude (5% threshold) for each active site in each TIME implanted showed changes over time. For some electrodes (e.g., electrodes 1 and 3) a progressive increase over time was observed. In contrast, in electrodes 2, 4, 5 and 6, there was an increase in the threshold during the first two weeks that was later decreased (Fig. 2). The 5% threshold of the contacts located inside the nerve was $70 \mu\text{A} \pm 10 \text{ SEM}$ ($n=6/\text{group}$), while nearly half of the ASs was outside and showed a 5% threshold of $300 \mu\text{A} \pm 70 \text{ SEM}$ (Fig. 2) in the first day of the implant. Moreover, a shift from the original position (day 0) for some implanted electrodes was observed, as the ASs with lower threshold changed during the follow-up (Fig. 2). In consequence, only the best AS (i.e., the lowest threshold value which would indicate the best position inside the nerve) for each muscle in each electrode was chosen for comparison between dexamethasone and saline-treated animals.

Focusing on the results of the different thresholds needed to elicit a 5%, 36%, 50% and 95% (Fig. 3 A-D) of the maximum CMAP amplitude, all animals showed a clear increase in the first week of follow-up, with a stabilization at day 14 and 30 after the implant (two-way ANOVA vs time, $p<0.05$). Moreover, rats receiving dexamethasone had significantly lower values for GM and TA muscles (two-way ANOVA vs saline, $p<0.05$) in comparison with the saline-treated group (Fig. 3), indicating that the treatment limited the initial increase in tissue resistance. Moreover, the treated group still maintained lower values after 1 month of implant, showing that electrodes implanted in dexamethasone-treated rats required less current than saline ones (Fig.3).

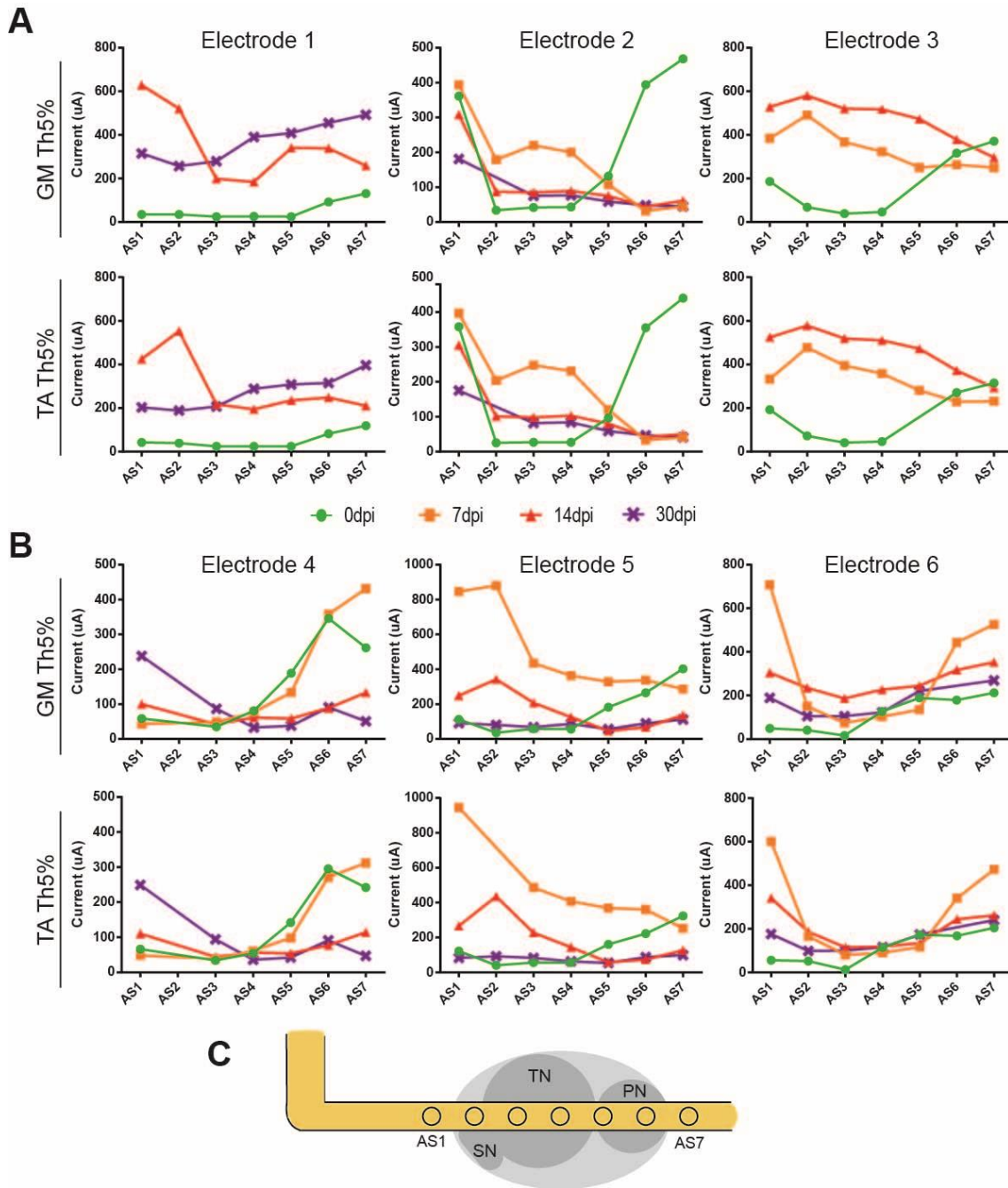


Figure 2. Evolution of 5% threshold values for each AS in implanted TIMEs over time. Stimulus current needed to evoke a CMAP of 5% the maximal amplitude in gastrocnemius (GM) and tibialis anterior (TA) muscles (5% threshold) by three different (A) saline or (B) dexamethasone-treated electrodes over time. (C) Schematic view of a TIME implanted in the fascicles (SN: sural nerve, TN: tibial nerve, PN: peroneal nerve) of the sciatic nerve with the ideal position of the active sites (from AS1 to AS7). Note the increase in threshold values over time (e.g., electrode 3) and the changes in the AS with the lowest threshold value likely due to AS displacement in the nerve (e.g., electrode 6).

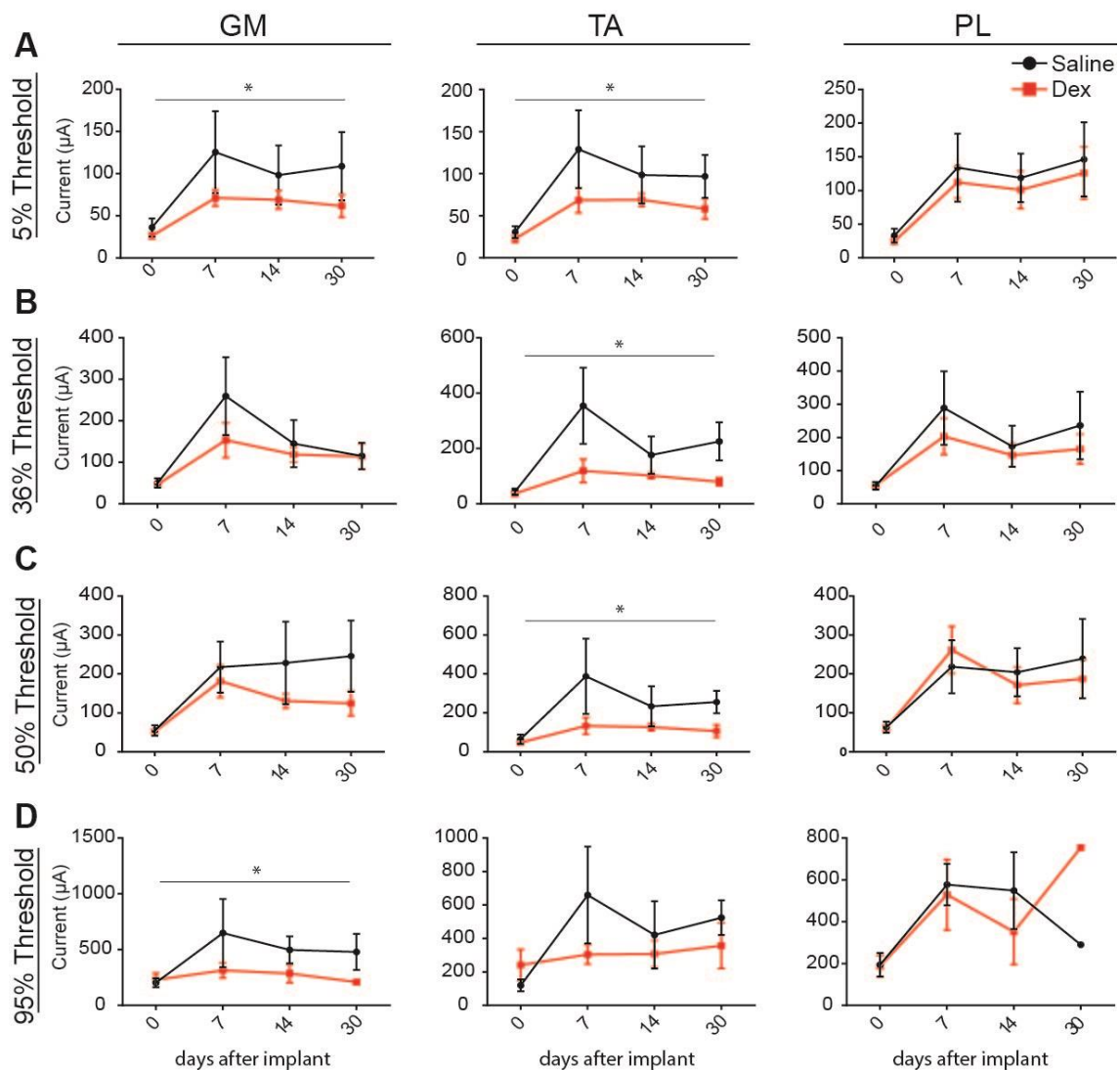


Figure 3. Differences in current values needed to evoke the (A) 5%, (B) 36%, (C) 50% or (D) 95% of the maximum CMAP of gastrocnemius (GM), tibialis anterior (TA) and plantar interossei (PL) muscles between saline and dexamethasone-treated groups over time. * $p < 0.05$ s saline group, two-way ANOVA.

Additionally, the total amount of working ASs able to evoke a 5%, 36%, 50% or 95% of the maximum CMAP decreased over time for both groups, with animals receiving the dexamethasone treatment maintaining more working ASs, although without significant differences (Fig. 4).

The selectivity of stimulation (SI) for the three different muscles tested innervated by the sciatic nerve was also calculated. The SI for GM and TA muscles were maintained during the follow-up, without differences between both groups. In the case of the PL muscle, the SI decreased from 0 to 30 days after the implant in treated and saline animals (two-way ANOVA vs time, $p < 0.001$) (Fig.5A). On the other hand, while there were no differences in

the SI between groups, the current needed to achieve the maximum SI was lower, although not significantly, in the dexamethasone-treated animals (Fig. 5B), according to the previous result in threshold current (Fig. 3).

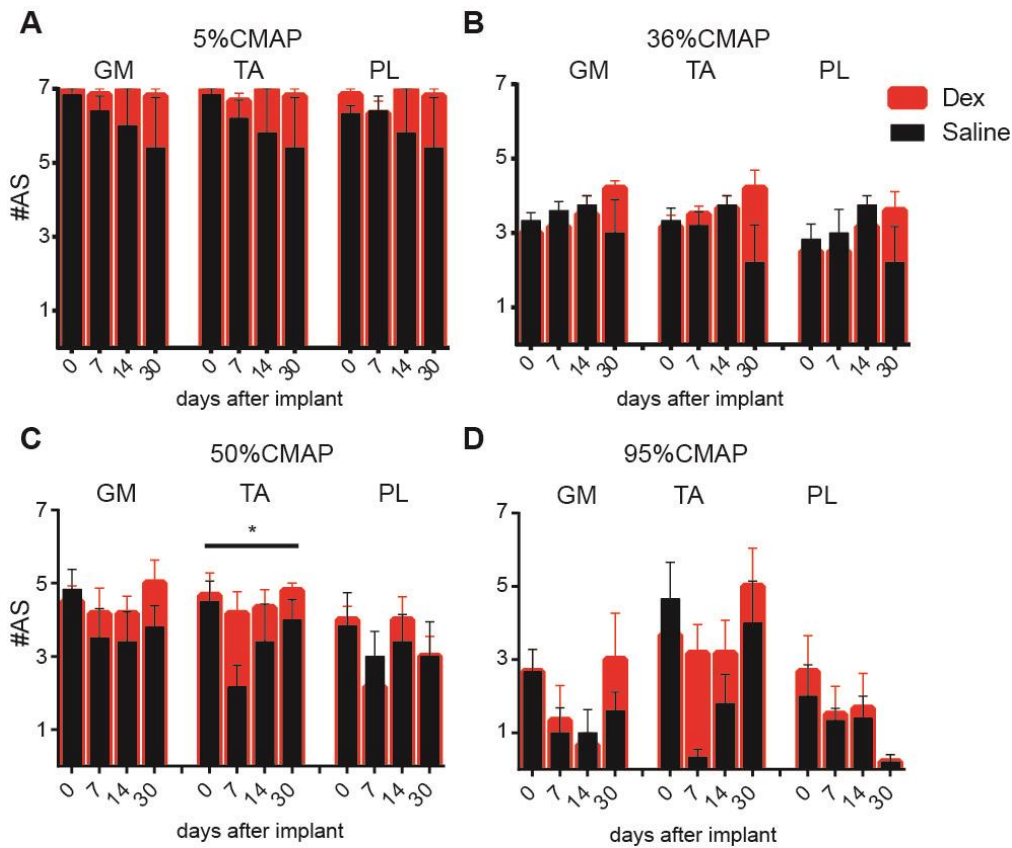


Figure 4. Number of working AS able to evoke CMAPs of (A) 5%, (B) 36%, (C) 50% and (D) 95% of the maximum CMAP amplitude of gastrocnemius (GM), tibialis anterior (TA) and plantar interossei (PL) muscles, in the saline and dexamethasone-treated groups at different time points. * $p < 0.05$ vs saline group, two-way ANOVA.

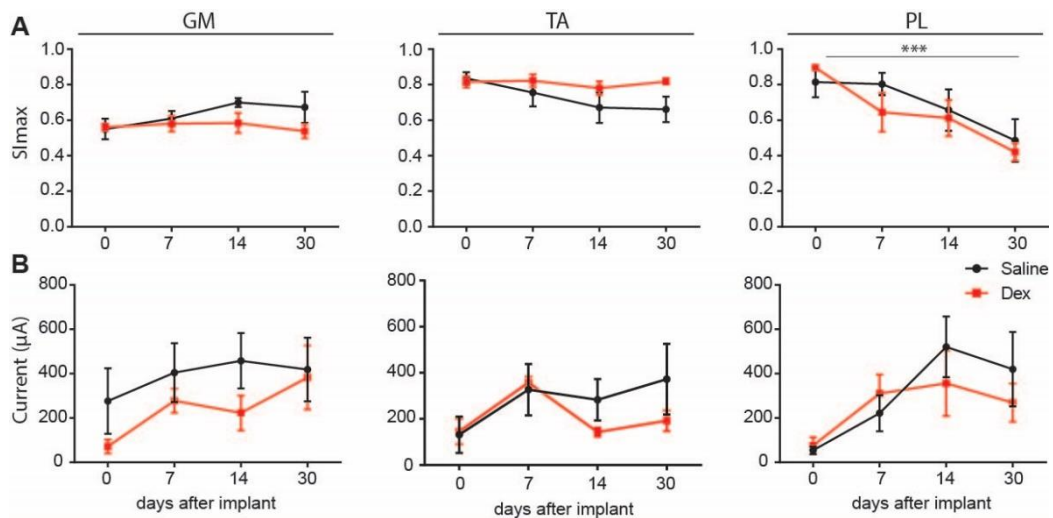


Figure 5. (A) Maximal selectivity index (SImax) and (B) current needed to achieve the SImax for gastrocnemius (GM), tibialis anterior (TA) and plantar interossei (PL) muscles over time in saline and dexamethasone-treated groups. *** $p < 0.001$ vs time, two-way ANOVA.

Nerve signals recording results

Electrical stimulation of the distal nerve was used to generate afferent CNAPs conducted orthodromically by the sciatic nerve and recorded from the different ASs in the implanted TIME. The maximum amplitude recorded for the CNAP decrease over time for both groups (two-way ANOVA vs time, $p < 0.05$). Electrodes under dexamethasone treatment appeared to record CNAPs of slightly higher amplitudes, although not significantly, than saline-treated electrodes during the first two weeks of follow-up (Fig. 6A). Electroneurographic recordings were also performed during mechanical stimulation of the hind paw sole. Moreover, the SNR value drastically decreased from 0 to 7 days after the implant, and remained unchanged until 30 days (Fig. 6 B, C), without differences between the two groups at any studied time point. Finally, dexamethasone treatment resulted in a higher number of ASs capable of recording afferent signals during mechanical stimulation during the follow-up (Fig.6D).

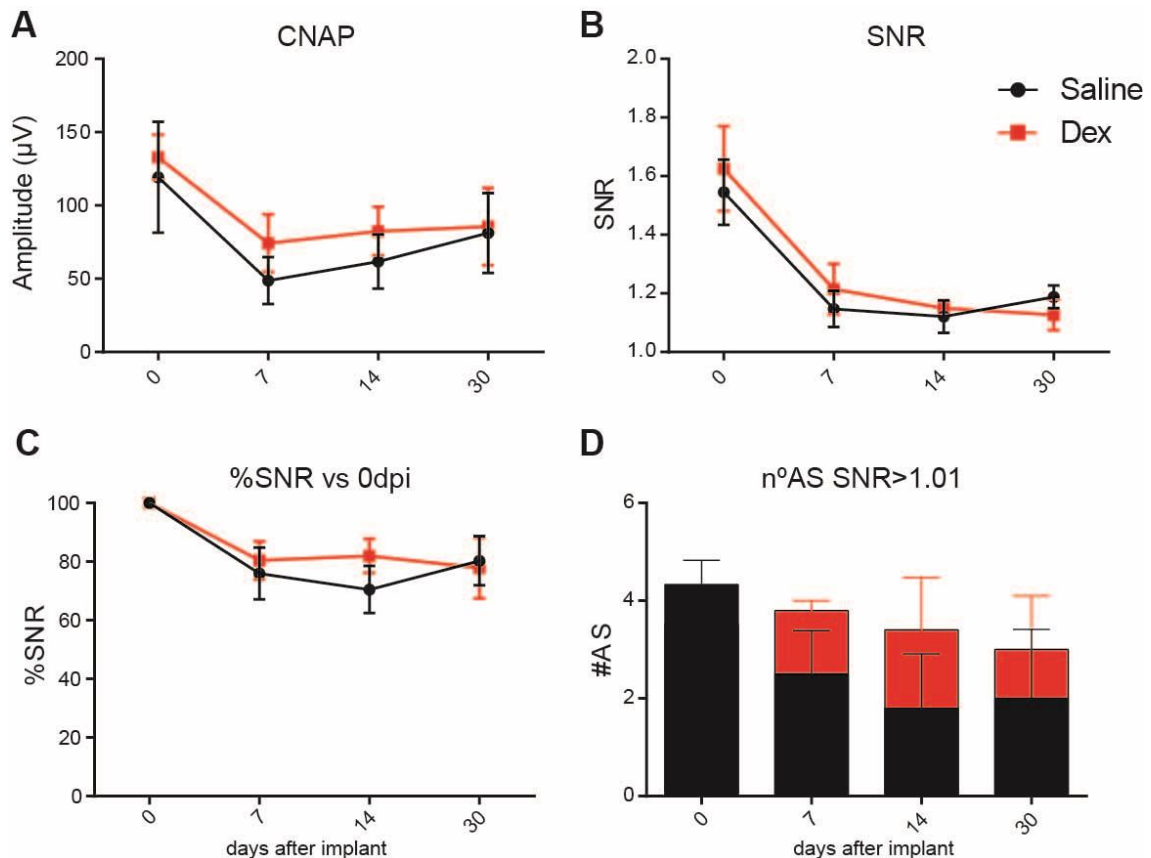


Figure 6. Recording evoked neural activity over time. (A) Maximum CNAP amplitude recorded by TIME in saline and dexamethasone-treated rats. (B) Signal-to-noise ratio (SNR) of sensory afferent signals induced by mechanical stimulation on the sole during time after implantation in saline and dexamethasone-treated rats. (C) Decrease of the SNR with respect to acute recordings (day 0) in saline and dexamethasone-treated groups. (D) Number of AS that recorded nerve signals with an SNR above 1.01 along time.

Nerve histology

Histological evaluation after 3 months of TIME implant showed that most of the electrodes implanted were within the fascicles of the sciatic nerve, traversing peroneal and tibial fascicles (Fig. 7A, B). Although axons were still close to the active sites, the electrodes were surrounded by a thick capsule of fibrotic tissue, as shown by the hematoxylin-eosin staining and no noticeable differences between dexamethasone and saline groups were observed. Moreover, foreign body giant cells (FBGCs) (McNally and Anderson, 2011) were present in close contact with the polyimide substrate, indicative of the second anti-inflammatory phase of the FBR (Fig. 7C, D).

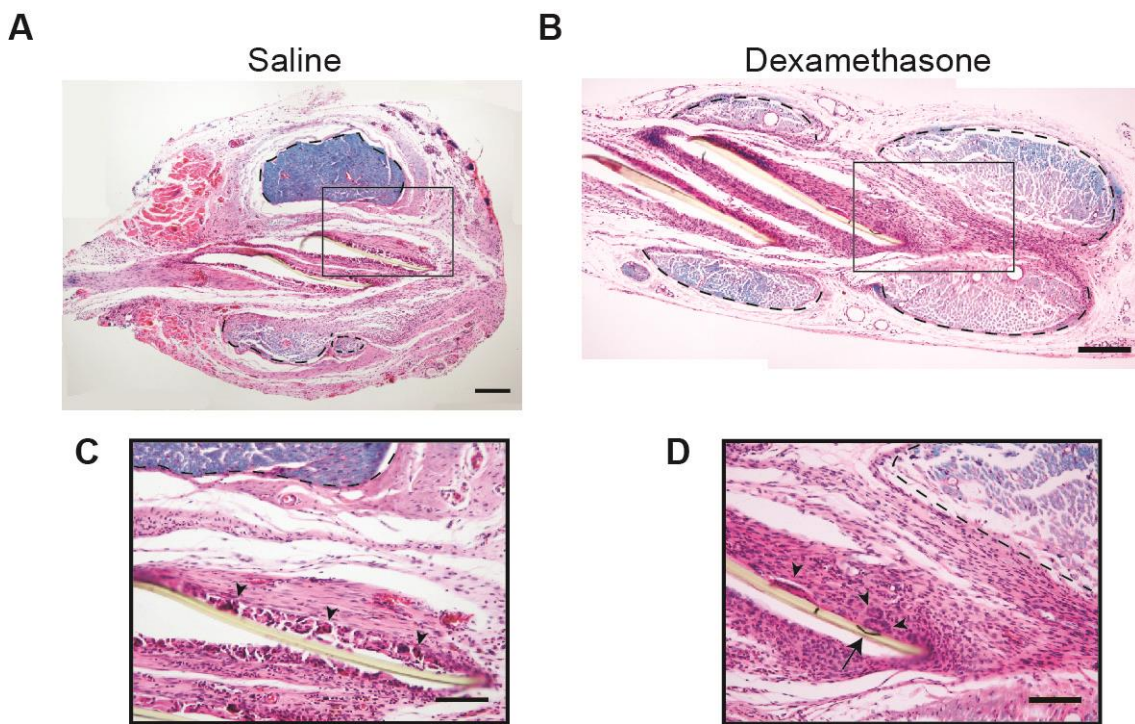


Figure 7. Histological evaluation of TIME electrodes after 12 weeks of implant with (A) saline or (B) dexamethasone treatment. Dotted lines delimit nerve fascicles. Note the empty spaces due to sample processing. Insets from (C) saline and (D) dexamethasone-treated rats showing an ASs inside the nerve (arrow in D) and foreign body giant cells (FBGCs; arrowheads in C and D). Scale bars in (A-B) 200 μ m and (C-D) 100 μ m.

DISCUSSION

Neural electrodes are a key component of interfaces for the communication between the nervous system and bionic prostheses. Despite the considerable advances achieved in biomaterial and electrode designs (Boddupalli et al., 2016; Navarro et al., 2005; Tyler et al., 2015), improved stability is desired to maintain the functionality of the implanted electrodes over long periods of time. One of the factors that contributes to the failure or decline of function of neural implants is the FBR (de la Oliva et al., 2017). The encapsulation of the implanted devices enlarges the distance between the axons membrane and the active sites and also increases the tissue resistance, resulting in an increase in the current needed to stimulate the neurons and the axons and also a decrease of the SNR during recordings. This study combines two of the most promising strategies to improve the long-term functionality of neural implants in peripheral nerves: transversal and flexible intraneural electrodes (i.e., TIME) and anti-inflammatory treatment (i.e., dexamethasone) by systemic administration.

TIME electrodes have been previously shown to provide good stimulation capabilities in animal models (Badia et al., 2016, 2011a) and humans (Oddo et al., 2016; Raspopovic et al., 2014). Although these studies reported adequate values of impedance and injected charge for useful stimulation in human patients, an increase in the stimulation threshold was observed during the first month of implant. Our present results are in agreement since the stimulation current needed to activate the nerve increased during the first weeks of implant, followed by a stabilization of the threshold values. Moreover, the selectivity indices achieved in this work are similar to those shown in previous studies with intraneural electrodes (Badia et al., 2011a; Cutrone et al., 2015; Wurth et al., 2017), confirming the stable selectivity in chronic implants despite the increased threshold.

TIME electrode was designed as a bidirectional interface, capable of stimulating as well as recording nerve signals. However, few works have focused on the recording capabilities of this type of electrode and only in acute conditions (Badia et al., 2016). Our results on chronically implanted TIME electrodes show a marked decrease in the amplitude of the recorded signals, either compound or single action potentials from one week post-implant, although later they stabilized in the following weeks.

Several studies have looked for the effect of anti-inflammatory drugs on the FBR to neural implants, with positive effects on electrode functionality and on the amount of FBR (Boehler et al., 2017; Park et al., 2015; Spataro et al., 2005; Zhong and Bellamkonda, 2007). However, this is the first work in which it has been evaluated with intraneural electrodes in the

peripheral nerve. The present results indicate that dexamethasone administration substantially decreased the stimulation threshold values during the first month of implant. Throughout the course of this first month, the inflammation of the first phase of the FBR peaks (de la Oliva et al., 2017) and dexamethasone treatment not only decreases the amount of inflammatory macrophages within the nerve but also shrinks the capsule around intraneural devices (De la Oliva et al., submitted, Chapter 3). On the other hand, dexamethasone treatment did not improve the capability for recording neural signals. The quality of the recorded signal relies on the amplitude of that signal and the placement of the AS with respect to the activated axons. Since the amplitude of nerve signals is on the scale of microvolts, the distance between the axons and the AS and the capsule tissue characteristics become critical to have a good SNR. The FBR adds about 30 μm of separation between the ASs and the axons in longitudinal implants (de la Oliva et al., 2017), but it seems larger in transversal implants (Wurth et al., 2017; present study). In addition, the fibrotic capsule formed around the electrode will presumably offer a higher resistivity, that might be comparable to that of the perineurium (Weerasuriya et al., 1984), than the endoneurial tissue in the nerve. Probably due to the decrease in capsule thickness produced by dexamethasone treatment, there were more AS able of recording small nerve signals.

These results showed a positive effect of dexamethasone treatment on the functionality of intraneural electrodes during the first month of implant. Other previously proposed strategies try to deliver different drugs locally on the implant side. However, these strategies have some limitations in the case of intraneural electrodes, such as the nerve size. Thus, local delivery systems are difficult to adapt to intraneural electrodes. Our results demonstrated that systemic administration of anti-inflammatory drugs would be useful and easily to apply. Moreover, stronger effects could be expected in more stable models of electrode implantation, such those observed in brain implants (Boehler et al., 2017), or in larger nerves (i.e., human implants), since the size mismatch between rat nerves and the implanted electrodes is more prominent than in other species.

In conclusion, dexamethasone treatment improves the stimulation and recording capabilities of implanted transversal electrodes after implant, being a feasible option to improve the functionality of chronic implanted electrodes. Further studies to improve electrode stability and signal recording and decoding are needed to ensure electrode functionality over time.

ACKNOWLEDGEMENTS

This research was supported by the European Union FPT-ICT project NEBIAS under contract number 611687, FEDER funds, and TERCEL (RD12/0019/0011) and CIBERNED (CB06/05/1105) funds from the Instituto de Salud Carlos III of Spain. The ICN2 is funded by the CERCA programme / Generalitat de Catalunya, and it is also supported by the Severo Ochoa programme of the Spanish Ministry of Economy, Industry, and Competitiveness (MINECO, grant no. SEV-2013-0295). The authors thank Monica Espejo and Jessica Jaramillo for technical help. Paul Cvancara, Matthias Müller and Thomas Stieglitz from IMTEK, University of Freiburg, provided the TIME devices used in the study.

REFERENCES

- Anderson, J.M., Rodriguez, A., Chang, D.T., 2008. Foreign body reaction to biomaterials. *Semin. Immunol.* <https://doi.org/0.1016/j.smim.2007.11.004>
- Badia, J., Boretius, T., Andreu, D., Azevedo-Coste, C., Stieglitz, T., Navarro, X., 2011a. Comparative analysis of transverse intrafascicular multichannel, longitudinal intrafascicular and multipolar cuff electrodes for the selective stimulation of nerve fascicles. *J. Neural Eng.* 8, 36023. <https://doi.org/10.1088/1741-2560/8/3/036023>
- Badia, J., Boretius, T., Pascual-Font, A., Udina, E., Stieglitz, T., Navarro, X., 2011b. Biocompatibility of chronically implanted transverse intrafascicular multichannel electrode (TIME) in the rat sciatic nerve. *IEEE Trans. Biomed. Eng.* 58, 2324–2332. <https://doi.org/10.1109/TBME.2011.2153850>
- Badia, J., Raspopovic, S., Carpaneto, J., Micera, S., Navarro, X., 2016. Spatial and Functional Selectivity of Peripheral Nerve Signal Recording With the Transversal Intrafascicular Multichannel Electrode (TIME). *IEEE Trans. Neural Syst. Rehabil. Eng.* 24, 20–27. <https://doi.org/10.1109/TNSRE.2015.2440768>
- Balaji, A., Jaganathan, S.K., Vellayappan, M. V., John, A.A., Subramanian, A.P., SelvaKumar, M., Mohandas, H., Sundar Raj, M., Supriyanto, E., 2015. Prospects of common biomolecules as coating substances for polymeric biomaterials. *RSC Adv.* 5, 69660–69679. <https://doi.org/10.1039/c5ra12693b>
- Boddupalli, A., Zhu, L., Bratlie, K.M., 2016. Methods for Implant Acceptance and Wound Healing: Material Selection and Implant Location Modulate Macrophage and Fibroblast Phenotypes. *Adv. Healthc. Mater.* <https://doi.org/10.1002/adhm.201600532>
- Boehler, C., Kleber, C., Martini, N., Xie, Y., Dryg, I., Stieglitz, T., Hofmann, U.G.G., Asplund, M., 2017. Actively controlled release of Dexamethasone from neural microelectrodes in a chronic in vivo study. *Biomaterials* 129, 176–187. <https://doi.org/10.1016/j.biomaterials.2017.03.019>
- Chen, S., Allen, M.G., 2012. Extracellular matrix-based materials for neural interfacing. *MRS Bull.* 37, 606–613. <https://doi.org/10.1557/mrs.2012.120>
- Christensen, M.B., Pearce, S.M., Ledbetter, N.M., Warren, D.J., Clark, G. a, Tresco, P. a, 2014. The foreign body response to the Utah Slant Electrode Array in the cat sciatic nerve. *Acta Biomater.* 10, 4650–60. <https://doi.org/10.1016/j.actbio.2014.07.010>
- Coutinho, A.E., Chapman, K.E., 2011. The anti-inflammatory and immunosuppressive effects of glucocorticoids, recent developments and mechanistic insights. *Mol. Cell. Endocrinol.* 335, 2–13. <https://doi.org/10.1016/j.mce.2010.04.005>

- Cutrone, A., Del Valle, J., Santos, D., Badia, J., Filippeschi, C., Micera, S., Navarro, X., Bossi, S., 2015. A three-dimensional self-opening intraneural peripheral interface (SELINe). *J. Neural Eng.* 12, 16016. <https://doi.org/10.1088/1741-2560/12/1/016016>
- de la Oliva, N., Navarro, X., del Valle, J., 2017. Time course study of long-term biocompatibility and foreign body reaction to intraneural polyimide-based implants. *J. Biomed. Mater. Res. Part A* 1–29. <https://doi.org/10.1002/jbm.a.36274>
- FitzGerald, J.J., 2016. Suppression of scarring in peripheral nerve implants by drug elution. *J. Neural Eng.* 13, 26006. <https://doi.org/10.1088/1741-2560/13/2/026006>
- Kastellorizios, M., Papadimitrakopoulos, F., Burgess, D.J., 2015. Multiple tissue response modifiers to promote angiogenesis and prevent the foreign body reaction around subcutaneous implants. *J. Control. Release* 214, 103–11. <https://doi.org/10.1016/j.jconrel.2015.07.021>
- Kim, Y., Romero-Ortega, M.I., 2012. Material considerations for peripheral nerve interfacing. *MRS Bull.* 37, 573–581. <https://doi.org/10.1557/mrs.2012.99>
- McNally, A.K., Anderson, J.M., 2011. Macrophage fusion and multinucleated giant cells of inflammation. *Adv. Exp. Med. Biol.* 713, 97–111. https://doi.org/10.1007/978-94-007-0763-4_7
- Navarro, X., Krueger, T.B., Lago, N., Micera, S., Stieglitz, T., Dario, P., 2005. A critical review of interfaces with the peripheral nervous system for the control of neuroprostheses and hybrid bionic systems. *J. Peripher. Nerv. Syst.* 10, 229–58. <https://doi.org/10.1111/j.1085-9489.2005.10303.x>
- Noorisafa, F., Razmjou, A., Emami, N., Low, Z.-X., Korayem, A.H., Kajani, A.A., 2016. Surface modification of polyurethane via creating a biocompatible superhydrophilic nanostructured layer: role of surface chemistry and structure. *J. Exp. Nanosci.* 8080, 1–23. <https://doi.org/10.1080/17458080.2016.1188223>
- Norton, L.W., Koschwanetz, H.E., Wisniewski, N.A., Klitzman, B., Reichert, W.M., 2007. Vascular endothelial growth factor and dexamethasone release from nonfouling sensor coatings affect the foreign body response. *J. Biomed. Mater. Res. - Part A* 81, 858–869. <https://doi.org/10.1002/jbm.a.31088>
- Oddo, C.M., Raspopovic, S., Artoni, F., Mazzoni, A., Spigler, G., Petrini, F., Giambattistelli, F., Vecchio, F., Miraglia, F., Zollo, L., Di Pino, G., Camboni, D., Carrozza, M.C., Guglielmelli, E., Rossini, P.M., Faraguna, U., Micera, S., 2016. Intraneural stimulation elicits discrimination of textural features by artificial fingertip in intact and amputee humans. *Elife* 5, 1–27. <https://doi.org/10.7554/eLife.09148>
- Park, S.J., Lee, Y.J., Heo, D.N., Kwon, I.K., Yun, K.S., Kang, J.Y., Lee, S.H., 2015. Functional nerve cuff

electrode with controllable anti-inflammatory drug loading and release by biodegradable nanofibers and hydrogel deposition. *Sensors Actuators, B Chem.* 215, 133–141. <https://doi.org/10.1016/j.snb.2015.03.036>

Raspopovic, S., Capogrosso, M., Petrini, F.M., Bonizzato, M., Rigosa, J., Di Pino, G., Carpaneto, J., Controzzi, M., Boretius, T., Fernandez, E., Granata, G., Oddo, C.M., Citi, L., Ciancio, a. L., Cipriani, C., Carrozza, M.C., Jensen, W., Guglielmelli, E., Stieglitz, T., Rossini, P.M., Micera, S., 2014. Restoring Natural Sensory Feedback in Real-Time Bidirectional Hand Prostheses. *Sci. Transl. Med.* 6, 222ra19-222ra19. <https://doi.org/10.1126/scitranslmed.3006820>

Rossini, P.M., Micera, S., Benvenuto, A., Carpaneto, J., Cavallo, G., Citi, L., Cipriani, C., Denaro, L., Denaro, V., Di Pino, G., Ferreri, F., Guglielmelli, E., Hoffmann, K.P., Raspopovic, S., Rigosa, J., Rossini, L., Tombini, M., Dario, P., 2010. Double nerve intraneural interface implant on a human amputee for robotic hand control. *Clin. Neurophysiol.* 121, 777–783. <https://doi.org/10.1016/j.clinph.2010.01.001>

Skousen, J.L., Bridge, M.J., Tresco, P. a, 2014. A strategy to passively reduce neuroinflammation surrounding devices implanted chronically in brain tissue by manipulating device surface permeability. *Biomaterials* 36, 33–43. <https://doi.org/10.1016/j.biomaterials.2014.08.039>

Sommakia, S., Lee, H.C., Gaire, J., Otto, K.J., 2014. Materials approaches for modulating neural tissue responses to implanted microelectrodes through mechanical and biochemical means. *Curr. Opin. Solid State Mater. Sci.* 18, 319–328. <https://doi.org/10.1016/j.cossms.2014.07.005>

Spataro, L., Dilgen, J., Retterer, S., Spence, a. J., Isaacson, M., Turner, J.N., Shain, W., 2005. Dexamethasone treatment reduces astroglia responses to inserted neuroprosthetic devices in rat neocortex. *Exp. Neurol.* 194, 289–300. <https://doi.org/10.1016/j.expneurol.2004.08.037>

Tyler, D.J., Polasek, K.H., Schiefer, M.A., 2015. *Peripheral Nerve Interfaces, Nerves and Nerve Injuries.* Elsevier Ltd. <https://doi.org/10.1016/B978-0-12-802653-3.00112-3>

Veraart, C., Grill, W.M., Mortimer, J.T., 1993. Selective control of muscle activation with a multipolar nerve cuff electrode. *IEEE Trans. Biomed. Eng.* 40, 640–653. <https://doi.org/10.1109/10.237694>

Ward, K.W., 2008. A review of the foreign-body response to subcutaneously-implanted devices: the role of macrophages and cytokines in biofouling and fibrosis. *J. diabetes Sci. Technol.* 2, 768–777. <https://doi.org/10.1177/193229681200600201>

Weerasuriya, A., Spangler, R.A., Rapoport, S.I., Taylor, R.E., 1984. AC impedance of the perineurium of the frog sciatic nerve. *Biophys. J.* 46, 167–74. [https://doi.org/10.1016/S0006-3495\(84\)84009-](https://doi.org/10.1016/S0006-3495(84)84009-6)

6

Wurth, S., Capogrosso, M., Raspopovic, S., Gandar, J., Federici, G., Kinany, N., Cutrone, A., Piersigilli, A.,

Pavlova, N., Guiet, R., Taverni, G., Rigosa, J., Shkorbatova, P., Navarro, X., Barraud, Q., Courtine, G., Micera, S., 2017. Long-term usability and bio-integration of polyimide-based intra-neural stimulating electrodes. *Biomaterials* 122, 114-129. <https://doi.org/10.1016/j.biomaterials.2017.01.014>

Zhong, Y., Bellamkonda, R. V, 2007. Dexamethasone-coated neural probes elicit attenuated inflammatory response and neuronal loss compared to uncoated neural probes. *Brain Res.* 1148, 15-27. <https://doi.org/10.1016/j.brainres.2007.02.024>

GENERAL DISCUSSION

Neuroprostheses are electromechanical systems intended to restore the lost functions after an injury to the nervous system or due to a partial or total limb amputation. In the case of limb prostheses for amputations, the link with the peripheral nervous system seems more advantageous than the access to the brain. A neural interface for the control of a bionic prosthesis should detect the descending motor signals to control the prosthetic device but also stimulate the nervous tissue to send an ascending sensory feedback to inform the nervous system about the action and sensing performed by the prosthesis. State-of-the-art hand bionic prostheses aim to mimic a large number of potential movements performed by the hand and the enormous amount of sensory information captured by skin and muscle receptors. Thus, the number of interfacing channels and the precision of the intercommunication need to be high. Regarding neuroprostheses for upper limb amputee patients, intraneural electrodes have been presented as the best strategy to selectively stimulate and record from axons in the peripheral nerves (del Valle and Navarro, 2013; Tyler et al., 2015). To accomplish its purpose, neural interfaces should be biocompatible and remain stable when chronically implanted. In addition, the electrodes should maintain proper function as long as needed. However, a progressive loss of electrode functionality has been reported in chronic human studies (Raspovic et al., 2014; Rossini et al., 2010; Wark et al., 2014), due to, among other factors, the biological response to the implanted device in the body, known as FBR (Anderson et al., 2008; Kenneth Ward, 2008). In the present thesis, a characterization of the FBR to polymer-based devices implanted in the peripheral nerve has been first performed, in order to determine the main targets amenable to modifications, and consequently we have assayed which treatments may be more effective to reduce and modulate this FBR, hence improving the long-term functionality of implanted electrodes in the peripheral nerve.

First of all, a characterization of a new intraneural interface was performed in chapter 1 (Mueller et al., 2017) in collaboration with Thomas Stieglitz and coworkers from IMTEK (Freiburg, Germany). Taking advantage of the successful design of the polyimide-based TIME interface, that is, transversally implanted in peripheral nerves, the new interface developed was made in Parylene C instead of polyimide. Parylene C is a polymer that has been widely used as an insulator for brain interfaces and other medical devices (Hassler et al., 2010; Kim and Meng, 2016; Schmidt et al., 1988). It is an FDA approved material for clinical applications, and different studies have shown good biocompatible characteristics (T. Y. Chang et al., 2007; Lecomte et al., 2017). In the case of intraneural

interfaces, the mechanical properties of Parylene C offer the possibility to integrate several active sites in both sides of the substrate, reducing the thickness of the implanted interface (Mueller et al., 2016) and thus reducing the size of the implanted device. In the histological analyses performed in Chapter 1, the Parylene C-based interface showed excellent biocompatibility and safety, as no signs of degeneration nor changes in the nerve architecture or the number of myelinated fibers were observed. Besides, the selectivity of the stimulation indicates that the interface position within the nerve was stable over time. However, an increase in the threshold of stimulation – the current needed to evoke a muscle response - was observed from 2 to 4 weeks after implant. Previous studies with intraneural (Oddo et al., 2016; Raspopovic et al., 2014; Rossini et al., 2010), extraneural (Fisher et al., 2009; Polasek et al., 2009; Tan et al., 2013) and even brain interfaces (Biran et al., 2005; Mercanzini et al., 2010; Nolte et al., 2015) have also reported an increase in the threshold of stimulation and a progressive decrease in the overall functionality.

These changes in electrode functionality could be attributed to electrochemical changes in the active sites inducing changes in conductivity, erosion of the metal sites, mechanical tensions of the wires, cell death and the biological response to the implanted device, which separate and isolate the electrode with a capsule tissue that increases the resistance and the distance between the nerve tissue and the active sites. In fact, an increase in the tissue deposition around the Parylene C electrodes was observed over time. According to the increase in the threshold of stimulation, the main tissue deposition seemed to occur during the first two weeks after the implantation, being stabilized thereafter. Such a capsule was similar to that reported in previous studies chronically implanting longitudinal (Lago et al., 2007) as well as transversal intraneural electrodes (Badia et al., 2011b; Wurth et al., 2017).

In order to depict the cellular and molecular events of the FBR after device implantation in peripheral nerves, we performed the experiments reported in Chapter 2 using longitudinal intraneural devices implanted up to 8 months. This characterization should help to eventually test treatments in further works to improve the functionality of intraneural electrodes. The description of the FBR was focused on two different polymers: polyimide, the current material used as a substrate of neural interfaces (Boretius et al., 2010; Lago et al., 2007; Rousche et al., 2001; Rubehn and Stieglitz, 2010), and Parylene C, a polymer previously used as an insulator in brain interfaces (Fekete and Pongrácz, 2017; Lecomte et al., 2017; Seymour and Kipke, 2007; Takeuchi et al., 2005) but also promoted for intraneural electrodes as shown in Chapter 1 (Mueller et al., 2017). Similar to previous studies with longitudinal intraneural devices (Lago et al., 2007), no damage or degeneration

of the implanted nerve were observed with polyimide nor Parylene C devices at any time point. These results confirmed the biocompatible characteristics of Parylene C as there were no harmful effects affecting nerve function (T. Y. Chang et al., 2007; Winslow et al., 2010).

With regard to the molecular and cellular processes associated with the FBR, several studies have characterized these events in subcutaneous and peritoneal implants (Anderson et al., 2008; Kenneth Ward, 2008; Luttikhuisen et al., 2006). According to them, FBR has a first inflammatory phase followed by an anti-inflammatory and tissue remodeling phase, which results in the tissue encapsulation of the device. Our results from Chapter 2 are in agreement with this pattern, where infiltration of polymorphonuclear cells and monocytes/macrophages was observed rapidly after the implant of both polyimide and Parylene C devices. Macrophages were the main cell type present in the first inflammatory phase of the FBR, starting to surround the longitudinal implants just after 1 day and generating a first capsule around the devices. These cells produced a peak of infiltration 2 weeks after the implant invading all the endoneurium and this maximum coincided with the highest thickness of the tissue capsule around both polyimide and Parylene C devices. Thus, the link between inflammation and the encapsulation process has been correlated for intraneural devices. From 2 to 8 weeks post-implant, infiltrating cells started to leave the nerve tissue. The clearance of immune cells occurred earlier in sham animals, whom only received the surgical implantation leaving no implant inside, than in implanted animals, indicating that the device implanted, and not only the surgical implantation, is contributing to the inflammatory process. With regard to the two materials implanted, there were no differences in the infiltration dynamics or in the number of inflammatory cells at any studied time-point.

On the other hand, the clearance of immune cells may indicate the transition from the first pro-inflammatory phase of the FBR to the subsequent anti-inflammatory and remodeling phase. This second phase is characterized by the production and stabilization of a tissue capsule around the implant. In fact, FBGCs – results of macrophage fusion (Sheikh et al., 2015) – were present in the capsules for both materials, as a hallmark of the anti-inflammatory and tissue remodeling phase. In the case of polyimide device, the thickness of the capsule peaked at 2 weeks and progressively decreased until stabilization after 8 weeks. In contrast, capsule around Parylene C devices also peaked after 2 weeks but, after a slight stabilization at 4 weeks, it continued increasing up to its maximum after 16 weeks. By then, the capsule to both materials appeared full of collagen fibers. Besides, the increase in the thickness of the capsule was accompanied of a change in the cellular integration of the capsule for both materials, from iba1 macrophages by week 2 and 4 to CD90 fibroblasts

from 8 weeks onwards. In the case of Parylene C, macrophages seemed to remain longer than in polyimide capsules, what may indicate a higher stimulation of the inflammatory phase by Parylene C. However, molecular analyses of cytokines and other related molecules such as TGF β indicated no changes in the amount of those molecules between Parylene C and polyimide responses at any time point. In fact, there were no differences not even with sham animals. This could be explained by the fact that cytokines highest levels are normally produced within the first hours or days after injury (Baldwin and Hunt, 2008; Luttikhuisen et al., 2006; Rodriguez et al., 2009) and, by then, the FBR processes and the wound healing processes due to the implantation procedure are happening simultaneously. Nevertheless, the chemical surface of polymers would also explain, at least in part, these results. Jones and coworkers showed that hydrophilic surfaces promote less cellular adhesion but a higher cytokine production (Jones et al., 2007). Although both materials show a hydrophobic behavior with contact angles ranging from 80 to 100°, Parylene C can be considered more hydrophilic than polyimide (T. Y. Chang et al., 2007; Ghosh et al., 1997; Richardson et al., 1993), which could explain the higher matrix deposition due to a higher inflammatory environment. Moreover, the degradation ratio of polymers has also been related to the molecular environment. Biodegradable materials would stimulate higher presence of polymorphonuclear cells and M1-like macrophages, with higher phagocytic capacity, to eliminate the implant. In contrast, non-biodegradable materials would stimulate a more M2-like and tissue deposition environment, to isolate the implant in case that macrophages cannot phagocyte it (Boddupalli et al., 2016; Veiseh et al., 2015). In that sense, Parylene C physical characteristics (i.e., degradation dynamics, stiffness, hardness ...) might be different from those of polyimide, thus stimulating different environments.

In general terms, it is accepted that the FBR has two main phases: a first pro-inflammatory phase followed by a second anti-inflammatory and remodeling phase, with different time progression depending on the host tissue. In peritoneal FBR models, myeloid cells and macrophages peak after 1 week of device implantation, and macrophage to myofibroblasts transition have been reported by week 4 (Mooney et al., 2010). On the other hand, the FBR in the CNS is completed by microglial cells, as inflammatory cells, and astroglial cells, main responsible of the glial scar around the device implanted and the tissue injury (Kozai et al., 2015; Polikov et al., 2005). The fact that only two cell populations – macrophages and fibroblasts, mainly – participate in the capsule formation not only in peripheral nerves but also in other tissues and to different materials indicates the conservation and generalization of the response, although with differences in the time progression of the response. This could be useful when searching for treatments to reduce this response and lengthening the lifespan of implanted devices. Even though, the

specificities of the FBR seem to be determined not only by the tissue in which the device is implanted but also by the type and size of the material implanted (Boddupalli et al., 2016; Veiseh et al., 2015). Therefore, studies for each material and each host tissue are needed to determine the specific FBR progression in time and to develop helpful strategies to modulate this response in order to improve the functional outcome of implanted devices.

As reviewed in the introduction part, different strategies have been developed to reduce the inflammatory process and the encapsulation of implanted devices. These strategies range from the use of different materials with modified surface characteristics to pharmacological approaches depending on the device final function. With regard to neural electrodes, few studies have focused on strategies to modulate the FBR and to improve the stimulation and recording capabilities of implanted electrodes (Norton et al., 2007; Park et al., 2015; Vince et al., 2005). According to the phases characterized in the FBR to intraneural devices, in Chapter 3 we tested several drugs, from anti-inflammatory (dexamethasone, ibuprofen, maraviroc, and clodronate) to anti-fibrotic (sildenafil) drugs, to modulate the response to Parylene C devices for 2 weeks, as in that point is when the peak in cell infiltration and capsule thickness occur. Systemic administration was chosen since it facilitates the combination of different FBR modulatory drugs at different time points after implantation, according to the time-window of effectiveness for each drug. Indeed, by using systemic administration, we aimed to make a feasible screening of different drugs with the potential to prevent the FBR.

Our results show that only dexamethasone treatment significantly reduces both cellular infiltration and tissue capsule thickness after 2 weeks of the implant of both Parylene C and polyimide devices. These results agree with previous studies in which a reduced scar tissue formation was reported after systemic (Spataro et al., 2005) and local (FitzGerald, 2016; Zhong and Bellamkonda, 2007) dexamethasone administration. Moreover, our results have shown for the first time that at least two weeks of dexamethasone are needed to significantly reduce the infiltration of immune cells and the thickness of the capsule in peripheral nerves. The effect achieved during the first two weeks is maintained after 8 weeks of implant, suggesting that this initial period is predictive of the later chronic FBR. Once more, knowledge of the FBR progression in each host tissue is essential to determine the useful time-window of each drug in order to modulate the reaction. Furthermore, the beneficial effects of dexamethasone treatment were also observed in the FBR to polyimide devices, where there was a significant decrease in capsule thickness after 2 and 8 weeks of implant. Thus, although some differences have been described in the chronic development of the tissue capsule between polyimide and Parylene

C devices, dexamethasone is decreasing the first pro-inflammatory phase to both materials, thus reducing the following tissue deposition. This result corroborates the generalization of the FBR, even the differences that can arise due to the implanted material or the host tissue.

In contrast to dexamethasone, the other studied anti-inflammatory drugs (i.e., ibuprofen and clodronate) do not have the same effect. While there was a reduction in inflammatory cells infiltration in the sciatic nerve after 2 weeks, no changes in tissue deposition were observed. These results could point out the mechanisms through which dexamethasone is doing its positive effect. Ibuprofen is an NSAID, known to exert an anti-inflammatory effect by the inhibition of cyclooxygenase 1 and 2 enzymes. Clodronate induces apoptosis of circulating monocytes/macrophages. Dexamethasone acts through the glucocorticoid receptor, having a much broader spectrum of actions (Coutinho and Chapman, 2011), from anti-inflammatory to immunosuppressive effects. Thus, the reduction of infiltrating macrophages and the decrease of immune mediators achieved also with ibuprofen and clodronate treatments would not be enough to reduce the encapsulation of implanted devices. A combination of both ibuprofen and clodronate treatments may have similar effects than dexamethasone. However, since clodronate is not a good option for human use as it stimulates the apoptosis of circulating monocytes/macrophages, the combination of both drugs would not be a feasible strategy. On the other hand, the elucidation of the exact pathway that dexamethasone is modulating to reduce the tissue encapsulation may give further targets to developed treatments with fewer side-effects than this classical corticosteroid. In that regard, maraviroc, an antagonist of CCR5, was also administered for 2 weeks with the longitudinal FBR model in peripheral nerves. However, maraviroc did not reduce macrophages infiltration nor tissue deposition in the implanted nerves. Despite the role of CCR5 in different fibrotic models to recruit monocytes/macrophages (Berres et al., 2010; Sahin and Wasmuth, 2013; Seki et al., 2009), we did not observe any beneficial effect of its blockage in our model of FBR in peripheral nerves. This receptor can also be activated by other molecules, such as CCL2 and CCL3 (Sahin and Wasmuth, 2013). Besides, CCR5 is not the only chemokine receptor implicated in monocyte/macrophage recruitment and progression of the inflammatory response (Ishida et al., 2007; Sahin and Wasmuth, 2013) and different molecules act during the FBR, such as CCL2/MCP-1, CCL3/MIP1 α , TNF α , granulocyte-macrophage colony stimulating factor (GM-CSF) or IL-6.

As expected from previous studies using sildenafil for reducing fibrosis development (Valente et al. 2003; Noel et al. 2012; Percival et al. 2012), we found a significant reduction in capsule thickness. However, the effect was not as marked as with dexamethasone. This could be due to the two main phases of the FBR, one pro-inflammatory

followed by a second one anti-inflammatory and tissue remodeling (Anderson et al. 2008). Thus, dexamethasone might be modulating both phases while the other treatments assessed only act by reducing either activation of the inflammatory cells or the tissue deposition and remodeling. Given the similarities in the FBR with other types of devices, such as multielectrode arrays (Christensen et al., 2014) and transversal electrodes (Wurth et al., 2017), dexamethasone treatment will be likely useful to modulate the FBR to different electrode designs for peripheral nerves.

However, despite the reduction of the FBR to substrate polymers (i.e., Parylene C and polyimide) obtained with dexamethasone, still some encapsulation appeared around the implanted devices. The ultimate question is how this reduction in capsule thickness may improve the functionality of intraneural interfaces in terms of stimulation and nerve signal recording. In Chapter 4 we combined the best two solutions that have been found up to date. On the one hand, polyimide as a substrate of the neural interface, considering the FBR progression in chronic time-points around Parylene C devices. Although it is an FDA approved material and the Parylene C-based interface showed good functional performance *in vivo* (Mueller et al., 2017), polyimide-based intraneural interfaces have been already used with human volunteers with promising results (Oddo et al., 2016; Raspopovic et al., 2014; Rossini et al., 2010). On the other hand, systemic dexamethasone was administered due to the reduction achieved in cell infiltration and capsule thickness. Thus, transversal polyimide-based intraneural interfaces (TIME electrodes) were chronically implanted for 3 months to evaluate its stimulation and recording capabilities after systemic dexamethasone treatment. While a longitudinal implant model was used to characterize the FBR in Chapter 2, a transversal electrode was used to test whether dexamethasone improves its functionality over time in Chapter 4. The transversal electrode was chosen because it is more clinically relevant than the longitudinal one since TIME electrodes allow to target different fascicles within the same nerve (Badia et al., 2011a). However, the implantation of transversal devices is usually less accurate than longitudinal devices and it also implies greater damage of the epineurium in comparison to longitudinal implantation. Hence, to characterize the FBR, the longitudinal implant was chosen because of its better reproducibility and to better study only the FBR inside the nerve, without confounding factors due to tissue damage. Moreover, the use of non-functional longitudinal devices and the absence of wires that may induce some tethering forces in the nerve (Navarro et al., 2005) avoids external artifacts in the creation of a FBR and focus only in the material reaction in comparison with those studies that used wired or active electrodes (Christensen et al., 2016; Wark et al., 2014; Wurth et al., 2017).

The implanted TIME electrodes have shown similar stimulation and recording capabilities in our results in comparison with previous studies in acute conditions (Badia et al., 2016, 2011a). In the saline-treated animals, a progressive increase in the threshold of stimulation – the current needed to evoke a muscular response – was observed over time. In fact, this increase coincided in time with the first inflammatory phase of the FBR, as it occurred during the first weeks after the implant. Dexamethasone treatment significantly reduced the threshold of stimulation during the first month of implant. From our previous results on FBR progression (Chapter 2), the tissue deposition is stabilized from 4 weeks onwards for polyimide devices. Moreover, dexamethasone significantly decreased the tissue deposition after 2 and 8 weeks of treatment (Chapter 3). Therefore, the decrease in the threshold of stimulation can be directly related to the decrease in the cell infiltration and tissue deposition. Even though, no differences in tissue deposition were observed between groups in the histological analysis after 3 months. The fact that dexamethasone apparently did not reduce the tissue deposition could be due to that in the transversal model there is much more contamination from the epineurium and the perineurium tissues. Therefore, the connective tissue and the new deposited tissue around the electrode due to the FBR do not easily differentiate in the transversal model. On the other hand, the transversal model allows evaluating not only the effect of dexamethasone on the FBR to active sites inside the nerve but also to active sites outside the nerve. In fact, in dexamethasone-treated animals, there was a higher number of active sites able to evoke a muscle response over time. This could be due to the fact that dexamethasone is indeed reducing the tissue deposition around the implanted electrode, although no noticeable differences were observed in the histological analysis.

As expected, there were no differences in the stimulation selectivity between groups, as this aspect depends more on the position with respect the fibers to stimulate than in the few microns of the tissue capsule generated. On the other hand, recording capabilities did not show a clear improvement after dexamethasone treatment. The quality of the recorded signal relies on the amplitude of nerve signals and on the localization of the active sites concerning the fibers that are generating the electric signals. Since the amplitude of nerve signals is within the scale of microvolts, the position of the electrode active sites after the implant and the nerve fibers becomes more critical to have a good SNR than the capsule generated due to the FBR. However, due to dexamethasone decrease in capsule thickness, there were more AS able to record small nerve signals, similarly to the stimulation results.

Overall, these results showed a useful effect of dexamethasone treatment on the functionality of intraneural electrodes during the first month of implant. Besides, most of the strategies try to deliver the different drugs locally on the implant side with controlled-

released coatings or nanoparticles. However, these strategies have some limitations in the case of intraneural electrodes, such as the nerve size since the coatings would increase the thickness of the device implanted. Thus, local delivery systems are difficult to adapt to intraneural electrodes. Our results have demonstrated that systemic administration of anti-inflammatory drugs would be likewise useful and easily to apply to modulate the FBR to intraneural interfaces. Nevertheless, FBR is not the only nor the most important factor related to the decrease in electrode functionality. Hence, further studies to improve electrode stability and signal recording and decoding are needed to ensure electrode functionality over time.

CONCLUSIONS

The main conclusions of this thesis are summarized as:

1. A new design of intraneural electrode was made on Parylene C, based on the transversal intraneural electrode TIME model.
 - 1.1. The new electrode design has been optimized for allowing implantation in small peripheral nerves, such as the rat sciatic nerve.
 - 1.2. It shows good biocompatibility and does not produce any functional or structural damage in the rat sciatic nerve after 3 and 12 months of implantation.
 - 1.3. The implanted electrode allowed for good stimulation selectivity.
 - 1.4. However, the intensity of stimulation required to evoke the muscle responses increased with time from two weeks after the implant. This functional decline might be related to the progressive tissue encapsulation observed around the implanted electrode.

2. The biocompatibility and the foreign body reaction to polyimide and Parylene C based devices chronically implanted in the peripheral nerve have been characterized:
 - 2.1 A chronic longitudinal implant model has been designed, which allows reproducible evaluation of the foreign body reaction and avoids confounding factors from variations in the implant placement and tethering forces by connectors.
 - 2.2 Both Polyimide and Parylene C can be considered as biocompatible materials, as they do not cause any alteration in the nerve structure, axonal number and in the nerve function after up to 8 months of implantation.
 - 2.3 The implantation surgery, evaluated in the sham animals, produced an infiltration of macrophages in the nerve that is resolved in 2 weeks. No signs of scar tissue were observed at later time points.

- 2.4 The implanted devices produced increased macrophage recruitment, which started to resolve by 8 weeks, but still remained higher than in intact nerve after 8 months for both materials.
- 2.5 A progressive tissue encapsulation was formed around both polyimide and Parylene C devices. The capsule thickness for polyimide devices peaked at 2 weeks and was maintained thereafter, whereas the capsule around Parylene C devices peaked also after 2 weeks, but then increased again up to a maximum at 16 weeks.
- 2.6 Macrophages are the main cells surrounding the intraneural device from 1 day until 4 weeks. Fibroblasts appear by 8 weeks at the edge of the capsule, coinciding with production and organization of collagen fibrils. Two zones are distinguished within the capsule: an inner zone containing macrophages, and an outer zone with fibroblasts.
- 2.7 With polyimide devices fibroblasts have mostly substituted macrophages by 16 weeks, in Parylene C devices macrophages stayed longer, in contact with the device. This may indicate higher stimulation of the inflammatory phase by Parylene C. There were no differences between materials in the amount or size of FBGCs.
- 2.8 Molecular analysis of cytokines and inflammatory mediators revealed a pro-inflammatory peak for both material implants at early time points. There were only a few significant differences in the response to implanted devices with respect to the sham surgical procedure. CCL2 and CCL3 were increased in both materials in comparison to sham animals, and CXCL2 increased, although not significantly, in Parylene C compared with polyimide devices.
- 2.9 Provided the higher tissue capsule induced by Parylene C in comparison with polyimide implants, Parylene C may not be a good option to be used as substrate for chronic implanted intraneural electrodes.
3. The two main phases described in the foreign body reaction (FBR) determine possible therapeutic strategies to modulate the response:

- 3.1 Systemic anti-inflammatory treatments, such as dexamethasone, ibuprofen, and clodronate, significantly reduced the number of infiltrating macrophages in the nerve after 2 weeks of Parylene C implants.
 - 3.2 Only dexamethasone significantly reduced the capsule thickness after 2 weeks. At least 2 weeks of dexamethasone administration are needed to significantly reduce the FBR after 2 and 8 weeks of implant.
 - 3.3 Dexamethasone similarly modulates the FBR after 2 and 8 weeks of implant of polyimide devices.
 - 3.4 Systemic administration of anti-inflammatory drugs is a feasible option to modulate the FBR to intraneural devices.
 - 3.5 Maraviroc, a CCR5 antagonist, does not have any effect on the FBR to Parylene C devices.
 - 3.6 Sildenafil, used as an anti-fibrotic drug, reduced the thickness of the capsule but did not affect the number of infiltrating cells after 2 weeks of Parylene C implant.
4. The functional outcome of chronic implanted polyimide transversal electrodes under systemic dexamethasone treatment has been evaluated over 3 months:
 - 4.1 The intensity of stimulation in the saline-treated animals increased during the first two weeks of implant and then it stabilized. Dexamethasone treatment significantly reduced the intensity of stimulation in comparison to saline-treated animals.
 - 4.2 The stimulation selectivity did not change over time nor between treatment groups.
 - 4.3 Dexamethasone treatment did not improve the recording sensitivity of intraneural electrodes after one month of implant.
 - 4.4 Systemic administration of dexamethasone shows a positive effect on the functionality of intraneural electrodes during the first months of implant, particularly for the stimulation properties.

REFERENCES

- Abe, R., Donnelly, S.C., Peng, T., Bucala, R., Metz, C.N., 2001. Peripheral Blood Fibrocytes: Differentiation Pathway and Migration to Wound Sites. *J. Immunol.* 166, 7556–7562. <https://doi.org/10.4049/jimmunol.166.12.7556>
- Albrecht, E., Kern, C., Kirkham, K.R., 2015. A systematic review and meta-analysis of perineural dexamethasone for peripheral nerve blocks. *Anaesthesia.* <https://doi.org/10.1111/anae.12823>
- Allodi, I., Udina, E., Navarro, X., 2012. Specificity of peripheral nerve regeneration: interactions at the axon level. *Prog. Neurobiol.* 98, 16–37. <https://doi.org/10.1016/j.pneurobio.2012.05.005>
- Amiji, M., Park, H., Park, K., 1992. Study on the prevention of surface-induced platelet activation by albumin coating. *J. Biomater. Sci. Polym. Ed.* 3, 375–388. <https://doi.org/10.1163/156856292X00196>
- Anderson, J.M., Jiang, S., 2017. Implications of the Acute and Chronic Inflammatory Response and the Foreign Body Reaction to the Immune Response of Implanted Biomaterials, in: *The Immune Response to Implanted Materials and Devices.* Springer International Publishing, Cham, pp. 15–36. https://doi.org/10.1007/978-3-319-45433-7_2
- Anderson, J.M., Rodriguez, A., Chang, D.T., 2008. Foreign body reaction to biomaterials. *Semin. Immunol.* 20, 86–100. <https://doi.org/10.1016/j.smim.2007.11.004>
- Asplund, M., Thaning, E., Lundberg, J., Sandberg-Nordqvist, A.C., Kostyszyn, B., Inganäs, O., von Holst, H., 2009. Toxicity evaluation of PEDOT/biomolecular composites intended for neural communication electrodes. *Biomed. Mater.* 4, 45009. <https://doi.org/10.1088/1748-6041/4/4/045009>
- Aszmann, O.C., Vujaklija, I., Roche, A.D., Salminger, S., Herceg, M., Sturma, A., Hruby, L.A., Pittermann, A., Hofer, C., Amsuess, S., Farina, D., 2016. Elective amputation and bionic substitution restore functional hand use after critical soft tissue injuries. *Sci. Rep.* 6, 34960. <https://doi.org/10.1038/srep34960>
- Badia, J., Boretius, T., Andreu, D., Azevedo-Coste, C., Stieglitz, T., Navarro, X., 2011a. Comparative analysis of transverse intrafascicular multichannel, longitudinal intrafascicular and multipolar cuff electrodes for the selective stimulation of nerve fascicles. *J. Neural Eng.* 8, 36023. <https://doi.org/10.1088/1741-2560/8/3/036023>
- Badia, J., Boretius, T., Pascual-Font, A., Udina, E., Stieglitz, T., Navarro, X., 2011b. Biocompatibility of chronically implanted transverse intrafascicular multichannel electrode (TIME) in the rat sciatic nerve. *IEEE Trans. Biomed. Eng.* 58, 2324–2332. <https://doi.org/10.1109/TBME.2011.2153850>
- Badia, J., Pascual-Font, A., Vivó, M., Udina, E., Navarro, X., 2010. Topographical distribution of motor fascicles in the sciatic-tibial nerve of the rat. *Muscle Nerve* 42, 192–201. <https://doi.org/10.1002/mus.21652>
- Badia, J., Raspopovic, S., Carpaneto, J., Micera, S., Navarro, X., 2016. Spatial and Functional Selectivity of Peripheral Nerve Signal Recording With the Transversal Intrafascicular Multichannel Electrode (TIME). *IEEE Trans. Neural Syst. Rehabil. Eng.* 24, 20–27. <https://doi.org/10.1109/TNSRE.2015.2440768>
- Badylak, S.F., Gilbert, T.W., 2008. Immune response to biologic scaffold materials, *Seminars in Immunology.* <https://doi.org/10.1016/j.smim.2007.11.003>
- Balaji, A., Jaganathan, S.K., Vellayappan, M. V., John, A.A., Subramanian, A.P., SelvaKumar, M., Mohandas, H., Sundar Raj, M., Supriyanto, E., 2015. Prospects of common biomolecules as

- coating substances for polymeric biomaterials. *RSC Adv.* 5, 69660–69679. <https://doi.org/10.1039/c5ra12693b>
- Baldwin, L., Hunt, J.A., 2008. The in vivo cytokine release profile following implantation. *Cytokine* 41, 217–222. <https://doi.org/10.1016/j.cyto.2007.11.015>
- Bayramoğlu, G., Yilmaz, M., Batislam, E., Arica, M.Y., 2008. Heparin-coated poly(hydroxyethyl methacrylate/albumin) hydrogel networks: In vitro hemocompatibility evaluation for vascular biomaterials. *J. Appl. Polym. Sci.* 109, 749–757. <https://doi.org/10.1002/app.28062>
- Berres, M.-L., Koenen, R.R., Rueland, A., Zaldivar, M.M., Heinrichs, D., Sahin, H., Schmitz, P., Streetz, K.L., Berg, T., Gassler, N., Weiskirchen, R., Proudfoot, A., Weber, C., Trautwein, C., Wasmuth, H.E., 2010. Antagonism of the chemokine Ccl5 ameliorates experimental liver fibrosis in mice. *J. Clin. Invest.* 120, 4129–40. <https://doi.org/10.1172/JCI41732>
- Biddiss, E., Beaton, D., Chau, T., 2007. Consumer design priorities for upper limb prosthetics. *Disabil. Rehabil. Assist. Technol.* 2, 346–357. <https://doi.org/10.1080/17483100701714733>
- Biddiss, E., Chau, T., 2007. Upper-Limb Prosthetics. *Am. J. Phys. Med. Rehabil.* 86, 977–987. <https://doi.org/10.1097/PHM.0b013e3181587f6c>
- Biran, R., Martin, D.C., Tresco, P.A., 2005. Neuronal cell loss accompanies the brain tissue response to chronically implanted silicon microelectrode arrays. *Exp. Neurol.* 195, 115–126. <https://doi.org/10.1016/j.expneurol.2005.04.020>
- Blair, E.A., Erlanger, J., 1933. Comparison of Properties of Individual Axons in the Frog. *Exp. Biol. Med.* 30, 728–729. <https://doi.org/10.3181/00379727-30-6647>
- Boddupalli, A., Zhu, L., Bratlie, K.M., 2016. Methods for Implant Acceptance and Wound Healing: Material Selection and Implant Location Modulate Macrophage and Fibroblast Phenotypes. *Adv. Healthc. Mater.* <https://doi.org/10.1002/adhm.201600532>
- Boehler, C., Kleber, C., Martini, N., Xie, Y., Dryg, I., Stieglitz, T., Hofmann, U.G., Asplund, M., 2017. Actively controlled release of Dexamethasone from neural microelectrodes in a chronic in vivo study. *Biomaterials* 129, 176–187. <https://doi.org/10.1016/j.biomaterials.2017.03.019>
- Boehler, R.M., Graham, J.G., Shea, L.D., 2011. Tissue engineering tools for modulation of the immune response. *Biotechniques*. <https://doi.org/10.2144/000113754>
- Boretius, T., Badia, J., Pascual-Font, A., Schuettler, M., Navarro, X., Yoshida, K., Stieglitz, T., 2010. A transverse intrafascicular multichannel electrode (TIME) to interface with the peripheral nerve. *Biosens. Bioelectron.* 26, 62–69. <https://doi.org/10.1016/j.bios.2010.05.010>
- Borkner, C.B., Wohlrab, S., Möller, E., Lang, G., Scheibel, T., 2017. Surface Modification of Polymeric Biomaterials Using Recombinant Spider Silk Proteins. *ACS Biomater. Sci. Eng.* 3, 767–775. <https://doi.org/10.1021/acsbomaterials.6b00306>
- Bosse, F., 2012. Extrinsic cellular and molecular mediators of peripheral axonal regeneration. *Cell Tissue Res.* 349, 5–14. <https://doi.org/10.1007/s00441-012-1389-5>
- Bossi, S., Benvenuto, A., Wieringa, P., Di Pino, G., Guglielmelli, E., Boretius, T., Stieglitz, T., Navarro, X., Micera, S., 2010. Preliminary investigations on laminin coatings for flexible polyimide/platinum thin films for PNS applications, in: 2010 Annual International Conference of the IEEE Engineering in Medicine and Biology Society, EMBC'10. pp. 1527–1530. <https://doi.org/10.1109/IEMBS.2010.5626831>
- Bostock, H., 1983. The strength-duration relationship for excitation of myelinated nerve: computed dependence on membrane parameters. *J. Physiol.* 341, 59–74. <https://doi.org/10.1113/jphysiol.1983.sp014792>
- Bota, P.C.S., Collie, A.M.B., Puolakkainen, P., Vernon, R.B., Sage, E.H., Ratner, B.D., Stayton, P.S., 2010. Biomaterial topography alters healing in vivo and monocyte/macrophage activation in vitro. *J.*

Biomed. Mater. Res. Part A 95A, 649–657. <https://doi.org/10.1002/jbm.a.32893>

- Branner, A., Stein, R.B., Fernandez, E., Aoyagi, Y., Normann, R.A., 2004. Long-Term Stimulation and Recording with a Penetrating Microelectrode Array in Cat Sciatic Nerve. *IEEE Trans. Biomed. Eng.* 51, 146–157. <https://doi.org/10.1109/TBME.2003.820321>
- Branner, A., Stein, R.B., Normann, R.A., 2001. Selective stimulation of cat sciatic nerve using an array of varying-length microelectrodes. *J. Neurophysiol.* 85, 1585–1594.
- Bucala, R., Spiegel, L.A., Chesney, J., Hogan, M., Cerami, A., 1994. Circulating Fibrocytes Define a New Leukocyte Subpopulation That Mediates Tissue Repair.
- Burck, J.M., Bigelow, J.D., Harshbarger, S.D., 2011. Revolutionizing Prosthetics: Systems Engineering Challenges and Opportunities. *JOHNS HOPKINS APL Tech. Dig.* 30.
- Burgess, D.J., Wang, Y., Vaddiraju, S., Gu, B., Papadimitrakopoulos, F., 2015. Foreign Body Reaction to Implantable Biosensors: Effects of Tissue Trauma and Implant Size. *J. Diabetes Sci. Technol.* 9, 966–977. <https://doi.org/10.1177/1932296815601869>
- Cain, D.W., Cidlowski, J.A., 2017. Immune regulation by glucocorticoids. *Nat. Rev. Immunol.* 17, 233–247. <https://doi.org/10.1038/nri.2017.1>
- Can, A.A., Can, A.A., Gamze Bölükbaşı Ateş, 2016. Silk as a Natural Biopolymer for Tissue Engineering, in: *Advanced Surfaces for Stem Cell Research*. John Wiley & Sons, Inc., Hoboken, NJ, USA, pp. 381–400. <https://doi.org/10.1002/9781119242642.ch13>
- Cao, H., Mchugh, K., Chew, S.Y., Anderson, J.M., 2009. The topographical effect of electrospun nanofibrous scaffolds on the in vivo and in vitro foreign body reaction. *J. Biomed. Mater. Res. Part A* 9999A, NA-NA. <https://doi.org/10.1002/jbm.a.32609>
- Capogrosso, M., Milekovic, T., Borton, D., Wagner, F., Martin Moraud, E., Mignardot, J.-B., Buse, N., Gandar, J., Barraud, Q., Xing, D., Rey, E., Duis, S., Jianzhong, Y., Li, W.K.D.K.Q., Detemple, P., Denison, T., Micera, S., Bezard, E., Bloch, J., Courtine, G., 2016. A brain-spinal interface alleviating gait deficits after spinal cord injury in primates. *Nature In Press*, 284–288. <https://doi.org/10.1038/nature20118>
- Ceballos, D., Valero-Cabr, A., Valderrama, E., Schttler, M., Stieglitz, T., Navarro, X., 2002. Morphologic and functional evaluation of peripheral nerve fibers regenerated through polyimide sieve electrodes over long-term implantation. *J. Biomed. Mater. Res.* 60, 517–528. <https://doi.org/10.1002/jbm.10099>
- Chadwell, A., Kenney, L., Thies, S., Galpin, A., Head, J., 2016. The reality of myoelectric prostheses: Understanding what makes these devices difficult for some users to control. *Front. Neurobot.* 10. <https://doi.org/10.3389/fnbot.2016.00007>
- Chang, S.K., Hum, O.S., Moscarello, M.A., Neumann, A.W., Zingg, W., Leutheusser, M.J., Ruegsegger, B., 1977. Platelet adhesion to solid surfaces. The effects of plasma proteins and substrate wettability. *Med. Prog. Technol.* 5, 57–66.
- Chang, T.Y., Yadav, V.G., De Leo, S., Mohedas, A., Rajalingam, B., Chen, C.L., Selvarasah, S., Dokmeci, M.R., Khademhosseini, A., 2007. Cell and protein compatibility of parylene-C surfaces. *Langmuir* 23, 11718–11725. <https://doi.org/10.1021/la7017049>
- Chen, G., Kawazoe, N., Tateishi, T., 2008. Effects of ECM Proteins and Cationic Polymers on the Adhesion and Proliferation of Rat Islet Cells. *Open Biotechnol. J.* 2, 133–137. <https://doi.org/10.2174/1874070700802010133>
- Christensen, M.B., Pearce, S.M., Ledbetter, N.M., Warren, D.J., Clark, G. a, Tresco, P. a, 2014. The foreign body response to the Utah Slant Electrode Array in the cat sciatic nerve. *Acta Biomater.* 10, 4650–60. <https://doi.org/10.1016/j.actbio.2014.07.010>
- Christensen, M.B., Wark, H.A., Hutchinson, D.T., 2015. A Histological Analysis of Human Median and

Ulnar Nerves Following Implantation of Utah Slanted Electrode Arrays. *Biomaterials*. <https://doi.org/10.1016/j.biomaterials.2015.11.012>

- Ciancio, A.L., Cordella, F., Barone, R., Romeo, R.A., Bellingegni, A.D., Sacchetti, R., Davalli, A., Di Pino, G., Ranieri, F., Di Lazzaro, V., Guglielmelli, E., Zollo, L., 2016. Control of Prosthetic Hands via the Peripheral Nervous System. *Front. Neurosci.* 10, 116. <https://doi.org/10.3389/fnins.2016.00116>
- Clark, G.A., Ledbetter, N.M., Warren, D.J., Harrison, R.R., 2011. Recording sensory and motor information from peripheral nerves with Utah Slanted Electrode Arrays. *Proc. Annu. Int. Conf. IEEE Eng. Med. Biol. Soc. EMBS* 4641–4644. <https://doi.org/10.1109/IEMBS.2011.6091149>
- Clark, G.A., Wendelken, S., Page, D.M., Davis, T., Wark, H.A.C., Normann, R.A., Warren, D.J., Hutchinson, D.T., 2014. Using multiple high-count electrode arrays in human median and ulnar nerves to restore sensorimotor function after previous transradial amputation of the hand. 2014 36th Annu. Int. Conf. IEEE Eng. Med. Biol. Soc. EMBC 2014 1977–1980. <https://doi.org/10.1109/EMBC.2014.6944001>
- Clements, I.P., Mukhatyar, V.J., Srinivasan, A., Bentley, J.T., Andreasen, D.S., Bellamkonda, R. V., 2013. Regenerative scaffold electrodes for peripheral nerve interfacing. *IEEE Trans. Neural Syst. Rehabil. Eng.* 21, 554–566. <https://doi.org/10.1109/TNSRE.2012.2217352>
- Cordella, F., Ciancio, A.L., Sacchetti, R., Davalli, A., Cutti, A.G., Guglielmelli, E., Zollo, L., 2016. Literature Review on Needs of Upper Limb Prosthesis Users. *Front. Neurosci.* 10, 209. <https://doi.org/10.3389/fnins.2016.00209>
- Corradetti, B. (editor), 2017. *The Immune Response to Implanted Materials and Devices*. <https://doi.org/10.1007/978-3-319-45433-7>
- Coutinho, A.E., Chapman, K.E., 2011. The anti-inflammatory and immunosuppressive effects of glucocorticoids, recent developments and mechanistic insights. *Mol. Cell. Endocrinol.* 335, 2–13. <https://doi.org/10.1016/j.mce.2010.04.005>
- Cowley, J., Resnik, L., Wilken, J., Smurr Walters, L., Gates, D., 2017. Movement quality of conventional prostheses and the DEKA Arm during everyday tasks. *Prosthet. Orthot. Int.* 41, 33–40. <https://doi.org/10.1177/0309364616631348>
- Cui, C., Schwendeman, S.P., 2007. One-step surface modification of poly(lactide-co-glycolide) microparticles with heparin. *Pharm. Res.* 24, 2381–2393. <https://doi.org/10.1007/s11095-007-9378-1>
- Cui, X., Lee, V.A., Raphael, Y., Wiler, J.A., Hetke, J.F., Anderson, D.J., Martin, D.C., 2001. Surface modification of neural recording electrodes with conducting polymer/biomolecule blends. *J. Biomed. Mater. Res.* 56, 261–272. [https://doi.org/10.1002/1097-4636\(200108\)56:2<261::AID-JBM1094>3.0.CO;2-I](https://doi.org/10.1002/1097-4636(200108)56:2<261::AID-JBM1094>3.0.CO;2-I)
- Cui, X., Wiler, J., Dzaman, M., Altschuler, R.A., Martin, D.C., 2003. In vivo studies of polypyrrole/peptide coated neural probes. *Biomaterials* 24, 777–787. [https://doi.org/10.1016/S0142-9612\(02\)00415-5](https://doi.org/10.1016/S0142-9612(02)00415-5)
- Cutrone, A., Del Valle, J., Santos, D., Badia, J., Filippeschi, C., Micera, S., Navarro, X., Bossi, S., 2015. A three-dimensional self-opening intraneural peripheral interface (SELINe). *J. Neural Eng.* 12, 16016. <https://doi.org/10.1088/1741-2560/12/1/016016>
- Dang, T.T., Bratlie, K.M., Bogatyrev, S.R., Chen, X.Y., Langer, R., Anderson, D.G., 2011. Spatiotemporal effects of a controlled-release anti-inflammatory drug on the cellular dynamics of host response. *Biomaterials* 32, 4464–4470. <https://doi.org/10.1016/j.biomaterials.2011.02.048>
- Darby, I.A., Laverdet, B., Bonté, F., Desmouliere A., 2014. Fibroblasts and myofibroblasts in wound healing. *Clin Cosmet Investig Dermatol.* 7, 301–311. [10.2147/CCID.S50046](https://doi.org/10.2147/CCID.S50046)

- Davis, T.S., Wark, H.A.C., Hutchinson, D.T., Warren, D.J., O'Neill, K., Scheinblum, T., Clark, G.A., Normann, R.A., Greger, B., O'Neill, K., Scheinblum, T., Clark, G.A., Normann, R.A., Greger, B., 2016. Restoring motor control and sensory feedback in people with upper extremity amputations using arrays of 96 microelectrodes implanted in the median and ulnar nerves. *J. Neural Eng.* 13, 36001. <https://doi.org/10.1088/1741-2560/13/3/036001>
- del Valle, J., Navarro, X., 2013. Interfaces with the peripheral nerve for the control of neuroprostheses. *Int. Rev. Neurobiol.* 109, 63–83. <https://doi.org/10.1016/B978-0-12-420045-6.00002-X>
- Delgado-Martinez, I., Righi, M., Santos, D., Cutrone, A., Bossi, S., D'Amico, S., Del Valle, J., Micera, S., Navarro, X., Silva, F.R.D.O., Gomes, L., 2017. Fascicular nerve stimulation and recording using a novel double-aisle regenerative electrode. *J. Neural Eng.* 14, 46003. <https://doi.org/10.1016/j.colsurfa.2007.04.052>
- Deng, Y., Ren, J., Chen, G., Li, G., Wu, X., Wang, G., Gu, G., 2017. Chitosan-Hyaluronic Acid Based Hydrogels for Abdominal Tissue Regeneration 1–13. <https://doi.org/10.1038/s41598-017-02962-z>
- Dhillon, G.S., Horch, K.W., 2005. Direct neural sensory feedback and control of a prosthetic arm. *IEEE Trans. Neural Syst. Rehabil. Eng.* 13, 468–472. <https://doi.org/10.1109/TNSRE.2005.856072>
- DiEgidio, P., Friedman, H.I., Gourdie, R.G., Riley, A.E., Yost, M.J., Goodwin, R.L., 2014. Biomedical Implant Capsule Formation: Lessons Learned and the Road Ahead. *Ann. Plast. Surg.* 0, 1–10. <https://doi.org/10.1097/SAP.0000000000000287>
- Donaldson, P.E.K., 1989. Encapsulating microelectronic implants in one-part silicone rubbers. *Med. Biol. Eng. Comput.* 27, 93–94. <https://doi.org/10.1007/BF02442177>
- Edell, D.J., 1986. A Peripheral Nerve Information Transducer for Amputees: Long-Term Multichannel Recordings from Rabbit Peripheral Nerves. *IEEE Trans. Biomed. Eng. BME-33*, 203–214. <https://doi.org/10.1109/TBME.1986.325892>
- Erlanger, J., Gasser, H. S., 1937. *Electrical signs of nervous activity.* Oxford, England: Univ. Penn. Press.
- Fattahi, P., Yang, G., Kim, G., Abidian, M.R., 2014. A Review of Organic and Inorganic Biomaterials for Neural Interfaces. *Adv. Mater.* 1846–1885. <https://doi.org/10.1002/adma.201304496>
- Fekete, Z., Pongrácz, A., 2017. Multifunctional soft implants to monitor and control neural activity in the central and peripheral nervous system: A review. *Sensors Actuators, B Chem.* 243, 1214–1223. <https://doi.org/10.1016/j.snb.2016.12.096>
- Finch, J., 2011. The ancient origins of prosthetic medicine. *Lancet.* [https://doi.org/10.1016/S0140-6736\(11\)60190-6](https://doi.org/10.1016/S0140-6736(11)60190-6)
- Fisher, L.E., Tyler, D.J., Anderson, J.S., Triolo, R.J., 2009. Chronic stability and selectivity of four-contact spiral nerve-cuff electrodes in stimulating the human femoral nerve. *J. Neural Eng.* 6, 46010. <https://doi.org/10.1088/1741-2560/6/4/046010>
- FitzGerald, J.J., 2016. Suppression of scarring in peripheral nerve implants by drug elution. *J. Neural Eng.* 13, 26006. <https://doi.org/10.1088/1741-2560/13/2/026006>
- Fliegel, O., Feuer, S., 1966. Historical Development of Lower-Extremity Prostheses. *Orthop. Prosthet. Appl. J.* 47, 313–324.
- Gaudet, A.D., Popovich, P.G., Ramer, M.S., 2011. Wallerian degeneration: gaining perspective on inflammatory events after peripheral nerve injury. *J. Neuroinflammation* 8, 110. <https://doi.org/10.1186/1742-2094-8-110>
- Gebelein, C.G., Carraher, C.E., 2007. Silicones in Medical Applications, in: *Bioactive Polymeric Systems, An Overview.* pp. 61–161. <https://doi.org/10.1002/jbm.1043>
- Geelhood, S.J., Horbett, T.A., Ward, W.K., Wood, M.D., Quinn, M.J., 2007. Passivating protein coatings

- for implantable glucose sensors: Evaluation of protein retention. *J. Biomed. Mater. Res. - Part B Appl. Biomater.* 81, 251–260. <https://doi.org/10.1002/jbm.b.30660>
- Ghosh, I., Konar, J., Bhowmick, A.K., 1997. Surface properties of chemically modified polyimide films. *J. Adhes. Sci. Technol.* 11, 877–893. <https://doi.org/10.1163/156856197X00967>
- Gorman, P.H., Mortimer, J.T., 1983. The Effect of Stimulus Parameters on the Recruitment Characteristics of Direct Nerve Stimulation. *IEEE Trans. Biomed. Eng. BME-30*, 407–414. <https://doi.org/10.1109/TBME.1983.325041>
- Green, R.A., Lovell, N.H., Wallace, G.G., Poole-Warren, L.A., 2008. Conducting polymers for neural interfaces: Challenges in developing an effective long-term implant. *Biomaterials* 29, 3393–3399. <https://doi.org/10.1016/j.biomaterials.2008.04.047>
- Grill, W.M., Mortimer, J.T., 1996. Quantification of recruitment properties of multiple contact cuff electrodes. *IEEE Trans. Rehabil. Eng.* 4, 49–62. <https://doi.org/10.1109/86.506402>
- Gunasekera, B., Saxena, T., Bellamkonda, R., Karumbaiah, L., 2015. Intracortical Recording Interfaces: Current Challenges to Chronic Recording Function. *ACS Chem. Neurosci.* 6, 68–83. <https://doi.org/10.1021/cn5002864>
- Haipeng, G., Yinghui, Z., Jianchun, L., Yandao, G., Nanming, Z., Xiufang, Z., 2000. Studies on nerve cell affinity of chitosan-derived materials. *J. Biomed. Mater. Res.* 52, 285–295. [https://doi.org/10.1002/1097-4636\(200011\)52:2<285::AID-JBM7>3.0.CO;2-G](https://doi.org/10.1002/1097-4636(200011)52:2<285::AID-JBM7>3.0.CO;2-G)
- Hanisch, U.-K., Kettenmann, H., 2007. Microglia: active sensor and versatile effector cells in the normal and pathologic brain. *Nat. Neurosci.* 10, 1387–1394. <https://doi.org/10.1038/nn1997>
- Hascup, E.R., af Bjerken, S., Hascup, K.N., Pomerleau, F., Huettl, P., Strömberg, I., Gerhardt, G.A., 2009. Histological studies of the effects of chronic implantation of ceramic-based microelectrode arrays and microdialysis probes in rat prefrontal cortex. *Brain Res.* 1291, 12–20. <https://doi.org/10.1016/j.brainres.2009.06.084>
- Hashim, N.A., Abd Razak, N.A. bin, Gholizadeh, H., Osman, N.A.A., 2017. Analysis of voluntary opening Ottobock Hook and Hosmer Hook for upper limb prosthetics: a preliminary study. *Biomed. Eng. / Biomed. Tech.* 62, 447–454. <https://doi.org/10.1515/bmt-2016-0130>
- Hassler, C., Von Metzen, R.P., Ruther, P., Stieglitz, T., 2010. Characterization of parylene C as an encapsulation material for implanted neural prostheses. *J. Biomed. Mater. Res. - Part B Appl. Biomater.* 93, 266–274. <https://doi.org/10.1002/jbm.b.31584>
- Haugland, M.K., Hoffer, J.A., Sinkjaer, T., 1994. Skin contact force information in sensory nerve signals recorded by implanted cuff electrodes. *IEEE Trans. Rehabil. Eng.* 2, 18–28. <https://doi.org/10.1109/86.296346>
- Heiduschka, P.; Thanos, S., 1998. Implantable bioelectronic interfaces for lost nerve functions. *Prog Neurobiol.* 55, 433–461. [https://doi.org/10.1016/S0301-0082\(98\)00013-6](https://doi.org/10.1016/S0301-0082(98)00013-6)
- Henze, D.A., Borhegyi, Z., Csicsvari, J., Mamiya, A., Harris, K.D., Buzsáki, G., 2000. Intracellular features predicted by extracellular recordings in the hippocampus in vivo. *J. Neurophysiol.* 84, 390–400. <https://doi.org/10.1152/jn.2000.84.3.390>
- Heo, D.N., Ko, W.-K., Lee, W.J., Lee, S.J., Lee, D., Heo, M., Rim, H., Bae, M.S., Lee, J.B., Ahn, B.-S., Kwon, I.K., 2016a. Enhanced Biocompatibility of Polyimide Film by Anti-Inflammatory Drug Loading. *J. Nanosci. Nanotechnol.* 16, 8800–8804. <https://doi.org/10.1166/jnn.2016.12482>
- Heo, D.N., Song, S.J., Kim, H.J., Lee, Y.J., Ko, W.K., Lee, S.J., Lee, D., Park, S.J., Zhang, L.G., Kang, J.Y., Do, S.H., Lee, S.H., Kwon, I.K., 2016b. Multifunctional hydrogel coatings on the surface of neural cuff electrode for improving electrode-nerve tissue interfaces. *Acta Biomater.* 39, 25–33. <https://doi.org/10.1016/j.actbio.2016.05.009>
- Hetrick, E.M., Prichard, H.L., Klitzman, B., Schoenfisch, M.H., 2007. Reduced foreign body response at

- nitric oxide-releasing subcutaneous implants. *Biomaterials* 28, 4571–4580. <https://doi.org/10.1016/j.biomaterials.2007.06.036>
- Hezi-Yamit, A., Sullivan, C., Wong, J., David, L., Chen, M., Cheng, P., Shumaker, D., Wilcox, J.N., Udipi, K., 2009. Impact of polymer hydrophilicity on biocompatibility: Implication for DES polymer design. *J. Biomed. Mater. Res. - Part A* 90, 133–141. <https://doi.org/10.1002/jbm.a.32057>
- Hirsh, S.L., McKenzie, D.R., Nosworthy, N.J., Denman, J.A., Sezerman, O.U., Bilek, M.M.M., 2013. The Vroman effect: Competitive protein exchange with dynamic multilayer protein aggregates. *Colloids Surfaces B Biointerfaces* 103, 395–404. <https://doi.org/10.1016/j.colsurfb.2012.10.039>
- Horch, K., Meek, S., Taylor, T.G., Hutchinson, D.T., 2011. Object discrimination with an artificial hand using electrical stimulation of peripheral tactile and proprioceptive pathways with intrafascicular electrodes. *IEEE Trans. Neural Syst. Rehabil. Eng.* 19, 483–489. <https://doi.org/10.1109/TNSRE.2011.2162635>
- Hu, W.J., Eaton, J.W., Ugarova, T.P., Tang, L.P., 2001. Molecular basis of biomaterial-mediated foreign body reactions. *Blood* 99, 3908.
- Ige, O.O., Umoru, L.E., Aribu, S., 2012. Natural Products: A Minefield of Biomaterials. *ISRN Mater. Sci.* 2012, 1–20. <https://doi.org/10.5402/2012/983062>
- Ishida, Y., Kimura, A., Kondo, T., Hayashi, T., Ueno, M., Takakura, N., Matsushima, K., Mukaida, N., 2007. Essential Roles of the CC Chemokine Ligand 3-CC Chemokine Receptor 5 Axis in Bleomycin-Induced Pulmonary Fibrosis through Regulation of Macrophage and Fibrocyte Infiltration. *Am. J. Pathol.* 170, 843–854. <https://doi.org/10.2353/ajpath.2007.051213>
- Jan, E., Hendricks, J.L., Husaini, V., Richardson-Burns, S.M., Sereno, A., Martin, D.C., Kotov, N.A., 2009. Layered carbon nanotube-polyelectrolyte electrodes outperform traditional neural interface materials. *Nano Lett.* 9, 4012–4018. <https://doi.org/10.1021/nl902187z>
- Janeway, C.A., Travers, P., Walport, M., Shlomchik, M., 2001. *Immunobiology: The Immune System In Health And Disease*, *Immuno Biology* 5. Garland Pub. <https://doi.org/10.1111/j.1467-2494.1995.tb00120.x>
- Jones, J.A., Chang, D.T., Meyerson, H., Colton, E., Il, K.K., Matsuda, T., Anderson, J.M., 2007. Proteomic analysis and quantification of cytokines and chemokines from biomaterial surface-adherent macrophages and foreign body giant cells. *J. Biomed. Mater. Res. - Part A* 83, 585–596. <https://doi.org/10.1002/jbm.a.31221>
- Kang, Y., Kim, J., Lee, Y.M., Im, S., Park, H., Kim, W.J., 2015. Nitric oxide-releasing polymer incorporated ointment for cutaneous wound healing. *J. Control. Release* 220, 624–630. <https://doi.org/10.1016/j.jconrel.2015.08.057>
- Kastellorizios, M., Papadimitrakopoulos, F., Burgess, D.J., 2015a. Multiple tissue response modifiers to promote angiogenesis and prevent the foreign body reaction around subcutaneous implants. *J. Control. Release* 214, 103–111. <https://doi.org/10.1016/j.jconrel.2015.07.021>
- Kastellorizios, M., Papadimitrakopoulos, F., Burgess, D.J., 2015b. Prevention of foreign body reaction in a pre-clinical large animal model. *J. Control. Release* 202, 101–107. <https://doi.org/10.1016/j.jconrel.2015.01.038>
- Kigerl, K. a, Gensel, J.C., Ankeny, D.P., Alexander, J.K., Donnelly, D.J., Popovich, P.G., 2009. Identification of two distinct macrophage subsets with divergent effects causing either neurotoxicity or regeneration in the injured mouse spinal cord. *J. Neurosci.* 29, 13435–44. <https://doi.org/10.1523/JNEUROSCI.3257-09.2009>
- Kim, B.J., Meng, E., 2016. Micromachining of Parylene C for bioMEMS. *Polym. Adv. Technol.* 27, 564–576. <https://doi.org/10.1002/pat.3729>

- Kim, D.H., Martin, D.C., 2006. Sustained release of dexamethasone from hydrophilic matrices using PLGA nanoparticles for neural drug delivery. *Biomaterials* 27, 3031–3037. <https://doi.org/10.1016/j.biomaterials.2005.12.021>
- Kim, J., 2002. Protein adsorption on polymer particles. *J. Biomed. Mater. Res.* 21, 4373–4381. <https://doi.org/10.1002/jbm.820210202>
- Kim, Y., Romero-Ortega, M.I., 2012. Material considerations for peripheral nerve interfacing. *MRS Bull.* 37, 573–580. <https://doi.org/10.1557/mrs.2012.99>
- Klopfleisch, R., 2016. Macrophage reaction against biomaterials in the mouse model - Phenotypes, functions and markers. *Acta Biomater.* 43, 3–13. <https://doi.org/10.1016/j.actbio.2016.07.003>
- Kovacs, G.T.A., Stormont, C.W., Rosen, J.M., 1992. Regeneration microelectrode array for peripheral nerve recording and stimulation. *IEEE Trans. Biomed. Eng.* 39, 893–902. <https://doi.org/10.1109/10.256422>
- Kozai, T.D.Y., Jaquins-Gerstl, A.S., Vazquez, A.L., Michael, A.C., Cui, X.T., 2015. Brain tissue responses to neural implants impact signal sensitivity and intervention strategies. *ACS Chem. Neurosci.* 6, 48–67. <https://doi.org/10.1021/cn500256e>
- Krarpup, C., Loeb, G.E., Pezeshkpour, G.H., 1989. Conduction studies in peripheral cat nerve using implanted electrodes: III. The effects of prolonged constriction on the distal nerve segment. *Muscle Nerve* 12, 915–928. <https://doi.org/10.1002/mus.880121108>
- Kuiken, T.A., Li, G., Lock, B.A., Lipschutz, R.D., Miller, L.A., Stubblefield, K.A., Englehart, K., 2011. Targeted muscle reinnervation for real-time myoelectric control of multifunction artificial arms. *Jama* 301, 619–628. <https://doi.org/10.1001/jama.2009.116.Targeted>
- Kuiken, T. a, Marasco, P.D., Lock, B. a, Harden, R.N., Dewald, J.P. a, 2007. Redirection of cutaneous sensation from the hand to the chest skin of human amputees with targeted reinnervation. *Proc. Natl. Acad. Sci. U. S. A.* 104, 20061–20066. <https://doi.org/10.1073/pnas.0706525104>
- Kyberd, P.J., 2017. Assessment of Functionality of Multifunction Prosthetic Hands. *J. Prosthetics Orthot.* 29, 103–111. <https://doi.org/10.1097/JPO.0000000000000139>
- Lacour, S.P., Courtine, G., Guck, J., 2016. Materials and technologies for soft implantable neuroprostheses. *Nat. Rev. Mater.* 1, 16063. <https://doi.org/10.1038/natrevmats.2016.63>
- Lacour, S.P., FitzGerald, J.J., Lago, N., Tarte, E., McMahon, S., Fawcett, J., 2009. Long micro-channel electrode arrays: A novel type of regenerative peripheral nerve interface. *IEEE Trans. Neural Syst. Rehabil. Eng.* 17, 454–460. <https://doi.org/10.1109/TNSRE.2009.2031241>
- Lago, N., Ceballos, D., J Rodríguez, F., Stieglitz, T., Navarro, X., 2005. Long term assessment of axonal regeneration through polyimide regenerative electrodes to interface the peripheral nerve. *Biomaterials* 26, 2021–2031. <https://doi.org/10.1016/j.biomaterials.2004.06.025>
- Lago, N., Yoshida, K., Koch, K.P., Navarro, X., 2007. Assessment of biocompatibility of chronically implanted polyimide and platinum intrafascicular electrodes. *IEEE Trans. Biomed. Eng.* 54, 281–290. <https://doi.org/10.1109/TBME.2006.886617>
- Lapidot, S., Meirovitch, S., Sharon, S., Heyman, A., Kaplan, D.L., Shoseyov, O., 2012. Clues for biomimetics from natural composite materials. *Nanomedicine* 7, 1409–1423. <https://doi.org/10.2217/nnm.12.107>
- Larsen, J.O., Thomsen, M., Haugland, M., Sinkjær, T., 1998. Degeneration and regeneration in rabbit peripheral nerve with long-term nerve cuff electrode implant: A stereological study of myelinated and unmyelinated axons. *Acta Neuropathol.* 96, 365–378. <https://doi.org/10.1007/s004010050907>
- Latour, R.A., 2008. Biomaterials : Protein – Surface Interactions. *Encycl. Biomater. Biomed. Eng.* 3434. <https://doi.org/10.3109/E-EBBE-120041856>

- Lawrence, S.M., Dhillon, G.S., Jensen, W., Yoshida, K., Horch, K.W., 2004. Acute peripheral nerve recording characteristics of polymer-based longitudinal intrafascicular electrodes. *IEEE Trans. Neural Syst. Rehabil. Eng.* 12, 345–348. <https://doi.org/10.1109/TNSRE.2004.831491>
- Lawrence, S.M., Larsen, J.O., Horch, K.W., Riso, R., Sinkjr, T., 2002. Long-term biocompatibility of implanted polymer-based intrafascicular electrodes. *J. Biomed. Mater. Res.* 63, 501–506. <https://doi.org/10.1002/jbm.10303>
- Lawrence, T., Gilroy, D.W., 2007. Chronic inflammation: a failure of resolution? *Int. J. Exp. Pathol.* 88, 85–94. <https://doi.org/10.1111/j.1365-2613.2006.00507.x>
- Lech, M., Anders, H.J., 2013. Macrophages and fibrosis: How resident and infiltrating mononuclear phagocytes orchestrate all phases of tissue injury and repair. *Biochim. Biophys. Acta - Mol. Basis Dis.* 1832, 989–997. <https://doi.org/10.1016/j.bbadis.2012.12.001>
- Lecomte, A., Castagnola, V., Descamps, E., Dahan, L., Blatché, M.C., Dinis, T.M., Leclerc, E., Egles, C., Bergaud, C., 2015. Silk and PEG as means to stiffen a parylene probe for insertion in the brain: toward a double time-scale tool for local drug delivery. *J. Micromechanics Microengineering* 25, 125003. <https://doi.org/10.1088/0960-1317/25/12/125003>
- Lecomte, A., Degache, A., Descamps, E., Dahan, L., Bergaud, C., 2017. In vitro and in vivo biostability assessment of chronically-implanted Parylene C neural sensors. *Sensors Actuators B Chem.* <https://doi.org/10.1016/j.snb.2017.05.057>
- Lee, H.C., Ejserholm, F., Gaire, J., Currllin, S., Schouenborg, J., Wallman, L., Bengtsson, M., Park, K., Otto, K.J., 2017. Histological evaluation of flexible neural implants; flexibility limit for reducing the tissue response? *J. Neural Eng.* 14, 36026. <https://doi.org/10.1088/1741-2552/aa68f0>
- Lee, Y.J., Kim, H.J., Kang, J.Y., Do, S.H., Lee, S.H., 2017. Biofunctionalization of Nerve Interface via Biocompatible Polymer-Roughened Pt Black on Cuff Electrode for Chronic Recording. *Adv. Healthc. Mater.* 6. <https://doi.org/10.1002/adhm.201601022>
- Leventhal, D.K., Cohen, M., Durand, D.M., 2006. Chronic histological effects of the flat interface nerve electrode. *J. Neural Eng.* 3, 102–113. <https://doi.org/10.1088/1741-2560/3/2/004>
- Leventhal, D.K., Durand, D.M., 2004. Chronic measurement of the stimulation selectivity of the flat interface nerve electrode. *IEEE Trans. Biomed. Eng.* 51, 1649–1658. <https://doi.org/10.1109/TBME.2004.827535>
- Loeb, G.E., Peck, R.A., 1996. Cuff electrodes for chronic stimulation and recording of peripheral nerve activity. *J. Neurosci. Methods* 64, 95–103. [https://doi.org/10.1016/0165-0270\(95\)00123-9](https://doi.org/10.1016/0165-0270(95)00123-9)
- Luttikhuisen, D.T., Harmsen, M.C., Luyn, M.J.A. Van, 2006. Cellular and Molecular Dynamics in the Foreign Body Reaction. *Tissue Eng.* 12, 1955–1970. <https://doi.org/10.1089/ten.2006.12.1955>
- Malagodi, M.S., Horch, K.W., Schoenberg, A.A., 1989. An intrafascicular electrode for recording of action potentials in peripheral nerves. *Ann. Biomed. Eng.* 17, 397–410. <https://doi.org/10.1007/BF02368058>
- Martin, P., Leibovich, S.J., 2005. Inflammatory cells during wound repair: The good, the bad and the ugly. *Trends Cell Biol.* <https://doi.org/10.1016/j.tcb.2005.09.002>
- McCreery, D., Cogan, S., Kane, S., Pikov, V., 2016. Correlations between histology and neuronal activity recorded by microelectrodes implanted chronically in the cerebral cortex. *J. Neural Eng.* 13, 36012. <https://doi.org/10.1088/1741-2560/13/3/036012>
- McDonald, B., Pittman, K., Menezes, G.B., Hirota, S.A., Slaba, I., Waterhouse, C.C.M., Beck, P.L., Muruve, D.A., Kubers, P., 2010. Intravascular Danger Signals Guide Neutrophils to Sites of Sterile Inflammation. *Science* (80-.). 330.
- McNally, A.K., Anderson, J.M., 2011. Macrophage fusion and multinucleated giant cells of

- inflammation. *Adv. Exp. Med. Biol.* 713, 97–111. https://doi.org/10.1007/978-94-007-0763-4_7
- McNally, A.K., DeFife, K.M., Anderson, J.M., 1996. Interleukin-4-induced macrophage fusion is prevented by inhibitors of mannose receptor activity. *Am. J. Pathol.* 149, 975–85.
- McNaughton, T.G., Horch, K.W., 1996. Metallized polymer fibers as leadwires and intrafascicular microelectrodes. *J. Neurosci. Methods* 70, 103–110. [https://doi.org/10.1016/S0165-0270\(96\)00111-2](https://doi.org/10.1016/S0165-0270(96)00111-2)
- McNeal, D.R., 1976. Analysis of a Model for Excitation of Myelinated Nerve. *IEEE Trans. Biomed. Eng. BME-23*, 329–337. <https://doi.org/10.1109/TBME.1976.324593>
- Mercanzini, A., Reddy, S.T., Velluto, D., Colin, P., Maillard, A., Bensadoun, J.C., Hubbell, J.A., Renaud, P., 2010. Controlled release nanoparticle-embedded coatings reduce the tissue reaction to neuroprostheses. *J. Control. Release* 145, 196–202. <https://doi.org/10.1016/j.jconrel.2010.04.025>
- Merrill, D.R., Bikson, M., Jefferys, J.G.R., 2005. Electrical stimulation of excitable tissue: design of efficacious and safe protocols. *J. Neurosci. Methods* 141, 171–198. <https://doi.org/10.1016/j.jneumeth.2004.10.020>
- Metallo, C., Trimmer, B.A., 2015. Silk coating as a novel delivery system and reversible adhesive for stiffening and shaping flexible probes. *J. Biol. Methods* 2, 13. <https://doi.org/10.14440/jbm.2015.41>
- Mighri, N., Mao, J., Mighri, F., Aji, A., Rouabhia, M., 2015. Chitosan-Coated Collagen Membranes Promote Chondrocyte Adhesion, Growth, and Interleukin-6 Secretion. *Materials (Basel)*. 8, 7673–7689. <https://doi.org/10.3390/ma8115413>
- Miller, L.A., Stubblefield, K.A., Lipschutz, R.D., Lock, B.A., Kuiken, T.A., 2008. Improved Myoelectric Prosthesis Control Using Targeted Reinnervation Surgery: A Case Series. *IEEE Trans Neural Syst Rehabil Eng* 16, 4650. <https://doi.org/10.1109/TNSRE.2007.911817>
- Millstein, S.G., Heger, H., Hunter, G. a, 1986. Prosthetic use in adult upper limb amputees: a comparison of the body powered and electrically powered prostheses. *Prosthet. Orthot. Int.* 10, 27–34. <https://doi.org/10.3109/03093648609103076>
- Mohan, T., Niegellhell, K., Nagaraj, C., Reishofer, D., Spirk, S., Olschewski, A., Stana Kleinschek, K., Kargl, R., 2017. Interaction of Tissue Engineering Substrates with Serum Proteins and Its Influence on Human Primary Endothelial Cells. *Biomacromolecules* 18, 413–421. <https://doi.org/10.1021/acs.biomac.6b01504>
- Mooney, J.E., Rolfe, B.E., Osborne, G.W., Sester, D.P., van Rooijen, N., Campbell, G.R., Hume, D.A., Campbell, J.H., 2010. Cellular Plasticity of Inflammatory Myeloid Cells in the Peritoneal Foreign Body Response. *Am. J. Pathol.* 176, 369–380. <https://doi.org/10.2353/ajpath.2010.090545>
- Moore, L.B., Kyriakides, T.R., 2015. Molecular characterization of macrophage-biomaterial interactions. *Adv. Exp. Med. Biol.* 865, 109–122. https://doi.org/10.1007/978-3-319-18603-0_7
- Moore, L.B., Sawyer, A.J., Charokopos, A., Skokos, E.A., Kyriakides, T.R., 2015. Loss of monocyte chemoattractant protein-1 alters macrophage polarization and reduces NFκB activation in the foreign body response. *Acta Biomater.* 11, 37–47. <https://doi.org/10.1016/j.actbio.2014.09.022>
- Morais, J.M., Papadimitrakopoulos, F., Burgess, D.J., 2010. Biomaterials/tissue interactions: possible solutions to overcome foreign body response. *AAPS J.* 12, 188–196. <https://doi.org/10.1208/s12248-010-9175-3>
- Mueller, M., Boehler, C., Jaeger, J., Asplund, M., Stieglitz, T., 2016. A double-sided fabrication process

- for intrafascicular parylene C based electrode arrays, in: 2016 38th Annual International Conference of the IEEE Engineering in Medicine and Biology Society (EMBC). IEEE, pp. 2798–2801. <https://doi.org/10.1109/EMBC.2016.7591311>
- Mueller, M., de la Oliva, N., del Valle, J., Delgado-Martínez, I., Navarro, X., Stieglitz, T., 2017. Rapid prototyping of flexible intrafascicular electrode arrays by picosecond laser structuring. *J. Neural Eng.* 14, 66016. <https://doi.org/10.1088/1741-2552/aa7eea>
- Müller, M., Leonhard, C., Krauthausen, M., Wacker, K., Kiefer, R., 2010. On the longevity of resident endoneurial macrophages in the peripheral nervous system: A study of physiological macrophage turnover in bone marrow chimeric mice. *J. Peripher. Nerv. Syst.* 15, 357–365. <https://doi.org/10.1111/j.1529-8027.2010.00295.x>
- Nair, L.S., Laurencin, C.T., 2007. Biodegradable polymers as biomaterials. *Prog. Polym. Sci.* <https://doi.org/10.1016/j.progpolymsci.2007.05.017>
- Navarro, X., Calvet, S., Butí, M., Gómez, N., Cabruja, E., Garrido, P., Villa, R., Valderrama, E., 1996. Peripheral nerve regeneration through microelectrode arrays based on silicon technology. *Restor. Neurol. Neurosci.* 9, 151–160. <https://doi.org/10.3233/RNN-1996-9303>
- Navarro, X., Calvet, S., Rodríguez, F.J., Stieglitz, T., Blau, C., Butí, M., Valderrama, E., Meyer, J.U., 1998. Stimulation and recording from regenerated peripheral nerves through polyimide sieve electrodes. *J. Peripher. Nerv. Syst.* 3, 91–101.
- Navarro, X., Krueger, T.B., Lago, N., Micera, S., Stieglitz, T., Dario, P., 2005. A critical review of interfaces with the peripheral nervous system for the control of neuroprostheses and hybrid bionic systems. *J. Peripher. Nerv. Syst.* 10, 229–58. <https://doi.org/10.1111/j.1085-9489.2005.10303.x>
- Navarro, X., Verdú, E., 2004. Cell transplants and artificial guides for nerve repair, in: *Brain Damage and Repair. From Molecular Research to Clinical Therapy.* pp. 451–471. https://doi.org/10.1007/1-4020-2541-6_29
- Nerlich, A.G., Zink, A., Szeimies, U., Hagedorn, H.G., 2000. Ancient Egyptian prosthesis of the big toe. *Lancet.* [https://doi.org/10.1016/S0140-6736\(00\)03507-8](https://doi.org/10.1016/S0140-6736(00)03507-8)
- Noel, S., Dhooghe, B., Leal, T., 2012. PDE5 Inhibitors as Potential Tools in the Treatment of Cystic Fibrosis. *Front. Pharmacol.* 3, 167. <https://doi.org/10.3389/fphar.2012.00167>
- Nolta, N.F., Christensen, M.B., Crane, P.D., Skousen, J.L., Tresco, P.A., 2015. BBB leakage, astrogliosis, and tissue loss correlate with silicon microelectrode array recording performance. *Biomaterials* 53, 753–762. <https://doi.org/10.1016/j.biomaterials.2015.02.081>
- Noorisafa, F., Razmjou, A., Emami, N., Low, Z.-X., Korayem, A.H., Kajani, A.A., 2016. Surface modification of polyurethane via creating a biocompatible superhydrophilic nanostructured layer: role of surface chemistry and structure. *J. Exp. Nanosci.* 8080, 1–23. <https://doi.org/10.1080/17458080.2016.1188223>
- Norton, L.W., Koschwanez, H.E., Wisniewski, N.A., Klitzman, B., Reichert, W.M., 2007. Vascular endothelial growth factor and dexamethasone release from nonfouling sensor coatings affect the foreign body response. *J. Biomed. Mater. Res. - Part A* 81, 858–869. <https://doi.org/10.1002/jbm.a.31088>
- Norton, L.W., Tegnell, E., Toporek, S.S., Reichert, W.M., 2005. In vitro characterization of vascular endothelial growth factor and dexamethasone releasing hydrogels for implantable probe coatings. *Biomaterials* 26, 3285–3297. <https://doi.org/10.1016/j.biomaterials.2004.07.069>
- Oddo, C.M., Raspopovic, S., Artoni, F., Mazzoni, A., Spigler, G., Petrini, F., Giambattistelli, F., Vecchio, F., Miraglia, F., Zollo, L., Di Pino, G., Camboni, D., Carrozza, M.C., Guglielmelli, E., Rossini, P.M., Faraguna, U., Micera, S., 2016. Intraneural stimulation elicits discrimination of textural features by artificial fingertip in intact and amputee humans. *Elife* 5, 1–27.

<https://doi.org/10.7554/eLife.09148>

- Oughlis, S., Changotade, S., Poirier, F., Cieutat, A.-M., Rohman, G., Peltzer, J., Migonney, V., Lataillade, J.-J., Lutomski, D., 2016. Improved proliferation and osteogenic differentiation of human mesenchymal stem cells on a titanium biomaterial grafted with poly(sodium styrene sulphonate) and coated with a platelet-rich plasma proteins biofilm. *J. Bioact. Compat. Polym.* 31, 568–582. <https://doi.org/10.1177/0883911516643105>
- Pacelli, S., Manoharan, V., Desalvo, A., Lomis, N., Jodha, K.S., Prakash, S., Paul, A., 2015. Tailoring biomaterial surface properties to modulate host-implant interactions: implication in cardiovascular and bone therapy. *J. Mater. Chem. B* 4, 1586–1599. <https://doi.org/10.1039/C5TB01686J>
- Park, H.J., Durand, D.M., 2015. Motion control of the rabbit ankle joint with a flat interface nerve electrode. *Muscle and Nerve* 52, 1088–1095. <https://doi.org/10.1002/mus.24654>
- Park, S.J., Lee, Y.J., Heo, D.N., Kwon, I.K., Yun, K.S., Kang, J.Y., Lee, S.H., 2015. Functional nerve cuff electrode with controllable anti-inflammatory drug loading and release by biodegradable nanofibers and hydrogel deposition. *Sensors Actuators, B Chem.* 215, 133–141. <https://doi.org/10.1016/j.snb.2015.03.036>
- Percival, J.M., Whitehead, N.P., Adams, M.E., Adamo, C.M., Beavo, J. a, Froehner, S.C., 2012. Sildenafil reduces respiratory muscle weakness and fibrosis in the mdx mouse model of Duchenne muscular dystrophy. *J. Pathol.* 228, 77–87. <https://doi.org/10.1002/path.4054>
- Polasek, K.H., Hoyen, H.A., Keith, M.W., Kirsch, R.F., Tyler, D.J., 2009. Stimulation stability and selectivity of chronically implanted multicontact nerve cuff electrodes in the human upper extremity. *IEEE Trans. Neural Syst. Rehabil. Eng.* 17, 428–437. <https://doi.org/10.1109/TNSRE.2009.2032603>
- Polikov, V.S., Tresco, P.A., Reichert, W.M., 2005. Response of brain tissue to chronically implanted neural electrodes. *J. Neurosci. Methods* 148, 1–18. <https://doi.org/10.1016/j.jneumeth.2005.08.015>
- Ranck, J.B., 1975. Which elements are excited in electrical stimulation of mammalian central nervous system: A review. *Brain Res.* 98, 417–440. [https://doi.org/10.1016/0006-8993\(75\)90364-9](https://doi.org/10.1016/0006-8993(75)90364-9)
- Raspopovic, S., Capogrosso, M., Petrini, F.M., Bonizzato, M., Rigosa, J., Di Pino, G., Carpaneto, J., Controzzi, M., Boretius, T., Fernandez, E., Granata, G., Oddo, C.M., Citi, L., Ciancio, a. L., Cipriani, C., Carrozza, M.C., Jensen, W., Guglielmelli, E., Stieglitz, T., Rossini, P.M., Micera, S., 2014. Restoring Natural Sensory Feedback in Real-Time Bidirectional Hand Prostheses. *Sci. Transl. Med.* 6, 222ra19–222ra19. <https://doi.org/10.1126/scitranslmed.3006820>
- Raspopovic, S., Carpaneto, J., Udina, E., Navarro, X., Micera, S., 2010. On the identification of sensory information from mixed nerves by using single-channel cuff electrodes. *J. Neuroeng. Rehabil.* 7, 17. <https://doi.org/10.1186/1743-0003-7-17>
- Resnik, L., Klinger, S.L., Etter, K., 2014. The DEKA Arm: Its features, functionality, and evolution during the Veterans Affairs Study to optimize the DEKA Arm. *Prosthet. Orthot. Int.* 38, 492–504. <https://doi.org/10.1177/0309364613506913>
- Richardson, R.R., Miller, J.A., Reichert, W.M., 1993. Polyimides as biomaterials: preliminary biocompatibility testing. *Biomaterials* 14, 627–635. [https://doi.org/10.1016/0142-9612\(93\)90183-3](https://doi.org/10.1016/0142-9612(93)90183-3)
- Rodriguez, A., Meyerson, H., Anderson, J.M., 2009. Quantitative in vivo cytokine analysis at synthetic biomaterial implant sites. *J. Biomed. Mater. Res. - Part A* 89, 152–159. <https://doi.org/10.1002/jbm.a.31939>
- Rodriguez, F.J., Ceballos, D., Schuttler, M., Valero, A., Valderrama, E., Stieglitz, T., Navarro, X., 2000. Polyimide cuff electrodes for peripheral nerve stimulation. *J. Neurosci. Methods* 98, 105–118.

[https://doi.org/10.1016/S0165-0270\(00\)00192-8](https://doi.org/10.1016/S0165-0270(00)00192-8)

- Rosen, J.M., Grosser, M., Hentz, V.R., 1990. Preliminary experiments in nerve regeneration through laser-drilled holes in silicon chips. *Restor. Neurol. Neurosci.* 2, 89–102. <https://doi.org/10.3233/RNN-1990-2205>
- Rosenthal, F., 1972. Extracellular potential fields of single PT-neurons. *Brain Res.* 36, 251–263. [https://doi.org/10.1016/0006-8993\(72\)90733-0](https://doi.org/10.1016/0006-8993(72)90733-0)
- Rossini, P.M., Micera, S., Benvenuto, A., Carpaneto, J., Cavallo, G., Citi, L., Cipriani, C., Denaro, L., Denaro, V., Di Pino, G., Ferreri, F., Guglielmelli, E., Hoffmann, K.P., Raspopovic, S., Rigosa, J., Rossini, L., Tombini, M., Dario, P., 2010. Double nerve intraneural interface implant on a human amputee for robotic hand control. *Clin. Neurophysiol.* 121, 777–783. <https://doi.org/10.1016/j.clinph.2010.01.001>
- Rousche, P.J., Pellinen, D.S., Pivin, D.P., Williams, J.C., Vetter, R.J., Kipke, D.R., 2001. Flexible polyimide-based intracortical electrode arrays with bioactive capability. *IEEE Trans. Biomed. Eng.* 48, 361–370. <https://doi.org/10.1109/10.914800>
- Rubehn, B., Stieglitz, T., 2010. In vitro evaluation of the long-term stability of polyimide as a material for neural implants. *Biomaterials* 31, 3449–3458. <https://doi.org/10.1016/j.biomaterials.2010.01.053>
- Rutten, W.L.C., Smit, J.P.A., Frieswijk, T.A., Bielen, J.A., Brouwer, A.L.H., Buitenweg, J.R., Heida, C., 1999. Neuro-electronic interfacing with multielectrode arrays. *IEEE Eng. Med. Biol. Mag.* 18, 47–55. <https://doi.org/10.1109/51.765188>
- Rutten, W.L.C., van Wier, H.J., Put, J.H.M., 1991. Sensitivity and selectivity of intraneural stimulation using a silicon electrode array. *IEEE Trans. Biomed. Eng.* 38, 192–198. <https://doi.org/10.1109/10.76386>
- Sahin, H., Wasmuth, H.E., 2013. Chemokines in tissue fibrosis. *Biochim. Biophys. Acta - Mol. Basis Dis.* 1832, 1041–1048. <https://doi.org/10.1016/j.bbadis.2012.11.004>
- Sarkar, K., Xue, Y., Sant, S., 2017. Host Response to Synthetic Versus Natural Biomaterials, in: *The Immune Response to Implanted Materials and Devices: The Impact of the Immune System on the Success of an Implant*. pp. 1–241. <https://doi.org/10.1007/978-3-319-45433-7>
- Schiefer, M.A., Freeberg, M., Pinault, G.J.C., Anderson, J., Hoyen, H., Tyler, D.J., Triolo, R.J., 2013. Selective activation of the human tibial and common peroneal nerves with a flat interface nerve electrode. *J. Neural Eng.* 10, 56006. <https://doi.org/10.1088/1741-2560/10/5/056006>
- Schiefer, M., Tan, D., Sidek, S.M., Tyler, D.J., 2016. Sensory feedback by peripheral nerve stimulation improves task performance in individuals with upper limb loss using a myoelectric prosthesis. *J. Neural Eng.* 13, 16001. <https://doi.org/10.1088/1741-2560/13/1/016001>
- Schmidt, E.M., McIntosh, J.S., Bak, M.J., 1988. Long-term implants of Parylene-C coated microelectrodes. *Med. Biol. Eng. Comput.* 26, 96–101. <https://doi.org/10.1007/BF02441836>
- Schultz, A.E., Kuiken, T.A., 2011. Neural Interfaces for Control of Upper Limb Prostheses: The State of the Art and Future Possibilities. *PM R* 3, 55–67. <https://doi.org/10.1016/j.pmrj.2010.06.016>
- Seki, E., De Minicis, S., Gwak, G.Y., Kluwe, J., Inokuchi, S., Bursill, C.A., Llovet, J.M., Brenner, D.A., Schwabe, R.F., 2009. CCR1 and CCR5 promote hepatic fibrosis in mice. *J. Clin. Invest.* 119, 1858–1870. <https://doi.org/10.1172/JCI37444.1858>
- Seymour, J.P., Kipke, D.R., 2007. Neural probe design for reduced tissue encapsulation in CNS. *Biomaterials* 28, 3594–3607. <https://doi.org/10.1016/j.biomaterials.2007.03.024>
- Sheikh, Z., Brooks, P.J., Barzilay, O., Fine, N., Glogauer, M., 2015. Macrophages, foreign body giant cells and their response to implantable biomaterials. *Materials (Basel)*. <https://doi.org/10.3390/ma8095269>

- Smit, J.P.A., Rutten, W.L.C., Boom, H.B.K., 1999. Endoneural selective stimulating using wire-microelectrode arrays. *IEEE Trans. Rehabil. Eng.* 7, 399–412. <https://doi.org/10.1109/86.808943>
- Smith, J.A., Das, A., Ray, S.K., Banik, N.L., 2011. Role of pro-inflammatory cytokines released from microglia in neurodegenerative diseases. *Brain Res. Bull.* 87. <https://doi.org/10.1016/j.brainresbull.2011.10.004>
- Smith, J.K., Myers, K.P., Holloway, R.G., Landau, M.E., 2014. Ethical considerations in elective amputation after traumatic peripheral nerve injuries. *Neurol. Clin. Pract.* 4, 280–286. <https://doi.org/10.1212/CPJ.0000000000000049>
- Spataro, L., Dilgen, J., Retterer, S., Spence, a. J., Isaacson, M., Turner, J.N., Shain, W., 2005. Dexamethasone treatment reduces astroglia responses to inserted neuroprosthetic devices in rat neocortex. *Exp. Neurol.* 194, 289–300. <https://doi.org/10.1016/j.expneurol.2004.08.037>
- Stieglitz, T., 2001. Flexible biomedical microdevices with double-sided electrode arrangements for neural applications. *Sensors Actuators, A Phys.* 90, 203–211. [https://doi.org/10.1016/S0924-4247\(01\)00520-9](https://doi.org/10.1016/S0924-4247(01)00520-9)
- Stieglitz, T., Beutel, H., Keller, R., Blau, C., Meyer, J.-U., 1997a. Development of flexible stimulation devices for a retina implant system, in: *Proceedings of the 19th Annual International Conference of the IEEE Engineering in Medicine and Biology Society*. IEEE, pp. 2307–2310. <https://doi.org/10.1109/IEMBS.1997.758825>
- Stieglitz, T., Beutel, H., Meyer, J.-U., 1997b. A flexible, light-weight multichannel sieve electrode with integrated cables for interfacing regenerating peripheral nerves. *Sensors Actuators A Phys.* 60, 240–243. [https://doi.org/10.1016/S0924-4247\(97\)01494-5](https://doi.org/10.1016/S0924-4247(97)01494-5)
- Stieglitz, T., Beutel, H., Schuettler, M., Meyer, J.-U., 2000. Micromachined, Polyimide-Based Devices for Flexible Neural Interfaces. *Biomed. Microdevices* 2, 283–294. <https://doi.org/10.1023/A:1009955222114>
- Sussman, E.M., Halpin, M.C., Muster, J., Moon, R.T., Ratner, B.D., 2014. Porous implants modulate healing and induce shifts in local macrophage polarization in the foreign body reaction. *Ann. Biomed. Eng.* 42, 1508–1516. <https://doi.org/10.1007/s10439-013-0933-0>
- Szarowski, D.H., Andersen, M.D., Retterer, S., Spence, A.J., Isaacson, M., Craighead, H.G., Turner, J.N., Shain, W., 2003. Brain responses to micro-machined silicon devices. *Brain Res.* 983, 23–35. [https://doi.org/10.1016/S0006-8993\(03\)03023-3](https://doi.org/10.1016/S0006-8993(03)03023-3)
- Takeuchi, S., Ziegler, D., Yoshida, Y., Mabuchi, K., Suzuki, T., 2005. Parylene flexible neural probes integrated with microfluidic channels. *Lab Chip* 5, 519–523. <https://doi.org/10.1039/b417497f>
- Tan, D., Schiefer, M.A., Keith, M.W., Anderson, J.R., Tyler, J., Tyler, D.J., 2014. A neural interface provides long-term stable natural touch perception. *Sci. Transl. Med.* 6, 257ra138–257ra138. <https://doi.org/10.1126/scitranslmed.3008669>
- Tan, D., Schiefer, M., Keith, M.W., Anderson, R., Tyler, D.J., 2013. Stability and selectivity of a chronic, multi-contact cuff electrode for sensory stimulation in a human amputee, in: *2013 6th International IEEE/EMBS Conference on Neural Engineering (NER)*. IEEE, pp. 859–862. <https://doi.org/10.1109/NER.2013.6696070>
- Tarique, A.A., Logan, J., Thomas, E., Holt, P.G., Sly, P.D., Fantino, E., 2015. Phenotypic, functional, and plasticity features of classical and alternatively activated human macrophages. *Am. J. Respir. Cell Mol. Biol.* 53, 676–688. <https://doi.org/10.1165/rcmb.2015-00120C>
- Tortora, G.J., Derrickson, B., 2014. *Principles of Anatomy & Physiology 14th Edition*, Wiley.
- Tyler, D.J., Durand, D.M., 2002. Functionally selective peripheral nerve stimulation with a flat

- interface nerve electrode. *IEEE Trans. Neural Syst. Rehabil. Eng.* 10, 294–303. <https://doi.org/10.1109/TNSRE.2002.806840>
- Tyler, D.J., Polasek, K.H., Schiefer, M.A., 2015. *Peripheral Nerve Interfaces, Nerves and Nerve Injuries*. Elsevier Ltd. <https://doi.org/10.1016/B978-0-12-802653-3.00112-3>
- Upshaw, B., Sinkjaer, T., 1998. Digital signal processing algorithms for the detection of afferent nerve activity recorded from cuff electrodes. *IEEE Trans. Rehabil. Eng.* 6, 172–181. <https://doi.org/10.1109/86.681183>
- Valente, E.G. a, Vernet, D., Ferrini, M.G., Qian, A., Rajfer, J., Gonzalez-Cadavid, N.F., 2003. L-Arginine and phosphodiesterase (PDE) inhibitors counteract fibrosis in the Peyronie's fibrotic plaque and related fibroblast cultures. *Nitric Oxide - Biol. Chem.* 9, 229–244. <https://doi.org/10.1016/j.niox.2003.12.002>
- Vass, K., Hickey, W.F., Schmidt, R.E., Lassmann, H., 1993. Bone marrow-derived elements in the peripheral nervous system. An immunohistochemical and ultrastructural investigation in chimeric rats. *Lab. Invest.* 69, 275–82.
- Weiseh, O., Doloff, J.C., Ma, M., Vegas, A.J., Tam, H.H., Bader, A.R., Li, J., Langan, E., Wyckoff, J., Loo, W.S., Jhunjhunwala, S., Chiu, A., Siebert, S., Tang, K., Hollister-Lock, J., Aresta-Dasilva, S., Bochenek, M., Mendoza-Elias, J., Wang, Y., Qi, M., Lavin, D.M., Chen, M., Dholakia, N., Thakrar, R., Lacić, I., Weir, G.C., Oberholzer, J., Greiner, D.L., Langer, R., Anderson, D.G., 2015. Size- and shape-dependent foreign body immune response to materials implanted in rodents and non-human primates. *Nat. Mater.* 14, 643–51. <https://doi.org/10.1038/nmat4290>
- Veraart, C., Grill, W., Mortimer, J.T., 1993. Selective stimulation of muscle activation with a multipolar nerve cuff electrode. *IEEE TBME.* 40, 640–653. [10.1109/10.237694](https://doi.org/10.1109/10.237694)
- Vince, V., Brelen, M.E., Delbeke, J., Colin, I.M., 2005. Anti-TNF α reduces the inflammatory reaction associated with cuff electrode implantation around the sciatic nerve. *J. Neuroimmunol.* 165, 121–128. <https://doi.org/10.1016/j.jneuroim.2005.04.019>
- Vroman, L., 1988. The life of an artificial device in contact with blood: initial events and their effect on its final state. *Bull. N. Y. Acad. Med.* 64, 352–357.
- Vroman, L., Adams, A., Fischer, G., Munoz, P., 1980. Interaction of high molecular weight kininogen, factor XII, and fibrinogen in plasma at interfaces. *Blood* 55.
- Vroman, L., Adams, A.L., Brakman, M., 1985. Lack of exchange among plasma proteins in narrow spaces on glass, demonstrated with metal oxide coatings. *Pathophysiol. Haemost. Thromb.* 15, 300–303. <https://doi.org/10.1159/000215163>
- Wang, P.H., Tsai, C.L., Wu, K.C., Shao, C.J., Kuo, L.C., Jou, I.M., 2015. Effects of Different Dosage of Dexamethasone on Behavioral, Electrophysiological, and Histomorphological Recovery in a Chronic Sciatic Nerve Compression Model. *Pain Med. (United States)* 16, 765–776. <https://doi.org/10.1111/pme.12680>
- Wang, W., Collinger, J.L., Degenhart, A.D., Tyler-Kabara, E.C., Schwartz, A.B., Moran, D.W., Weber, D.J., Wodlinger, B., Vinjamuri, R.K., Ashmore, R.C., Kelly, J.W., Boninger, M.L., 2013. An Electrographic Brain Interface in an Individual with Tetraplegia. *PLoS One* 8, 1–8. <https://doi.org/10.1371/journal.pone.0055344>
- Ward, K., 2008. A review of the foreign-body response to subcutaneously-implanted devices: the role of macrophages and cytokines in biofouling and fibrosis. *J. Diabetes Sci. Technol.* 2, 768–77. <https://doi.org/10.1177/193229680800200504>
- Wark, H.A.C., Mathews, K.S., Normann, R.A., Fernandez, E., 2014. Behavioral and cellular consequences of high-electrode count Utah Arrays chronically implanted in rat sciatic nerve. *J. Neural Eng.* 11, 46027. <https://doi.org/10.1088/1741-2560/11/4/046027>

- Warwick, K., Gasson, M., Hutt, B., Goodhew, I., Kyberd, P., Andrews, B., Teddy, P., Shad, A., 2003. The application of implant technology for cybernetic systems. *Arch. Neurol.* 60, 1369–1373. <https://doi.org/10.1001/archneur.60.10.1369>
- Weyhe, D., Cobb, W., Lecuivre, J., Alves, A., Ladet, S., Lomanto, D., Bayon, Y., 2015. Large pore size and controlled mesh elongation are relevant predictors for mesh integration quality and low shrinkage? Systematic analysis of key parameters of meshes in a novel minipig hernia model. *Int. J. Surg.* 22, 46–53. <https://doi.org/10.1016/j.ijisu.2015.07.717>
- Willerth, S.M., Sakiyama-Elbert, S.E., 2007. Approaches to neural tissue engineering using scaffolds for drug delivery. *Adv. Drug Deliv. Rev.* <https://doi.org/10.1016/j.addr.2007.03.014>
- Williams, D.F., 2008. On the mechanisms of biocompatibility. *Biomaterials* 29, 2941–2953. <https://doi.org/10.1016/j.biomaterials.2008.04.023>
- Williams, D.F., 1987. Definitions in biomaterials: proceedings of a consensus conference of the European Society for Biomaterials, Definitions in biomaterials: proceedings of a consensus conference of the European Society for Biomaterials.
- Winslow, B.D., Christensen, M.B., Yang, W.K., Solzbacher, F., Tresco, P.A., 2010. A comparison of the tissue response to chronically implanted Parylene-C-coated and uncoated planar silicon microelectrode arrays in rat cortex. *Biomaterials* 31, 9163–9172. <https://doi.org/10.1016/j.biomaterials.2010.05.050>
- Wurth, S., Capogrosso, M., Raspopovic, S., Gandar, J., Federici, G., Kinany, N., Cutrone, A., Piersigilli, A., Pavlova, N., Quiet, R., Taverni, G., Rigosa, J., Shkorbatova, P., Navarro, X., Barraud, Q., Courtine, G., Micera, S., 2017. Long-term usability and bio-integration of polyimide-based intra-neural stimulating electrodes. *Biomaterials* 122, 114–129. <https://doi.org/10.1016/j.biomaterials.2017.01.014>
- Wynn, T. a, 2013. Mechanism of fibrosis: therapeutic translation for fibrotic disease. *Nat. Med.* 18, 1028–1040. <https://doi.org/10.1038/nm.2807.Mechanisms>
- Xie, Y., Martini, N., Hassler, C., Kirch, R.D., Stieglitz, T., Seifert, A., Hofmann, U.G., 2014. In vivo monitoring of glial scar proliferation on chronically implanted neural electrodes by fiber optical coherence tomography. *Front. Neuroeng.* 7, 34. <https://doi.org/10.3389/fneng.2014.00034>
- Yao, G.L., Kiyama, H., 1995. Dexamethasone enhances level of GAP-43 mRNA after nerve injury and facilitates re-projection of the hypoglossal nerve. *Mol. Brain Res.* 32, 308–312. [https://doi.org/10.1016/0169-328X\(95\)00091-6](https://doi.org/10.1016/0169-328X(95)00091-6)
- Yoshida, K., Jovanović, K., Stein, R.B., 2000. Intrafascicular electrodes for stimulation and recording from mudpuppy spinal roots. *J. Neurosci. Methods* 96, 47–55. [https://doi.org/10.1016/S0165-0270\(99\)00176-4](https://doi.org/10.1016/S0165-0270(99)00176-4)
- Young, A.T., Cornwell, N., Daniele, M.A., 2017. Neuro-Nano Interfaces: Utilizing Nano-Coatings and Nanoparticles to Enable Next-Generation Electrophysiological Recording, Neural Stimulation, and Biochemical Modulation. *Adv. Funct. Mater.* 1700239. <https://doi.org/10.1002/adfm.201700239>
- Yuan, Y., Chesnutt, B.M., Wright, L., Haggard, W.O., Bumgardner, J.D., 2008. Mechanical property, degradation rate, and bone cell growth of chitosan coated titanium influenced by degree of deacetylation of chitosan. *J. Biomed. Mater. Res. Part B Appl. Biomater.* 86B, 245–252. <https://doi.org/10.1002/jbm.b.31012>
- Zecca, M., Micera, S., Carrozza, M.C., Dario, P., 2002. Control of multifunctional prosthetic hands by processing the electromyographic signal. *Crit. Rev. Biomed. Eng.* 30, 459–85.
- Zhang, J., Wang, J., Wei, Y., Gao, C., Chen, X., Kong, W., Kong, D., Zhao, Q., 2016. ECM-mimetic heparin glycosaminoglycan-functionalized surface favors constructing functional vascular smooth muscle tissue in vitro. *Colloids Surfaces B Biointerfaces* 146, 280–288.

<https://doi.org/10.1016/j.colsurfb.2016.06.023>

Zhong, C., Ke, D., Wang, L., Lu, Y., Wang, L., 2017. Bioactive interpenetrating polymer networks for improving the electrode/neural-tissue interface. *Electrochem. commun.* 79, 59–62. <https://doi.org/10.1016/j.elecom.2017.04.015>

Zhong, Y., Bellamkonda, R. V, 2007. Dexamethasone-coated neural probes elicit attenuated inflammatory response and neuronal loss compared to uncoated neural probes. *Brain Res.* 1148, 15–27. <https://doi.org/10.1016/j.brainres.2007.02.024>

Zuo, K.J., Olson, J.L., 2014. The evolution of functional hand replacement: From iron prostheses to hand transplantation. *Can. J. Plast. Surg.* 22, 44–51.

ANNEX

Published manuscripts from the work of this thesis:

Peer reviewed publications

Chapter 1: Mueller M, de la Oliva N, del Valle J, Delgado-Martinez I, Navarro X, Stieglitz T. 2017. **Rapid prototyping of flexible intrafascicular electrode arrays by picosecond laser structuring.** Journal of Neural Engineering 14 066016.

Chapter 2: de la Oliva N, Navarro X, del Valle J. 2017. **Time course study of long-term biocompatibility and foreign body reaction to intraneural polyimide-based implants.** Journal of Biomedical Materials Research Part A doi: 10.1002/jbm.a.36274.

Under revision

Chapter 3: de la Oliva N, Navarro X, del Valle J. **Dexamethasone reduces the foreign body reaction to intraneural electrode implants in the peripheral nerve of the rat.** The Anatomical Record.

In preparation

Chapter 2: de la Oliva N, Mueller M, Stieglitz T, Navarro X, del Valle J. **On the use of Parylene C polymer as substrate for peripheral nerve electrodes.**

Chapter 4: de la Oliva N, del Valle J, Delgado-Martinez I, Navarro X. **Dexamethasone improves long-term function of transversal intraneural electrodes**

Time course study of long-term biocompatibility and foreign body reaction to intraneural polyimide-based implants

Natalia de la Oliva ¹, Xavier Navarro ¹, Jaume del Valle ^{1,2}

¹Department of Cell Biology, Physiology and Immunology, Universitat Autònoma de Barcelona, and Centro de Investigaci^on Biomèdica en Red en Enfermedades Neurodegenerativas (CIBERNED), Institute of Neurosciences, Bellaterra, 08193 Barcelona, Spain

²Catalan Institute of Nanoscience and Nanotechnology (ICN2), CSIC and BIST, Campus UAB, Bellaterra, 08193 Barcelona, Spain

Received 24 May 2017; revised 6 October 2017; accepted 17 October 2017

Published online 00 Month 2017 in Wiley Online Library (wileyonlinelibrary.com). DOI: 10.1002/jbm.a.36274

Abstract: The foreign body reaction (FBR) against an implanted device is characterized by the formation of a fibrotic tissue around the implant. In the case of interfaces for peripheral nerves, used to stimulate specific group of axons and to record different nerve signals, the FBR induces a matrix deposition around the implant creating a physical separation between nerve fibers and the interface that may reduce its functionality over time. In order to understand how the FBR to intraneural interfaces evolves, polyimide non-functional devices were implanted in rat peripheral nerve. Functional tests (electrophysiological, pain and locomotion) and histological evaluation demonstrated that implanted devices did not cause any alteration in nerve function, in myelinated axons or in nerve architecture. The inflammatory response due to the surgical implantation decreased after 2 weeks. In contrast, inflammation was higher and more prolonged in the device implanted nerves with a

peak after 2 weeks. With regard to tissue deposition, a tissue capsule appeared soon around the devices, acquiring maximal thickness at 2 weeks and being remodeled subsequently. Immunohistochemical analysis revealed two different cell types implicated in the FBR in the nerve: macrophages as the first cells in contact with the interface and fibroblasts that appear later at the edge of the capsule. Our results describe how the FBR against a polyimide implant in the peripheral nerve occurs and which are the main cellular players. Increasing knowledge of these responses will help to improve strategies to decrease the FBR against intraneural implants and to extend their usability. © 2017 Wiley Periodicals, Inc. *J Biomed Mater Res Part A*: 00B:000–000, 2017.

Key Words: foreign body reaction, peripheral nerve interface, biocompatibility, polyimide, nerve electrode

How to cite this article: de la Oliva N, Navarro X, del Valle J. 2017. Time course study of long-term biocompatibility and foreign body reaction to intraneural polyimide-based implants. *J Biomed Mater Res Part A* 2017;00A:000–000.

INTRODUCTION

Neuroprostheses aimed to restore the loss of motor and sensory function after a limb amputation try to link the peripheral nervous system with electromechanical prostheses by means of neural electrodes. Advanced neuroprostheses rely on the capability to interface specific groups of nerve fibers within the nerve for obtaining different motor signals and for stimulating selective populations of sensory afferents. Some authors consider intraneural electrodes as the most adequate type, as they allow for higher selectivity of recording and stimulation, lower intensity for stimulation and increased signal-to-noise ratio of recordings compared with extraneural electrodes.^{1–3} Several intraneural electrodes, such as multielectrode arrays,^{4–8} longitudinal

(LIFE),^{9,10} and transversal (TIME)^{11,12} intrafascicular electrodes have shown good performance for the bidirectional interface with the peripheral nerve. Intraneural electrodes should remain within the nerve for months or years and be able to record high quality motor nerve signals and to selectively stimulate small groups of afferent axons to evoke sensory activity for a successful performance over time.^{13–16} Consequently, they have to show good biocompatibility and stability.

However, during chronic implantations made in human subjects, it has been observed a reduction in the functionality of electrode active sites^{14,17} or an increase in the threshold needed for stimulation¹⁵ along time, thus limiting the prospective use of intraneural electrodes. Such failures could be attributed to electromechanical erosion of the

Additional Supporting Information may be found in the online version of this article.

Correspondence to: J. del Valle; e-mail: jaume.delvalle@uab.cat

Contract grant sponsor: Seventh Framework Programme FPT-ICT project NEBIAS; contract grant number: 611687

Contract grant sponsor: CIBERNED; contract grant number: CB06/05/1105

Contract grant sponsor: TERCEL; contract grant number: RD12/0019/0011

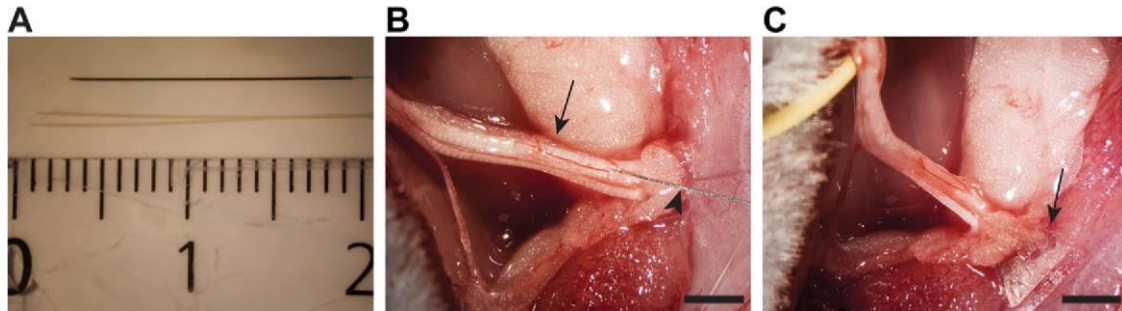
Contract grant sponsor: European Regional Development Funds (ERDF)

Contract grant sponsor: Severo Ochoa programme of the Spanish Ministry of Economy, Industry and Competitiveness (MINECO; contract grant number: SEV-2013-0295 v-

© 2017 WILEY PERIODICALS, INC.

FIGURE 1. Surgical procedure. (A) Photograph of the LIFE device implanted (bottom) and the implantation needle used (top). (B) Needle used for the implantation piercing (arrowhead) the sciatic nerve (arrow) of a rat. (C) Device implanted (arrow points to the triangle base) in the sciatic nerve. Scale bar in (B–C) 51 mm.

metal sites, fatigue of the connections, changes in conductivity, cell death and to the biological response of the nerve tissue against the electrode implant. Regarding the latter, experimental studies



have reported that the implanted electrode becomes encapsulated by host cells, creating a separation between the electrode and the nerve fibers to be interfaced.^{10,11,18,19}

The foreign body reaction (FBR) is the first response of the nonspecific immune system against an implanted device. It is characterized by a primarily inflammatory phase triggered by macrophages and leukocytes, that is followed by a fibrotic phase in which fibroblasts are responsible for the formation of a fibrotic tissue around the implant.²⁰ Despite the FBR has been widely studied and the progression of this response is well known in subcutaneous,^{21–23} peritoneal,^{24,25} and even central nervous system implants,^{26–28} few studies have focused on the peripheral nervous system^{29–32} and a detailed description of the long-term response against implanted interfaces in peripheral nerves and its time-course is still needed. In order to characterize the cellular processes participating in the FBR to an intraneural electrode, which may allow to identify new targets to modulate this response and enhance the interface functionality, we have studied from 1 day to 8 months the progression of the FBR to LIFE nerve implants made of polyimide, a material widely used in the fabrication of peripheral nerve interfaces,^{10,12,19,33} in the rat sciatic nerve.

MATERIALS AND METHODS

Animals and surgical procedures

Female Sprague-Dawley rats weighing 250–300 g were used (n5 6–8/group). All surgeries were performed under ketamine and xylazine anesthesia (90/10 mg/kg i.p.). The sciatic nerve was surgically exposed at the mid thigh and carefully freed from adherences to surrounding tissues. Passive devices of polyimide 20 mm long, 200 μm wide, and 10 μm thick [Fig. 1(A)] were inserted longitudinally in the tibial branch of the sciatic nerve with the help of a straight needle attached to a 10–0 loop thread (STC-6, Ethicon). The thread is passed between the two arms of the device and pulls the arrow-shaped center of the electrode strip [Fig. 1(B,C)], as previously described for the insertion of LIFE.¹⁰ Longitudinal implant was chosen because of its better reproducibility in comparison with TIME implant and to better study only the FBR inside the nerve. A group of animals underwent a sham operation with the same surgical procedures but the device was implanted and instantly removed leaving no implant inside the nerve. Moreover, a group of intact animals was included for reference of normal nerves (Supporting Information Fig. S1).

Adequate measures were taken to reduce the number of animals used and to minimize pain and animal discomfort during surgery and in the postoperative follow-up. After surgeries animals were left to recover under a warm environment and were housed at 22 ± 0.28°C under a 12:12 h light cycle with food and water access ad libitum. All experimental procedures performed were approved by the Ethical Committee of the Universitat Autònoma de Barcelona in accordance with the European Communities Council Directive 2010/63/EU.

After 1, 2, 4 days and 2, 4, 8, 16, and 32 weeks postimplant, animals were deeply anesthetized with an overdose of pentobarbital, injected intracardially with 1000 UI of heparin per kg body weight and perfused transcardially with 4% PFA in phosphate buffer (PB). After the perfusion, the sciatic nerve segment including the implant was collected and kept in 30% sucrose in PB for immunohistochemistry, in 70% ethanol for paraffin embedding or in 3% glutaraldehyde–3% paraformaldehyde in PB for light and electron microscopy.

Functional evaluation

The functional properties of the nerves that had been implanted were evaluated by means of nerve conduction, algometry, and locomotion tests over time after the implant. Nerve conduction test was performed by stimulating the sciatic nerve proximally with single electrical pulses and recording the compound muscle action potentials (CMAPs) of the gastrocnemius medialis muscle as previously described in.¹⁹ The nociceptive threshold to mechanical stimuli was evaluated by means of an electronic Von Frey algometer (Bioseb, Chaville, France) following the same protocol described before.³⁴ Rats were placed on a wire net platform in plastic chambers, and a metal tip applied to the sole of the hind paw until the rat withdrew the paw in response to the stimulus. The walking track test was performed to assess locomotor function

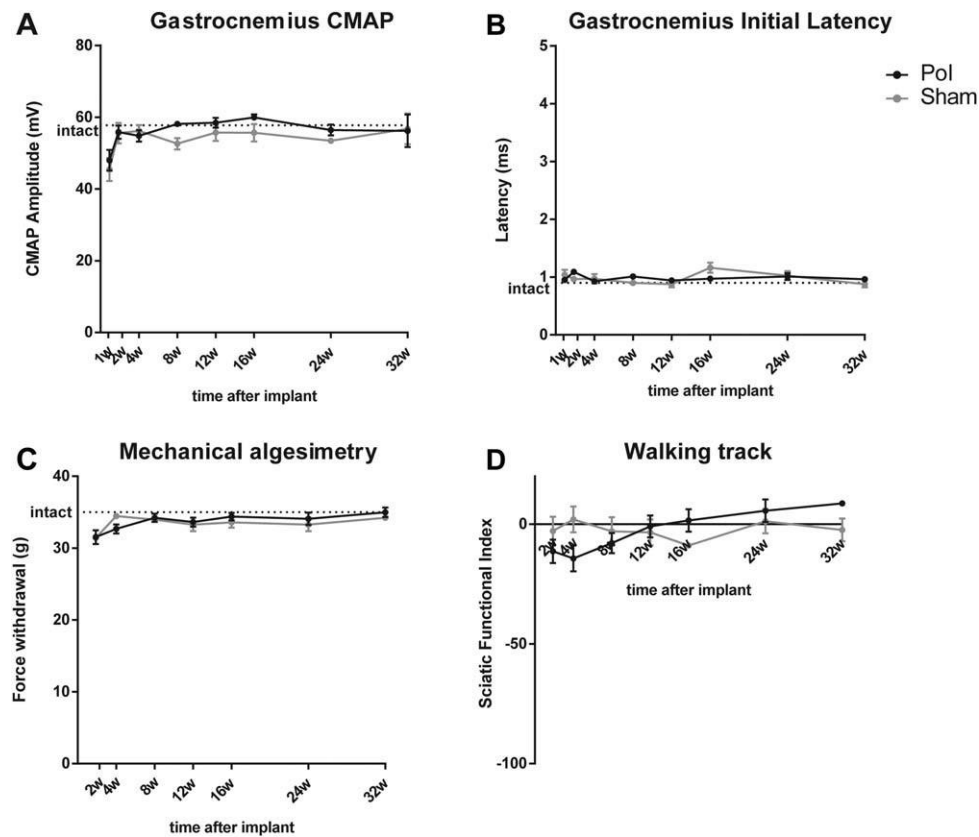


FIGURE 2. Functional evaluation of implanted nerves. No alterations were found in the (A) amplitude and (B) initial latency of the gastrocnemius CMAP of implanted and sham animals. (C) Pain threshold assessed by Von Frey mechanical algesimetry in the hind paw. (D) SFI of sham and implanted animals. Dotted lines indicate values from intact animals.

after the implant. The plantar surface of the hind paws was painted with black ink and the rat was left to walk along a corridor. The print length, the distance between the first and fifth toes and between the second and fourth toes were measured to calculate the Sciatic Functional Index (SFI).³⁵

Morphological evaluation

In order to evaluate the microstructure of the implanted nerves and the myelinated nerve fibers, segments fixed in 3% glutaraldehyde-3% paraformaldehyde were postfixed in 2% OsO₄ for 2 h, dehydrated through ethanol series and embedded in epon resin. Semithin sections (0.5 mm thick) were stained with toluidine blue and examined by light microscopy. The number of myelinated fibers in the implanted tibial nerve was counted in images taken at 100x chosen by systematic random sampling of squares representing at least 30% of the nerve cross-sectional area. The cross-sectional area of the whole sciatic nerve was measured at 43 with a microscope BX51 (Olympus) and a DP73 digital camera (Olympus) and the total number of myelinated fibers estimated. The thickness of the deposited tissue around the implant was measured as the distance between each side of the device and the closest myelinated axon, using ImageJ software.³⁶

Transmission electron microscopy (TEM) was used to evaluate the ultrastructure of the tissue and collagen deposition

around the polyimide device in transverse nerve sections. Ultrathin sections of the entire nerve were cut, mounted on formvar 200 mesh copper grids and contrasted with uranyl acetate/lead citrate. A TEM microscope (JEM 1400) was used to take pictures of the area with the implanted device, to analyze the encapsulating tissue and the surrounding nerve fibers at different time points.

Immunohistochemistry

Nerve segments containing the implanted polyimide device were serially cut into 15 mm thick sections in 10 slides with 12 slices each with a cryostat (Leica CM190, Leica Microsystems). Nerve sections were blocked with normal donkey serum and incubated overnight at 48C with primary antibodies rabbit anti-iba1 (Wako, 191947, 1:500) and mouse anti-CD-68 clone ED1 (Abcam, ab31630, 1:500) for macrophages and mouse anti-CD90 clone OX-7 (BD Pharmingen, 554897, 1:150) for fibroblasts. Slides were then washed with 0.1% Tween 20 buffer solution and incubated with AlexaFluor 594 donkey anti-rabbit (Invitrogen, A21207, 1:200) and 488 donkey anti-mouse (Invitrogen, A21202, 1:200) secondary antibodies for 1 h at room temperature. Finally, sections were mounted with mowiol containing DAPI (0.1 lg/mL, Sigma).

To quantify the amount of infiltrating macrophages, images of the whole tibial nerve with iba1 or ED1 immunostaining were

analyses were conducted by using GraphPad Prism software. Statistical significance was considered when $p < 0.05$.

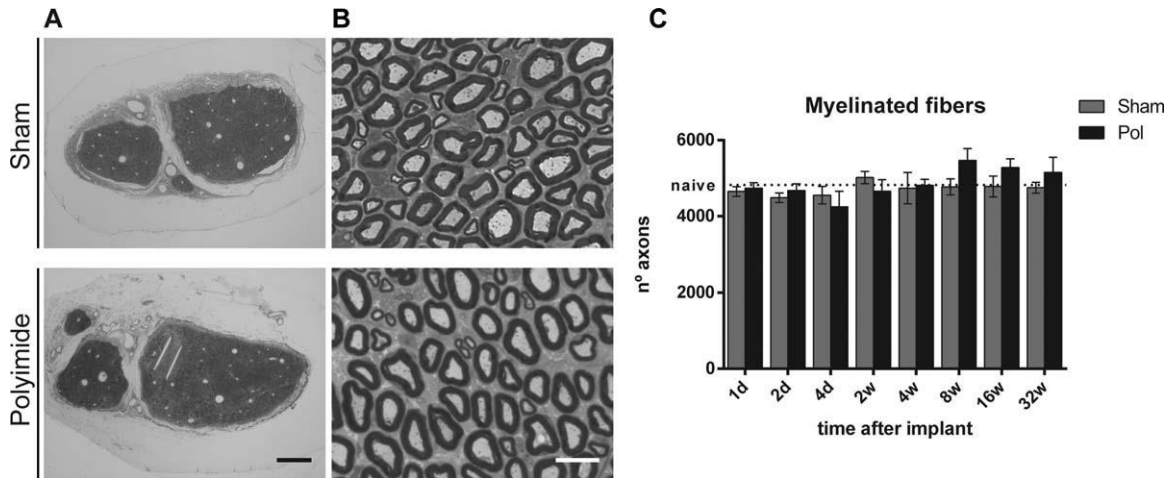


FIGURE 3. Histological evaluation of implanted nerves. (A) Low and (B) high magnification images of semithin sections of sham (top) and implanted (bottom) nerves after 2 weeks of surgery. (C) Quantification of myelinated fibers in sham and implanted nerves. The dotted line indicates the mean number of intact tibial nerves. Scale bar in (A) 5200 μm and (B) 510 μm .

taken with an epifluorescence microscope (BX51, Olympus) attached to a digital camera (DP73, Olympus) and equally treated to adjust brightness and contrast. Then, the background was subtracted and a threshold of detection and binarization was applied. Iba1 or ED1 positive cells were counted in the whole area of the tibial nerve, excluding the implant device and the tissue capsule using the command “Analyze Particles” of ImageJ.

Paraffin embedding and hematoxylin-eosin staining

To determine the amount of foreign body giant cells (FBGCs) around the implant, nerve segments containing the implanted device were dehydrated with increasing ethanol series, followed by increasing xylene series and finally embedded in paraffin. Then, 5 mm thick serial sections were cut with a microtome (Leica RM 2255). To study FBGCs, slides were deparaffinized using two xylene rinses of 15 min each and rehydrated with decreasing ethanol series and 5 min in water. Then, slides were immersed in hematoxylin Harris solution (Fluka, Sigma) for 7 min and washed in water followed by 1% HCl in ethanol solution for 20 s. Finally, sections were washed again with water and stained with Eosin Y (Merck Millipore) for 5 min. Sections were dehydrated with series of graded ethanol rinses and mounted with DPX (Sigma). Then, the number of FBGCs was counted under the microscope in each stained section and expressed as FBGCs per mm of implant length. Moreover, pictures of every FBGC were taken and the diameter was measured with ImageJ.

Statistical analysis

Results are expressed as mean \pm SEM. Means were compared with one or two-way ANOVA followed by Bonferroni post hoc test for differences between groups or times. To quantify the linear relationship between two variables, the Pearson’s correlation coefficient and the p values of the Fisher test were calculated. All

RESULTS

Longitudinal neural implants do not cause functional damage in the implanted nerves

Functional studies performed over time (from week 1 up to month 8) postimplant did not show any changes in nerve conduction, pain thresholds or locomotion (Fig. 2). Histological evaluation of polyimide implanted nerves revealed that all the implanted devices were placed within the tibial nerve [Fig. 3(A)]. Light microscopy observations showed normal fascicular architecture and axonal morphology of both implanted and sham implanted nerves, similar to intact sciatic nerves [Fig. 3(A,B)] and the number of myelinated fibers showed no differences between groups [Fig. 3(C)]. Moreover, no obvious signs of axonal degeneration or demyelination due to the surgery or the implanted device within the nerve were found, indicating that the implant model used was useful to assess the FBR to the polyimide device, without confounding factors that might be due to tissue damage.

Nerve response and tissue capsule formation

The tissue encapsulation around the polyimide implant was evaluated under light microscopy. Whereas in the sham nerves there was no evidence of wound or tissue aggregation at any time point [Fig. 4(B)], the surrounding of the implant was rapidly modified in the device implanted nerves [Fig. 4(A)]. The thickness of the tissue encapsulation around the implant showed a gradual increase from 2 days to 2 weeks post-implant when it reached its maximum, and a slight decrease and compaction thereafter [Fig. 4(C)].

Detailed analysis of the encapsulating tissue under light and TEM showed several changes in the surroundings of the device. Thus, at day one only some erythrocytes could be seen near the implant and axons were still in close contact with the polyimide. After 4 days, some amoeboid cells had already arrived at the

vicinity of the polyimide device [Fig. 5(A)] and started to organize creating a small gap between the implant and the axons. At 2 and 4 weeks post-

and organization of new collagenous fibrils that progressively filled the area formerly occupied by spindle-shaped and ameboid cells [Fig. 5(D–F) and insets].

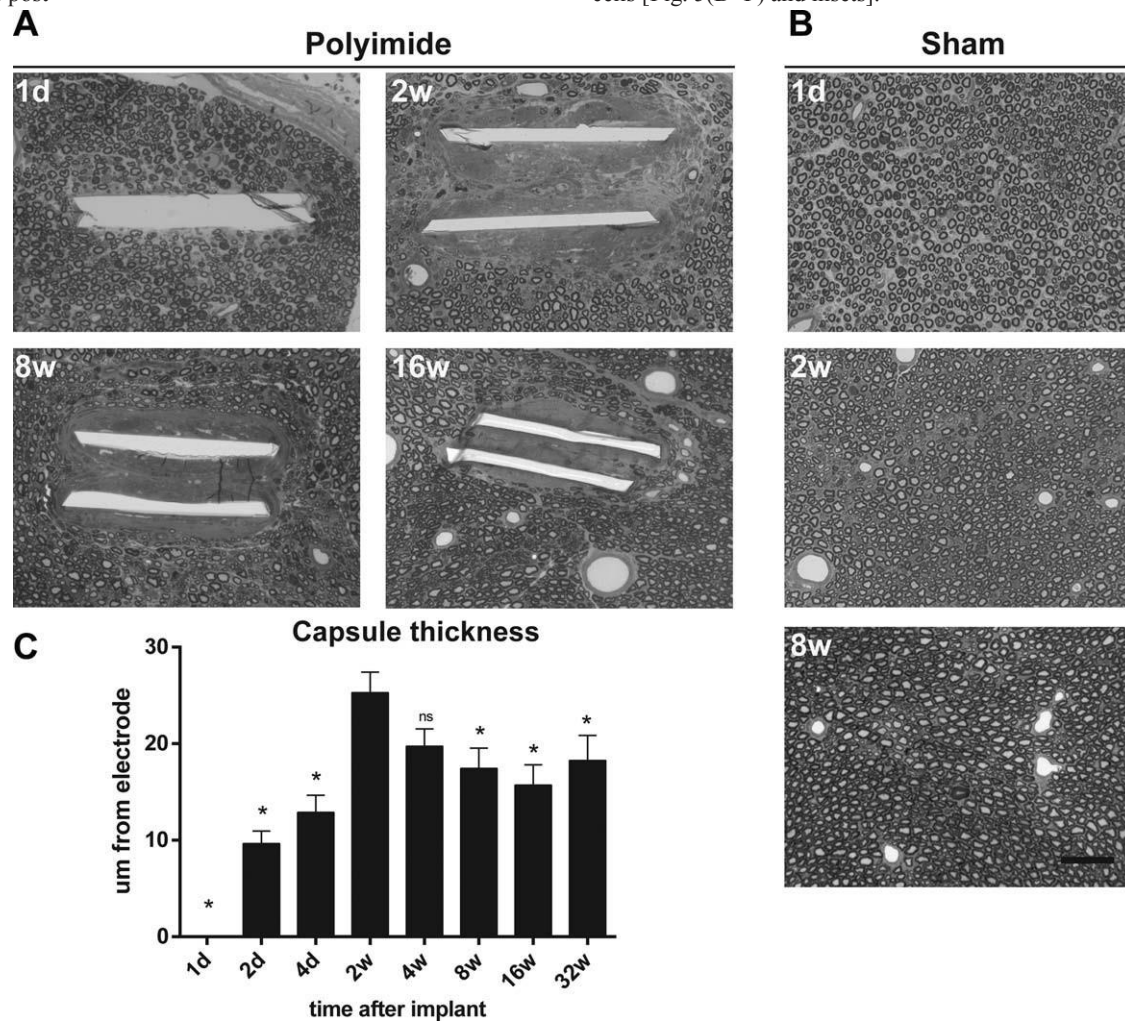


FIGURE 4. Histological progression of capsule tissue around the implants. (A) Representative images of time progression of the capsule around polyimide implants. (B) No signs of tissue aggregation can be observed in sham nerves. (C) Measurements of capsule thickness along time.

* $p < 0.05$ versus 2 weeks. Scale bar 550 μm .

implant, the capsule that separated the axons and the polyimide implant appeared as a more compacted tissue containing mainly ameboid-shaped cells and the characteristic collagen organization of the endoneurium was not distinguished in the surroundings of the implant [Fig. 5(B,D)]. At 8 weeks, two zones could be differentiated in the encapsulating tissue, with an inner area stocked with ameboid cells as in the previous time points, and an outer region composed of layers of parallel spindle-shaped cells [Fig. 5(C,E)]. Although this disposition was very similar after 16 weeks, the presence of ameboid cells seemed to slightly decline, but it was at 32 weeks post-implant that only spindle-shape cells were seen in the capsule [Fig. 5(F)] with no presence of ameboid cells. Moreover, these changes in the cellular type from 8 to 32 weeks also correlated with a progressive organization of the extracellular matrix of the capsule, with an increased deposition

Cellular characterization of the FBR

To evaluate the inflammatory response due to the surgery or the implant, we assessed the presence of Iba1 labeled macrophages in the whole tibial nerve. Whereas in intact nerves a few macrophages were seen (Supporting Information Fig. S1), the number of Iba1 positive macrophages started to increase within the implanted nerves one day after surgery both in polyimide device and in sham groups [Fig. 6(A,B)]. The inflammatory response caused solely by the surgery, evaluated in sham rats with no implants left within the nerve, peaked at 4 days and decreased noticeably at 2 and 4 weeks, reaching similar values than intact animals from week 8 onwards [Fig. 6(C)]. In contrast, the inflammatory reaction due to the implanted device peaked at 2 weeks and took more time to resolve, with a slight decrease at 4 weeks that persisted 8 weeks after the implant. Finally, at week 16 and 32, the number of macrophages showed a further decrease but with still significantly more Iba1⁺ cells than sham and intact

animals [Fig. 6(C)]. To characterize these infiltrating macrophages, the amount

reported.³⁷ However, the evolution of ED1⁺ cells was very similar to that of Iba1⁺ cells [Fig. 7(B)], with a peak at 2 weeks after the

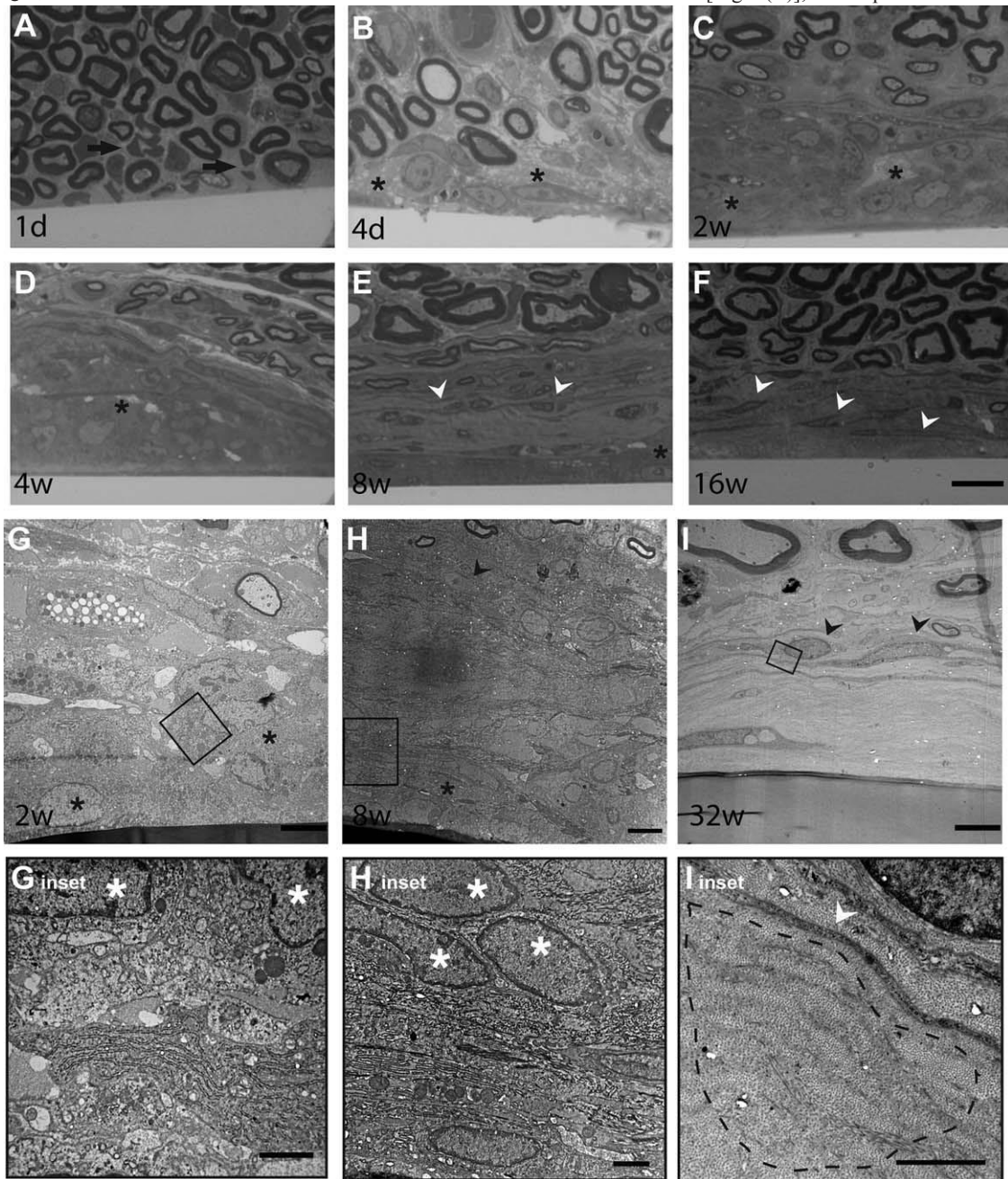


FIGURE 5. Tissue capsule development around the implant (bottom). Images of semithin sections showing changes in the capsule. At (A) day 1, erythrocytes (arrow) can be seen near the implant. After 4 days, 2, and 4 weeks (B–D) ameboid cells (asterisks) are forming the capsule. After 8 and 16 weeks (E,F), the capsule is already compacted and spindle-shape cells (arrowheads) are seen within. (G–I) Representative TEM images taken at different time points showing the ameboid-shaped cells (asterisks) in the inner zone of the capsule at 2 weeks and the spindle-shaped cells (arrowheads) in the outer zone at 8 and 32 weeks. Insets of G–I show high-magnification view of changes at 2 (I inset), 8 (H inset) and 32 weeks (I inset). A lenticular collagen fibril architecture of the extracellular matrix (dotted line area) is defined at 32 weeks. Scale bar 510 nm (A–F), 5 nm (G–I), 2 nm (insets).

of macrophages that presented positivity for the CD-68 ED1 antigen [Fig. 7(A)] was quantified. As expected, all the CD68⁺ cells were also stained with the Iba1 antibody, while several Iba1⁺ macrophages did not express the ED1 antigen as previously

reported. Hence, the amount of CD-68⁺ and Iba1⁺ cells maintained a ratio of 1:3 (SEM 0.26), following a significant positive relationship [Fig. 7(C)].

To further investigate how the tissue capsule is formed around the implant, we focused on the two main cell populations involved in the FBR process: macrophages and fibroblasts.³⁸ In the host

fusion appeared soon after the polyimide device implantation and its number increased over time [Fig. 9(A,B)]. The FBGCs seen in this model had many nuclei mainly in the cellular periphery,³⁹ as

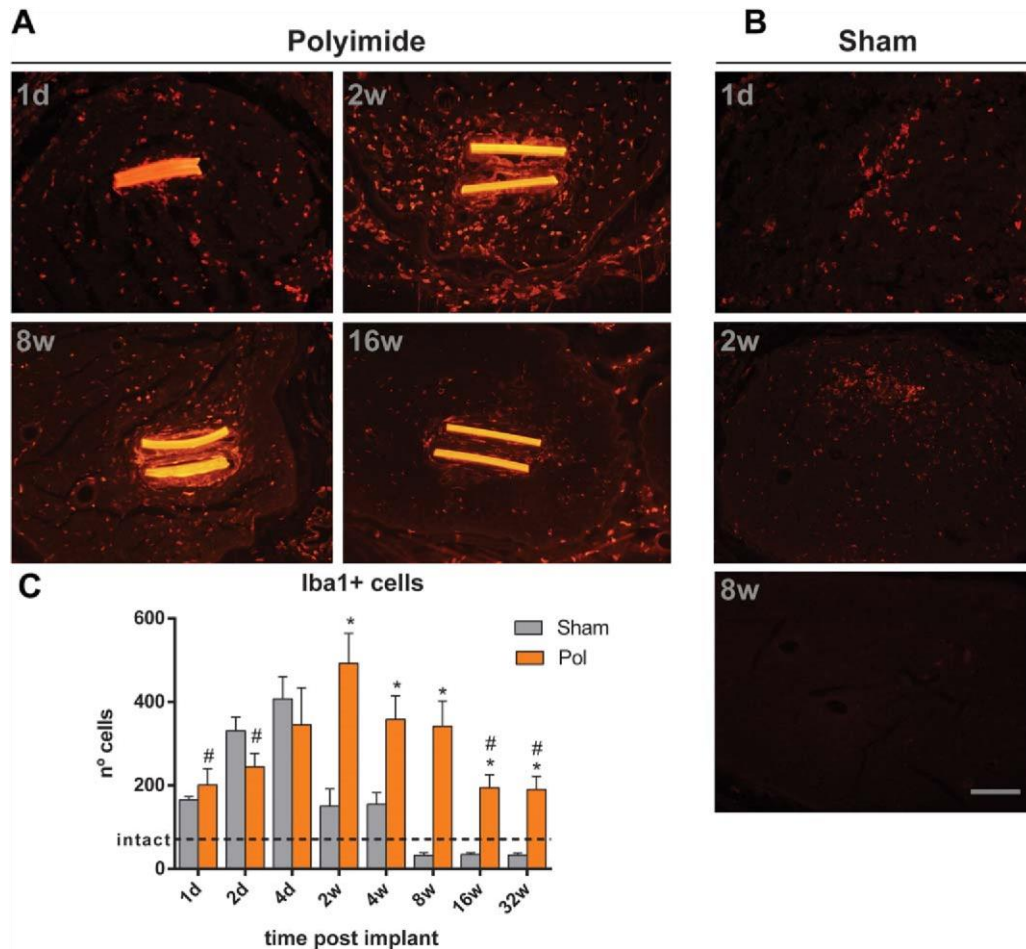


FIGURE 6. Inflammatory cells in the implanted nerves. Representative images of macrophages labeled with Iba1 at different times points in (A) implanted and (B) sham nerves. (C) Quantification of the number of Iba1 positive cells along time in implanted and sham animals. Dotted line indicates the mean of intact nerves. * $p < 0.05$ vs. sham. # $p < 0.05$ versus 2 weeks. Scale bar 5100 nm.

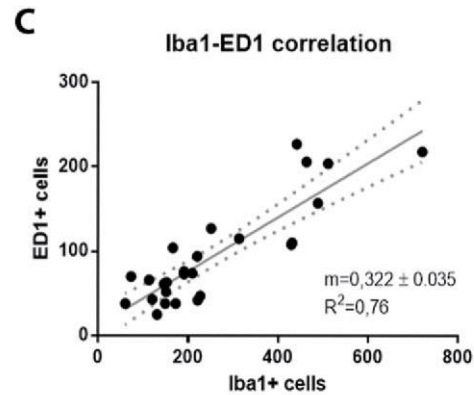
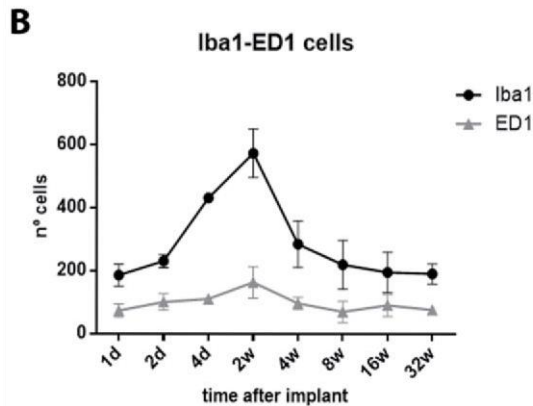
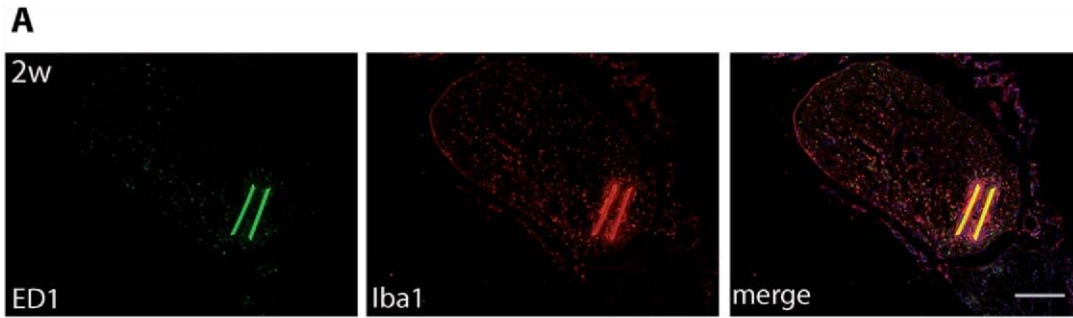
response in the implanted peripheral nerves, macrophages were the first cells to arrive [Fig. 8(A)] and rapidly surround the device from day 2–4 up to 4 weeks after implant [Fig. 8(B–E)]. Indeed, after 2 and 4 weeks, the capsule around the device was mainly formed by compacted macrophagic cells expressing Iba1 in close contact with the device, in a similar disposition of the round-shape cells observed by TEM in Figure 4. By week 8, some CD90⁺ fibroblasts started to appear in the edge of the capsule, between the inner macrophage layer and the surrounding nerve fibers [Fig. 8(F)], confirming the observations under light and electron microscopy. After 16 weeks, although the number of cells in the capsule decreased, Iba1⁺ macrophages were still in contact with the device and CD90⁺ fibroblasts were in the outer layer of the capsule, in contact with nerve fibers [Fig. 8(G)]. After 32 weeks of implant, most cells in the capsule were CD90⁺ fibroblasts within a well-organized extracellular matrix [Fig. 8(H)].

Finally, the amount and size of FBGCs were also measured as another hallmark of FBR. These cells resulting from macrophage

expected with the presence of foreign bodies. By week 2 these cells were easily recognizable around the implant, becoming stabilized in number and size [Fig. 9(B,C)] up to 8 weeks. From week 16 onwards, the amount of these cells started to decline concomitantly with the emergence of fibroblasts and the decline of macrophages both in the nerve and the capsule. On the other hand, the diameter of these cells increased progressively from the first day up to week 2. From 2 up to 16 weeks post-implant the size of the FBGCs remained stable and it was slightly increased at 32 weeks.

DISCUSSION

After the implant of any biomaterial in the body, acute and chronic cellular and tissue responses occur.^{20,40} These events include inflammatory response, FBR, and fibrous encapsulation of the implanted device.^{41,42} The peripheral nervous system is not an exception¹⁰ and it is a serious problem when the active sites of



implanted intraneural interfaces have to be in intimate contact with nerve fibers to have a proper functionality. Although many studies have

FIGURE 7. ED1-Iba1 macrophage staining over time. (A) Representative images of ED1 (green) and Iba1 (red) labeling after 2 weeks of implant; cell nuclei can be seen in blue by DAPI staining. (B) Quantification of the number of ED1 positive cells and Iba1 positive cells over time. (C) Correlation between number of ED1 and Iba1 positive cells. The solid gray line represents the linear regression (slope significantly different from zero, $p < 0.001$), while the dotted line represents the 95% CI. Scale bar 5200 nm.

reported good results regarding stimulation and recording of the interface has been reported.¹⁴ The encapsulating tissue of nerve signals in short-term studies, a progressive loss of use reduces the amplitude of recordable axonal impulses function of intraneural electrodes that reduce the useful life and increases the intensity needed for axonal excitation due

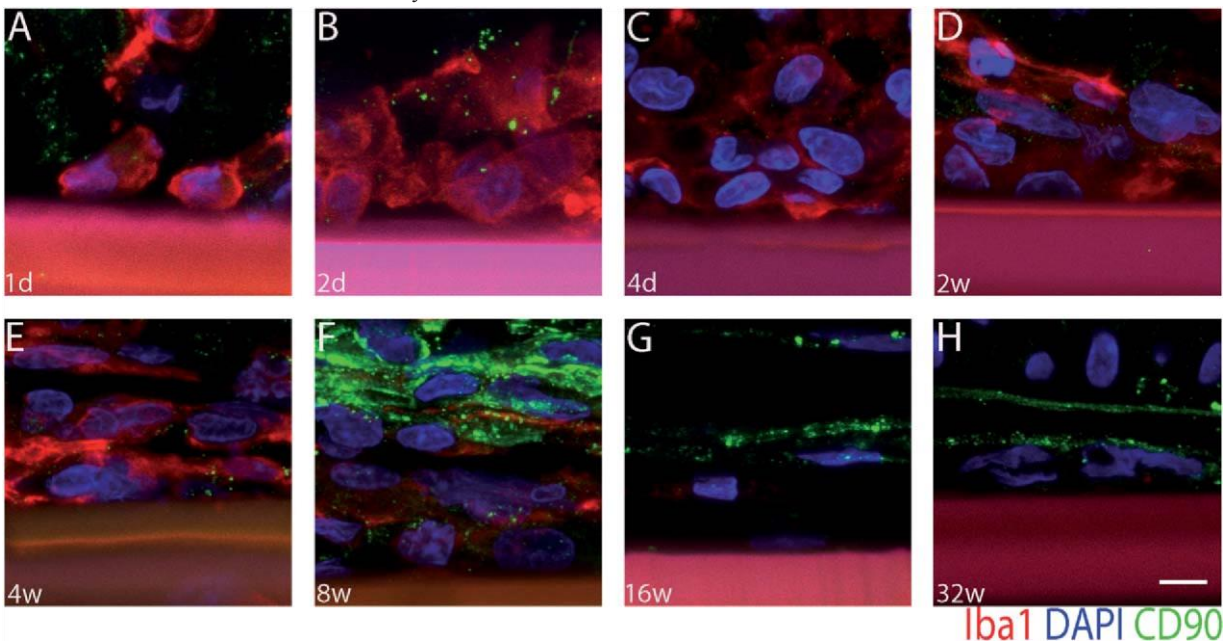


FIGURE 8. Cellular events in the tissue capsule around the device. Representative confocal images of cells in the capsule from 1 day to 32 weeks. Macrophages (red) are in contact with the device until 16 weeks. Fibroblasts (green) appear at 4–8 weeks and are located in the periphery of the capsule, in contact with nerve fibers. Scale bar 515 μ m.

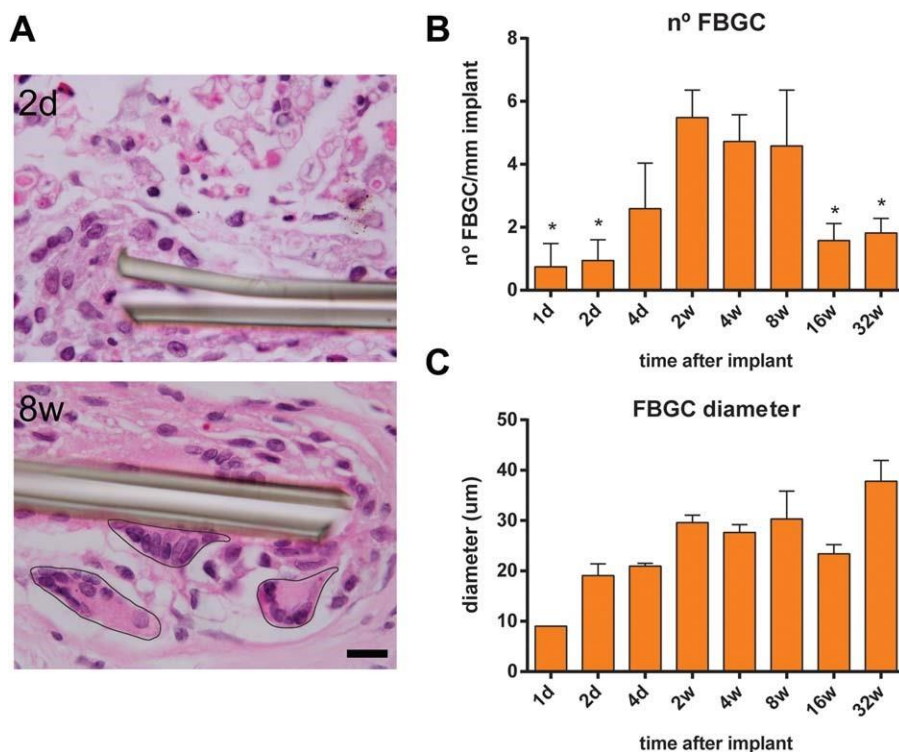


FIGURE 9. Foreign body giant cells as a hallmark of the FBR. (A) Presence of FBGCs in the surface of the device observed with hematoxylineosin at different time points. (B) Number and (C) diameter of FBGCs on the device over time. * $p < 0.05$ versus 2 weeks. Scale bar 515 μ m.

to the interposition of the fibrous tissue between the active sites in the electrode and the axons. Although stimulation can be maintained over time at the cost of increasing the intensity of stimuli,¹⁵ recording of nerve signals is more critically affected given the low amplitude of axonal impulses recorded extracellularly, in the range of microvolts, that cannot be increased, and the influence of distance between active site and recorded cells in quality of signal recordings.⁴³ Whereas the rationale to explain the functional decrease in chronic electrodes has been hypothesized and modeled,^{44,45} the exact mechanisms that explain the possible role of the FBR in electrode failure have not yet been elucidated.⁴⁶

Some reports have characterized the FBR to intraneural implants in cats³¹ and in humans,²⁹ but these studies were conducted after implantation of rigid multielectrode Utah slanted arrays and the stiffness of these electrodes has been reported to contribute to traumatic nerve injuries and an increased FBR.⁴⁷ However, here we describe in detail the progression of the FBR to LIFE intraneural devices fabricated with polyimide, a flexible material that can deform in 3D and adapt with the nerve,⁴⁸ widely used in the fabrication of nerve electrodes tested in rats^{19,32,49} and in humans.^{14–16} The implant of wired active electrodes may induce tethering forces resulting in damage to the nerve tissue^{29–32} but not directly contribute to the FBR. Thus, the use of non-functional devices avoided external artifacts in the creation of a FBR and provided a more reproducible model to focus only on the nerve

reaction to the implant. Therefore, the information in this study may help to design novel strategies for modulating the FBR against electrodes placed within the peripheral nerve.

Unlike other fibrotic responses in pathological conditions where scar tissue impairs proper function of the organ,^{50,51} our results showed that the new tissue formation in the peripheral nerve did not have a negative impact on its function after careful implantation, as previously reported when implanting LIFE¹⁰ or even TIME electrodes.¹¹ Electrophysiological tests of the implanted nerves did not show alterations in the onset and the amplitude of the evoked compound action potentials along the 8 months of implantation. Besides, there were no functional alterations observed in nociceptive and in locomotion tests. These results were corroborated by histological observations of implanted and sham nerves, where the normal fascicular architecture was preserved, and no evidence of axonal damage and distal degeneration were observed at all the studied time points. This is an important point, since the LIFE implant of the thin film polyimide device, mimicking the use of tf-LIFEs, allowed us to investigate the FBR against the device, without relevant contributions of tissue damage due to the surgical procedure or to the mechanical stress of connected wires.

In order to understand how the FBR evolves, we first studied the infiltration of macrophages in the nerve as a sign of the immune response. Whereas in the sham group, that had received the same surgical procedure as implanted animals but leaving no implant in the nerve, the inflammatory reaction was low and time-

limited, in the device implanted group there were more infiltrating macrophages during a longer time, becoming chronic. This evolution corresponds to the FBR widely studied in other tissues, which normally has an acute inflammatory phase that may become chronic with time.²⁰ Regarding the phenotype of the infiltrating macrophages, the ED1 clone of CD68 was proposed as a marker of activated or inflammatory macrophages.⁵² The evolution of ED1⁺ macrophages, comprehending about a third of those labeled with Iba1 in the nerve, was similar to the evolution of the total Iba1⁺ cell population, increasing to a peak between 1 and 2 weeks and slowly disappearing later, as also found in a previous report.³² These observations suggest that ED1 labels a subpopulation of macrophages rather than a different pro-inflammatory reactive subclass, all stained with Iba1. Thus, description of nerve macrophages need to be made using reliable macrophage markers, such as Iba1³⁷ or F4/80,⁵³ and additional measurements of Ly6C, CX3CR1, CCR2, and CD62L, rather than only ED1 labeling, should be performed for a better characterization of macrophage activation.⁵⁴

We also assessed the progressive formation of an encapsulating tissue around the polyimide device. One day after the implantation the body started to react against the foreign device with changes in the surrounding as seen by electron microscopy. Nevertheless, there was no real capsule until four days and the thickness peaked by 2 weeks. From week 4 to the end of the follow-up, the capsule was progressively decreasing in thickness until stabilization. This dynamic in the capsule formation is coincident in time with the infiltration of macrophages in the nerve due to the implant described here, which also peaked after 2 weeks and started to decrease thereafter. It has been shown that macrophages and phagocytes are related to the nature of the material implanted and its degradation dynamics.^{55,56} Thus, biodegradable materials would stimulate more M1 phenotype and phagocytic environment to eliminate the implant. In contrast, non-biodegradable materials would stimulate more M2, pro-fibrotic and tissue remodeling environment, with the contribution of FBGCs and matrix deposition. In fact, fused macrophages forming FBGCs were found surrounding the implanted device as early as 1 day after the implant contributing to the FBR, and their size did not change substantially throughout the study, except for a slight increase seen at 32 weeks, probably due to further stabilization and fusion of these cells. The amount of FBGCs increased gradually to reach a maximum at 2 weeks, similar to the density of Iba1 cells and the capsule thickness, but declined slower than macrophages in the nerve. At late time, 16 and 32 weeks, when macrophages have practically disappeared from the nerve, the presence of these FBGCs also declined as a hallmark of the chronic phase of FBR.⁴² FBGCs are found only within the tissue capsule where tissue reactivity and inflammation is higher than within the nerve endoneurium, and these cells have been linked to the tissue formation around implants.⁵⁷ Therefore, the decline of FBGCs could indicate an intermediate step between the predominant presence of macrophages to fibroblasts around the implant, when the tissue capsule switches from a phagocytic state to a barrier forming state due to the presence of a non-

phagocytatable foreign body. Taking our results into account, polyimide intraneural implants could be stimulating the second scenario, regarding the presence of FBGCs and the resolution of the inflammatory response in the nerve in comparison to the remodeling response.

Although the appearance of the different cells and the characteristics of the encapsulation in the peripheral nerve seem to follow a similar pattern to the FBR described in subcutaneous implants, there are differences in the timecourse of the cellular events between subcutaneous⁴¹ and nerve implants.^{10,32} Thus, during the acute inflammatory phase of the FBR, macrophages and other immune cells, such as mast cells and neutrophils, start to surround the foreign body and to bind to adsorbed proteins on the device surface in a process called biofouling that will stimulate the subsequent phases.⁴¹ The accumulation of these cells around the device would contribute to the proinflammatory environment which leads to the subsequent chronic inflammation and tissue remodeling phase.²⁰ During the first weeks after the intraneural implant, there is a marked presence of round-shaped macrophages surrounding the device without evidence of other cell types. As a matter of fact, Wurth et al.³² reported a zone of increased cellularity around the implant being both fibroblasts and monocytes the main components of the tissue capsule as early as 1 week after implantation of a transverse type electrode. In our study we also observed a tissue capsule with increased cellularity, but we found that macrophages are the main cells that populate this capsule from 1 day to 4 weeks, without presence of monocytes which are rarely found within the peripheral nerve,^{58,59} or fibroblasts that were not seen until 8 weeks after the implant at the edge of the capsule. Later on, the occurrence of macrophages declines while fibroblasts increase at 16 weeks. Finally, 8

months after the implantation, macrophages almost disappeared from the encapsulating tissue and fibroblasts became more numerous, forming a permanent connective capsule. These changes in the cellularity of the capsule correlate with an increasing deposition of extracellular matrix mainly formed by collagen fibrils. Therefore, subcutaneous implantation models may give an indication on different strategies to decrease the tissue reaction in the nerve, but the use of an intraneural model is necessary for an optimal understanding of the nerve FBR provided the different evolution of cellular events in time.

In conclusion, our study characterizes the FBR against an intraneural passive polyimide electrode. The advantages of using a LIFE device are that the implant creates a stable environment of 10–15 mm inside the nerve that creates a reliable model with high reproducibility to study the FBR throughout the nerve. In our model, the FBR stems from the relationship between the endoneurium and the device itself without the confounding contribution of other external factors, such as variability of implantation, electrical stimulation, or tethering forces of the wires. Our results help to understand the FBR to intraneural electrodes and provide the bases for developing new strategies to reduce this reaction and, thus, lengthen the lifespan of intraneural interfaces.

ACKNOWLEDGMENTS

The authors thank Monica Espejo and Jessica Jaramillo for the technical help, and Servei de Microscopia (UAB) for help with TEM images. The ICN2 is funded by the CERCA programme/ Generalitat de Catalunya. The authors would like to express their special appreciation to Matthias Mueller and Thomas Stieglitz from IMTEK, University of Freiburg for providing the polyimide devices.

REFERENCES

- Yoshida K, Pellinen D, Rousche P, Kipke D. Development of the Thin-film Longitudinal Intra-fascicular Electrode. Proceedings of the 5th Annual Conference of the International Functional Electrical Stimulation Society 2000;279–281.
- Badia J, Boretius T, Andreu D, Azevedo-Coste C, Stieglitz T, Navarro X. Comparative analysis of transverse intrafascicular multichannel, longitudinal intrafascicular and multipolar cuff electrodes for the selective stimulation of nerve fascicles. *J Neural Eng* [Internet] 2011;8:36023. Available from: <http://www.scopus.com/inward/record.url?eid=52-s2.0-79957935921&partnerID=5tZ0tx3y1>
- Micera S, Navarro X, Carpaneto J, Citi L, Tonet O, Rossini PM, Carrozza MC, Hoffmann KP, Vivo M, Yoshida K, Dario P. On the use of longitudinal intrafascicular peripheral interfaces for the control of cybernetic hand prostheses in amputees. *IEEE Trans Neural Syst Rehabil Eng* 2008;16:453–472.
- Branner A, Normann RA. A multielectrode array for intrafascicular recording and stimulation in sciatic nerve of cats. *Brain Res Bull* 2000;51:293–306.
- Branner A, Stein RB, Normann RA. Selective stimulation of cat sciatic nerve using an array of varying-length microelectrodes. *J Neurophysiol* 2001;85:1585–1594.
- Clark GA, Ledbetter NM, Warren DJ, Harrison RR. Recording sensory and motor information from peripheral nerves with Utah Slanted Electrode Arrays. *Proc Annu Int Conf IEEE Eng Med Biol Soc EMBS*. 2011;4641–4644.
- Wark HA, Sharma R, Mathews KS, Fernandez E, Yoo J, Christensen MB, Tresco P, Rieth L, Solzbacher F, Normann RA, Tathireddy P. A new high-density (25 electrodes/mm²) penetrating microelectrode array for recording and stimulating sub-millimeter neuroanatomical structures. *J Neural Eng* [Internet] 2013;10: 45003. Available from: <http://www.ncbi.nlm.nih.gov/pubmed/23723133>
- Clark GA, Wendelken S, Page DM, Davis T, Wark HAC, Normann RA, Warren DJ, Hutchinson DT. Using multiple high-count electrode arrays in human median and ulnar nerves to restore sensorimotor function after previous transradial amputation of the hand. *36th Annu Int Conf IEEE Eng Med Biol Soc EMBC* 2014. 2014;1977–80.
- Malmstrom J, McNaughton T, Horch K. Recording properties and biocompatibility of chronically implanted polymer-based intrafascicular electrodes. *Ann Biomed Eng* 1998;26:1055–1064.
- Lago N, Yoshida K, Koch KP, Navarro X. Assessment of biocompatibility of chronically implanted polyimide and platinum intrafascicular electrodes. *IEEE Trans Biomed Eng* 2007;54:281–290.
- Badia J, Boretius T, Pascual-Font A, Udina E, Stieglitz T, Navarro X. Biocompatibility of chronically implanted transverse intrafascicular multichannel electrode (TIME) in the rat sciatic nerve. *IEEE Trans Biomed Eng* 2011;58:2324–2332. Available from: <http://www.scopus.com/inward/record.url?eid=52-s2.0-79957942755&partnerID=5tZ0tx3y1>
- Boretius T, Badia J, Pascual-Font A, Schuettler M, Navarro X, Yoshida K, Stieglitz T. A transverse intrafascicular multichannel electrode (TIME) to interface with the peripheral nerve. *Biosens Bioelectron* 2010;26:62–69. Available from: <http://www.scopus.com/inward/record.url?eid=52-s2.0-84055161627&partnerID=5tZ0tx3y1>
- Dhillon GS, Horch KW. Direct neural sensory feedback and control of a prosthetic arm. *IEEE Trans Neural Syst Rehabil Eng* 2005;13: 468–472.
- Rossini PM, Micera S, Benvenuto A, Carpaneto J, Cavallo G, Citi L, Cipriani C, Denaro L, Denaro V, Di Pino G, Ferreri F, Guglielmelli E, Hoffmann KP, Raspovic S, Rigosa J, Rossini L, Tombini M, Dario P. Double nerve intraneural interface implant on a human amputee for robotic hand control. *Clin Neurophysiol* 2010;121:777–783. Available from: <https://doi.org/10.1016/j.clinph.2010.01.001>
- Raspovic S, Capogrosso M, Petrini FM, Bonizzato M, Rigosa J, Di Pino G, Carpaneto J, Controzzi M, Boretius T, Fernandez E, Granata G, Oddo CM, Citi L, Ciancio A, Cipriani C, Carrozza MC, Jensen W, Guglielmelli E, Stieglitz T, Rossini PM, Micera S. Restoring natural sensory feedback in real-time bidirectional hand prostheses. *Sci Transl Med* 2014;6:222ra19–222ra19. Available from: <http://stm.sciencemag.org/cgi/doi/10.1126/scitranslmed.3006820>
- Oddo CM, Raspovic S, Artoni F, Mazzoni A, Spigler G, Petrini F, Giambattistelli F, Vecchio F, Miraglia F, Zollo L, Di Pino G, Camboni D, Carrozza MC, Guglielmelli E, Rossini PM, Faraguna U, Micera S. Intraneural stimulation elicits discrimination of textural features by artificial fingertip in intact and amputee humans. *Elife* 2016;5:1–27. Available from: <http://elifesciences.org/lookup/doi/10.7554/eLife.09148>
- Warwick K, Gasson M, Hutt B, Goodhew I, Kyberd P, Andrews B, Teddy P, Shad A. The application of implant technology for cybernetic systems. *Arch Neurol* 2003;60:1369–1373. Available from: <https://doi.org/10.1001/archneur.60.10.1369>
- Branner A, Stein RB, Fernandez E, Aoyagi Y, Normann RA. Long-term stimulation and recording with a penetrating microelectrode array in cat sciatic nerve. *IEEE Trans Biomed Eng* 2004;51:146–157.
- Cutrone A, Del Valle J, Santos D, Badia J, Filippeschi C, Micera S, Navarro X, Bossi S. A three-dimensional self-opening intraneural peripheral interface (SELINE). *J Neural Eng* 2015;12:0. Available from: <https://doi.org/10.1088/1741-2560/0/0/000000>
- Anderson JM, Rodriguez A, Chang DT. Foreign body reaction to biomaterials. *Semin Immunol* 2008;20:86.
- Gretzer C, Emanuelsson L, Liljensten E, Thomsen P. The inflammatory cell influx and cytokines changes during transition from acute inflammation to fibrous repair around implanted materials. *J Biomater Sci Polym Ed* 2006;17:669–687.
- Fet N, Alizai PH, Fragoulis A, Wruck C, Pufe T, Tolba RH, Neumann UP, Klinge U. In vivo characterisation of the inflammatory reaction following mesh implantation in transgenic mice models. *Langenbecks Arch Surg*. Springer Verlag 2014;399:579–588.
- Kastellorizios M, Papadimitrakopoulos F, Burgess DJ. Multiple tissue response modifiers to promote angiogenesis and prevent the foreign body reaction around subcutaneous implants. *J Control Release* 2015;214:103–111.
- Robitaille R, Dusseault J, Henley N, Desbiens K, Labrecque N, Hall JP. Inflammatory response to peritoneal implantation of alginate-poly-L-lysine microcapsules. *Biomaterials* 2005;26:4119–4127.
- Le SJ, Gongora M, Zhang B, Grimmond S, Campbell GR, Campbell JH, Rolfe BE. Gene expression profile of the fibrotic response in the peritoneal cavity. *Differentiation*. Elsevier 2010;79: 232–243.
- Biran R, Martin DC, Tresco PA. Neuronal cell loss accompanies the brain tissue response to chronically implanted silicon microelectrode arrays. *Exp Neurol* 2005;195:115–126.
- Polikov VS, Tresco PA, Reichert WM. Response of brain tissue to chronically implanted neural electrodes. *J Neurosci Methods* 2005;148:1–18.
- Yanagihara T, Goldstein NP, Svien HJ, Bahn RC. Foreign body reaction of the brain: Enzyme-histochemical study in dogs. *Neurology* 1967;17:337. Available from: <http://www.neurology.org/content/17/4/337.short>
- Christensen MB, Wark HA, Hutchinson DT. A histological analysis of human median and ulnar nerves following implantation of Utah slanted electrode arrays. *Biomaterials* 2016;77:235–242. Available from: <https://doi.org/10.1016/j.biomaterials.2015.11.012>
- Wark HA, Mathews KS, Normann RA, Fernandez E. Behavioral and cellular consequences of high-electrode count Utah Arrays chronically implanted in rat sciatic nerve. *J Neural Eng* 2014;11: 46027. Available from: <http://www.ncbi.nlm.nih.gov/pubmed/25031219> <http://stacks.iop.org/1741-2552/11/i5/a5046027>
- Christensen MB, Pearce SM, Ledbetter NM, Warren DJ, Clark GA, Tresco PA. The foreign body response to the Utah Slant Electrode Array in the rat sciatic nerve. *Acta Biomater* [Internet]. Acta Materialia Inc 2014;10:4650–4660. Available from: <https://doi.org/10.1016/j.actbio.2014.07.010>
- Wurth S, Capogrosso M, Raspovic S, Gandar J, Federici G, Kinany N, Cutrone A, Piersigilli A, Pavlova N, Guiet R, Taverni G, Rigosa J, Shkarbatova P, Navarro X, Barraud Q, Courtine G, Micera S. Long-term usability and bio-integration of

- polyimidebased intra-neural stimulating electrodes. *Biomaterials* [Internet]. Elsevier Ltd 2017;122:114–129. Available from: <https://doi.org/10.1016/j.biomaterials.2017.01.014>
33. Rubehn B, Stieglitz T. In vitro evaluation of the long-term stability of polyimide as a material for neural implants. *Biomaterials*. Elsevier Ltd 2010;31:3449–3458.
 34. Santos D, Wieringa P, Moroni L, Navarro X, Del Valle J. PEOT/PBT guides enhance nerve regeneration in long gap defects. *Adv Healthcare Mater* 2017;6:1600298. Available from: <http://www.ncbi.nlm.nih.gov/pubmed/27973708>
 35. de Medinaceli L, Freed WJ, Wyatt RJ. An index of the functional condition of rat sciatic nerve based on measurements made from walking tracks. *Exp Neurol* 1982;77:634–643.
 36. Schneider CA, Rasband WS, Eliceiri KW. NIH Image to ImageJ: 25 years of image analysis. *Nat Methods* 2012;9:671–675. Available from: <https://doi.org/10.1038/nmeth.2089>
 37. Ito D, Tanaka K, Suzuki S, Dembo T, Fukuuchi Y. Enhanced expression of Iba1, ionized calcium-binding adapter molecule 1, after transient focal cerebral ischemia in rat brain. *Stroke* 2001;32: 1208–1215. Available from: <http://stroke.ahajournals.org/content/32/5/1208.full.pdf>
 38. Anderson JM. Future challenges in the in vitro and in vivo evaluation of biomaterial biocompatibility. *Regen Biomater* 2016;3: rbw001. Available from: <http://rb.oxfordjournals.org/lookup/doi/10.1093/rb/rbw001>
 39. McNally AK, Anderson JM. Macrophage fusion and multinucleated giant cells of inflammation. *Adv Exp Med Biol* 2011; 713:97–111.
 40. Luttkhuizen DT, Harmsen MC, Van Luyn MJA. Cellular and molecular dynamics in the Foreign Body Reaction. *Tissue Eng* 2006;10:77–96. discussion 97.
 41. Ward KW. A review of the foreign-body response to subcutaneously-implanted devices: the role of macrophages and cytokines in biofouling and fibrosis. *J Diab Sci Technol* 2008;2: 768–777.
 42. Sheikh Z, Brooks PJ, Barzilay O, Fine N, Glogauer M. Macrophages, foreign body giant cells and their response to implantable biomaterials. *Materials (Basel)* 2015;8:5671–5701. Available from: <http://www.mdpi.com/1996-1944/8/9/5269/>
 43. Henze D, Borhegyi Z, Csicsvari J, Mamiya A, Harris K, Buzsaki G. Intracellular features predicted by extracellular recordings in the hippocampus in vivo. *J Neurophysiol* 2000;84:390–400. Available from: <http://www.ncbi.nlm.nih.gov/pubmed/10899213>
 44. Micera S, Citi L, Rigosa J, Carpaneto J, Raspopovic S, Di Pino G, Rossini L, Yoshida K, Denaro L, Dario P, Rossini PM. Decoding information from neural signals recorded using intraneural electrodes: Toward the development of a neurocontrolled hand prosthesis. *Proc IEEE* 2010;98:407–417.
 45. Raspopovic S, Capogrosso M, Micera S. A computational model for the stimulation of rat sciatic nerve using a transverse intrafascicular multichannel electrode. *IEEE Trans Neural Syst Rehabil Eng* 2011;19:333–344.
 46. Raspopovic S, Petrini FM, Zelechowski M, Valle G. Framework for the development of neuroprostheses: from basic understanding by sciatic and median nerves models to bionic legs and hands. *Proc IEEE* 2017;105:34–49.
 47. Lacour SP, Benmerah S, Tarte E, FitzGerald J, Serra J, McMahon S, Fawcett J, Graudejus O, Yu Z, Morrison B. Flexible and stretchable micro-electrodes for in vitro and in vivo neural interfaces. *Med Biol Eng Comput* 2010;48:945–954. Available from: <http://www.ncbi.nlm.nih.gov/pubmed/20535574>
 48. del Valle J, Navarro X. Interfaces with the peripheral nerve for the control of neuroprostheses. *Int Rev Neurobiol* 2013;109:63–83.
 49. Delgado-Martinez I, Righi M, Santos D, Cutrone A, Bossi S, D'Amico S, Del Valle J, Micera S, Navarro X. Fascicular nerve stimulation and recording using a novel double-aisle regenerative electrode. *J Neural Eng* [Internet] 2017;14:46003. Available from: <http://iopscience.iop.org/10.1088/1741-2552/aa6bac>
 50. Duffield JS. Cellular and molecular mechanisms in kidney fibrosis. *J Clin Invest* 2014;124:2299–2306.
 51. Gross TJ, Hunninghake GW. Idiopathic pulmonary fibrosis. *N Engl J Med* 2001;345:517–525.
 52. Damoiseaux JG, Dopp EA, Calame W, Chao D, MacPherson GG, Dijkstra CD. Rat macrophage lysosomal membrane antigen recognized by monoclonal antibody ED1. *Immunology* 1994;83:140–147.
 53. Martinez-Muriana A, Mancuso R, Francos-Quijorna I, Olmos-Alonso A, Osta R, Perry VH, Navarro X, Gomez-Nicola D, Lopez-Vales R. CSF1R blockade slows the progression of amyotrophic lateral sclerosis by reducing microgliosis and invasion of macrophages into peripheral nerves. *Sci Rep* 2016;6:25663. Available from: <https://doi.org/10.1038/srep25663>
 54. Geissmann F, Jung S, Littman DR. Blood monocytes consist of two principal subsets with distinct migratory properties. *Immunity* 2003;19:71–82.
 55. Veisoh O, Doloff JC, Ma M, Vegas AJ, Tam HH, Bader AR, Li J, Langan E, Wyckoff J, Loo WS, Jhunjhunwala S, Chiu A, Siebert S, Tang K, Hollister-Lock J, Aresta-Dasilva S, Bochenek M, Mendoza-Elias J, Wang Y, Qi M, Lavin DM, Chen M, Dholakia N, Thakrar R, Lacik I, Weir GC, Oberholzer J, Greiner DL, Langer R, Anderson DG. Size- and shape-dependent foreign body immune response to materials implanted in rodents and non-human primates. *Nat Mater* 2015;14:643–651.
 56. Boddupalli A, Zhu L, Bratlie KM. Methods for implant acceptance and wound healing: material selection and implant location modulate macrophage and fibroblast phenotypes. *Adv Healthcare Mater* 2016; 5:2575–2594. Available from: <http://doi.wiley.com/10.1002/adhm.201600532>
 57. Anderson JM, McNally AK. Biocompatibility of implants: Lymphocyte/macrophage interactions. *Semin Immunopathol* 2011;33:221–233.
 58. Ginhoux F, Jung S. Monocytes and macrophages: developmental pathways and tissue homeostasis. *Nat Rev Immunol* 2014; 14 VN-r:392–404. Available from: <http://www.nature.com/doi/10.1038/nri3671>
 59. Jakubczak CV, Randolph GJ, Henson PM. Monocyte differentiation and antigen-presenting functions. *Nat Rev Immunol* 2017;17:349–362. Available from: <http://www.nature.com/doi/10.1038/nri.2017.28>